



The
University
Of
Sheffield.

Roller compaction: Effect of morphology and amorphous content of different types of lactose

Chalak S. Omar

A thesis submitted in partial fulfilment of the requirements for the degree
of
Doctor of Philosophy

Department of Chemical and Biological Engineering
The University of Sheffield

Supervised by:
Prof. Agba D. Salman
Prof. Michael J. Hounslow

December 2016

ABSTRACT

Roller compaction is a dry granulation process in which high stresses are applied on the powder using two counter-rotating rollers to produce compacts which can then be milled into granules. Roller compaction is a complex process and very sensitive to the primary powder properties. The process is not fully understood due to the diversity of materials properties which could be different even for similar materials. For example, particles of lactose (an important material in food and pharmaceutical industries) can be found in different morphologies as well as different amorphous contents. This thesis aims to understand the behaviour of various types of lactose (with different morphologies and amorphous contents) during roller compaction at different humidity conditions and process parameters, and attempts to improve the quality of ribbons using various approaches.

Three types of lactose powders were used: anhydrous SuperTab21AN, spray dried SuperTab11SD which are agglomerated forms of lactose, and α -lactose monohydrate 200M which is non-agglomerated. The morphology of the particle was found to have a significant effect on single particle strength. The strength of a single particle of the non-agglomerated type of lactose (200M) was higher in comparison with the agglomerated types (21AN and SD). The lowest strength was shown by particles of spray dried (SD) lactose due to its agglomerated structure. During the roller compaction experiments, an online thermal camera was used to record the temperature of ribbon which was considered as a key factor to describe the behaviour of powder undergoing roller compaction. It was found that the morphology and amorphous content of the powder have a significant effect on the ribbon properties. The agglomerated type of lactose (21AN and SD) showed better binding capacity compare to the non-agglomerated type (200M). The best binding capacity was shown by the agglomerated types of lactose which contain the highest percentage of the amorphous form. It was found that there is a relationship between the tensile strength of the produced ribbon and the strength of a single particle of the starting powder. The stronger the primary particle of the initial powder the weaker the ribbon after roller compaction. It was also found that there is a relationship between the surface temperature of the ribbon during production and its resultant tensile strength: the higher the temperature of the ribbon during production the higher the ribbon tensile strength. This means that the temperature of the ribbon may be

used to predict the tensile strength of the produced ribbon, regardless of the type of lactose.

The changes in the relative humidity (RH) conditions during powder storage were shown to have a significant effect on powder and ribbon properties. It was found that powders conditioned at different RH values exhibited different behaviours in the compaction zone which was evident by the PIV (Particle Image Velocimetry) experiments. The optimum storage conditions for all three types of lactose were found to be in the range of 20% - 40% RH. Within this range, wider ribbons with a minimum amount of fines were produced.

The online thermal imaging was found to be a useful technique to describe the difference in ribbon properties at different process parameters. The process parameter of the roller compactor (roller speed, roller gap and the feeder screw speed) was shown to have a significant effect on the ribbon properties.

The results showed that ribbons with homogeneous properties (e.g. porosity and strength) along the width can be obtained using a new roller with a novel curved design. The curved roller was able to apply a more uniform stress on the powder along the width of the roller surface and resulted in a significant reduction in the percentage of fines in the product. This approach can be used in different industries to overcome the non-uniformity of ribbon properties across the width and reduce the undesirably large amount of fines which have a negative impact on the final product.

Acknowledgements

First of all, I would like to thank my academic supervisors Prof. Agba D. Salman and Prof. Michael J. Hounslow for their supervision. Special thank with my sincere gratitude goes to Prof. Agba D. Salman for his continuous support, advice and encouragements throughout my PhD study. Your valuable guidance has been extremely helpful all the time during the research and writing of my thesis, much appreciated.

I am grateful to The Higher Committee for Education Development in Iraq for funding my PhD study.

I would also like to thank all the members of the Particle Product Group (PPG) for all their support and help. Special thanks to Dr Ranjit Dhenge for all your advice and excellent feedback and comments while reading my thesis. Great thank to Syed for his continuous help, Mohammed for making the PhD life enjoyable, Menan, Riyadh, for being good neighbours. Thanks to William, JianKai, Arthi, Sushma and Ai Qing for being good colleagues and friends. Thank you Ali, Osama, Bilal, Kawther, Wafaa, Alan and Mingzhe wish you all the best in your study.

I reserve my special thanks to GOD for his great graces, help and conciliation. Great thanks, gratitude and love to my family: my wife, daughter and little son for making me forget the hard time in the university and giving me a great support, motivation and encouragements. My deep respect and thank to my mother, father, brother and sisters who have always supported me in every step in my life. I would like to thank my mother and father-in-law and extended family for their support and encouragements.

List of Publications and Presentations

- Omar, C.S., et al., Roller compaction: Effect of relative humidity of lactose powder. **European Journal of Pharmaceutics and Biopharmaceutics**, 2016. **106**: p. 26-37.
- Omar, C.S., et al., Roller compaction: Effect of morphology and amorphous content of lactose powder on product quality. **International Journal of Pharmaceutics**, 2015. **496**(1): p. 63-74.
- Omar, C.S., et al., Roller compaction: Reducing the percentage of fines in the product using lactose powders at different relative humidities. Poster presentation at the 12th UK Particle Technology Forum, Manchester, UK. 16th-17th September 2014.
- Omar, C.S., et al., Roller compaction: Effect of amorphous content of lactose upon product properties. Conference paper and oral presentation at the 21st International Congress of Chemical and Process Engineering Chisa, Prague, Czech Republic. 23rd-27th August 2014. Paper No. 1221.
- Omar, C.S., et al., Roller compaction: Comparison of ribbon and granule properties using different types of lactose. Poster presentation at the 6th International Granulation Workshop, Sheffield, UK. 26th-28th June 2013.

TABLE OF CONTENTS

Abstract	I
Acknowledgements	III
List of Publications and Presentations	IV
Table of Contents	V
List of Figures	IX
List of Tables	XVIII
Nomenclature	XIX
Chapter 1 Introduction	1
1.1 Granulation.....	1
1.2 Types of granulation.....	1
1.3 Roller compaction	2
1.4 Roller compaction challenges	4
1.5 Aim of the research	5
1.6 Overview of thesis.....	6
Chapter 2 Literature Review	8
2.1 Compaction process and bonding mechanisms.....	8
2.2 Material	10
2.2.1 Structure	10
2.2.2 Amorphous and crystalline lactose.....	12
2.2.3 Determination of lactose amorphous content	13
2.3 Experimental studies on powder compaction.....	15
2.3.1 Effect of primary powder properties (Morphology and amorphous content)	15
2.3.1.1 Direct compaction	15
2.3.1.2 Roller compaction	17
2.3.2 Effect of powder moisture content	19
2.3.2.1 Direct compaction	20
2.3.2.2 Roller compaction	23
2.3.3 Effect of the process parameter	27
2.3.3.1 Effect of the feeder screw speed.....	28
2.3.3.2 Effect of the roller speed	28
2.3.3.3 Effect of the gap between the rollers.....	30
2.3.4 Amount of fines (non-compacted powder)	32
2.4 Inhomogeneity across ribbon width	34

2.5	Theoretical models in roller compaction.....	40
2.5.1	Johanson Model.....	40
2.5.2	The slab model:	44
2.5.3	Thin layer model	46
2.5.4	Finite element method (FEM)	47
Chapter 3	Materials and methods.....	51
3.1	Material	51
3.1.1	Lactose	51
3.1.2	Primary particle size distribution	53
3.2	Methods.....	53
3.2.1	Differential Scanning Calorimetry (DSC).....	53
3.2.2	Fourier Transform Near Infrared (FT-NIR)	53
3.2.3	Powder preparation	55
3.2.4	Powder moisture content.....	55
3.2.5	Powder flow property.....	55
3.2.5.1	Shear cell tester	55
3.2.5.2	Repose angle	57
3.2.5.3	Compressibility index	57
3.2.6	Compressibility factor of the powders	57
3.2.7	Roller compaction	58
3.2.8	Online thermal imaging.....	60
3.2.9	Determination of the fine percentage	61
3.2.10	Strength of ribbon.....	61
3.2.11	Ribbon porosity using X-ray tomography.....	62
3.2.12	Scanning Electron Microscopy	62
Chapter 4	Properties of the primary powders.....	63
4.1	Particle size distribution of the primary powders.....	63
4.2	Quantification of the amorphous content of powders	64
4.2.1	Differential Scanning Calorimetry (DSC).....	64
4.2.2	Fourier Transform Near Infrared (FT-NIR)	66
4.3	Preparation of the powder prior to compaction.....	70
4.3.1	Powder weight changes in the climatic chamber	70
4.4	Emissivity of the powder.....	71
4.5	X-ray tomography of the primary particles	72
4.6	Single primary particle strength	74
Chapter 5	Effect of morphology and amorphous content.	79
5.1	Introduction	79

5.2	Preparation of powders.....	80
5.3	Scanning electron microscopy (SEM) of the primary powder.....	80
5.4	Production of ribbon.....	82
5.5	Effect of morphology and amorphous content.....	82
5.5.1	Stress applied on the powder during roller compaction.....	82
5.5.2	Surface temperature and strength of the ribbon.....	86
5.5.3	Scanning electron microscopy (SEM) for Ribbons.....	97
5.5.4	Percentage of fines and width of ribbon.....	100
5.5.4.1	Relationship between the fine percentage and ribbon width.....	102
5.5.4.2	Relationship between the fine percentage and ribbon temperature.....	103
5.5.5	Temperature distribution across the width of ribbon.....	106
5.5.6	Ribbon porosity.....	108
5.6	Effect of amorphous content.....	111
5.7	Effect of morphology.....	114
5.8	Conclusion.....	115
Chapter 6	Effect of the relative humidity on the product quality.....	117
6.1	Introduction.....	117
6.2	Preparation of the powders.....	118
6.3	Production of ribbon.....	118
6.4	Particle Image Velocimetry (PIV).....	119
6.5	Results and discussion.....	121
6.5.1	Powder water content.....	121
6.5.2	Powder flow properties.....	122
6.5.3	Amount of fines in the product.....	126
6.5.4	Velocity of powders during roller compaction (PIV).....	128
6.5.5	Width of the ribbon.....	132
6.5.6	Compressibility of the powders at different RH conditions.....	134
6.5.7	Ribbon tensile strength.....	135
6.5.8	Ribbon surface structure (SEM).....	139
6.5.9	Porosity of ribbons.....	141
6.6	Conclusion.....	144
Chapter 7	Roller compaction at different process parameters.....	146
7.1	Introduction.....	146
7.2	Preparation of the powders.....	147
7.3	Production of ribbon.....	147
7.4	Result and discussion.....	147
7.4.1	Effect of the roller speed.....	147

7.4.2	Effect of the gap between the rollers.....	154
7.4.3	Effect of temperature of the starting powder.....	162
7.4.4	Effect of the feeder screw speed.....	169
7.5	Conclusion.....	174
Chapter 8	Inhomogeneity of ribbon across the width.....	176
8.1	Introduction.....	176
8.2	Powder preparation.....	177
8.3	Production and characterisation of ribbon.....	177
8.3.1	The novel design of the curved roller.....	178
8.4	Result and discussion.....	180
8.4.1	Temperature profile across roller width.....	180
8.5	Measurements of the stress during the roller compaction.....	181
8.5.1	Calibration of the pressure film.....	182
8.5.2	Determination of the stress profile across roller width.....	184
8.6	Fines percentage and width of ribbon.....	189
8.7	Local strength across the width of the ribbon.....	191
8.8	Ribbon surface structure.....	194
8.9	X-ray.....	197
8.10	Conclusion.....	201
Chapter 9	Conclusion and future work.....	203
9.1	Conclusion.....	203
9.2	Future work.....	205
References	207
Appendix A: NIR spectra for lactose 21AN and 200M.....	215
Appendix B: Inhomogeneity of ribbon property across the width (lactose 21AN and lactose SD).....	216

LIST OF FIGURES

Figure 1.1: Different designs for rollers: (A) vertical design, (B) incline design, and (C) horizontal design [6].	3
Figure 1.2: Schematic diagram of the roller compaction process showing different regions [6].	4
Figure 2.1: Sorption isotherm (22°C) for crystalline and amorphous materials [18].	12
Figure 2.2: The crushing strength of tablets compressed at 75 MPa from spray dried lactose with different size [21].	16
Figure 2.3: Tablet specific surface area (measured by mercury porosimetry) of α -lactose monohydrate (\square) and anhydrous α -lactose(\circ) [33].	17
Figure 2.4: Tablet porosity for α -lactose monohydrate (\square , \blacksquare) and anhydrous α -lactose(\circ , \bullet), using two methods: Calculation (\circ , \square), and mercury porosimetry (\bullet , \blacksquare) [33].	17
Figure 2.5: Tensile strength of tablets for amorphous lactose at different storage conditions. Open symbols represent 0% RH; closed symbols represent 22% RH. Square=5-10 μ m; circle= 10-25 μ m; triangle=20-50 μ m [31].	21
Figure 2.6: Porosity of tablets for amorphous lactose at different storage conditions. Open symbols represent 0% RH; closed symbols represent 22% RH. Square=5-10 μ m; circle= 10-25 μ m; triangle=20-50 μ m [31].	21
Figure 2.7: Effect of water content and hydraulic pressure on fragment size (d_{50}) of the ribbon after milling [51].	24
Figure 2.8: Effect of water content and hydraulic pressure on ribbon porosity [51].	25
Figure 2.9: Effect of moisture content on the tensile strength of roller compacted ribbon (solid grey line) and compacts prepared using rectangular die (dashed line). Arrow means a decrease in roller speed (7.2, 6, 5 rpm) for the roller compactor and increase in compaction pressure for the rectangular compacts [40].	26
Figure 2.10: Effect of the roller speed and gap on the maximum pressure applied during roller compaction, the theoretical values are obtained from Johanson's model [66].	30
Figure 2.11: Transmission of light through sodium chloride compact [79].	35
Figure 2.12: Simulation results using FEM showing the effect of side seal friction on the roller pressure and density of ribbon across the width [11].	36
Figure 2.13: average relative density along the width of the ribbon using three analysis methods [68].	38
Figure 2.14: the concave-convex rollers designed by Funakoshi et al. [83].	39
Figure 2.15: Relationship between uni-axial stress and compact density [7].	41
Figure 2.16: Schematic diagram of roll press [85].	41
Figure 2.17. Stresses applied to the material in the nip region [90].	45
Figure 2.18: Densification of powder using thin layer model [91].	47

Figure 2.19: Effect of the powder feeding stress on the maximum roll pressure [90]... 48	48
Figure 2.20: Roller pressure and shear stress at a different rolling angle [11]..... 49	49
Figure 3.1: Scanning Electron Microscope images of as-received powders: 21AN (A, B), 200M (C, D), SD (E, F) at 50× magnifications (A, C, E) and 300× (B, D, F)..... 52	52
Figure 3.2: Yield locus and Mohr circle obtained from the ring shear tester..... 56	56
Figure 3.3: Determination of the compressibility factor (K)..... 58	58
Figure 3.4: Alexanderwerk WP120 Roller Compactor. 59	59
Figure 3.5: Design of the rollers showing the front cheek plate. 60	60
Figure 3.6: Schematic diagram of the online thermal imaging and the humidity generator setup..... 61	61
Figure 3.7: Schematic diagram of the three point bend test. 62	62
Figure 4.1: Particle size distribution for the three types of lactose. 63	63
Figure 4.2: Heat flow through pure amorphous lactose VS temperature and time in the DSC. 65	65
Figure 4.3: Normalized DSC data for the three types of lactose used in this study. 66	66
Figure 4.4: NIR spectra of lactose SD with different amorphous content. 67	67
Figure 4.5: Second derivative of the NIR spectra of lactose SD with different amorphous content..... 67	67
Figure 4.6: Actual amorphous content versus calculated amorphous content of anhydrous lactose SuperTab21AN. 68	68
Figure 4.7: Actual amorphous content versus calculated amorphous content of α -lactose monohydrate200M. 69	69
Figure 4.8: Actual amorphous content versus calculated amorphous content for spray dried lactose SuperTab1SD. 69	69
Figure 4.9: Weight change with time for powders conditioned at 40% RH at 25°C in the climatic chamber..... 71	71
Figure 4.10: X-ray images of particles of lactose 200M. 73	73
Figure 4.11: X-ray images of particles of lactose 21AN..... 73	73
Figure 4.12: X-ray images of particles of lactose SD..... 74	74
Figure 4.13: Porosity of the primary particles determined using X-ray tomography..... 74	74
Figure 4.14: Zwick- Roell setup to measure the strength of a single primary particle. . 75	75
Figure 4.15: Force vs displacement curve for a single particle of 200M 76	76
Figure 4.16: Force vs displacement curve for a single particle of 21AN..... 76	76
Figure 4.17: Force vs displacement curve for a single particle of SD..... 77	77
Figure 4.18: Strength of the primary particles of different types of lactose..... 77	77
Figure 4.19: Relationship between the primary particle porosity and strength..... 78	78
Figure 5.1: Scanning Electron Microscope images of sieved powders: 21AN (A, B), 200M (C, D), SD (E, F) at 100× magnifications (A, C, E) and 600× (B, D, F)..... 81	81

Figure 5.2: Thermal images of the three types of lactose at different compaction pressure.	87
Figure 5.3: Ribbon maximum temperature at different hydraulic pressures.	88
Figure 5.4: The Maximum force required to break ribbons produced from different types of lactose.	89
Figure 5.5: Tensile strength of ribbons produced from different types of lactose.	89
Figure 5.6: Cumulative size distribution of fragments of ribbons produced from α -lactose monohydrate 200M.	91
Figure 5.7: Cumulative size distribution of fragments of ribbons produced from anhydrous lactose SuperTab21AN.	91
Figure 5.8: Cumulative size distribution of fragments of ribbons produced from spray dried lactose SuperTab1SD.	92
Figure 5.9: Fragment size of ribbons produced from different types of lactose.	92
Figure 5.10: Relationship between the primary particle strength and ribbon tensile strength.	95
Figure 5.11: Relationship between ribbon temperature during production and ribbon tensile strength.	96
Figure 5.12: Scanning Electron Microscope images for ribbons produced at 100 bar from 21AN (A, B), 200M (C, D), and SD (E, F) at 100 \times magnifications (A, C, E) and 600 \times (B, D, F).	99
Figure 5.13: Scanning Electron Microscope images for ribbons produced at 30 bar from 21AN (A, B), 200M (C, D), and SD (E, F) at 100 \times magnifications (A, C, E) and 600 \times (B, D, F).	100
Figure 5.14: Fines weight percentage of different types of lactose at different hydraulic pressure.	101
Figure 5.15: Width of ribbon of different types of lactose at different hydraulic pressure.	102
Figure 5.16: Relationship between the width of the ribbon and the percentage of fines during roller compaction.	103
Figure 5.17: Example of the thermal images for ribbons produced at 100 bar (left), and the RGB stacks (right).	104
Figure 5.18: Fines percentage plotted against the ratio between the central region of ribbon and roller width, for different types of lactose at different hydraulic pressures.	105
Figure 5.19: Example of the thermal image of SD ribbon produced at 50 bar with a line drawn across the width.	106
Figure 5.20: Temperature distribution across the width of ribbon produced from α -lactose monohydrate 200M at different hydraulic pressure.	107
Figure 5.21: Temperature distribution across the width of ribbon produced from anhydrous 21AN lactose at different hydraulic pressure.	107

Figure 5.22: Temperature distribution across the width of ribbon produced from spray dried SD lactose at different hydraulic pressure.....	108
Figure 5.23: X-ray images for ribbon produced at 30 bar (top) and 100 bar bottom...	109
Figure 5.24: Porosity at the centre of ribbons of different types of lactose using X-ray.	110
Figure 5.25: Porosity at the edge of ribbons of different types of lactose using X-ray.	111
Figure 5.26: Tensile strength of ribbons produced from SD lactose containing different amorphous content.....	112
Figure 5.27: Tensile strength of ribbons produced from 200M lactose containing different amorphous content.....	112
Figure 5.28: Fines weight percentage of SD lactose containing different amorphous content.	113
Figure 5.29: Fines weight percentage of 200M lactose containing different amorphous content.	113
Figure 5.30: Surface temperature of ribbons of different types of lactose after removing the amorphous fraction.	114
Figure 5.31: Tensile strength of ribbons of different types of lactose after removing the amorphous fraction.	115
Figure 5.32: Fines weight percentage of different types of lactose after removing the amorphous fraction.	115
Figure 6.1: Representation of the area of investigation during PIV analysis.....	121
Figure 6.2: Water content of powders stored at different RH values.....	122
Figure 6.3: Powders flow function coefficient at different RH values, measured using the shear cell tester.	123
Figure 6.4: Effective angle of internal friction of powders at different relative humidity.	124
Figure 6.5: Repose angle of the powders equilibrated at different RH values.....	125
Figure 6.6: Compressibility index of the powders equilibrated at different RH values.	125
Figure 6.7: Fine percentage produced at different relative humidities for lactose 21AN.	127
Figure 6.8: Fine percentage produced at different relative humidities for lactose 200M.	128
Figure 6.9: Fine percentage produced at different relative humidities for lactose SD.	128
Figure 6.10: Velocity of 21AN lactose during roller compaction at different RH conditions.	129
Figure 6.11: Velocity of 200M lactose during roller compaction at different RH conditions.	129
Figure 6.12: Velocity of SD lactose during roller compaction at different RH conditions.	130

Figure 6.13: Microscope and X-ray Images of ribbon as an example to show the surface and structure across the width of the ribbon.....	131
Figure 6.14: Width of the ribbon at different relative humidities for lactose 21AN....	133
Figure 6.15: Width of the ribbon at different relative humidities for lactose 200M. ...	133
Figure 6.16: Width of the ribbon at different relative humidities for lactose SD.....	133
Figure 6.17: Compressibility factor (K) for the three types of lactose at different relative humidity conditions.	134
Figure 6.18: Tensile strength of the ribbon at different relative humidities for lactose 21AN.	135
Figure 6.19: Tensile strength of the ribbon at different relative humidities for lactose 200M.....	135
Figure 6.20: Tensile strength of the ribbon at different relative humidities for lactose SD.	136
Figure 6.21: Second derivative of the spectra for the SD lactose conditioned at 10% and 80% RH and pure amorphous lactose.	139
Figure 6.22: Scanning electron microscope images for ribbons produced at 100 bar from 21AN (A, B), 200M (C, D) and SD (E, F), at 20% RH (A, C, E) and 80% RH (B, D, F).	141
Figure 6.23: Porosity of ribbon of lactose 21AN at different RH condition.	142
Figure 6.24: Porosity of ribbon of lactose 200M at different RH condition.	143
Figure 6.25: Porosity of ribbon of lactose SD at different RH condition.....	143
Figure 7.1: Surface temperature of the ribbon during the production at different roller speed.	149
Figure 7.2: Fines percentage produced during the production of ribbon at different roller speed.	150
Figure 7.3: Width of ribbon produced from the three types of lactose at different roller speed.	151
Figure 7.4: Relationship between the fine percentage and the width of the ribbon.	151
Figure 7.5: Tensile strength of ribbon produced from the three types of lactose at different roller speed.....	152
Figure 7.6: Porosity of ribbon produced from the three types of lactose at different roller speed.	154
Figure 7.7: Feeder screw speed at different roller gap.	156
Figure 7.8: Maximum temperature of the ribbon during the production at different roller gap.	157
Figure 7.9: The percentage of fines produced with the ribbon during the production at different roller gap.	158
Figure 7.10: Width of ribbon produced from the three types of lactose at different roller gap.	159

Figure 7.11: Tensile strength of ribbon produced from the three types of lactose at different roller gap.	161
Figure 7.12: Porosity of ribbon produced from the three types of lactose at different roller gap.	162
Figure 7.13: Surface temperature of ribbon produced from the three types of lactose at different temperature of the starting powder.	163
Figure 7.14: The rate of heat loss from the three types of lactose.	165
Figure 7.15: Percentage of fines produced from the three types of lactose at different temperature of the starting powder.	165
Figure 7.16: Width of ribbon produced from the three types of lactose at different temperature of the starting powder.	166
Figure 7.17: Tensile strength of ribbon produced from the three types of lactose at different temperature of the starting powder.	167
Figure 7.18: Porosity of ribbon produced from the three types of lactose at different temperature of the starting powder.	168
Figure 7.19: Surface temperature of ribbon produced from the three types of lactose at different feeder screw speed.	170
Figure 7.20: Percentage of fines produced from the three types of lactose at different feeder screw speed.	171
Figure 7.21: Width of ribbon produced from the three types of lactose at different feeder screw speed.	172
Figure 7.22: Tensile strength of ribbon produced from the three types of lactose at different feeder screw speed.	173
Figure 7.23: Porosity of ribbon produced from the three types of lactose at different feeder screw speed.	174
Figure 8.1: The geometry of the new curved roller.	179
Figure 8.2: The setup of the rollers during the experiments using: (A) the standard flat rollers and (B) the new curved roller.	179
Figure 8.3: Temperature profile across the width of ribbon of lactose 200M during the roller compaction using the flat roller (A) and the curved roller (B) (◆ 20 bar, ■ 50 bar, ▲ 80 bar, × 100 bar).	181
Figure 8.4: The design of the Fujifilm pressure film.	181
Figure 8.5: Relationship between the density of the colour and the stress applied on the film (Fujifilm 2014).	182
Figure 8.6: Images of the standard coloured samples before and after processing.	183
Figure 8.7: Relationship between the density of the colour and the mean grey scale value.	183
Figure 8.8: Calibration curve showing the relationship between the mean grey scale value and the applied stress.	184
Figure 8.9: Images of the pressure film after compaction at 50 bar using the standard flat roller (left) and the new curved roller (right).	185

Figure 8.10: Grey scale images of the pressure film after compaction at 50 bar using the standard flat roller (left) and the new curved roller (right).....	186
Figure 8.11: Black and white images of the pressure film after compaction at 50 bar using the standard flat roller (left) and the new curved roller (right).	186
Figure 8.12: Stress distribution across the width of the flat roller (A) and the curved roller (B) during roller compaction of lactose 200M (◆ 20 bar, ■ 50 bar, ▲ 80 bar, × 100 bar).....	187
Figure 8.13: Stress distribution of the flat vs the curved roller using lactose 200M (◆ curved roller, ■ flat roller).....	188
Figure 8.14: Percentage of fines produced from lactose 200M using the standard flat roller and the new curved roller.....	189
Figure 8.15: Width of ribbon of lactose 200M produced using the standard flat roller and the new curved roller.	190
Figure 8.16: Fine percentage vs width of ribbon of lactose 200M.....	191
Figure 8.17: Example of ribbon sectioning method.	191
Figure 8.18: Local strength across the width of ribbon of 200M using the flat roller (A) and the curved roller (B) (◆ 20 bar, ■ 50 bar, ▲ 80 bar, × 100 bar).....	192
Figure 8.19: Local strength across the width of ribbon produced from 200M using the curved roller ◆, and the flat roller ■.	193
Figure 8.20: SEM images for ribbons produced from lactose 200M at 100 bar using the flat rollers; centre of ribbon (A, C, E) and edges of the ribbon (B, D, F), at 100× magnification (A, B), 300× (C, D), and 600× (E, F).....	195
Figure 8.21: SEM images for ribbons produced from lactose 200M at 100 bar using the curved rollers; centre of ribbon (A, C, E) and edges of the ribbon (B, D, F), at 100× magnification (A, B), 300× (C, D), and 600× (E, F).....	196
Figure 8.22: X-ray images for ribbon produced from lactose 200M using the flat rollers.	198
Figure 8.23: X-ray images for ribbon produced from lactose 200M using the curved roller.	199
Figure 8.24: Porosity across the width of ribbon of 200M using the flat roller (A) and the curved roller (B) (◆ 20 bar, ■ 50 bar, ▲ 80 bar, × 100 bar).....	200
Figure 8.25: Porosity across the width of ribbon produced from 200M using the curved roller ◆, and the flat roller ■.	201
Figure A.1: NIR spectra of lactose 200M with difference amorphous content.....	215
Figure A.2: NIR spectra of lactose 21AN with difference amorphous content.	215
Figure B.1: Temperature profile across the width of ribbon of lactose 21AN during the roller compaction using the flat roller (A) and the curved roller (B) (◆ 20 bar, ■ 50 bar, ▲ 80 bar, × 100 bar).	216

Figure B.2: Temperature profile across the width of ribbon of lactose SD during the roller compaction using the flat roller (A) and the curved roller (B) (◆ 20 bar, ■ 50 bar, ▲ 80 bar, × 100 bar).	216
Figure B.3: Stress distribution across the width of the flat roller (A) and the curved roller (B) during roller compaction of lactose 21AN (◆ 20 bar, ■ 50 bar, ▲ 80 bar, × 100 bar).....	217
Figure B.4: Stress distribution of the flat vs the curved roller using lactose 21AN (◆ curved roller, ■ flat roller).....	217
Figure B.5: Stress distribution across the width of the flat roller (A) and the curved roller (B) during roller compaction of lactose SD (◆ 20 bar, ■ 50 bar, ▲ 80 bar, × 100 bar).....	218
Figure B.6: Stress distribution of the flat vs the curved roller using lactose SD (◆ curved roller, ■ flat roller).....	218
Figure B.7: Percentage of fines produced from lactose 21AN using the standard flat roller and the new curved roller.....	219
Figure B.8: Percentage of fines produced from lactose SD using the standard flat roller and the new curved roller.	219
Figure B.9: Width of ribbon of lactose 21AN produced using the standard flat roller and the new curved roller.	220
Figure B.10: Width of ribbon of lactose SD produced using the standard flat roller and the new curved roller.	220
Figure B.11: Fine percentage vs width of ribbon of lactose 21AN.....	221
Figure B.12: Fine percentage vs width of ribbon of lactose SD.	221
Figure B.13: Local strength across the width of ribbon of 21AN using the flat roller (A) and the curved roller (B) (◆ 20 bar, ■ 50 bar, ▲ 80 bar, × 100 bar).....	222
Figure B.14: Local strength across the width of ribbon produced from 21AN using the curved roller◆, and the flat roller■.....	222
Figure B.15: Local strength across the width of ribbon of SD using the flat roller (A) and the curved roller (B) (◆ 20 bar, ■ 50 bar, ▲ 80 bar, × 100 bar).....	223
Figure B.16: Local strength across the width of ribbon produced from SD using the curved roller◆, and the flat roller■.....	223
Figure B.17: SEM images for ribbons produced from lactose 21AN at 20 bar using the flat rollers; centre of ribbon (A, C, E) and edges of the ribbon (B, D, F), at 50× magnification (A, B), 100× (C, D), and 300× (E, F).....	224
Figure B.18: SEM images for ribbons produced from lactose 21AN at 100 bar using the flat rollers; centre of ribbon (A, C, E) and edges of the ribbon (B, D, F), at 50× magnification (A, B), 100× (C, D), and 300× (E, F).....	225
Figure B.19: SEM images for ribbons produced from lactose 21AN at 20 bar using the curved rollers; centre of ribbon (A, C, E) and edges of the ribbon (B, D, F), at 50× magnification (A, B), 100× (C, D), and 300× (E, F).....	226

Figure B.20: SEM images for ribbons produced from lactose 21AN at 100 bar using the curved rollers; centre of ribbon (A, C, E) and edges of the ribbon (B, D, F), at 50× magnification (A, B), 100× (C, D), and 300× (E, F).....	227
Figure B.21: SEM images for ribbons produced from lactose SD at 20 bar using the flat rollers; centre of ribbon (A, C, E) and edges of the ribbon (B, D, F), at 50× magnification (A, B), 100× (C, D), and 300× (E, F).....	228
Figure B.22: SEM images for ribbons produced from lactose SD at 100 bar using the flat rollers; centre of ribbon (A, C, E) and edges of the ribbon (B, D, F), at 50× magnification (A, B), 100× (C, D), and 300× (E, F).....	229
Figure B.23: SEM images for ribbons produced from lactose SD at 20 bar using the curved rollers; centre of ribbon (A, C, E) and edges of the ribbon (B, D, F), at 50× magnification (A, B), 100× (C, D), and 300× (E, F).....	230
Figure B.24: SEM images for ribbons produced from lactose SD at 100 bar using the curved rollers; centre of ribbon (A, C, E) and edges of the ribbon (B, D, F), at 50× magnification (A, B), 100× (C, D), and 300× (E, F).....	231
Figure B.25: Porosity across the width of ribbon of 21AN using the flat roller (A) and the curved roller (B) (◆ 20 bar, ■ 50 bar, ▲ 80 bar, × 100 bar).....	232
Figure B.26: Porosity across the width of ribbon produced from 21AN using the curved roller◆, and the flat roller■.	232
Figure B.27: Porosity across the width of ribbon of SD using the flat roller (A) and the curved roller (B) (◆ 20 bar, ■ 50 bar, ▲ 80 bar, × 100 bar).....	233
Figure B.28: Porosity across the width of ribbon produced from SD using the curved roller◆, and the flat roller■.	233
Figure B.29: X-ray images for ribbon produced from lactose 21AN using the flat rollers.	234
Figure B.30: X-ray images for ribbon produced from lactose 21AN using the curved rollers.....	235
Figure B.31: X-ray images for ribbon produced from lactose SD using the flat rollers.	236
Figure B.32: X-ray images for ribbon produced from lactose SD using the curved rollers.....	237

LIST OF TABLES

Table 2.1: Physical and mechanical properties of ribbon from the roller compactor at different RH% and roller speed and constant screw speed, values inside brackets are the standard deviation of the mean, n= 8 [40].	27
Table 2.2: Effect of roller speed on ribbon physical properties using MCC at constant horizontal and vertical feed screw speed, values inside brackets are the %CV of the mean, n= 13 [61].	29
Table 2.3: Effect of roller speed on the physical properties of ribbon produced at constant compactor setting (^a roller speed/ horizontal feed screw/ and vertical feed screw), values inside brackets are the %CV of the mean, n=13 [61].	29
Table 4.1: Particle size data for the primary powders, measured by Camsizer XT.	63
Table 4.2: The amorphous content of different types of lactose (as-received powder) measured using FT-NIR.	70
Table 5.1: Material friction properties and compressibility factor for different types of lactose, each measurement was repeated at least 6 times.	83
Table 5.2: Nip angle for the three types of lactose calculated using Equation 2.7.	84
Table 5.3: The conversion between the hydraulic pressure and the roller force provided by Alexanderwerk.	85
Table 5.4: Maximum normal stress applied to different types of lactose at different hydraulic pressure.	86
Table 7.1: Design of the experiment used during the investigation of the roller speed.	148
Table 7.2: Feeder screw speed at different roller speed.	148
Table 7.3: Design of experiment during the investigation of the roller gap.	155
Table 7.4: Design of experiment during the investigation of the effect of the feeder screw speed.	169

Nomenclature

a_w	Water activity
b	Width of the ribbon
CI	Compressibility index
d	The average thickness of the compact at zero roller gap
D	Roller diameter
ffc	Flow function coefficient of the powder
F_{max}	Maximum force required to break the ribbon
h	Thickness of the slab in the slap model
K	Compressibility factor
L	Distance between the two supports in the three point bend test
p	Normal pressure applied to the slab in the slap model
P_m	Maximum stress applied by the roller on the powder in Johansons's model
R_F	Roll separating force
S	Roller gap
t	Thickness of ribbon
T_g	Glass transition temperature
W	Roller width.
$Y(\rho)$	Yield stress as a function of the slab density used in the slap model
ϕ_w	Angle of wall friction
θ	Angular position
θ_h	Entry angle (start of the slip region)
α	Nip angle

α_x	Instantaneous angle of the slab in the slab model
σ	Normal stress
σ_1	Consolidation stress calculated in the shear cell tester
σ_c	Unconfined yield strength calculated in the shear cell tester
σ_t	Ribbon tensile strength
σ_x	Stress acting in the rolling direction in slab model
σ_α	Normal stress at $\theta = \alpha$
σ_θ	Normal stress at $\theta = \theta$
ρ_B	Powder bulk density
ρ_T	Powder tap density
τ_f	Frictional stress used in the slab model
(δ)	Effective angle of internal friction
$\mu(p)$	Coefficient of friction used in the slab model

Abbreviations

SD	Spray dried lactose SuperTab11SD
21AN	Anhydrous lactose SuperTab21AN
200M	α -lactose monohydrate 200M
PIV	Particle Image Velocimetry

CHAPTER 1 INTRODUCTION

1.1 Granulation

Granulation is the size enlargement process of particles to improve the flowability, compressibility, compactibility and homogeneity of a downstream blend of materials. It is an essential process for converting fine powders into products with specific properties required in many industries such as pharmaceuticals, food, detergents, catalysts, ceramics and pesticides.

1.2 Types of granulation

There are three main product processing techniques that are commonly used to modify and improve the physical properties of materials in many industries: direct compression of powder, wet and dry granulation [1, 2]. In direct compression, powder blends are directly compressed into tablets using uniaxial compression machines without any pre-processing steps. However, some materials in the powder blends, e.g. APIs in the pharmaceutical industry, are difficult to directly compress or have poor flow properties which result in non-uniformity in die filling during tableting.

The necessity to achieve an adequate flowability of the powder and to attain a better uniformity of the final product, are the main reasons for the pre-treatment of the powder. There are generally two pre-treatment technologies of the powder: wet and dry granulation technologies.

In wet granulation technology, liquid or binder solution is added to a powder bed to produce granules with bridges between primary powder particles. The wet granulation process is usually followed by a drying step which is required to dry the liquid and result in solid bridges between the primary particles within the granules.

In dry granulation technology, high pressure is used to compress the primary powder particles into ribbons which are then milled to granules in different size classes. The most commonly used equipment which uses the dry granulation mechanism is the roller compactor which is a continuous process [3, 4].

The need for the dry granulation technology has been shown to increase and grow in many industries such as pharmaceuticals and food. This is due to the greater advantages of the dry granulation technology over the wet granulation which can be summarised as follow [2]:

- The risk of material degradation and modification during the drying process after the wet granulation. This risk is minimal with the dry granulation due to the absence of liquid.
- More space necessity to maintain and locate the machines required in wet granulation technology including the drying process.
- Lower operating costs in dry granulation compare to wet granulation due to the absence of the drying process which requires a higher amount of energy.
- The scale up in dry granulation is easier and less complicated compared to the wet granulation. This is because the wet granulation has more process parameters to consider which includes the liquid binder addition method and the complicated drying process.
- The liquid and the powder properties influence the interaction between the liquid and the powder during wetting and granulation processes. This is not applicable in dry granulation.

1.3 Roller compaction

The roller compaction process consists of three units working simultaneously: feeding, compaction and milling unit. The feeding unit provides and transports the powder to the compaction unit using different methods. The compaction unit consists of two counter-rotating rollers which come with different surfaces: smooth, fluted or knurled [5]. These two rollers are used to apply high stresses to the incoming powder to produce compacted material which is called a ribbon. The ribbon is then used to produce granules with the desired size after passing through a milling step. There are two different types of feeding system to feed the powder to the rollers; the gravity and the screw feeder system. The feeding system is dependent on the powder properties such as flow property and bulk density. The gravity feeding system is used for powders with good flowability. The screw feeder system is used for powders with low bulk density and poor flowability. There are also three different roller designs in the roller compactor; vertical, incline and horizontal roller design [6] as shown in Figure 1.1.

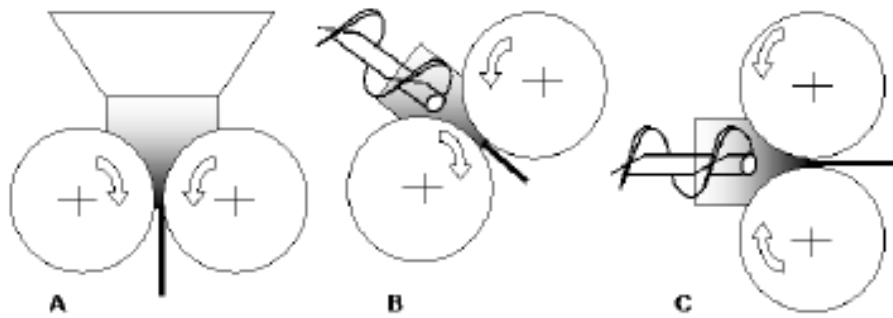


Figure 1.1: Different designs for rollers: (A) vertical design, (B) incline design, and (C) horizontal design [6].

During roller compaction, the material passes through three different regions; slip, nip and release regions as shown in Figure 1.2. The angular position of the material defines the boundary between different zones. Slip region (see Figure 1.2) has an angular position θ_h greater than the nip angle α . In the slip region, the speed of the roller is greater than the speed of the material so that the particles are slipping at the surface of the roller. The particles rearrange themselves in the slip region and the pressure exerted on the material is small in this region. In the nip region (an angular position equal or less than α) the material wall speed is equal to the speed of the roller. In the nip region and when the gap between the two rollers is at its minimum, densification of the powder occurs due to the high pressure exerted by the rollers. The release region begins when the gap between the rollers starts to increase. After the release region, the thickness of the ribbon may increase due to the elastic recovery, which may result in a ribbon with larger thickness than the roller gap [6, 7].

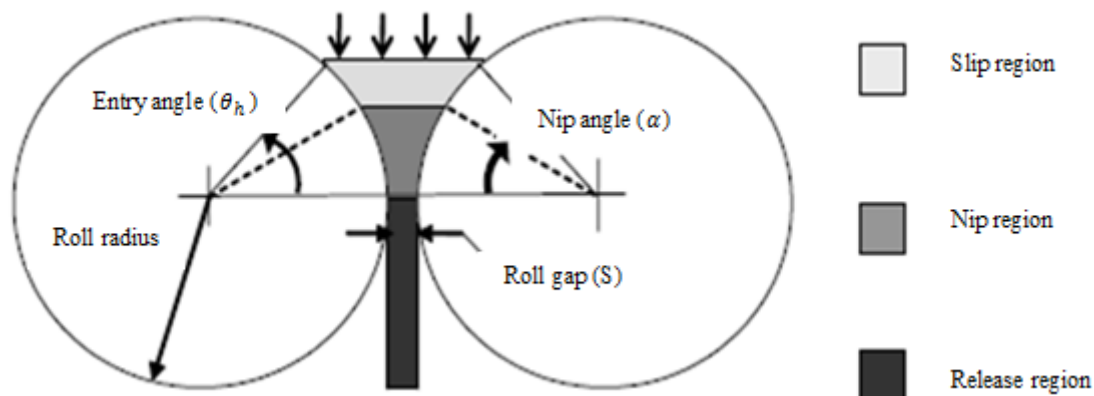


Figure 1.2: Schematic diagram of the roller compaction process showing different regions [6].

The main disadvantage of roller compaction is a large amount of fines that are produced during the process. The amount of fines is the amount of non-compacted powder which is produced with the ribbon and amount of fines which is produced after milling the ribbons to granules. Recycling the fines may solve this problem [1, 8].

1.4 Roller compaction challenges

Despite the advantages of the roller compaction over other techniques which mentioned earlier in Section 1.2, the technique has its disadvantages and drawbacks which cannot be ignored. The roller compaction is not well understood due to the complexity of the process and its sensitivity to the material properties. This becomes more problematic with the diversity in the material properties. For instance, particles of the same material can be found in different morphologies; it can exist either as a discrete entity or associated with other particles in an agglomerated structure. It can also be found either in crystalline or amorphous form. The morphology of the particle can have a significant effect on the powder flowability, the packing behaviour, and the consolidation during tableting [9]. The sensitivity of the primary powder to the ambient relative humidity can also be considered as a drawback in dry granulation especially when the weather is not stable throughout the year, resulting in varying product qualities.

The other disadvantage in the roller compaction is a large amount of non-compacted powder or fines which are associated with the ribbon during the roller compaction or produced during the milling process. The non-compacted powder can be recycled to

increase the yield and efficiency of the process; however, this could have a negative impact on the content uniformity of the final product [10]. The fines or the non-compacted powder produced from the ribbon during the compaction stage is due to the poor binding of the powder at the edges of ribbon as a result of a non-uniform stress distribution across the roller width. The non-uniformity of the stress distribution is another drawback of the roller compaction process which has a significant effect on the ribbon homogeneity across the width [11, 12]. The inhomogeneity of ribbon properties affects the final granule quality and other post granulation processes. Therefore, it is essential to obtain a uniform stress distribution across the roller width during the roller compaction in order to produce ribbons with a homogenous property across the width and improve the quality of the product.

1.5 Aim of the research

Lactose is one of the most important materials used in pharmaceutical and food industries to produce granulated materials. Particles of lactose can be found in different morphologies and it can also exist either in crystalline or amorphous form. The objective of this study is to understand the behaviour of various types of lactose during the roller compaction in a comprehensive perspective, finding the optimum relative humidity working condition for lactose and attempt to apply a uniform stress on the powder during the roller compaction. It is anticipated this will reduce the undesired fines percentage in the product, and produce ribbon with uniform properties across its width.

A detailed study will be performed to investigate how the primary particle morphology and the powder amorphous content will affect the strength and porosity of a single particle and, consequently, the ribbon properties after the roller compaction. The study will include an online recording of ribbon temperature during production using a thermal camera. This is intended to further understand the behaviour of lactose powders, and gain more information on the mechanisms occurred during roller compaction.

The work will also focus on the effect of the storage of powder at different relative humidity conditions on both the roller compaction behaviour and ribbon properties. The study will involve a Particle Image Velocimetry (PIV) technique to examine the velocity of the powders during the compaction process. The knowledge created from

such a study will help identify the optimum working conditions for roller compaction of different types of lactose.

The effect of the roller compaction process parameter will also be investigated. Experiments at different feeder screw speed, roller speed and the gap will be carried out and the properties of the ribbon (temperature, fine percentage, ribbon strength and porosity) will be related to the different process parameter.

To improve the roller compaction process, the inhomogeneity of ribbon property will be investigated in details using the different types of lactose. The stress applied across the roller width during the compaction will be obtained experimentally. The study will involve a presentation of a novel approach to overcome the non-uniform quality across the width of the ribbon. The thermal camera will be implemented to record the temperature profile of the ribbon during production, which gives an indication of the stress applied to the powder.

1.6 Overview of thesis

The outline of the thesis is as following:

- **Chapter 2** presents a review of literature related to the fundamentals during powder compaction and the effect of powder properties. It presents different methods in the literature used to quantify the powder amorphous content. In addition, the chapter includes a comprehensive review of work related to the area of this thesis and highlights the issues related to the process.
- **Chapter 3** describes the materials, main equipment and the general methods used to analyse both the raw material and the product.
- **Chapter 4** presents the properties of the primary powder used in this study. This includes the size, morphology, strength and porosity of the primary particles. Furthermore, the amorphous content in each type of lactose was quantified.
- **Chapter 5-8** correspond to the core results and discussion of the work.

In **Chapter 5** a comprehensive study was conducted to investigate the effect of the particle morphology and the powder amorphous content on the ribbon properties. An

online thermal camera was used to describe the behaviour of the powder undergoing roller compaction.

Chapter 6 focuses on the effect of the storage conditions (RH) on the moisture content and flowability of the powder and also on ribbon properties after the roller compaction. In addition, the chapter presents the velocity of particles during the roller compaction of powder stored at different RH values using the PIV technique.

In **Chapter 7** the effect of the process parameter of the roller compactor on the product properties will be investigated.

Chapter 8 focuses on the inhomogeneity of ribbon properties across the width. The chapter presents a novel approach to improve the compaction along the width of the roller and overcome the inhomogeneous property across the width of the ribbon.

- **Chapter 9** presents the overall conclusion of the thesis and recommends some future studies.

CHAPTER 2 LITERATURE REVIEW

This Chapter describes the work reported by various researchers in the field of dry granulation/ roller compaction and tableting. This includes the effect of powder amorphous content, powder moisture content and different process and formulation parameters on the product properties such as strength, porosity and the resultant granule size. Furthermore, the chapter includes literature concerning the measurement of the amorphous content of powder using different techniques.

2.1 Compaction process and bonding mechanisms

Compression of powder is a process of densification or volume reduction of a powder bed in a limited space, which is initiated due to the application of a force e.g. applying force to a powder bed between the rollers during roller compaction to produce ribbon. Upon applying a force onto a powder bed, the air between the particles is reduced and particles become closer to each other. This will lead to an increase in the interparticulate bonds and results in a transformation of the loose powder to a compact [13]. The transformation of a bulk powder to compacts, upon the application of a force, requires a number of mechanisms for the powder at different stages depending on the applied force [13-15]. During compression, the powder may pass through the following stages:

- Particle rearrangement
- Particle deformation
- Particle fragmentation
- Formation of interparticulate bond

Particle rearrangement is the first stage which occurs at low compaction forces. At this stage, particles start to come close to each other and arrange themselves to fill the spaces and the air start to leave which results in a reduction of volume and porosity of the powder bed. The particle rearrangement stage depends on the particle shape and the particle size distribution [2]. At higher compaction pressure, the reduction of the powder bed volume will be related to the particle deformation. The deformation of the particle can be irreversible by plastic deformation or reversible by elastic deformation

depending on the material properties. The powder bed volume reduction could also occur by particle fragmentation at higher compaction forces which then go through a secondary particle rearrangement and deformation. Particle fragmentation creates smaller fragments with new surface sites which result in an increase in the surface area available for bonding. All the volume reduction stages mentioned above can occur at the same time during powder compaction; however, only one of them usually dominates depending on the temperature and compression rate [2, 13-15].

The bonding mechanism between the primary particles is an important step in dry granulation and direct compression processes. It is an essential process for the formation of compacts with optimum product properties. Understanding the mechanism of bonding between the particles helps to design a new product and determine the final product properties such as the granule density, strength, compressibility and friability [2]. The bonding mechanisms between the particles during compaction have been described in the literature [15-17]. During compaction of a dry powder, the mechanisms of bonding between particles can be divided into three types [14, 15, 17].

- Solid bridges
- Attraction between the primary particles
- Particle mechanical interlocking

Solid bridge forms when particles come close to each other and molecules starts to move and fill the space between them by diffusion or melting. This type of bonding can be formed by contact melting as a result of high local stresses at the particle contact points which increases the local heat and initiate the melting at the contact points. Solid bridges can also be formed by sintering when the temperature is higher than the glass transition temperature of the amorphous powder which results in the transformation of the powder from its glassy state to the rubbery state, consequently, the formation of solid bridges. The attraction between the primary particles can be considered as electrostatic forces or Van der Waals forces which occur when the particles are very close to each other. The electrostatic forces are very weak compared to Van der Waals forces which is most likely occurs during the compression of powder. The mechanical interlocking between particles is related to the shape and the surface structure of the particles [14, 15, 17]. Smooth and spherical particle have less tendency to hook together in comparison to irregular or needle shape particles.

The different types of bonding mechanism mentioned above have different bond strength. Rumpf [17] investigated the strength of different types of bonds, and it was found that the solid bridge bonding between the particles is the strongest bonding mechanism.

2.2 Material

2.2.1 Structure

In the food and pharmaceutical industries, two main types of material can be used: crystalline material and amorphous material. During processing in the industry, different behaviour can be seen from these two types of material, due to their different structure. The molecules are organised in a tri-dimensional order in the crystalline material and, therefore, they are highly ordered with limited motion. The amorphous material, on the other hand, consists of disordered molecules or atoms which are distributed randomly in a matrix and, therefore, a free volume can be found in the structure. The free volume is the space which is not occupied by the molecules and it is an expression of the molecular mobility within the material. Changing the temperature and the pressure of the material affects the free volume and, consequently, the molecular mobility within the material [18].

The free volume and the molecular mobility increases with increasing the temperature of the material, and this effect is different in crystalline and amorphous structures. In crystalline material, increasing the temperature results in vibrating the molecules in their position within the structure until it reaches a defined temperature, known as the melting point, where the structure breaks down. However, there is no melting point for amorphous material, and the increase in the temperature results in a steady increase in the free volume and the molecular mobility. However, the free volume increases rapidly at a certain temperature range, known as the glass transition temperature. Molecules start to move and rotate past each other and the amorphous material transfers from the glassy state to the rubbery state. After a further increase in the temperature, exceeding the glass transition temperature, the material finally liquefies [19].

Moisture also has an effect on the properties of some materials used in food and pharmaceutical industries. The humidity of the atmosphere has a significant effect on

the powder moisture content. Therefore, it is important to know the relationship between the moisture content of the material and the atmosphere. The tendency of a material to hold water molecules from the atmosphere is called hygroscopicity. This is achieved by either adsorption on the surface of the material or absorption into the molecular structure. The water content of a material depends on its water activity, a_w , which is the vapour pressure of the air surrounding the material divided by the vapour pressure of pure water. At equilibrium, the relative humidity of the surrounding air is equal to the water activity of the material. The amount of water in a material, at a defined temperature, is related to the water activity of the material via the sorption isotherm [18, 19].

Crystalline and amorphous materials show different behaviour during exposure to a moist environment, because of differences in free volume. It is impossible for the crystalline material to absorb water from the atmosphere until a critical relative humidity, the deliquescence relative humidity, where the material dissolves completely. The water can adsorb onto the surface of the crystalline material and can exist as a monomolecular layer. The amorphous material, on the other hand, has no deliquescence relative humidity and it is more hygroscopic than crystalline material. This means that amorphous material absorbs more water which is stored in the amorphous structure. Figure 2.1 shows the sorption isotherm for different crystalline and amorphous materials [18].

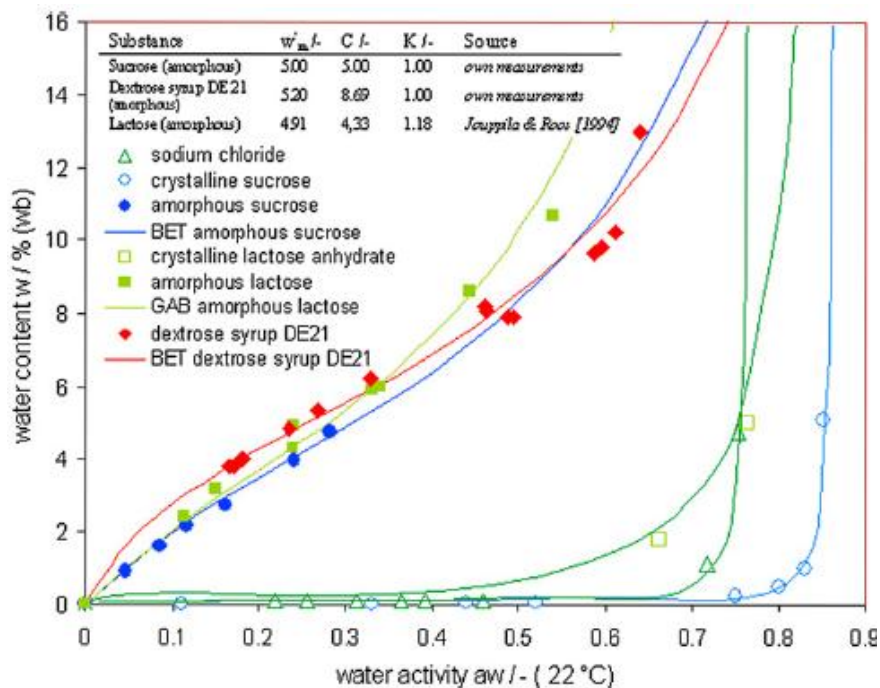


Figure 2.1: Sorption isotherm (22°C) for crystalline and amorphous materials [18].

2.2.2 Amorphous and crystalline lactose

Lactose is one of the most important raw materials used in the food and pharmaceutical industry. It can exist either in crystalline or amorphous form. The common forms of crystalline lactose are α -lactose monohydrate and lactose anhydrous. The manufacturing processes of these two types of crystalline lactose are different. Slow crystallisation, below 93.5°C, of a supersaturated solution, produces α -lactose monohydrate. However, lactose anhydrous is produced by drum drying of a supersaturated solution above 93.5°C. Amorphous lactose, on the other hand, has many origins. The presence of amorphous lactose in predominantly crystalline lactose has a significant effect on the moisture sorption isotherm [20] and also on the behaviour of the power during tableting [21].

Amorphous lactose can be produced by a fast removal of water from a solution of lactose so that lactose molecules have no enough time to arrange themselves and crystallise. This includes spray drying of a solution of lactose to remove the water very fast and to ensure a lack of time for lactose molecules to crystallise. The other method is the freeze drying of a solution of lactose to decrease the molecular mobility and then remove the water by sublimation [22].

Small amounts of amorphous lactose can be found in predominantly crystalline lactose. This can be produced during either the drying process after crystallisation or the milling process. After the crystallisation process and during the filtration some of the lactose dissolves on the surface of the particles, which then becomes amorphous lactose after drying. Milling is another source of amorphous lactose, and the more the heavy the milling process the more amorphous lactose is produced [23].

2.2.3 Determination of lactose amorphous content

The presence of amorphous lactose in predominantly crystalline lactose has a significant effect on the moisture sorption isotherm [20]. This may have a significant effect on powder properties during different processes. Therefore, it is essential to know the amount of amorphous form in the powder before processing. Several works have been carried out to determine the amorphous content in lactose samples using different techniques [22, 24-30].

Dynamic vapour sorption is a common method used to determine the amorphous content in lactose samples. The method is based on the moisture sorption isotherm and crystallisation of the amorphous part. It consists of drying a sample of lactose at 0% RH to remove all the moisture and then measuring the weight of the dry sample. The sample then treated at very high humidity, 90% RH, in a wetting step. During this step, the amorphous part absorbs water and the molecules become mobile and start to crystallise to monohydrate lactose. The wetting step is then followed by another drying step at 0% RH then the weight of the sample is measured. The difference in weight of the sample before and after the process is the amount of water produced during crystallisation, which can be used to determine the amorphous content of the sample [22, 24].

Calorimetry is another method used for the quantification of amorphous lactose. It depends on the energy of crystallisation of amorphous lactose when reaches the glass transition temperature. For example, differential scanning calorimetry (DSC) is used to study the heat flow through the sample with changing the temperature. Gombás et al. [26] studied the ability of a DSC and an X-ray diffractometer to quantify the crystallinity in amorphous/ crystalline blends. Mixtures with different amounts of amorphous lactose in crystalline lactose were prepared and used to determine the calibration data in both methods. It was found that DSC can be used for the quantification of amorphous lactose for mixtures above 20% amorphous. On the other

hand, X-ray powder diffraction was found to be a good method for the quantification of low amorphous content. The increase in scan rate in the DSC helps to detect the response of the glass transition temperature easier. Hyper-DSC was used by Saunders et al. [29] as an attempt to quantify low levels of amorphous content in a lactose sample using a scan rate of 500°C/min. It was found that Hyper-DSC, running at high scan rate, was able to detect the response of the glass transition temperature for samples containing 1.5% amorphous lactose.

Several other methods have been utilised to quantify the amorphous content such as near infrared (NIR), and Raman spectrometry. A combination of near infrared spectroscopy (NIR) with dynamic vapour sorption (DVS) was used by Hogan and Buckton [27] to quantify the amorphous content of lactose samples. They used mixtures of lactose with different amorphous content to obtain the calibration equation, which was then used to predict the amorphous content of other samples. It was found that the combination of NIR with DVS was able to predict as little as 1 mg of amorphous lactose in the sample. Raman spectroscopy was also found to be a powerful method to identify amorphous lactose and α -lactose monohydrate [28].

Gombás et al. [25] also used NIR to quantify the amorphous content of lactose samples. Amorphous lactose was obtained by spray drying a solution of lactose, and then mixing with crystalline lactose to obtain blends with different amorphous content. Multiple linear regression (MLR) was used to analyse the data and obtain the calibration equation. They found a close correlation between the actual and the predicted amorphous content. It was concluded that the NIR is a powerful method for the quantification of low amorphous content in lactose samples.

A comparison of different methods to determine the amorphous content of lactose samples was made by Lehto et al. [30]. Seven methods were utilised to quantify the amorphous content; these are differential scanning calorimetric DSC, step scan DSC SS-DSC, gravimetric moisture sorption GMS, solution calorimetry SC, X-ray powder diffraction XRPD, Raman spectrometry and isothermal microcalorimetry IMC. It was found that DSC showed variation in the results due to the overlapping of the peaks. Results from SC, Raman spectroscopy, GMS, XRPD, IMC, and SS-DSC were good and were consistent with each other. They reported that better results can be found by

combining two methods, and the use of Raman spectroscopy with IMC or GMS was recommended.

2.3 Experimental studies on powder compaction

2.3.1 Effect of primary powder properties (Morphology and amorphous content)

The properties of the primary particles can have a significant effect on the powder compression behaviour and the produced compacts properties. Morphology is a property of a material which is related to the external feature of the primary particle including the size, shape, aspect ratio or crystal habit (plate, needle, equant, etc.). Particles can exist as a discrete entity or they associate with other particles in one structure. The bond between the particles in the structure can be weak (i.e. agglomerate) or strong (i.e. aggregate) which behaves as discrete particles. The morphology of the primary particle can have a significant effect on the behaviour of the powder during compression and on the compact properties. It affects the powder flowability, the packing behaviour, and the consolidation during tableting. Therefore, it is essential to consider the morphology of the primary particles during formulation development [9].

2.3.1.1 Direct compaction

Previous work has been carried out to compare the tableting behaviour of different types of powder and examine the tablet properties [21, 31, 32]. As mentioned earlier, the presence of amorphous lactose in predominantly crystalline lactose has a significant effect on the powder behaviour during tableting.

Vromans et al. [21] studied the effect of amorphous content and primary particle size of lactose powder on tablet properties. They used spray dried lactose with different amorphous content and different particle size and then examined tablet crushing strength. They found that tablet crushing strength increased with increasing percentage of amorphous lactose in the powder and that tablets produced from smaller primary particle size showed higher crushing strength (Figure 2.2). It was concluded that amorphous lactose is acting as a binder during compaction. Sebhatu and Alderborn [31] confirmed the same result, in that amorphous lactose produce tablet with higher tensile strength than those of crystalline lactose. This was attributed to the higher deformability

of amorphous lactose particles compared to crystalline lactose, which increased the contact area between the particles. The presence of amorphous lactose in a predominantly crystalline lactose was also found to increase the powder plasticity [32].

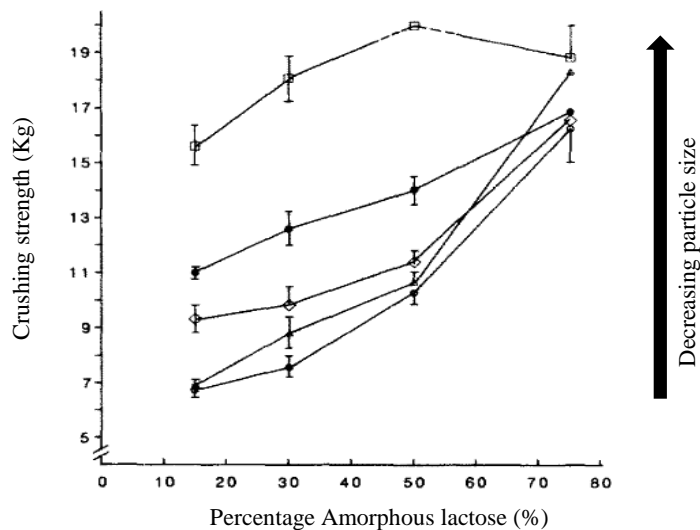


Figure 2.2: The crushing strength of tablets compressed at 75 MPa from spray dried lactose with different size [21].

In another study, Vromans et al. [33] studied the compaction behaviour of different types of lactose during tableting. They examined the strength and porosity of tablets of anhydrous α -lactose and α -lactose monohydrate at different compaction loads. It was found that tablets made from anhydrous α -lactose were stronger. It was suggested that the crushing strength of tablets depends on the degree of fragmentation of the material during compression, and anhydrous lactose showed a high degree of fragmentation during compression which was showed by the increase in tablet specific surface area (Figure 2.3). The increase in the degree of fragmentation of the powder particles increases the contact area between the particles, therefore increasing tablet strength. However, tablets made from both types of lactose showed almost similar overall porosity (Figure 2.4). Two methods were used to determine the porosity of tablet; calculation method from the dimensions of the tablet, and mercury porosimetry. For both types of lactose, it was found that tablet porosity was decreasing with increasing the compaction force.

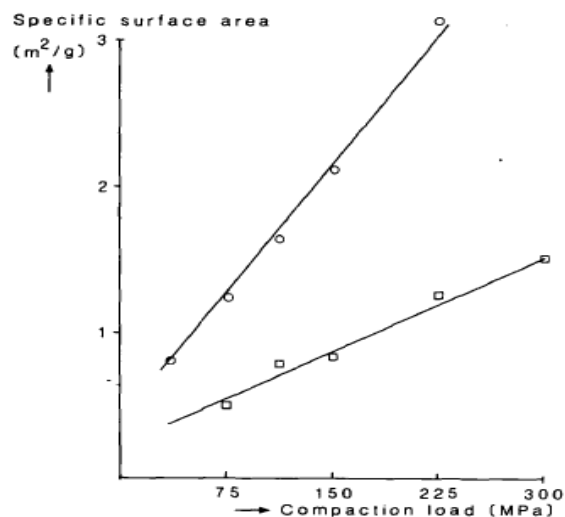


Figure 2.3: Tablet specific surface area (measured by mercury porosimetry) of α -lactose monohydrate (\square) and anhydrous α -lactose (\circ) [33].

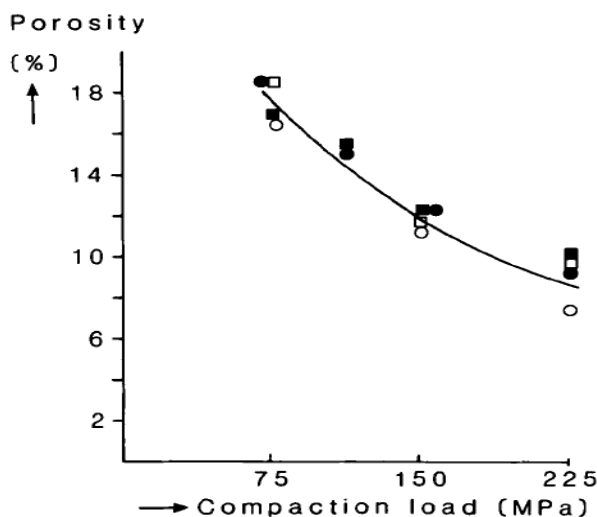


Figure 2.4: Tablet porosity for α -lactose monohydrate (\square , \blacksquare) and anhydrous α -lactose (\circ , \bullet), using two methods: Calculation (\circ , \square), and mercury porosimetry (\bullet , \blacksquare) [33].

Compaction pressure is the most important parameter that has a significant effect on the tablet strength and porosity. It was found that for both crystalline and amorphous material, tablet tensile strength increases and porosity decreases with increasing the compaction pressure during tableting [21, 31-40].

2.3.1.2 Roller compaction

Limited works have been carried out in roller compaction to study the effect of particle morphology on roller compaction of metal powders [41]. Chikosha et al. [41] investigated the rolling behaviour of titanium and titanium alloy powders with different particle morphology (spongy, angular and spherical) and different particle size. A

Cavallin rolling mill was used in the study which was equipped with a gravity feeding system and a roll with diameter and width of 55 mm and 110 mm respectively. It was concluded that the rolling behaviour enhanced with the variation in particle morphology from spherical, to angular to spongy looked particles. The spongy looked particle was found to produce denser strips in comparison to the other powders. The higher density of strips produced from the spongy powder was attributed to the higher compressibility of the powder.

The effect of the roller compaction of three types of calcium carbonate on compaction properties was also investigated by Bacher et al. [42]. Three types of calcium carbonate with different external surface features were used: a cubic calcite Scoralite, scalenohedral calcite Sturcal and ground Mikhart which had irregular and rough particles. It was found that the compressibility of Sturcal powder was higher in comparison with the other types of powder. The porosity, after roller compaction, was reduced and the compressibility of the Sturcal granules was lower than the corresponding powder. It was concluded that the compaction properties were influenced more by the physical attributes of the primary powder in comparison to the process parameters. Freitag and Kleinebudde [43] studied the effect of roller compaction on the tableting behaviour of inorganic materials. They used four types of magnesium carbonate with different properties (tap density, shape, surface texture and specific surface area). The primary particles used in this study were either pin-like or rounded in shape with different mean particle sizes. It was reported that materials with low tap density and high specific surface area are desirable in order to obtain a high degree of densification during tableting, even after the roller compaction

The term morphology can refer to the shape, aspect ratio or crystal habit of the particle. The work done in the literature was mostly focusing on the shape of the primary particle rather than the internal structure of the primary particle.

One previous work to study the roller compaction of lactose is by Inghelbrecht and Remon [44]. They investigated the effect of different process parameters using different types of lactose on the granule friability. It was found that granules produced from anhydrous lactose showed better quality (low friability) in comparison to lactose monohydrate and spray dried lactose. Although their work studied the influence of using different types of lactose on the granule quality using roller compaction, the effect

of the amorphous content of lactose powder on the product quality has received very limited attention.

Furthermore, the effect of particle morphology on the strength and porosity of a single particle has not been investigated and linked to the roller compaction process in the literature. It is anticipated that the strength and porosity of a single primary particle has a significant effect on both the behaviour of powder undergoing roller compaction and also on the ribbon properties.

Therefore, further work is required to explore the effect of amorphous lactose on roller compaction behaviour and ribbon properties (strength, porosity and fines percentage in the product). In addition, the effect of the morphology and the internal structure of the primary particles of different types of lactose are not fully understood and require further investigations. Such knowledge will help using an appropriate type of lactose while developing a new formulation which will help improving the product quality and reducing the undesired fine percentage in the product.

2.3.2 Effect of powder moisture content

Solids in the powder bed may interact with water vapour from the environment during the storage and processing of powders in areas with a high relative humidity. The water content of the powder can have a significant effect on the powder properties for example powder flow properties, stability and powder compaction behaviour during tableting [45-47]. Moisture can be adsorbed on the solid surface, or absorbed into the structure of the solid. It can also interact by capillary condensation into the small pores existing on the solid [48]. The adsorption and the absorption of moisture depend on the attraction between the solid surface and the molecules of the water, surface area, humidity and temperature [45].

Moisture can exist in food and pharmaceutical powders mainly in three forms: free, adsorbed on the particle surface or bound water in the molecular structure. The free water is located in the pores between the particles and on the surface of the particle and it can act as a solvent with similar physical properties as pure water. The adsorbed water is present on the solid surface with a physiochemical bind. The bound water is the water which cannot behave as pure water. This form of water is bound in the molecular

structure of the particle and it is less active than other forms of water, an example of bound water is the water of crystallisation and water of constitution [49, 50].

The existence of moisture in the material in different forms depends on the material structure (for example crystalline and amorphous). Due to the nature of the amorphous material, the moisture can be absorbed into the free volume within the material structure. This will influence the mobility of the molecules and the glass transition temperature of the material. The change in the glass transition temperature affects the state of the material (rubbery or glassy state), which will have an effect on the viscosity and the deformability of the powder. Applying force to an amorphous powder at this stage will affect the interparticulate forces and promote the sintering process between the particles at the contact points and create solid bridges [19, 51]. In crystalline material, moisture can be adsorbed onto the surface of the particle and create a monomolecular layer at low moisture content. This may result in smoothening the irregularities on the particle surface and therefore decrease the distance between two particles and increase the contact area [47, 52].

The powder moisture content may have a significant effect on the properties of the powder during different processing for example tableting [47]. The moisture content of the powder can affect the flow properties, compressibility and stability of the powder [48]. Some works have been carried out to study the effect of powder moisture content on the properties of compacts during tableting [31, 34, 40, 53-57].

2.3.2.1 Direct compaction

In direct compression or tableting, Vromans et al. [21] studied the effect of moisture content of spray dried lactose on tablet crushing strength using powder with varying amorphous content. It was found that at high amorphous content, tablet crushing strength was significantly dependent on the amount of water in the initial powder which was absorbed by the amorphous lactose. Increasing the water content of a powder increases the deformability of the powder, which increases the bonding area upon compaction and, therefore, increases the tensile strength and decreases the porosity of the tablets [31, 34]. Figure 2.5 and Figure 2.6 shows the tensile strength and the porosity, respectively, of tablets produced from fully amorphous lactose with different particle sizes and different water content. Powder with different water contents was achieved by storing them at different relative humidities (0% and 22% RH). It can be

seen that powders conditioned at 22% RH produced stronger tablets with less porosity than those conditioned at 0% RH. This means that tablet tensile strength increased and the porosity decreased with increasing the powder moisture content (22% RH). This was due to the fact that at higher moisture content, amorphous lactose particles exhibited higher deformability than those at lower moisture content, which resulted in decreasing the porosity and increasing the tablet strength [31].

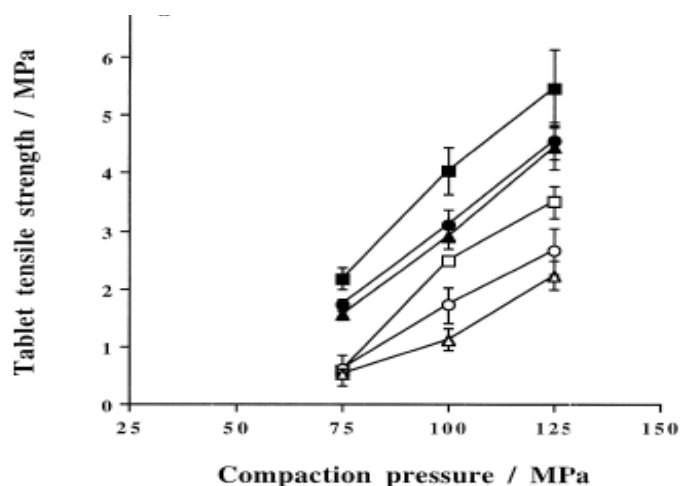


Figure 2.5: Tensile strength of tablets for amorphous lactose at different storage conditions. Open symbols represent 0% RH; closed symbols represent 22% RH. Square=5-10µm; circle=10-25µm; triangle=20-50µm [31].

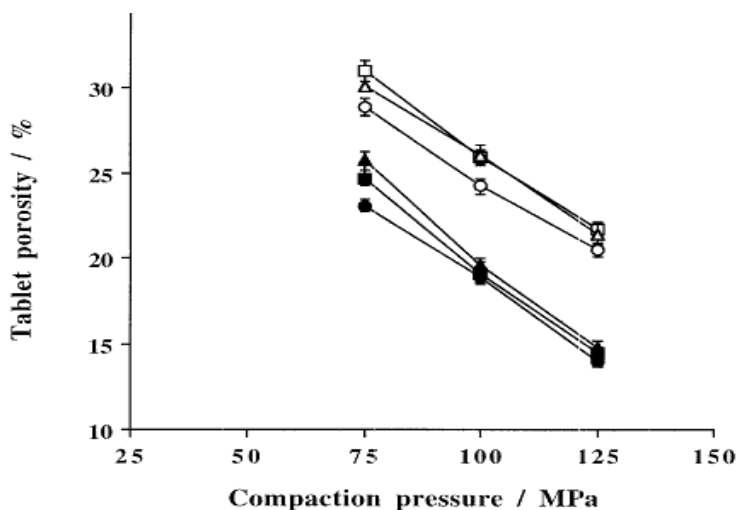


Figure 2.6: Porosity of tablets for amorphous lactose at different storage conditions. Open symbols represent 0% RH; closed symbols represent 22% RH. Square=5-10µm; circle=10-25µm; triangle=20-50µm [31].

Ollet et al. [53] studied the effect of powder water content on the compaction properties of crystalline and amorphous food powder. Different methods were used to obtain powders with different water content prior to tableting. Samples with different water

content were obtained by either storing the powder over saturated salt solution at different relative humidities or slowly spraying different amounts of water on the powder. The water content of powders was ranging as follows: potato starch (5.5-25.1%), maltodextrin (4.9- 11.2%), sucrose (0- 2.3%) and sodium chloride (0-4.6%). All the materials were then compacted using a compaction cell. They concluded that the stress of deformation during tableting was decreasing with increasing the water content of all materials. It was suggested that an increase in the powder water content increases the plasticisation for the amorphous material, while for crystalline material the water content had a lubricating effect. An increase in the water content of Maltodextrin was also found to increase the plastic deformation of the powder during compression [54].

A different result was found by Sun [57] who studied the effect of moisture content on compaction behaviour of Microcrystalline Cellulose MCC (Avicel PH-102). Powders with different water contents (1.63- 9%) were obtained by equilibrating the powders over different saturated salt solutions. Tablets were made by compressing the powders in a 10 mm diameter die using a hydraulic press. After compression, tablets were stored in sealed containers at the same humidity condition as the powder. The tensile strength of the tablet was measured (1- 2 hours) after the compression. It was found that tablet tensile strength increased and then decreased with increasing the moisture content of the powder. The increase in tablet tensile strength was explained by the increase in the plastic deformation with increasing the water content, which then increases the bonding area. The decrease in the tensile strength with a further increase in water content was attributed to the decrease in the bonding strength as a result of reducing the inter-particulate forces between particles. Microcrystalline Cellulose MCC (Avicel PH-200) with different concentrations of crystalline acetaminophen powder (APAP) was also used by Gupta et al. [55] in order to study the properties of tablets at different moisture content. Powders with different moisture content were achieved by storing the blends at different relative humidity (RH) conditions for 24 hours. It was found that the compact tensile strength was increasing slightly with increasing the relative humidity (moisture content) and reached equilibrium at 40% RH. However, there was an increase in compact relative density with increasing the powder moisture content.

2.3.2.2 Roller compaction

Some studies have been carried out to investigate the effect of the moisture content of different food and pharmaceutical powders in the roller compaction. It is believed that the water content of the starting material will have an effect on the roller compaction behaviour and on the product properties and this effect will be different depending on the powder properties [39, 40, 47, 51, 56, 58, 59].

The effect of moisture content of amorphous food powder on ribbon properties was studied by Osborne et al. [51]. Maltodextrin was stored at different relative humidities to obtain powders with different moisture content. Ribbons were then produced at different hydraulic pressure using Alexanderwerk WP120 roller compactor in a range of 30-180 bar, and the roller speed and the gap were kept constant at 3 rpm and 2 mm respectively. The strength of the ribbon was assessed using two methods; the ball milling method and the three point bend test. In the first method, ribbons were grinded under the same condition in the ball mill to obtain fragments. The fragment size distribution was then measured and related to the ribbon strength. Figure 2.7 illustrates the effect of the water content on the fragment size of the ribbon after milling. The term $(T_g - T)$ indicates the powder water content, as the water content affects the powder glass transition temperature (T_g). The lower the value of $(T_g - T)$ the higher the water content of the powder. It was found that ribbons produced from powder with high water content gave larger fragments than those of low water content which indicates that the ribbons were stronger. The increase in water content results in a decrease in the glass transition temperature of the powder and also a decrease in the powder viscosity [19]. It was hypothesised that the decrease in the powder viscosity resulted in a sintering process during compaction which forms strong bonds between the particles, therefore, increasing ribbon strength [19, 51]. In the second method, the three point bend test, the powder moisture content was found to have no influence on ribbon tensile strength at the same hydraulic pressure. This was attributed to the non-uniformity in ribbon density, and also to the large error bars associated with the result [51].

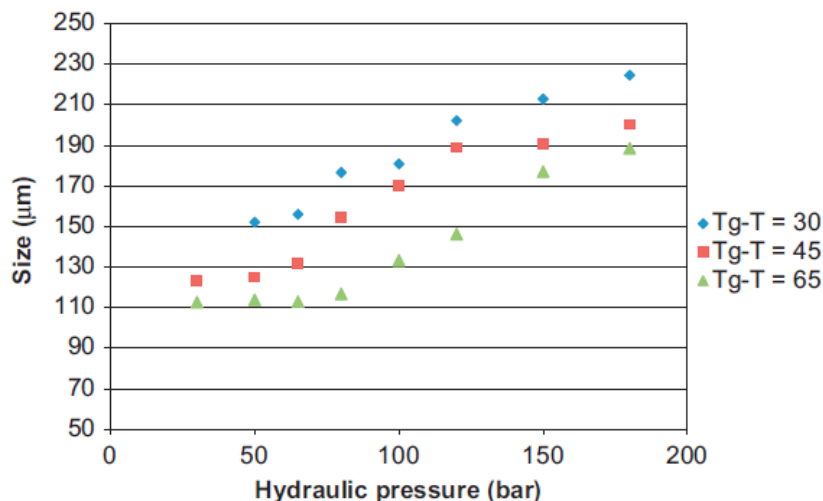


Figure 2.7: Effect of water content and hydraulic pressure on fragment size (d_{50}) of the ribbon after milling [51].

The porosity of the ribbon was also examined at different powder moisture content as shown in Figure 2.8 [51]. The porosity of the ribbon was determined from the mass and volume of the sample and using the true density of the powder. The average porosity was determined by considering the whole width of the ribbon, and the ribbon central porosity was calculated after removing approximately 10 mm from the edges of the ribbon. It was found that the powder moisture content had no significant effect on the average porosity of the ribbons, which can be seen from the large error bars shown in Figure 2.8. However, there was a significant effect of the water content of the initial powder upon the ribbon central porosity, where the central porosity decreased with increasing powder water content. This result was suggested to be due to a sintering process which happened during compaction of powder with high water content.

Figure 2.8 also shows that the average porosity is higher than the central porosity. This was attributed to the fact that the centre of the ribbon was denser in comparison to the edges, therefore removing the ribbon edges from either side resulted in a decrease in porosity.

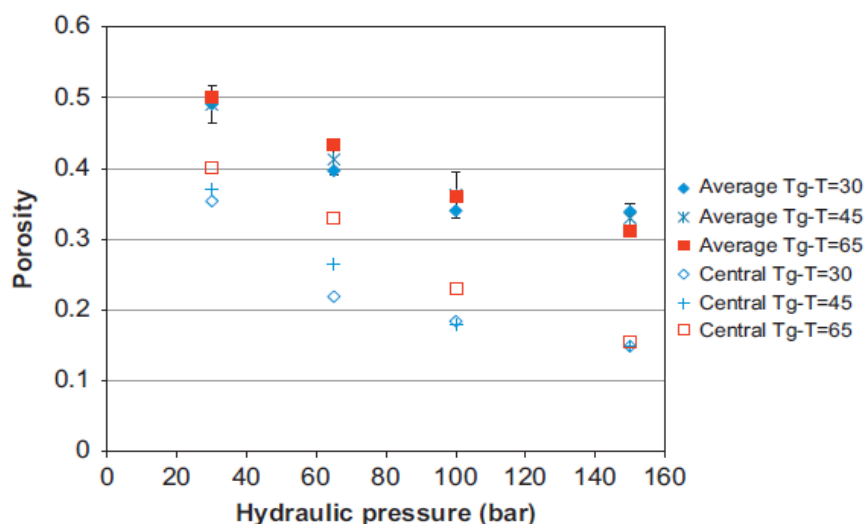


Figure 2.8: Effect of water content and hydraulic pressure on ribbon porosity [51].

The moisture content of the starting powder will have an effect not only on the produced ribbon properties but also on the powder behaviour during the roller compaction. The moisture content of the powder may have an effect on the powder flowability and compressibility [48]. The compressibility and the flow properties of the powder play a significant role during the roller compaction. The flowability of the powder determines the amount of the powder between the two rolls during compaction, especially for the gravity feeding systems. The powder compressibility defines the degree of the densification during compression.

Powder moisture content was found to affect the pressure (stress) applied by the rollers during roller compaction [56]. This study was carried out using Microcrystalline cellulose MCC (Avicel PH-102) with different water content. Different amounts of water (2.5-15%) were sprayed on the powder bed while agitated in a rotary mixer. It was found that the maximum pressure (stress) applied by the rollers was the same for powders with a water content below 10%. However, the value of the maximum pressure increased sharply at a water content of 11.44% and then decreased with further increase in water content. It was found that the increase in powder water content decreased the flowability and increased the cohesivity of the powder. It was hypothesised that the increase in the powder cohesivity resulted in increasing the amount of powder being gripped by the rollers, therefore, increasing the pressure applied to the powder. The decrease in the pressure with a further increase in water content was attributed to the lubricating effect of the water.

However, some other studies showed contradictions to the previous work, showing that compact tensile strength decreases with increasing the moisture content of a powder. Gupta et al. [39] studied the effect of moisture content of Microcrystalline Cellulose MCC (Avicel PH-200) on ribbon tensile strength. Ribbons were produced using a Chilsonator IR220 roller compactor at a constant feed rate by keeping both the horizontal and vertical screw speed constant at 30 rpm and 200 rpm respectively. The tensile strength was determined using the three point bend test. It was reported that the tensile strength of the ribbon decreased with increasing the powder moisture content. In another work [40] the same authors examined the effect of variation in the surroundings moisture on compaction and strength of ribbons of Microcrystalline Cellulose MCC (Avicel PH-200) in a blend with 10% acetaminophen (APAP). The same equipment and process parameters as the previous work were used. It was found that ribbon tensile strength increased with increasing the powder moisture content and then decreased with further increase in the moisture content (Figure 2.9).

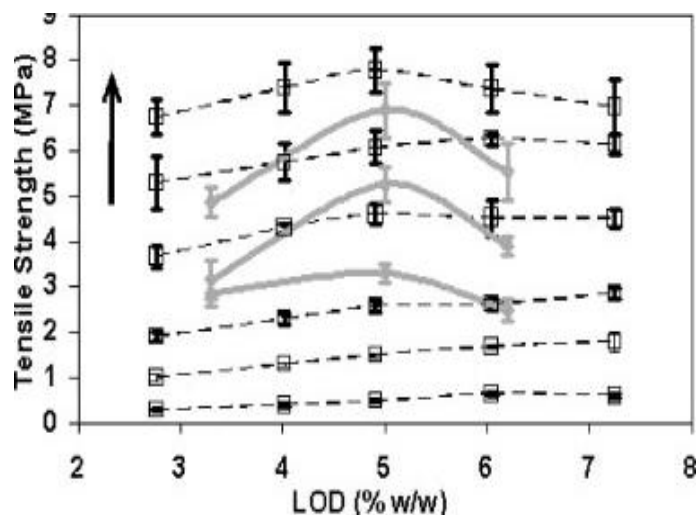


Figure 2.9: Effect of moisture content on the tensile strength of roller compacted ribbon (solid grey line) and compacts prepared using rectangular die (dashed line). Arrow means a decrease in roller speed (7.2, 6, 5 rpm) for the roller compactor and increase in compaction pressure for the rectangular compacts [40].

This behaviour was attributed to the presence of the APAP powder in the blend. An increase in moisture content resulted in facilitating the rearrangement of the APAP particles in the blend, which increases the formation of interparticulate bonds and leads to an increase in tensile strength. This is in contrast to the decrease in ribbon tensile strength with increasing moisture content for ribbons produced from 100% MCC in their previous work [39]. Therefore, the increase and then decrease in ribbon strength

with increasing moisture content was attributed to the opposite effect of the APAP and MCC with increasing in moisture content. The ribbon relative density was also found to increase (porosity decreased) with increasing the water content of the blend (Table 2.1). The authors suggested that this result was due to the powder blend, which contained 10% w/w APAP. Increasing moisture content facilitated the rearrangement of APAP particles in the blend during compaction. These rearrangements resulted in filling the voids between the MCC particles, therefore increasing the relative density of ribbon and, consequently, decreasing the porosity.

Table 2.1: Physical and mechanical properties of ribbon from the roller compactor at different RH% and roller speed and constant screw speed, values inside brackets are the standard deviation of the mean, n= 8 [40].

Property	RH	Roll speed (rpm)		
		5.0	6.0	7.2
Relative density	24	0.76 (0.01)	0.7 (0.01)	0.68 (0.01)
	45	0.79 (0.02)	0.78 (0.02)	0.72 (0.02)
	65	0.81 (0.03)	0.77 (0.02)	0.74 (0.02)
Tensile strength (MPa)	24	4.9 (0.3)	3.2 (0.4)	2.9 (0.3)
	45	6.9 (0.5)	5.3 (0.3)	3.3 (0.2)
	65	5.5 (0.6)	3.9 (0.2)	2.5 (0.2)

2.3.3 Effect of the process parameter

In the roller compaction, not only the primary powder properties affect the product properties, but also the process parameter during the ribbon production. There are few process parameters in the roller compactor which could be changed during production of compacts and granules. The compaction pressure, feeder screw speed, roller speed and the gap between the two rollers are the process parameters which affects the properties of ribbon and granules. Several works have been carried out to investigate the effect of the process parameter in roller compaction on the ribbon and granule properties using different types of powders.

Compaction pressure is the most significant parameter that affects ribbon properties, as the compaction pressure determines the stress acting on the powder during compression. Increasing the compaction pressure increases the strength and the density of ribbon and granules [8, 39, 40, 44, 51]. Roller speed, screw speed and the gap between the rollers

were also found to affect the quality of ribbon produced in the roller compactor [8, 44, 60, 61].

2.3.3.1 Effect of the feeder screw speed

The effect of process parameters on product quality has been investigated in the literature using different types of lactose [44], different types of MCC [60] and maize [8]. Process parameters were represented by the compaction pressure and the speed of the horizontal and vertical screws, while the product quality was represented by the granule friability. Lower granules friability was suggested to represent better quality of the product. It was found that the best product quality (low friability) for all materials was achieved by operating the roller compactor at high compaction pressure. The effect of the horizontal screw speed was different for different powders; the best quality of the product was obtained using low horizontal screw speed for lactose [44] and high horizontal screw speed for both MCC and maize [8, 60]. This could be due to the difference in flow properties of the powders. The vertical screw speed was the least important variable in the equipment; however, better quality of the product was obtained at higher vertical screw speed.

2.3.3.2 Effect of the roller speed

The speed of the roller, at constant feeder screw speed, affects the amount of powder between the rollers and also the dwell time of the powder in the compaction zone which may affect the strength of the ribbon. Increasing the roller speed, by keeping both horizontal and vertical screw speed constant, was found to decrease the force required to break the ribbon, consequently, decreasing ribbon tensile strength and density [39, 40, 61] as shown in Table 2.1 and Table 2.2. This was due to the fact that at constant feeder screw speed, an increase in the roller speed decreased the amount of powder in the compaction zone; therefore, ribbons were thinner, lesser in width and easier to break. The size of the granules produced after crushing the ribbon was also affected by the roller speed during the roller compaction [61]. It was found that granule size decreased with increasing the roller speed during ribbon production, this was due to the weaker ribbon which was produced at high roller speed [40, 61]. However, operating the roller compactor at constant (roller speed / horizontal feed screw / vertical feed screw constant at 1:5:25) ratios was found to have no effect on ribbon thickness, width, strength and density [61] as shown in Table 2.3. This was because the amount of powder between the

rollers was always the same; therefore, ribbons with similar thickness and width were produced.

Table 2.2: Effect of roller speed on ribbon physical properties using MCC at constant horizontal and vertical feed screw speed, values inside brackets are the %CV of the mean, n= 13 [61].

Roller speed (rpm)	Thickness (mm)	Width (mm)	Force (N)	Density (g/cm ³)
4	1.58 (1.0)	21.4 (0.1)	16.17 (8.9)	1.24
5	1.39 (1.7)	21.1 (0.1)	9.87 (11.8)	1.21
6	1.26 (1.3)	21.1(0.0)	5.03 (6.0)	1.09
7	1.16 (1.0)	20.9 (0.1)	3.07 (48)	1.04
8	1.12 (1.7)	20.8 (0.5)	1.91 (8.2)	0.92
9	1.08 (1.7)	20.7 (0.6)	1.43 (8.3)	0.88
10	1.06 (1.7)	20.0 (0.6)	0.87 (6.4)	0.8
11	1.02 (2.7)	20.0 (1.0)	0.69 (7.4)	0.78
12	1.00 (1.6)	19.0 (0.5)	0.41 (8.7)	0.71

Table 2.3: Effect of roller speed on the physical properties of ribbon produced at constant compactor setting (^a roller speed/ horizontal feed screw/ and vertical feed screw), values inside brackets are the %CV of the mean, n=13 [61].

Compactor setting ^a (rpm)	Thickness (mm)	Width (mm)	Force (N)	Density (g/cm ³)
4/20/100	1.21 (1.8)	20.8 (0.2)	3.95 (9.3)	1.06
6/30/150	1.21 (1.7)	20.8 (0.1)	3.53 (7.5)	1.04
8/40/200	1.19 (1.5)	20.8 (0.1)	3.89 (7.2)	1.07
10/50/250	1.19 (1.9)	20.8 (0.1)	3.89 (8.2)	1.07

An increase in the roller speed was also found to decrease the nip angle of MCC [62, 63] and Di-calcium phosphate dihydrate (DCPD) [64]. In addition, increasing the roller speed decreased the maximum pressure (stress) applied by the rollers on MCC powder [56, 65] as shown in Figure 2.10 and on (DCPD) powder [64]. This was suggested to be due to the insufficient amount of powder (provided by a gravity feeding system) available between the two rollers at a specific gap which decreases the stress applied on the powder [66]. The decrease in the stress applied on the powder, with increasing the roller speed, resulted in a reduction in ribbon strength [65]. The theoretical peak pressure values in Figure 2.10 were obtained using Johanson's model [7]. It can be seen that the roller speed has no effect on the theoretical peak pressure value, as the speed of the roller is not considered in Johanson's model.

The effect of the roller speed during production on the width and density of the ribbon was also investigated using MCC avicel PH102 by Miguélez-Morán et al. [67]. Wider ribbons were produced when lower roller speed used during the production. The relative density of the produced ribbon was also found to decrease slightly with increasing the roller speed. This was attributed to the fact that the lower speed of the roller enables more air to escape from the powder during densification, in addition, it allows more time for the particles to rearrange and deform [67].

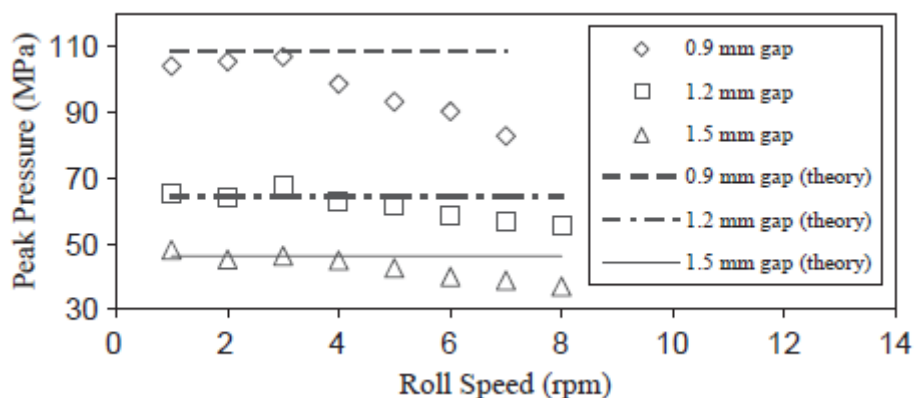


Figure 2.10: Effect of the roller speed and gap on the maximum pressure applied during roller compaction, the theoretical values are obtained from Johanson's model [65].

Osborne [59] studied the effect of the roller speed in Alexanderwerk WP120 roller compactor using Maltodextrin, NaCl, and microcrystalline cellulose MCC. It was found that the roller speed has a minor effect on the temperature of the ribbon during production; ribbons produced at higher roller speed had, slightly, a higher temperature than those at a lower speed. This was due to the increase in the internal friction between particles which was caused by the increase in the feeder screw speed while trying to maintain a constant gap at higher roller speed. The increase in the roller speed was found to have no effect on both the ribbon tensile strength and fragment size after milling the ribbon.

2.3.3.3 Effect of the gap between the rollers

The gap between the two rollers is one of the process parameters which can be changed during the roller compaction. In the roller compactor, one of the rollers is movable while the other is stationary; the movable roller helps to fix the gap between the rollers.

The gap determines the thickness of the produced ribbon, which may affect ribbon strength and porosity.

Bindhumadhavan et al. [65] attempted to investigate the effect of the process parameter (e.g. gap between the rollers) on the behaviour of microcrystalline cellulose undergoing roller compaction using a gravity feeding system. They examined the effect of the roller gap on the maximum pressure applied on the powder during compaction both experimentally and theoretically using Johanson's model. The maximum pressure applied on the powder during roller compaction was found to decrease with increasing the gap between the two rollers as shown in Figure 2.10. This could be due to the fact that increasing the gap between the rollers increases the amount of the powder in the gap region and reduces the applied stress on the powder.

Miguélez-Morán et al. [67] investigated the effect of the gap between the rollers on the ribbon relative density. Microcrystalline cellulose MCC was used as a model powder and ribbons were produced at two different gap settings. It was found that the average relative density of the ribbon was increasing with decreasing the gap between the rollers. This was due to the higher stress which was applied to the powder at lower roller gap, this is in agreement with the finding of Bindhumadhavan et al. [65] as shown in Figure 2.10. Osborne [59] investigated the effect of the roller gap on the properties of ribbon produced from Maltodextrin. Ribbon temperature was found to increase with increasing the roller gap due to the higher internal friction as a result of increased screw speed while attempting to maintain a constant gap. It was also found that the force required to break the ribbon increased with increasing the gap during the roller compaction. This was due to the fact that thicker ribbons require a higher force to break. However, after normalising the data by calculating the tensile strength of the ribbon which takes into consideration the dimensions of the ribbon, it was found that the tensile strength was decreasing with increasing the gap. This is believed to be due to the larger amount of powder available between the rollers at the larger gap, which decrease the stress applied to the material. The increase in the roller gap size during ribbon production was found to have no effect on the porosity of ribbon produced from Maltodextrin. However, the porosity of ribbon produced from sodium chloride was found to increase with increasing the gap size [59].

Inghelbrecht et al. [8] examined the effect of the gap between the two rollers on the friability of granule after crushing ribbon produced from maize powder. It was found that the friability of granules decreased with increasing the roller gap. This was due to the fact that at a high roller gap, compacts were thicker which produced granules with low friability. The decrease in the friability of the granules with increasing the roller gap gives an indication of stronger ribbon. This is in contradiction with the previous studies in that the increase in the roller gap resulted in a decrease in the maximum pressure applied and a decrease in the ribbon density, which gives an indication of weaker ribbon. The different results from these studies indicate that the effect of the gap during roller compaction may vary with different materials.

2.3.4 Amount of fines (non-compacted powder)

The main disadvantage of dry granulation using the roller compaction is a large amount of non-compacted material associated with the product. This non-compacted material also called the amount of fines, is a major problem in some industries, especially food and pharmaceutical (for example when active ingredient are involved in the pharmaceutical industry). The existence of a large amount of fines in the product increases its tendency to segregate, which is finally cause a content non-uniformity problems. In industry, it is well known that the process is combined with a recycling system in order to reuse the fines and increase the efficiency and the yield of the process. However, the fines may have different composition compare to the starting powder blend which means that the reuse of the fines will have a negative effect on the content uniformity of the product [10]. In addition, the re-compaction of the same material more than one time may affect the compactibility of the granule which then reduces the tablet tensile strength. The fines usually produce from the poor binding at the edges of the ribbon during the roller compaction [63] or after crushing of the ribbon during the milling process.

Limited works have been carried out to study the amount of fines associated with the ribbon during the roller compaction process [58, 68, 69]. The amount of fines associated with the ribbon during the roller compaction was investigated in the literature for different grades of microcrystalline cellulose MCC [69] and different types of mannitol and dicalcium phosphate (DCP) [68]. The fines were defined as fragments less than 1.6 mm in size which was separated from the ribbon by sieving. It was found that the

amount of fines produced with the ribbons during roller compaction was high for the direct compression qualities of powder which were manufactured by a spray dryer. They claimed that the spray dried particles may collapse during the roller compaction and produce smaller particles of which it will be difficult to create sufficient pressure on the powder between the rollers [68]. The large amount of fines produced from the spray dried qualities was also suggested to be due to the good flowability of the powder which enabled the particles escaping from the compaction zone. This phenomenon was reported to be more problematic in roller compactors with vertically designed feeding systems [70], the same type of feeding system which was used by [68].

Inghelbrecht and Remon [58] tried to enhance the granule quality in the roller compactor by reducing the amount of fines in the product. A mixture of 90% w/w of pharmatose 200M and 10% w/w of pharmacoat 606 (as a binder) was used. Powders with different water content were obtained prior to compaction by spraying different amounts of water onto the powder. They studied the amount of non-compacted powder produced with the ribbon and the amount of fines produced with granules after milling. It was found that the amount of non-compacted powder decreased with increasing the water content of the powder. Moreover, increasing the hydraulic pressure during production decreased both the non-compacted powder with the ribbon and the amount of fines with the granules after milling. However, powder water content above 11% was avoided due to the formation of lumps and the sticking of powder on the roller during production. It was reported that the optimum powder water content range was between 8 and 10%.

As mentioned earlier, the fines could also produce during crushing the ribbon in the milling system. Several works have been carried out to study the effect of formulation and different process parameters during milling on the amount of fines in the product [71-74].

Samanta et al.[71, 72] investigated the effect of the milling setting (after the roller compaction) on the amount of fines in the final product using a blend of lactose, MCC and Magnesium stearate. The fines were defined as the amount of the granules less than 180 μm . It was found that the minimum amount of fines was produced when the pre-breaking action of flakes used. This means that the fine percentage in the final product can be reduced when multiple stages of milling are used. In another study Bultmann

[73] attempted to reduce the amount of fines produced after milling the ribbons of microcrystalline cellulose. In the study, they defined the fines as particles with a size smaller than 100 μm . Their approach was using multiple compaction cycles in order to improve the quality of the product. It was concluded that the percentage of fine in the final product can be reduced when multiple compaction cycles of MCC are used. However, compaction of the same material more than one time affects the binding ability of the granules which has a negative effect on the properties (e.g. tensile strength) of the tablet. A study of the roller compaction of different types of mannitol was conducted by Wagner et al. [74]. They compared the roller compaction behaviour of five grades of spray dried mannitol with an untreated mannitol grade in terms of the amount of fines produced with the granules after crushing the ribbons. The fines were defined as particles of size equal or smaller than 90 μm . It was found that the untreated grade of mannitol produced a high amount of fines even after compaction at high pressure. However, the five grades of the spray dried mannitol resulted in granules with better flowability and a lesser amount of fines.

2.4 Inhomogeneity across ribbon width

As mentioned earlier, roller compaction is a process for converting fine powders into flakes or ribbons which will be then milled into granules. Ribbons are the intermediate product which controls the properties of the final granules. The density and the strength are the most important properties of the ribbon which affects the properties of the final granules [5, 75]. The homogeneity of density and strength distributions across the width of the ribbon affects the ribbon and granule properties [75]. The non-uniformity of the ribbon density across the width has been reported in several studies [11, 12, 63, 67, 75-79].

The nonuniformity of ribbon property across the width was first reported by Guigon and Simon [78, 79]. They carried out their work using a laboratory roll press equipped with rollers of 130 mm in diameter and a horizontal screw feeder. They investigated the density distribution across the compact width by measuring the transmitted light through compacts of sodium chloride. The difference in the light transmission through the sample (see Figure 2.11) was attributed to the difference in stress which was applied during compaction.

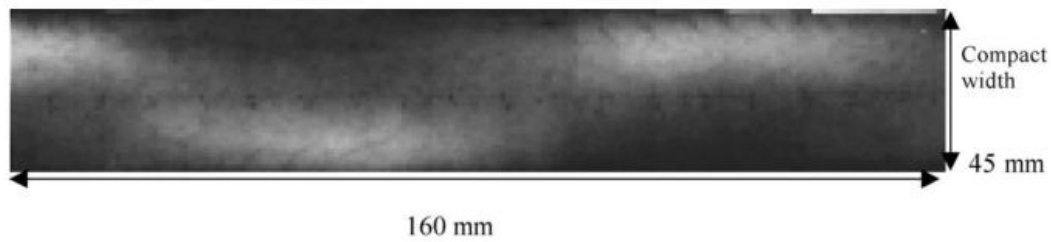


Figure 2.11: Transmission of light through sodium chloride compact [78].

It was found that the stress was not uniform across the width of the compacts as well as with time. The stress distribution across the width and with time was found to be periodical. This was attributed to the distribution of the feed pressure which was induced by the feeder screw.

A similar result was reported by Cunningham et al. [11] when studying the variation of the roller compaction process using finite element method FEM. A vertical screw feeder in the roller compactor was used to feed powder to the compaction zone. Similar to Guigon and Simon [78], they found that there was a fluctuation in the powder feeding which was due to the oscillating nature of the screw feeder. This resulted in non-uniformity in the stress applied on the material across the width of the roller. The simulation results from the FEM also showed that there was a difference in pressure and density of the compacts across the roller width. The density and the pressure distribution across the width of the ribbon were related to the side seal friction. Increasing the side seal friction decreased the pressure applied on the material at the edges, see Figure 2.12. This resulted in a density distribution across the width of the ribbon with lower density at the edges as shown in Figure 2.12.

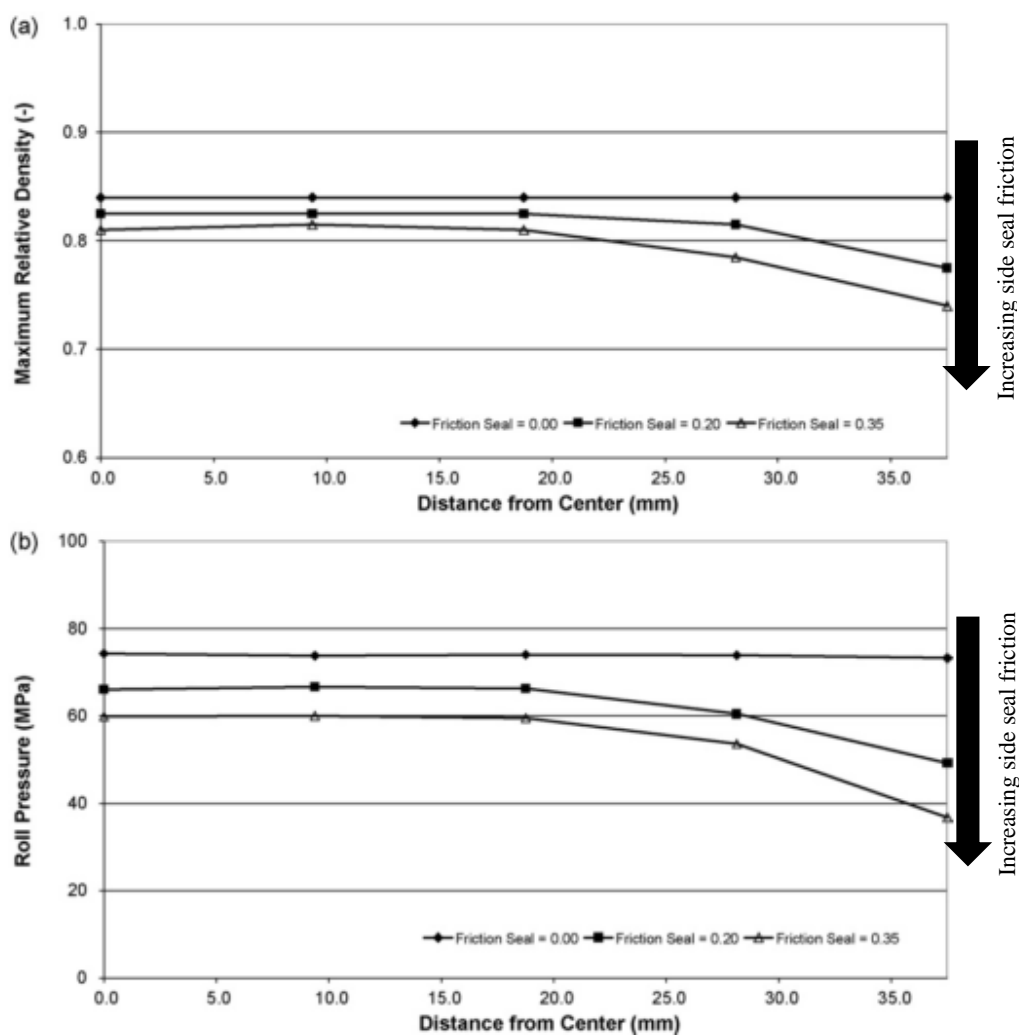


Figure 2.12: Simulation results using FEM showing the effect of side seal friction on the roller pressure and density of ribbon across the width [11].

The non-uniformity of powder flow and ribbon property across the width were later confirmed by Michrafy et al. [12] who studied the homogeneity of MCC ribbon across the width. They used a similar method to Guigon and Simon [78] for the homogeneity analysis (light transmission) as well as mercury porosimetry. It was reported that compacts showed periodic inhomogeneity represented by the light and dark regions across the width of the ribbon. The periodic heterogeneity across the compacts width was suggested to be due to the geometry of the screw, which resulted in a non-uniform powder feeding to the compaction zone. The mercury porosimetry was also used to measure the density of compacts over the width, and the result showed that ribbons have a higher density at the centre and low density at the sides. Both techniques, the light transmission and the mercury porosimetry, revealed a clear inhomogeneity in ribbon property across its width. However, it was claimed that the result from the two

techniques was not completely correlated. Michrafy et al. [12] further investigated the homogeneity of the ribbon across the width using a three-dimensional finite element modelling. The model was performed based on two assumptions; a constant feed velocity and a constant feed pressure. The model resulted in a uniform maximum stress and density across the compact width when constant feed pressure was assumed. Whereas, the stress and the density were not uniform across the width of the compacts (higher density and stress at the centre and lower at the edges) when constant feed velocity was assumed. This was attributed to the lesser amount of powder at the edges as a result of the forced flow of material. Recently, Muliadi et al. [75] developed a 3-D FEM simulation to predict the density distribution across the width of a ribbon and compared the results with the experimental values. A piston feeder was used to feed the powder to the compaction zone with a uniform stress. It was found that the increase in the powder feeding stress has a small effect on the ribbon density distribution, which was due to the change in roller gap with increasing the inlet stress. They reported that the density at the centre of ribbon was approximately 15% higher than that at the edges.

The influence of the powder feeding to the compaction zone was also investigated by Miguélez-Morán et al. [63]. A laboratory scale roller compactor was used in which the powder was fed using a gravity feeding system. The produced ribbons were sectioned into four pieces and the density of each piece was measured from their mass and volume. However, in their next work Miguélez-Morán et al. [67], three different methods have been used to examine the density across the width of the ribbon. The first method was the sectioning method which was the same method used in their earlier work, in the second method they used a micro-indentation across the ribbon width and the third method was using an X-ray micro-CT. It was concluded that the three methods of density measurement resulted in similar results as illustrated in Figure 2.13. It was found, from both studies, that the density of the ribbon was not uniform across the width, with high density at the centre and lower at the edges. This indicates that the material at the centre of the ribbon has been compacted more in comparison to the edges. This was attributed to the non-uniformity of the powder feeding from the hopper to the compaction zone, as more powder is fed to the middle of the roller and less at the edges due to the side seal friction and also powder being fed using gravity feeding system.

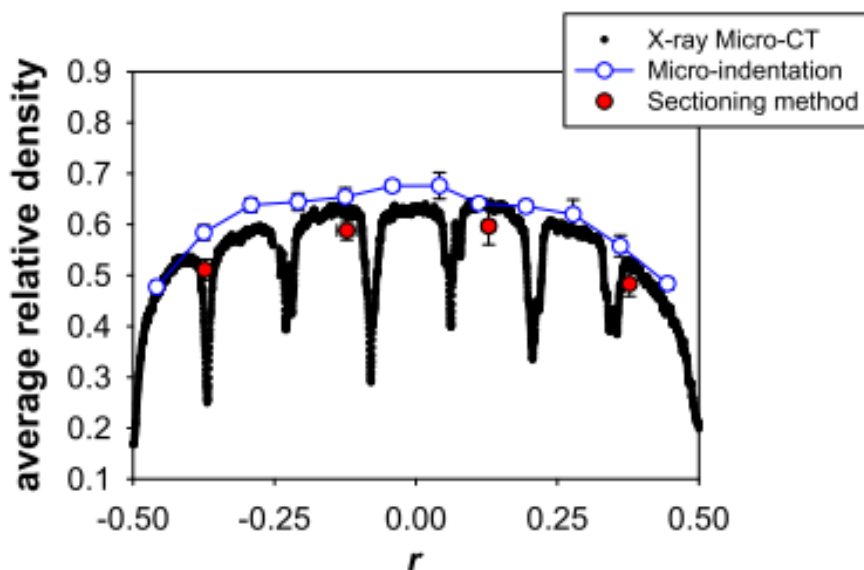


Figure 2.13: average relative density along the width of the ribbon using three analysis methods [67].

The heterogeneity of the ribbon properties across the width was also examined and confirmed experimentally by Akseli et al. [77] and Nesarikar et al. [80]. Non-destructive ultrasonic and X-ray tomography were used by Akseli et al. [77] to measure the density across the width of the ribbon. The acoustic pulse in the ultrasonic spectrum passes through the sample from particle to particle. The stronger the bonds between the particles the better the wave transmission, which means for denser ribbons the sound will travel faster through the sample. It was found that the average longitudinal phase velocity was higher for the middle section of the ribbon in comparison to the edges. This indicates that the ribbon has a higher density at the middle and lower density at the edges. This result was further confirmed by the X-ray images which showed similar observation. Nesarikar et al. [80] and Souihi et al. [81] used an instrumented roller compactor to measure the stress applied on the powder across the width of the roller. They installed three force transducers along the width of the roller, two at the edges and one at the centre of the roller. It was found that the normal stress value recorded by the sensor at the centre of the roller was higher than those recorded at the edges. Moreover, the recorded values of the normal stress from the side sensors showed greater variability in comparison to the one at the centre. This was attributed to the non-uniformity of the feeding pressure which was caused by the last flight of the feeding screw.

Limited work has been carried out to overcome the inhomogeneity issue of ribbon properties across the width. Funakoshi et al. [82] attempted to enhance the pressure distribution across the width of the roller by developing a pair of rollers with concave-convex edges. The concavity of the roller was formed by using flanges, or so-called “rims”, at the edges of the roller. They used flanges with a different angle in order to obtain wall slopes of 45° , 65° , 75° , and 90° . It was found that the use of the concave-convex rollers resulted in more uniform pressure distribution across the roller width in comparison to the ordinary flat rollers which showed higher pressure at the centre and lower at the edges. Furthermore, the amount of leaked powder during the roller compaction was depending on the angle of wall slope and the minimum amount of leaked powder was obtained at wall slope angle of 65° .

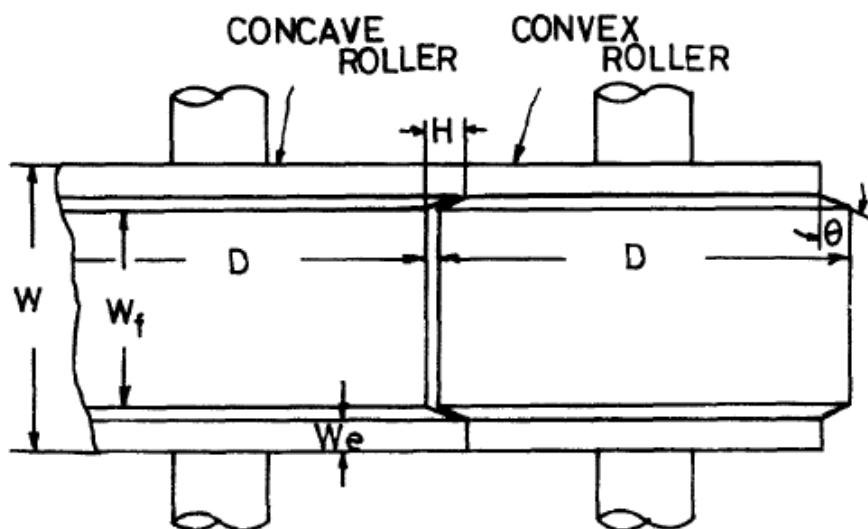


Figure 2.14: the concave-convex rollers designed by Funakoshi et al. [82].

Nowadays, rimmed rollers are offered by several roller compactors. The rimmed rollers are used instead of the cheek plates to help to reduce the side seal friction. The rimmed rolls and the ordinary cheek plates were recently used by Mazor et al. [76] in order to investigate the effect of the sealing system design on ribbon density distribution across the width using FEM modelling. They revealed that the use of the cheek plate sealing system resulted in a pressure and density non-uniformity across the width of the ribbon. The pressure and the density at the centre of the ribbon were higher in comparison to the edges. However, the use of the rimmed roller sealing system resulted in more

uniformity of the pressure applied on the powder and the density of ribbon across the width.

One of the reasons for the inhomogeneity of ribbon properties across the ribbon width is the powder flowability and the nature of the feeding from the screw feeder [11, 12, 63, 67, 78, 79]. This will result in less powder being present at the edges of the roller in comparison to the centre, therefore, less stress will be applied at the edges. The rimmed rollers were designed to overcome the side seal friction issue and reduce the amount of the leaked powder [76, 82]. However, it is believed that the rimmed roller is not capable of solving problems related to the powder flowability and powder availability across the width of the roller. Therefore, an alternative approach will be presented in this thesis to help to obtain uniform properties across the width of the ribbon.

2.5 Theoretical models in roller compaction

2.5.1 Johanson Model

The first model to predict the pressure distribution in the roller compactor was proposed by Johanson [7]. It assumes that the material is isotropic, frictional, compressible and cohesive and it follows the effective yield function which is proposed by Jenike and Shield [83]. The model utilises the roller geometry and the material physical properties to predict the stress distribution during the compaction. The main physical properties used in the model are the effective angle of internal friction, the angle of wall friction and the compressibility factor. The effective angle of internal friction (δ) and the angle of wall friction (ϕ_w) can be measured using a shear cell tester. The compressibility factor K can be obtained from the relationship between the uniaxial stress σ and the resulting bulk density (ρ), see Figure 2.15, using Equation. 2.1 [7].

$$\frac{\sigma_1}{\sigma_2} = \left(\frac{\rho_1}{\rho_2} \right)^K \quad 2.1$$

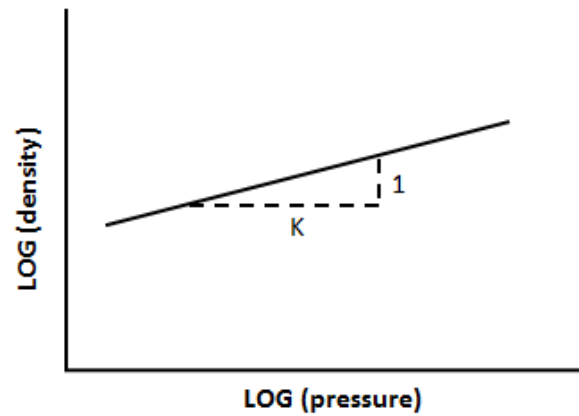


Figure 2.15: Relationship between uni-axial stress and compact density [7].

The model proposes that the compaction zone consists of two regions; slip and nip region. The boundary between these two regions is determined by the angular position (see Figure 2.16). In the slip region, the particles are slipping on the surface of the roller and the pressure gradient can be determined from Equation 2.2 [7].

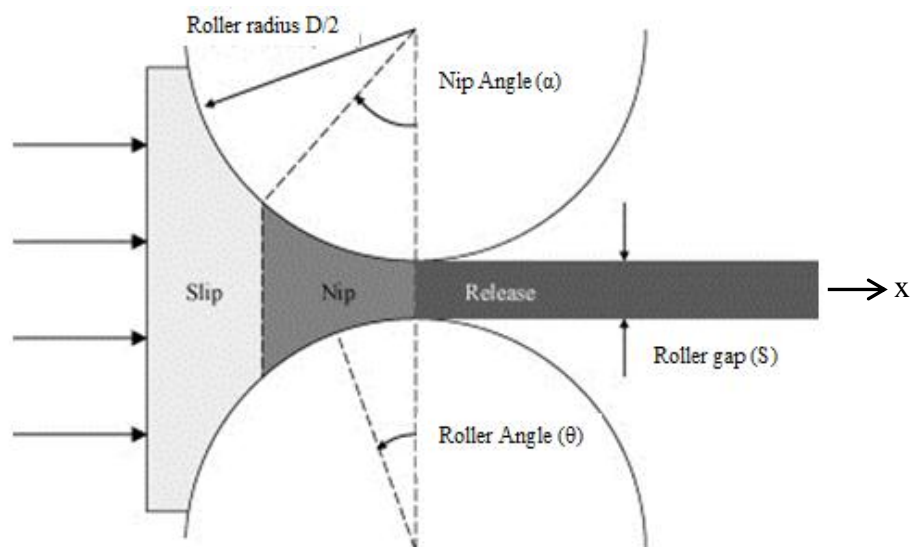


Figure 2.16: Schematic diagram of roll press [84].

$$\left. \frac{d\sigma}{dx} \right|_{slip} = \frac{4\sigma \left(\frac{\pi}{2} - \theta - \nu \right) \tan \delta}{\frac{D}{2} \left[1 + \frac{S}{D} - \cos \theta \right] [\cot(A - \mu) - \cot(A + \mu)]} \quad 2.2$$

where:

$$A = \frac{\theta + \nu + \pi/2}{2} \quad 2.3$$

$$\nu = \frac{1}{2} \left(\pi - \sin^{-1} \frac{\sin \phi_w}{\sin \delta} - \phi_w \right) \quad 2.4$$

$$\mu = \frac{\pi}{4} - \frac{\delta}{2} \quad 2.5$$

Where

δ The effective angle of internal friction

ϕ_w The angle of wall friction

θ Angular position

D Roller diameter

S Roller gap

The nip region starts when there is no relative movement between the material and the roller. The pressure gradient in the nip region can be determined from Equation 2.6 [7].

$$\left. \frac{d\sigma}{dx} \right|_{nip} = \frac{K \sigma \tan \theta \left(2 \cos \theta - 1 - \frac{S}{D} \right)}{\frac{D}{2} \left[\frac{d}{D} + \left(1 + \frac{S}{D} - \cos \theta \right) \cos \theta \right]} \quad 2.6$$

where d is the average thickness of the compact at zero roller gap.

The angular position at which the pressure gradient of the slip and the nip regions are equal is known as the nip angle α . Equating the pressure gradient of the two regions in Equations 2.2 and 2.6 resulted in Equation 2.7, which can be solved for the nip angle.

$$\begin{aligned}
& \frac{4\left(\frac{\pi}{2} - \alpha - \nu\right) \tan \delta}{\frac{D}{2} \left[1 + \frac{S}{D} - \cos \alpha\right] [\cot(A - \mu) - \cot(A + \mu)]} \\
& = \frac{K \tan \alpha \left(2 \cos \alpha - 1 - \frac{S}{D}\right)}{\frac{D}{2} \left[\frac{d}{D} + \left(1 + \frac{S}{D} - \cos \alpha\right) \cos \alpha\right]}
\end{aligned} \tag{2.7}$$

Once the nip angle is known, the roll separating force R_F can be calculated as shown in Equation 2.8 [7].

$$R_F = P_m W D F / 2 \tag{2.8}$$

where

$$F = \int_{\theta=0}^{\theta=\alpha} \left[\frac{(d + S)/D}{d/D + (1 + S/D - \cos \theta) \cos \theta} \right]^K \cos \theta \, d\theta \tag{2.9}$$

P_m is the maximum stress applied by the roller on the powder and W is roller width.

The mathematical model proposed by Johanson in 1965 played an important role in the design and operation of equipment and provided more understanding of the roller compaction process. It can be considered as a valuable tool for the prediction of parameters such as roller force and maximum stress applied to the powder during the roller compaction. This can be simply achieved by knowing both the powder properties (effective angle of internal friction, the angle of wall friction and compressibility factor) and some dimensions of the roller compactor (gap, width and diameter). Johanson's model has been used as a common investigation method and has been experimentally validated by several authors [59, 65, 85, 86]. Yusof et al. [85] used Johanson model for predicting the roller force and roller torque and compared the result with that measured experimentally using maize powder. It was concluded that the prediction of Johanson model was in agreement with the experimental result. Bindhumadhavan et al. [65] attempted to validate Johanson's model using a laboratory scale roller compactor with a gravity feeding system. The roller was equipped with a piezoelectric transducer which

measures the normal pressure profile during the roller compaction of microcrystalline cellulose PH102. It was concluded that the maximum pressure applied to the powder can be accurately predicted using Johanson's model since it showed a good agreement with the experimental result.

A comparison between Johanson's model and 2D FEM (finite element method) simulation was carried out by Muliadi et al. [86]. The two models were used to predict the nip angle, maximum normal stress and the relative density. In general, it was found that the nip angle predicted from Johanson's model showed the same trend as that predicted from the 2D FEM. However, the predicted maximum normal stress from Johanson's model was larger than that of the FEM simulation. This resulted in a relative density predicted from Johanson's model to be larger compared to the FEM simulation. It was concluded that the two models agreed better when the powder is more compressible, has a higher angle of wall friction and lower angle of internal friction.

More recently, Osborne [59] used Johanson's model for predicting the maximum normal stress applied on maltodextrin powder and validated the result experimentally. The maximum normal stress was measured experimentally using a prescale pressure film. It was found that there was a good agreement between the theoretical and experiment data, and Johanson's model can be used to predict the maximum normal stress applied on the powder during the roller compaction.

2.5.2 The slab model:

Another mathematical model that predicts the pressure distribution during powder densification is the slab method. It was first proposed and applied by Katashinskii [87] [88] to predict the stress distribution during metal powder rolling. The model uses the same method to Johanson while splitting the deformation zone between the two rolls, but this time, into trapezoidal slabs [89] as seen in Figure 2.17.

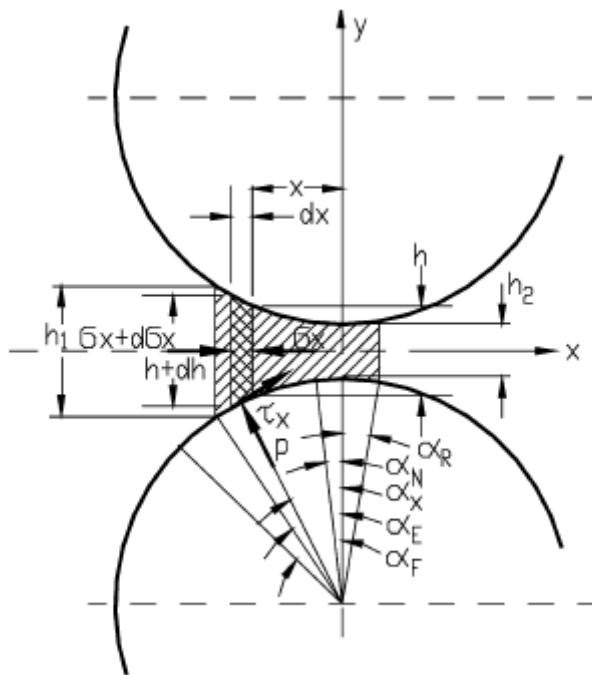


Figure 2.17. Stresses applied to the material in the nip region [89].

An equilibrium equation of the stress in the x direction was obtained from the force balance on the slab as shown in Equation 2.10, which expresses the principles of conservation of momentum.

$$\frac{\partial(h\sigma_x)}{\partial x} + 2(p \tan \alpha_x - \tau_f) = 0 \tag{2.10}$$

where:

h Thickness of the slab

σ_x Stress acting in the rolling direction

p Normal pressure applied to the slab

α_x Instantaneous angle

τ_f Frictional stress which can be expressed as follow:

$$\tau_f = Y(\rho): \quad \text{for } \mu(p)p \geq Y(\rho) \tag{2.11}$$

$$\tau_f = \mu(p)p: \quad \text{for } \mu(p)p < Y(\rho) \tag{2.12}$$

where $Y(\rho)$ is the yield stress as a function of the slab density which can be determined from compression test of the powder and $\mu(p)$ is the coefficient of friction which can be obtained by the annular friction tester [89].

The stress distribution between the rolls can be predicted after having both the nip angle and the position of the neutral plane which can be determined from experimental data. The initial density and the initial stress conditions were assumed. The density of the compacted powder was obtained from a compression test using the corresponding stress at each step. The assumed initial stress conditions were changed and the calculation was repeated until the compact density is equal to the ribbon density.

The necessity for the experimentally measured values of the nip angle and the required matching with the ribbon density reduce the predictive ability of the slab model. However, some studies were carried out in order to validate the slab model. Dec et al. [89] attempted to validate the slab model using laboratory roller compactor. The roller was fitted with a 12.4 mm diameter strain gauge transducer in order to measure the stress experimentally and then compare it to that of the model. During this study, seven different materials were tested to validate the model. In five of those materials, the predicted values from the model were greater than that of the experimental, while in the other two materials the values were smaller.

2.5.3 Thin layer model

Peter et al. [90] used a similar model as the slab model, known as the thin layer model. This model assumes that the powder deformation during the tableting process can be utilised in the roller compaction. The model assumes that the powder between the two rollers consists of thin layers with the same width and height and a specific density as shown in Figure 2.18. The amount of powders in each layer was assumed to remain constant at the different angular position. The pressure applied to each layer can be determined from the pressure-density relationship which can be obtained from the tableting experiments. Once the pressure is known, the force applied to each layer can be determined.

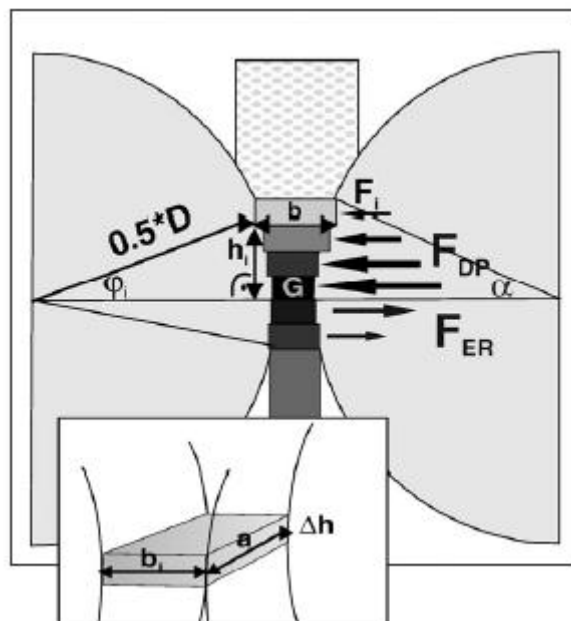


Figure 2.18: Densification of powder using thin layer model [90].

The model was tested and validated using four different materials and one powder blend in a Macro-Pactor roller compactor. The density of the produced ribbon from all powders was then compared to those predicted from the thin layer model. The result was different depending on the densification properties of the powders. For some material the accuracy of the model was less than $\pm 10\%$, and others around 50%. The drawback of the thin layer model is the necessity for a density-pressure relationship which could be difficult to interpret.

2.5.4 Finite element method (FEM)

The finite element method (FEM) has been used by Dec et al. [89] to investigate the behaviour of powder during roller compaction process. In this study, a two-dimensional model was developed to analyse the powder (Microcrystalline cellulose) compaction using ABAQUS code. The work investigated the effect of the powder friction coefficient and the powder feeding pressure on nip and neutral angles, roller force and roller torque. The constitutive model was based on a pressure-dependant yielding plasticity model (which was adapted from the Drucker-Prager/Cap model) with linear elasticity. The calibration of the rate-independent model was obtained from diametrical and simple compression tests in an instrumented die. For simplification of the model, the cohesion of the material was assumed to be zero, and the wall friction was assumed to follow the law of Coulomb friction. The angle of the internal friction was measured to be

65°. The simulation was run until steady state conditions (constant roller force and roller torque) were obtained. It was found that both the powder feeding stress (feed pressure applied to the mesh in the rolling direction) and the powder friction coefficient have a significant effect on the roller pressure. The maximum roller pressure increased with increasing the powder feed stress as shown in Figure 2.19. The maximum pressure was appeared at 0.5- 1.1° before the roller centre. For a given feed stress, an increase in the friction coefficient resulted in an increase in the maximum roller pressure. Moreover, relative density, roller torque and roller force were found to increase with increasing the feed stress and coefficient of friction.

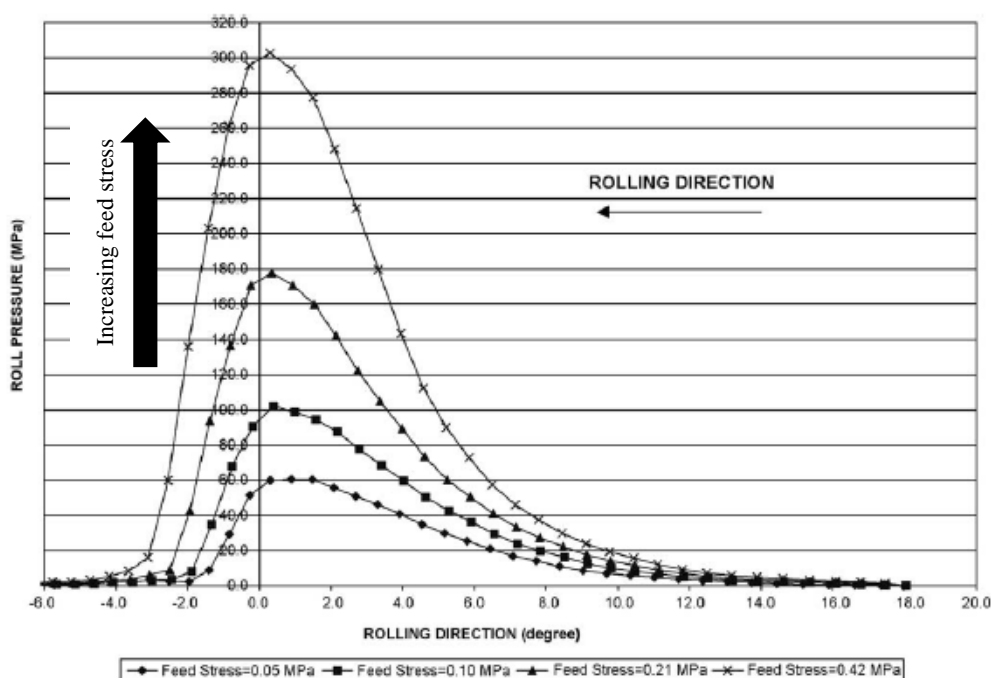


Figure 2.19: Effect of the powder feeding stress on the maximum roll pressure [89].

Cunningham et al. [11] carried out a study to understand the roller compaction of pharmaceutical powders both experimentally and theoretically using the finite element modelling. A blend of microcrystalline cellulose (MCC) with magnesium stearate MgSt was used as a model powder. In the experimental part of the work, they used an instrumented roller compactor equipped with a load cell on the roller of 100 mm diameter and 35 mm width. The load cell is capable of measuring the contact pressure (normal and shear stresses) in the rolling direction. It was found that the pressure of the rollers increased slowly at a rolling angle of -10° , and it reached a maximum pressure at an angle close to 0° as shown in Figure 2.20. They claimed that the determination of the

exact position of the maximum pressure was difficult as the pressure was recorded every 1° . It was reported that there was a difference in the maximum pressure along the width of the roller and the maximum pressure was off centre. The shear stress of the roller was found to increase slightly at the roll entry side then decreased to zero at the neutral angle (where the shear stress changes sign) then increased again with reversing the direction. To further investigate the variation during the roller compaction process, they developed 2D and 3D finite element models using Drucker-Prager/cap as a constitutive model to describe the powder mechanical properties. The 2D model showed that the maximum roller pressure and the final ribbon density increased with increasing the feed stress and the roll friction. The 3D model indicated that density and the roller pressure were lower at the edges of the roller due to the side seal friction. It was reported that the predictions from the models were following the experimental trends.

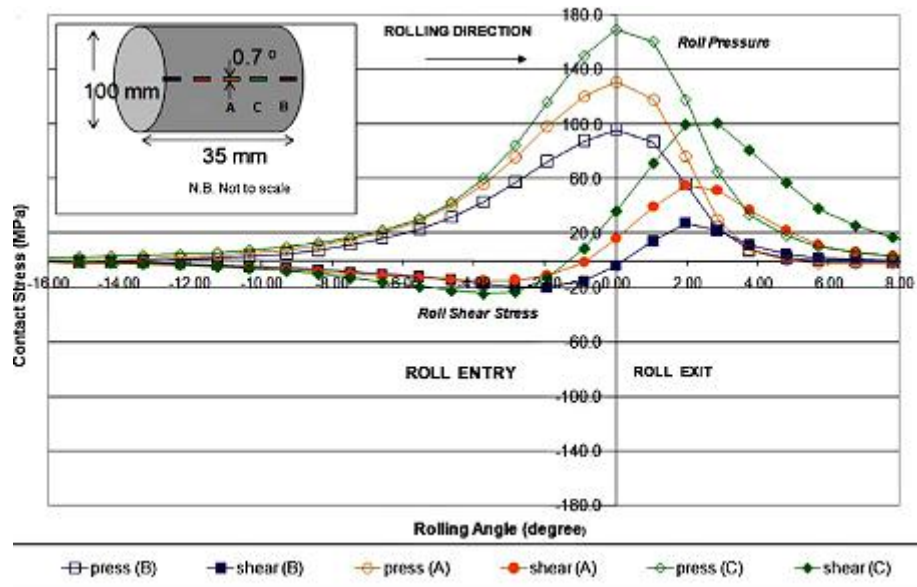


Figure 2.20: Roller pressure and shear stress at a different rolling angle [11].

Michrafy et al. [91] attempted to investigate the change of stress, velocity and density of the powder between the rollers during compaction. They developed a two-dimensional finite element model to understand the mechanism of powder (Avicel PH102) densification during roller compaction. Their work showed that there are three regions during the roller compaction process. The first region is the slide region where the powder flows by sliding mechanism in-between the rollers. The second region is the sticking region where the powder moves at the same velocity as the rollers and where the densification of the powder occurs due to the maximum pressure being applied by

the rollers on the powder in this region. The last region is the region where the compact realises from the gap by slipping and where the change of the shear stress sign occurs. It was found that the maximum pressure was achieved (-1.7°) before the minimum gap, which was in agreement with the observation of Dec et al. [89]. Michrafy et al. [91] also reported that the maximum density was achieved before the minimum gap where the maximum pressure of the roller was recorded. More recently, Muliadi et al. [75] developed a 3-D FEM simulation to predict the density of ribbon and compared the results with those determined experimentally. During the experiments, they used a piston feeder to feed the powder to the compaction zone with a uniform stress. They concluded that the predicted ribbon density from the FEM model was in agreement with those measured experimentally.

It can be concluded that the finite element modelling can be used to predict nip and neutral angles, relative density, force and torque of the roller [89]. However, the main challenge with the FEM is obtaining an acceptable input data to the model [89]. A better and more accurate material models could be used which describes the powder behaviour during compaction more realistically. In addition, the FEM simulation of the roller compaction was found to be restricted by the roller gap and the powder elasticity [75]. It was also claimed that the FEM model was not completely describing the complex behaviour of the powder during the roller compaction [91].

From all the studies mentioned above, it can be concluded that the behaviour of the powder undergoing roller compaction can be modelled using different mathematical models and computer simulations. However, each of these models has its disadvantages and drawback. Several studies showed that Johanson's model it is an accurate model for the prediction of the maximum stress applied on the powder during the roller compaction. The model is relatively simple and requires three properties of the powder (effective angle of internal friction, angle of wall friction and compressibility factor) and some dimensions of the roller compactor (gap, width and diameter) in order to predict the maximum normal stress. For these reasons, Johanson's model will be used in the current work to determine the maximum stress applied to different types of lactose during the roller compaction.

CHAPTER 3 MATERIALS AND METHODS

3.1 Material

3.1.1 Lactose

Lactose is the most important carbohydrate of the milk. It consists of one molecule of galactose and one molecule of glucose. Lactose can be found in either a crystalline state, where the molecules are highly ordered or in an amorphous state where the molecules are randomly arranged [92].

Three types of lactose were used in this study: α -lactose monohydrate 200M, anhydrous lactose SuperTab21AN and spray dried lactose SuperTab11SD (all lactose powders were supplied by DFE pharma, Germany). Different manufacturing processes are used in the production of these types of lactose. Anhydrous lactose SuperTab21AN is produced from the crystallisation of a supersaturated solution of lactose, above 93.5°C, using a roller dryer. Particles of anhydrous lactose are rough and brittle, see Figure 3.1 (A and B). Slow crystallisation, below 93.5°C, of a supersaturated solution of lactose, produces α -lactose monohydrate 200M, where each molecule of lactose is associated with one molecule of water which called water of crystallisation. Crystals of α -lactose monohydrate are brittle and hard with the tomahawk-like shape as can be seen in Figure 3.1 (C and D). Spray dried lactose SuperTab11SD is produced by spray drying a suspension of α -lactose monohydrate in lactose solution using a spray dryer. Because of the fast drying, the particles consist of crystalline and amorphous lactose, see Figure 3.1 (E and F) [92]. From Figure 3.1, it can be seen that there is a difference in particle shape and morphology for the three types of lactose. This is due to the difference in their manufacturing processes as mentioned earlier. The particles of anhydrous lactose SuperTab21AN and spray dried lactose SuperTab11SD are consisted of small crystals aggregated together in an agglomerated structure. However, α -lactose monohydrate particles consist of a single crystal with a smooth surface. The effect of the particle morphology will be investigated in details in Chapter 5.

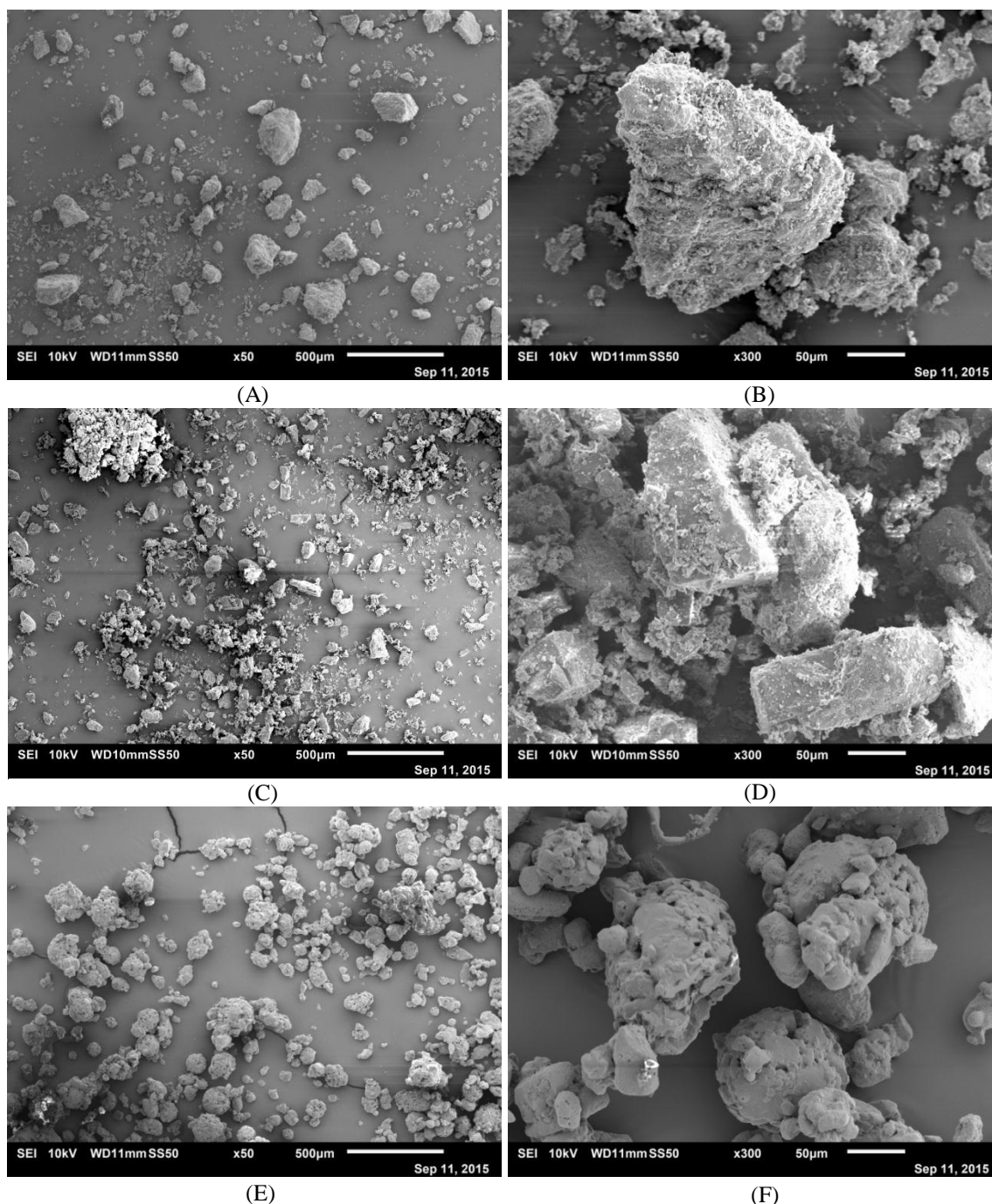


Figure 3.1: Scanning Electron Microscope images of as-received powders: 21AN (A, B), 200M (C, D), SD (E, F) at 50 \times magnifications (A, C, E) and 300 \times (B, D, F).

The three types of lactose contain different amounts of amorphous form. The anhydrous SuperTab21AN is crystalline lactose and is expected to contain no amorphous material. The α -lactose monohydrate is reported to contain a small amount of amorphous lactose. Spray dried lactose is reported to contain the highest amorphous content among the three types of lactose. However, it is important to determine the exact amorphous content of the three types of lactose, which will be presented in Section 4.2.

3.1.2 Primary particle size distribution

The particle size distribution of the primary powder for the three types of lactose (as-received) was measured using Camsizer XT (Retsch Technology GmbH, Germany) which operates based on image analysis. The equipment uses compressed air to disperse the small and cohesive particles which ensure record the properties of a single particle.

3.2 Methods

3.2.1 Differential Scanning Calorimetry (DSC)

An increase in the powder temperature increases the free volume and the molecular mobility in the molecular structure of the powder. This behaviour is different in crystalline and amorphous material as the free volume is different. At elevated temperature, amorphous lactose starts to crystallise. This transformation, amorphous to crystalline, results in a heat generation by the sample due to the fact that crystalline lactose is more stable than amorphous lactose, so the energy of the amorphous material is higher than the energy of the crystalline material.

Differential Scanning Calorimetry (METTLER TOLEDO, Switzerland) was used to study the heat flow through the sample and measure the change in energy with increasing the temperature. A small amount of powder (6-7 mg) of each type of lactose was used in the DSC and heated from 25°C to 240°C at a heating rate of 10°C/min.

3.2.2 Fourier Transform Near Infrared (FT-NIR)

Antaris II FT-NIR (Thermo Scientific, USA) was used to measure the amorphous content of the three types of lactose used in this study. NIR is a fast, non-destructive and non-invasive technique, in which sample preparation is not required, which means a reduction in analysis time. All materials and products absorb NIR radiation at a specific region or wavelength. NIR can be used to determine the physical and chemical information of a material. It can also be used to study polymorphism, blending, coating and drying [93].

Each type of lactose was mixed with pure amorphous lactose (which was obtained from the supplier, DFE Pharma) to obtain mixtures with different percentage of amorphous. These mixtures were then used to obtain the calibration data using NIR. The calibration data was then used to determine the amorphous content of the unknown samples.

To ensure using crystalline lactose in the mixture of amorphous/crystalline lactose, α -monohydrate lactose 200M, anhydrous lactose SuperTab21AN and spray dried lactose SuperTab11SD were stored in the climatic chamber (Binder KMF 240, Germany) at 70% RH and 25°C for one week. This will ensure the crystallisation of any amorphous fraction in the powder [25, 26, 94].

The crystalline lactose (the three types of lactose after crystallisation) and the pure amorphous lactose were kept in a desiccator over silica gel for another week to remove any moisture in the powder. A humidity meter was put with the samples in the desiccator to monitor the humidity (the meter reading was always around 3% RH) and ensure a dry environment. Three sets of mixtures of different amorphous content were prepared using the pure amorphous lactose with each type of crystalline lactose as follows:

- α -lactose monohydrate 200M + amorphous lactose: 1-15% (1% step intervals) as well as 20% amorphous.
- Spray dried SuperTap11SD + amorphous lactose: 1-15% (1% step intervals) as well as 20% amorphous.
- Anhydrous lactose SuperTab21AN + amorphous lactose: 1-15% amorphous (1% step intervals).

NIR spectra for the mixtures were collected using an Antaris FT-NIR. In order to obtain accurate results, each sample was scanned at least three times. The calibration model was derived for each mixture using the Partial Least Squares (PLS) algorithm using the Thermo Scientific TQ Analyst quantitative analysis software. The calibration data will be used to determine the amorphous content in each type of lactose which will be presented in Chapter 4.

3.2.3 Powder preparation

The three types of lactose used in this study were equilibrated prior to compaction using a Binder KMF 240 climatic chamber (Binder, Germany). The equilibration of powder in the climatic chamber is faster than in a desiccator, due the ability to control the air flow and temperature in the climatic chamber. Powders were spread in a thin layer in a plastic tray to increase the surface area of the powder. In order to know the time required for the powder to equilibrate, an experiment was conducted using the climatic chamber which will be presented in Chapter 4.

3.2.4 Powder moisture content

The moisture content of all powders was measured using Sartorius infrared moisture analyser (Sartorius, MA 35, Germany). This was done while investigating the effect of storage of powder at different relative humidity (RH) conditions on powder and ribbon properties. After conditioning the powders in the climatic chamber, the moisture content was measured by placing the powder in an aluminium pan and heated at 80°C for 10 min [95].

3.2.5 Powder flow property

The flowability of a material can be defined as the ability of the material to flow. It depends on both the material properties and the way the material is being stored, handled and processed in different equipment [96]. Flowability of a powder is difficult to be expressed as an absolute number, and it is always associated with the test method. The flowability of the three types of lactose in this work was measured using three different techniques as discussed below.

3.2.5.1 Shear cell tester

The flow properties of the primary powders were measured using a ring- shear cell tester RST-XS.s (Dr. Dietmar Schulze, Germany). The powder flowability was described by the flow function coefficient (*ffc*). The flow function coefficient of the powder is calculated from the consolidation stress σ_1 of the corresponding yield locus divided by the unconfined yield strength σ_c using Equation 3.1 [97].

$$ffc = \frac{\sigma_1}{\sigma_c} \quad 3.1$$

The consolidation stress and the unconfined yield strength can be determined from the Mohr stress circle which can be obtained from the yield locus using the ring shear tester as shown in Figure 3.2. According to Jenike [98], powders have an extremely poor flowability when $ffc \leq 1$, very poor for the range of (1-2), poor between (2-4), fair between (4-10) and a good flowability > 10 .

The ring shear tester was also used to determine the effective angle of internal friction (friction occurred between the particles while flowing) and the angle of wall friction (friction between the powder and a solid surface of equipment or a silo) [97, 99].

The yield locus was determined from the relationship between the shear stress and the applied normal stress, whereas, the wall yield locus was determined from the relationship between wall shear stress and wall normal stress using a stainless steel plate. Both the yield locus and the wall yield locus of all materials were measured using 5000 Pa as a normal load at preshear, and four different stress levels were used as the normal load at shear, with the lowest stress being 30% of the maximum.

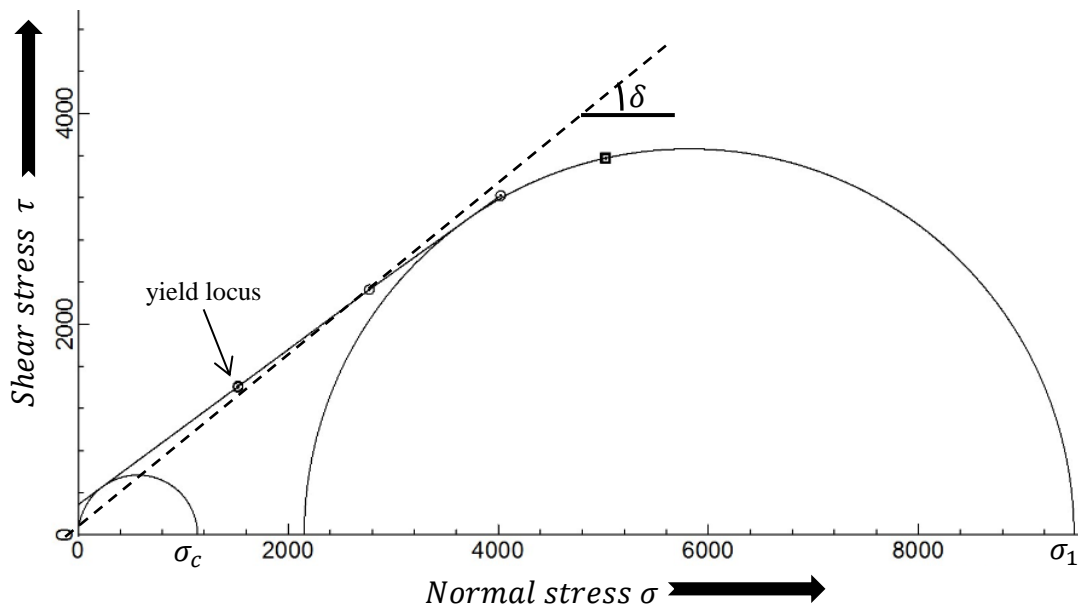


Figure 3.2: Yield locus and Mohr circle obtained from the ring shear tester.

3.2.5.2 Repose angle

The flowability of the primary powder for all materials was also represented by measuring the angle of repose. The angle of repose was measured using Mark 4 Powder Research Ltd (AOR tester, UK). Powders (100 g) were poured from a fixed height onto a flat surface and the angle between the slope of the heap of the powder and the horizontal were determined which represents the angle of repose. Generally, a lower repose angle of the powder indicates better flowability of the material [100-102].

3.2.5.3 Compressibility index

The compressibility index of the powders was also measured and used as an indirect method to represent the powder flow properties. Powders (250 g) were poured in 500 ml measuring cylinder and the bulk volume was recorded. The tapped volume was recorded after tapping the powder using a sieve shaker (Retsch Technology GmbH, Haan, Germany) at 0.2 mm amplitude for 1 min. The volumes of the powder before and after tapping were used to determine the bulk and the tapped densities. The compressibility index was calculated from the bulk and the tapped densities of the powder using Equation 3.2 [100]. Typically, the lower the compressibility index the better the flowability of the material.

$$CI = \frac{\rho_T - \rho_B}{\rho_T} \times 100 \quad 3.2$$

Where CI is the compressibility index, ρ_T is the tap density and ρ_B is the bulk density

3.2.6 Compressibility factor of the powders

The compressibility factor K can be obtained from the relationship between the uniaxial stress σ and the resulting powder bed density ρ using Equation 2.1 which was proposed by Johanson [7]. It was measured by compressing powders at different compression forces and determining the density of the powder bed. Powders of the same mass were compressed in a 12 mm diameter die using Instron testing machine (Instron 3367- USA) at different compression forces up to 15 KN (which results in 132 MPa) at 5 mm/min test speed. The applied force and the punch displacement were recorded during compression. The density of the powder bed was measured from the mass and volume of the powder. The volume of the powder bed was determined from the thickness of the

compacted powder, which can be obtained from the punch displacement, and the die cross sectional area. The force recorded during compression was divided by the die cross sectional area to determine the stress applied on the powder at a corresponding punch displacement. The stress applied on the powder was plotted against the density of the powder bed on a logarithmic scale as shown in Figure 3.3. The compressibility factor (K) was obtained from the slope of the line according to Equation 2.1; K is equal to the reciprocal of the slope of the line. The lower the value of the compressibility factor (K) the better the compressibility of the material [7]. A completely compressible material was reported to have a compressibility factor of $K= 0$ and for an incompressible material $K= \infty$ [7].

$$\frac{\sigma_1}{\sigma_2} = \left(\frac{\rho_1}{\rho_2}\right)^K \quad 2.1$$

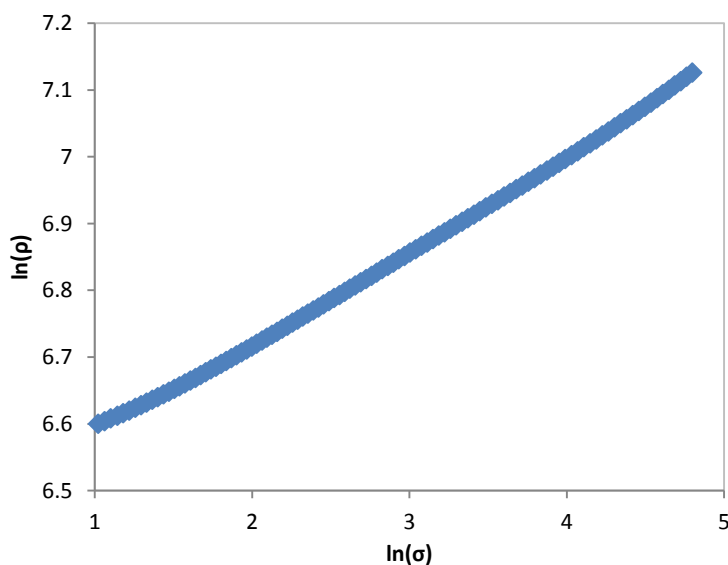


Figure 3.3: Determination of the compressibility factor (K).

3.2.7 Roller compaction

An Alexanderwerk WP120 (Alexanderwerk, Germany) roller compactor was used for the compaction of all types of lactose in this study (see Figure 3.4). The WP120 has three systems working simultaneously; the feeding system, compaction system and

milling system. The feeding system consists of a hopper for the powder and a horizontal screw feeder, which transports the powder from the hopper to the compaction system. Before the compaction system, on the screw feeder, there is a de-aeration system which takes the air out of the powder and improves powder flowability. The compaction system consists of two counter rotating rollers of 120 mm in diameter and 40 mm width with knurled surfaces. The two rollers apply high pressure on the powder using a hydraulic system, which gives a hydraulic pressure in the range of 18-230 bar. The time of compression can be controlled by changing the speed of the rollers from 3 to 13 rpm. The thickness of the ribbon can be defined by the gap between the two rollers which can be changed between 1-4 mm. There are two cheek plates on both sides of the rollers used to reduce the leakage of the powder during compression. Figure 3.5 shows the roller design.

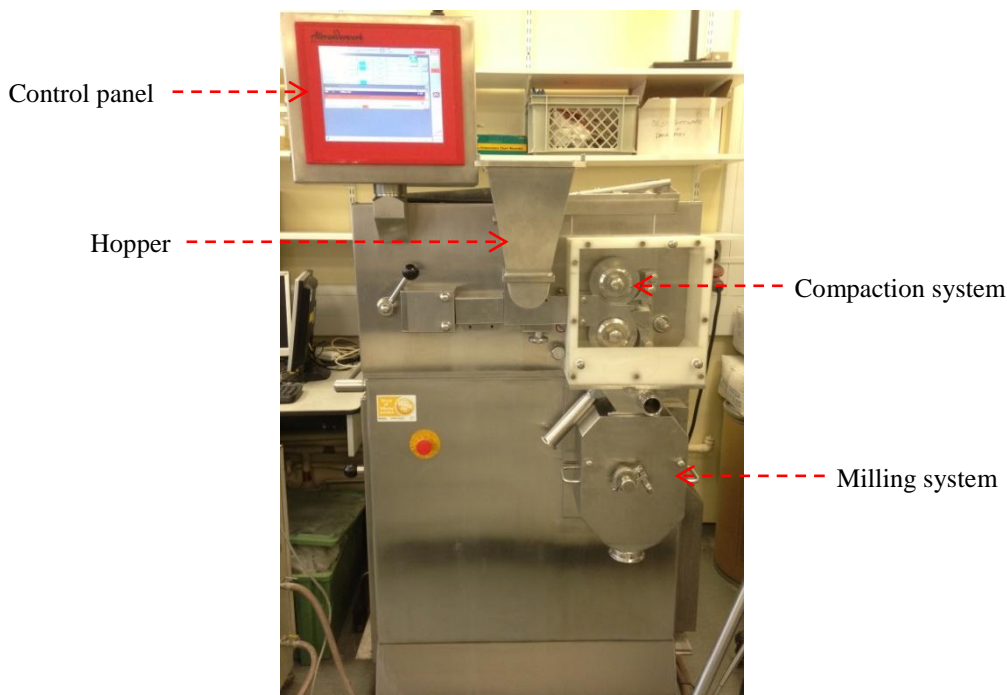


Figure 3.4: Alexanderwerk WP120 Roller Compactor.

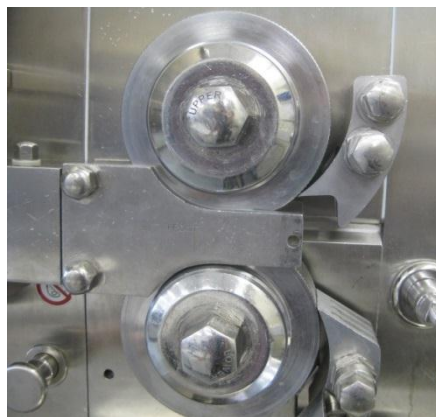


Figure 3.5: Design of the rollers showing the front cheek plate.

The WP120 is equipped with a feedback system which links the compaction system to the feeding system. The feedback system was used to control the gap between the two rollers, which determines the thickness of the ribbon. This is accomplished by changing the speed of the feeder screw until a defined roller gap is achieved.

During the roller compaction, a humidity generator GenRH-A (London, UK) was connected to the top of the hopper of the roller compactor. This was to ensure minimising the effect of the humidity in the laboratory on the powder properties during the production of ribbon. The setup of the humidity generator is shown in Figure 3.6. The humidity generator was operated at the same conditions as the climatic chamber; this ensured a constant humidity condition of the powder during roller compaction same as that used for the storage of the powder prior to compaction.

3.2.8 Online thermal imaging

The ribbon surface temperature was recorded during production using a FLIR A655sc thermal camera (FLIR-Sweden). The online thermal imaging setup is shown in Figure 3.6, where the camera was facing the two rollers and recording the temperature of the exiting ribbon directly. Ribbon temperature was recorded once the gap and pressure in the roller compactor had reached steady state. Each experiment was recorded for 60 seconds at a frame rate of 50 fps. Images from each experiment were then analysed using FLIR R&D software to find the maximum temperature in each frame. Then the average maximum temperatures for all frames were determined.

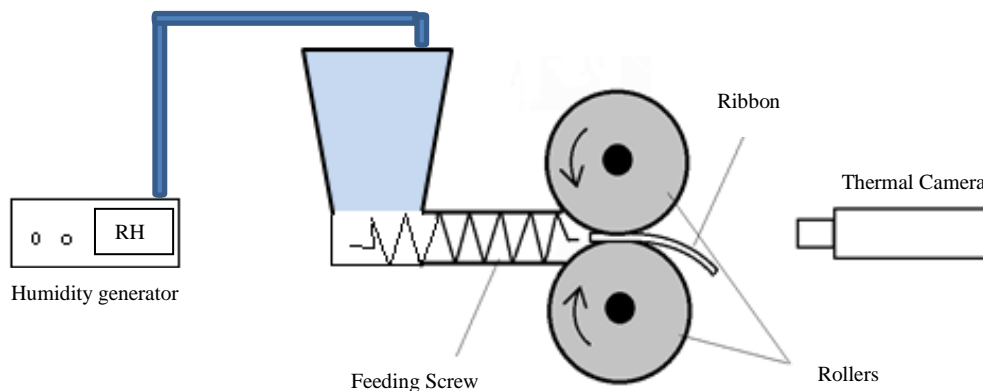


Figure 3.6: Schematic diagram of the online thermal imaging and the humidity generator setup.

3.2.9 Determination of the fine percentage

Due to the absence of liquid in dry granulation technology using the roller compaction, a considerable amount of fines or non-compacted powder produces with the ribbon as well as during the milling process. In this study, the amount of fines was defined as the amount of uncompacted powder (particles which are equal or smaller than the d_{90} of the original powder) which is produced along with the ribbon during the compaction process. To determine the amount of fines, the entire product (ribbon and fines) was collected for a set period of time during the operation of the roller compactor. Then the ribbons were separated from the fines by sieving (Retsch GmbH, Germany). From the total mass of the product and the mass of fines, the weight percentage of fines was determined.

3.2.10 Strength of ribbon

A Zwick/Roell Z 0.5 (Zwick/Roell, Germany) test machine was used to find the maximum force required for the ribbon to break using the three point bend setup [51, 103]. The setup consists of two supports to hold the ribbon, and a load is applied to the centre of the ribbon at a rate of 0.1 mm/min [104]. The maximum force was then recorded and used to determine the tensile strength of the ribbon.

Ribbon tensile strength was then determined using the force recorded by the Zwick/Roell, ribbon width and thickness, and the distance between two supports using Equation 3.3 [51, 105-109]. This measurement was repeated at least ten times for each

condition and an average was taken. Figure 3.7 shows a schematic diagram for the three point bend test.

$$\sigma_t = \frac{3F_{max}L}{2bt^2} \quad 3.3$$

where, σ_t is ribbon tensile strength (N/mm²), F_{max} is the maximum force required to break the ribbon (N), L is the distance between the two supports (mm), which was calculated depending on ribbon thickness using the formula $L = (16 \pm 1)t$ [105, 106]. b is width of the ribbon (mm), and t is the thickness of ribbon (mm).

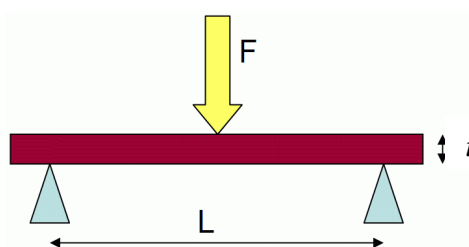


Figure 3.7: Schematic diagram of the three point bend test.

3.2.11 Ribbon porosity using X-ray tomography

X-ray images of ribbons produced from the roller compaction were obtained using microCT 35 (Scanco Medical AG, Switzerland). Samples of ribbon from different types of lactose were attached to a sample holder. The X-ray beam was operated at a voltage of 45 kV, a current of 177 μ A and a power of 8 W. The voxel size used was 3.5 μ m.

Images from the X-ray machine were then analysed using Image J software to determine the porosity of the ribbon. The black pixels in the X-ray images indicate the air (pores) and the white pixels indicate the powder. The number of black pixels (air) was determined and divided by the total number of pixels (air and powder); this ratio represents the porosity of the ribbon.

3.2.12 Scanning Electron Microscopy

Scanning electron microscopy JEOL JSM- 6010LA was used to obtain electron micrographs of the primary powders and of the ribbons after compaction of the powder in the roller compactor. In order to obtain good quality images of materials with low conductivity, e.g. lactose, the samples were coated with gold using AGAR sputter coater (AGAR, UK).

CHAPTER 4 PROPERTIES OF THE PRIMARY POWDERS

4.1 Particle size distribution of the primary powders

As mentioned in Section 3.1.1, the three types of lactose were produced using different production methods. The different production methods will result in the production of different types of lactose with different properties. The three types of lactose have different particle size distribution. Figure 4.1 shows the particle size distribution for the different types of lactose measured using the Camsizer XT as described in Chapter 3. Table 4.1 shows the particle size data (d_{10} , d_{50} and d_{90}) for the three types of lactose.

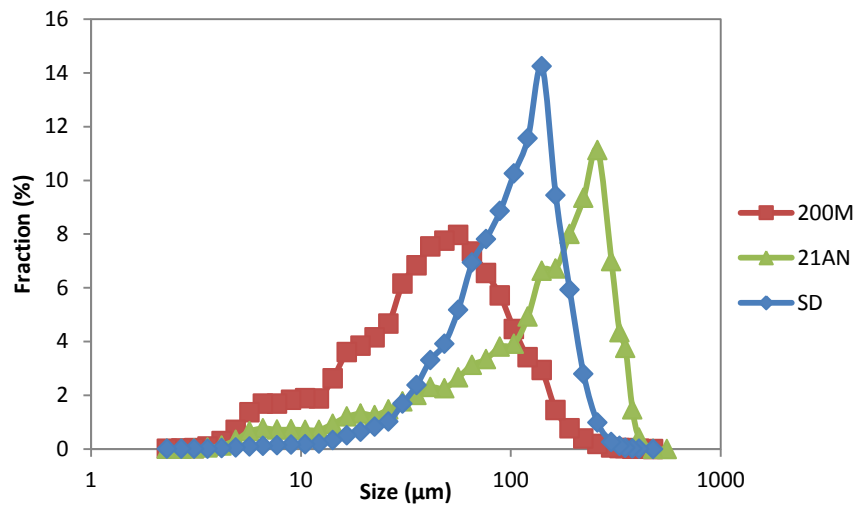


Figure 4.1: Particle size distribution for the three types of lactose.

Table 4.1: Particle size data for the primary powders, measured by Camsizer XT.

Powder	d_{10} (μm)	d_{50} (μm)	d_{90} (μm)
Anhydrous lactose SuperTab21AN	27.53	172.3	330.03
α - lactose monohydrate 200M	12.57	47.44	117.5
Spray dried lactose SuperTab11SD	45.08	113.48	191.33

4.2 Quantification of the amorphous content of powders

In order to know the exact amorphous content of all types of lactose used in this study, two methods were used to quantify the amorphous content in lactose samples; differential scanning calorimetry (DSC) and near infrared (NIR).

4.2.1 Differential Scanning Calorimetry (DSC)

Differential scanning calorimetry measures the heat flow through the sample with increasing temperature. A small amount of powder (6-7 mg) of each type of lactose was used in the DSC. Samples were heated from 25°C to 240°C and the heat flow through the sample was recorded.

Pure amorphous lactose, obtained from DFE Pharma, was used in the DSC to study the behaviour of the 100% amorphous lactose with increasing the temperature, and to compare this to the behaviour of the other three types of lactose. The heat flow through a sample of pure amorphous lactose was recorded in the DSC using three steps as shown in Figure 4.2. The first step was heating up the sample from 25°C to 120°C at 10°C/min. The second step was cooling down the sample from 120°C to -20°C at 10°C/min. The purpose of these two steps was to delete the thermal history which the sample could gain during storage or transportation.

In the third step, the sample was heated from -20°C to 240°C at 10°C/min and the heat flow was recorded at elevated temperature. The first change in the heat flow was recorded at 74.48°C, which represents the onset glass transition temperature of amorphous lactose. At this temperature, the material's molecular mobility increases and the powder will transform from its glassy state into the rubbery state. A further increase in the temperature resulted in the transformation of the amorphous lactose into crystalline lactose, also called crystallisation of lactose, which occurred at around 160°C. During the crystallisation process, the powder generates energy which is represented by the exothermic peak at 160°C in Figure 4.2. This is due to the fact that the amorphous form is an unstable form of lactose and has a high level of energy; therefore transformation from amorphous to crystalline generates heat or energy. The area of the crystallisation peak can be used to determine the amount of amorphous lactose in the sample; here the area represents 100% amorphous lactose.

A further increase in the temperature resulted in melting the powder, which is represented by the two endothermic peaks at around 220°C and 240°C. The two endothermic peaks are the melting points of both the α and β forms of lactose, as the crystallisation of amorphous lactose results in producing these two forms of crystalline lactose [26].

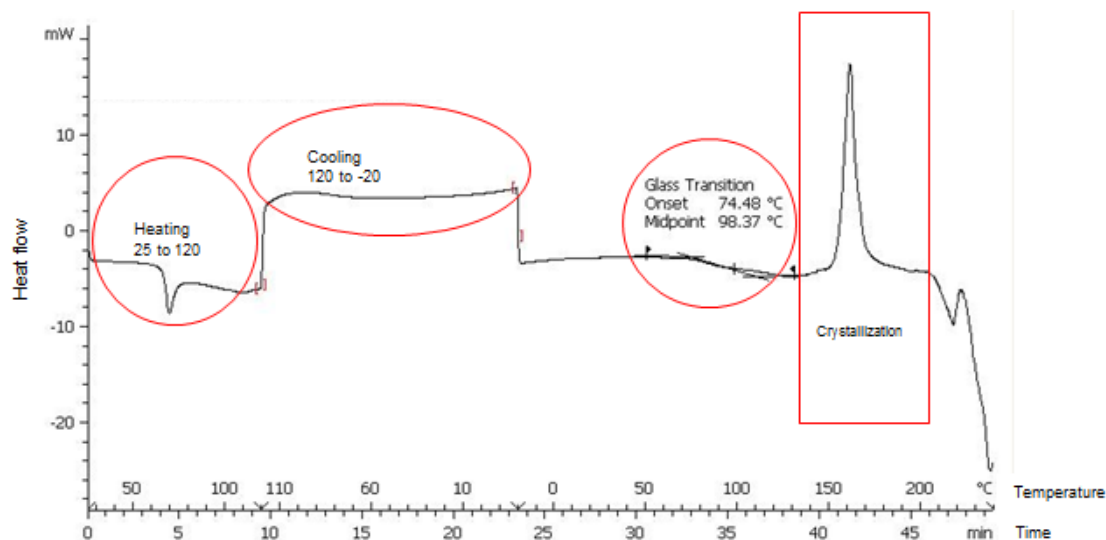


Figure 4.2: Heat flow through pure amorphous lactose VS temperature and time in the DSC.

For the three types of lactose used in this study, DSC experiments were conducted using 6-7 mg of sample and a heating range from 25°C to 240°C at 10°C/min. Figure 4.3 shows the normalised DSC data for the three types of lactose. Both α -lactose monohydrate 200M and spray dried lactose SuperTab11SD have two endothermic peaks. The first peak represents the loss of water of crystallisation which occurred at about 138-145°C for spray dried lactose SuperTab11SD and α -lactose monohydrate 200M. The second peak represents the melting point of α -lactose which was approximately 220°C. For anhydrous lactose SuperTab21AN, there is only one endothermic peak which represents the melting point of β lactose and it is below 240°C.

For all the three types of lactose, no exothermic peaks were found (which represented the crystallisation of amorphous lactose as mentioned earlier in Figure 4.2). This means that DSC was not able to predict the amorphous content of these samples. This could be due to the low amorphous content in these types of lactose. It was reported [26] that DSC is unable to predict the amorphous content for powder containing less than 20%

amorphous lactose. Therefore, another method was undertaken to measure the amorphous content of the lactose samples, i.e. the near infrared spectroscopy (NIR).

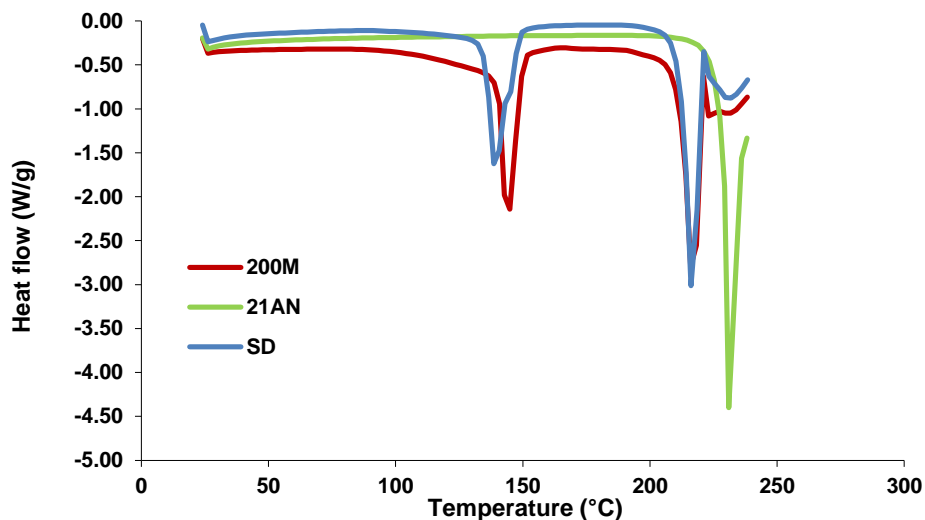


Figure 4.3: Normalized DSC data for the three types of lactose used in this study.

4.2.2 Fourier Transform Near Infrared (FT-NIR)

FT-NIR was used to quantify the amorphous content for the three types of lactose. Different material absorbs different amount of radiation at different wavelengths [93]. NIR is looking at the bond vibration between the molecules and atoms within the material [110], in crystalline lactose, the molecules are highly ordered while in amorphous the molecules are randomly ordered [18]. Applying an NIR radiation to these two materials will result in different bond vibration due to the difference in molecule arrangements. The change in vibration intensity or frequency will result in a change in the peak intensity and width of the spectra [111]. In the light of this fact, NIR can distinguish between different forms of lactose (amorphous and crystalline for example). First of all, mixtures with different amorphous content (known amorphous content) were required to obtain a calibration data, which was used later to measure the amorphous content of unknown samples. More details of the mixture preparation are given in Section 3.2.2.

NIR spectra of all mixtures with known amorphous content were collected using the Antaris II FT-NIR. Figure 4.4 shows an example of the NIR spectra of lactose SD with different (known) amorphous content. Similar data were obtained for lactose 200M and 21AN with different amorphous content (see Appendix A). The NIR spectra of all types

of lactose were analysed using the Thermo Scientific TQ Analyst quantitative analysis software.

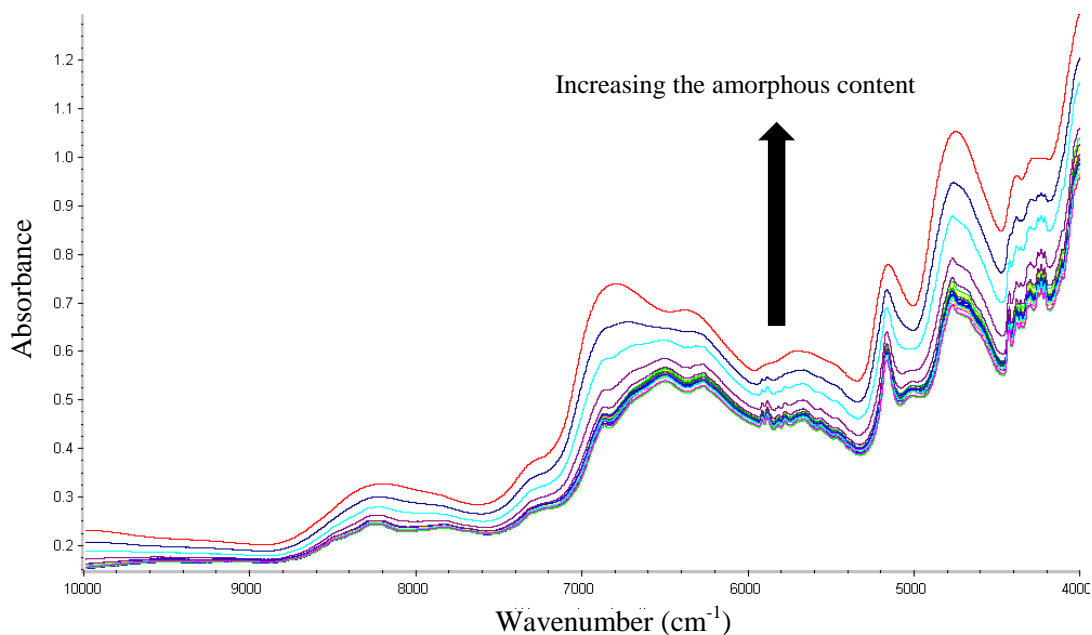


Figure 4.4: NIR spectra of lactose SD with different amorphous content.

To reduce the noise and eliminate the variations which are unrelated to the sample composition, the NIR spectra for all powders were pre-processed by determining the 2nd derivative of the spectra as shown in Figure 4.5.

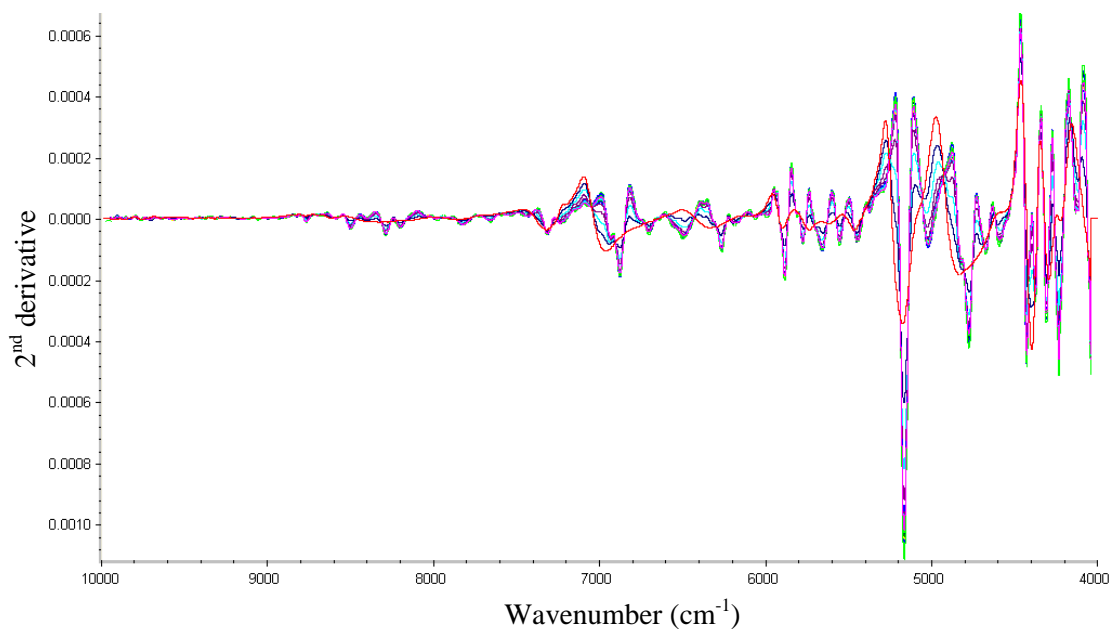


Figure 4.5: Second derivative of the NIR spectra of lactose SD with different amorphous content.

The calibration was performed for each type of lactose by applying a Partial Least Squares (PLS) regression using data of the second derivative of the spectra from the region 4936 to 7680 cm^{-1} . For all mixtures, some data were used to validate the calibration model. The calibration model was evaluated based on the correlation coefficient (R^2), root mean squared error of calibration (RMSEC) and root mean squared error of prediction (RMSEP).

Figure 4.6 shows the calculated amorphous content versus the actual amorphous content of lactose 21AN. The calibration data resulted in a correlation coefficient, R^2 , of 0.9965. The root mean squared error of calibration (RMSEC) of 0.386, and the root mean squared error of prediction (RMSEP) of 0.496.

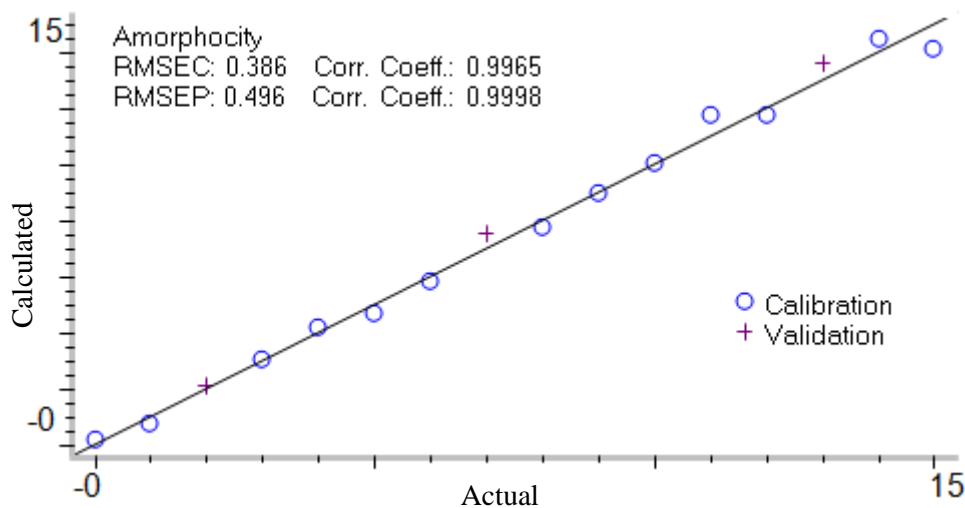


Figure 4.6: Actual amorphous content versus calculated amorphous content of anhydrous lactose SuperTab21AN.

The evaluation of the calibration data of α - lactose monohydrate 200M is illustrated in Figure 4.7. As shown, a correlation coefficient R^2 of 0.9958 was obtained for the model, a root mean squared error of calibration (RMSEC) of 0.497, and the root mean squared error of prediction (RMSEP) was 0.478.

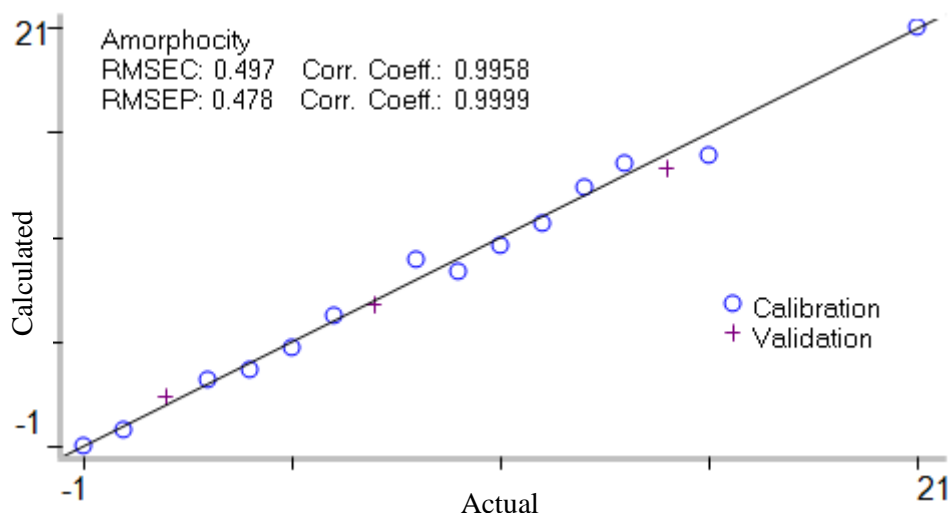


Figure 4.7: Actual amorphous content versus calculated amorphous content of α -lactose monohydrate200M.

The calibration model of spray dried lactose SuperTab11SD gave a correlation coefficient R^2 of 0.9939 and root mean squared error of calibration (RMSEC) of 0.613, and the root mean squared error of prediction (RMSEP) was 0.606. Figure 4.8 shows the goodness of the calibration model for spray dried lactose SuperTab11SD.

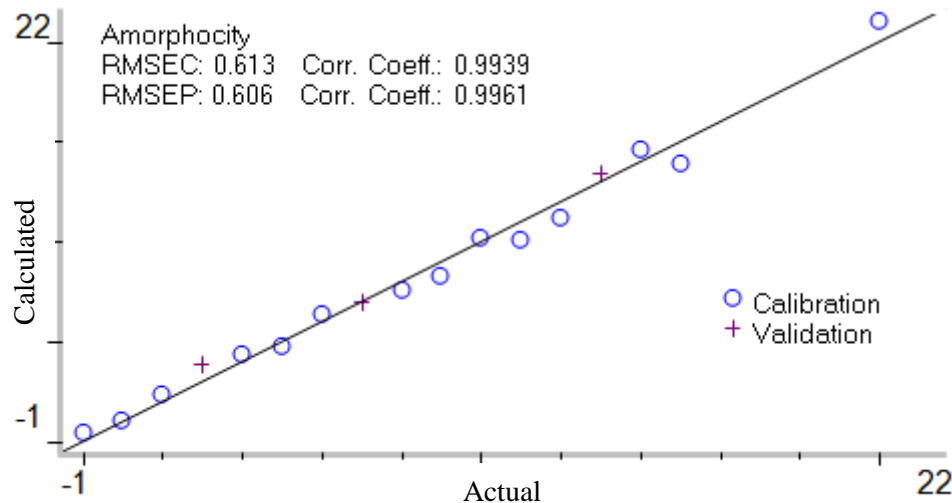


Figure 4.8: Actual amorphous content versus calculated amorphous content for spray dried lactose SuperTab11SD.

The three calibration models obtained for the three types of lactose were used to measure the amorphous content of unknown samples; i.e. the as-received lactose. Samples of anhydrous lactose SuperTab21AN, α -lactose monohydrate 200M and spray dried lactose SuperTab11SD were scanned three times using the FT-NIR. From both the

spectra of each type of lactose and the corresponding calibration model, the amorphous content of each type of lactose was found and is shown in Table 4.2.

Table 4.2: The amorphous content of different types of lactose (as-received powder) measured using FT-NIR.

Powder	Amorphous Content (%)
Anhydrous lactose SuperTab21AN	0.2
α -lactose monohydrate200M	2.67
Spray dried lactose SuperTab11SD	10.32

4.3 Preparation of the powder prior to compaction

Before the roller compaction process, the powders were conditioned in the climatic chamber at different conditions as described in Section 3.2.3. In order to know the time required for the powder to equilibrate in the chamber, an experiment was carried out using the climatic chamber as described below.

4.3.1 Powder weight changes in the climatic chamber

In the climatic chamber, the change in mass of the powder was monitored over six days. Four samples of each type of lactose (~7 g) were put in small containers and stored in the climatic chamber at 40% RH and 25°C. A very precise balance with four digits accuracy was used to measure the mass of the samples every 24 h.

The change of the powder weight was calculated and plotted with the time as shown in Figure 4.9. It was found that the powder weight did not change after the third day of storage in the climatic chamber. Therefore, three days was a sufficient amount of time for the powder to equilibrate.

As a result, all types of lactose were stored in the climatic chamber for three days at different relative humidities prior to roller compaction.

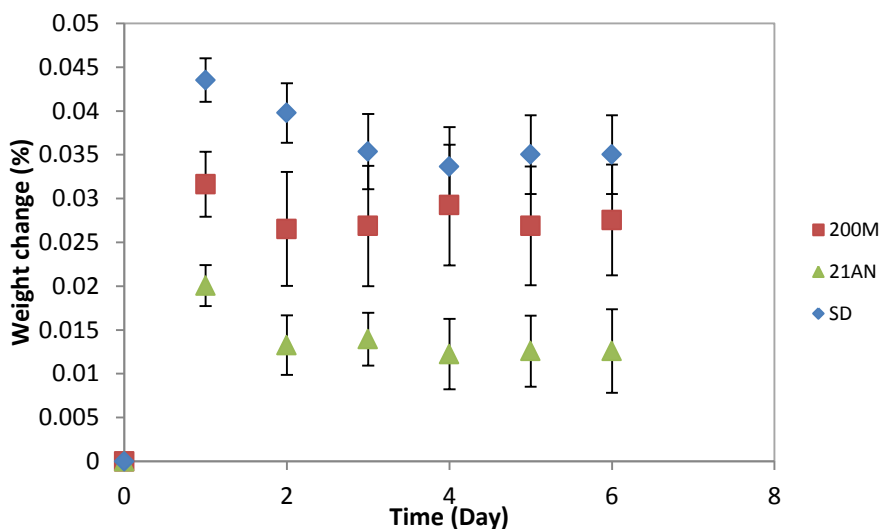


Figure 4.9: Weight change with time for powders conditioned at 40% RH at 25°C in the climatic chamber

4.4 Emissivity of the powder

The most important factor which needs to be taken into account when measuring the temperature of a material using infrared camera is the emissivity. The emissivity is the ability of the surface of material to emit energy by infrared radiation [112]. It is basically the ratio between the amounts of energy radiated by an object to the amount of energy radiated by a black body. Different materials have different values of emissivity.

The emissivity of lactose was found using the International Standards Organization method (ISO 18434-1). The method involves using a material of known emissivity to measure the emissivity of an unknown material. In this study, electric PVC black tape was chosen, which has an emissivity value of 0.95. Part of a lactose ribbon was covered with the tape and then the whole ribbon was heated in an oven to 60°C. Thermal images were then taken using a thermal camera and the temperature of the tape was determined using an emissivity value of 0.95. The emissivity of the other part of the lactose ribbon was then adjusted until the same temperature as the tape was obtained; this is the emissivity of lactose which was 0.98.

A second approach was taken to determine the emissivity of lactose which involved a thermometer to obtain the actual temperature of the powder, which was then compared to the reading of the thermal camera. A hotplate was used to heat the powder to 60°C, and the surface temperature of the powder was obtained using the thermometer whilst

thermal images were taken by the camera. The temperature from the thermometer was then entered into the FLIR software to obtain the emissivity of lactose which was 0.98. The value of the emissivity obtained from the two methods agreed with each other.

4.5 X-ray tomography of the primary particles

The different manufacturing process of the different types of lactose is believed to result in particles with different morphology and porosity. X-ray tomography (Scanco Medical AG, Switzerland) was used to determine the porosity of the primary particles of the different types of lactose; the method is outlined in Section 3.2.11. The X-ray tomography can also be used to identify the morphology and the internal structure of the primary particles. Figures 4.10-4.12 show some X-ray images of particles of 200M, 21AN and SD lactose respectively. It can be seen that there is a significant difference in the internal structure of the primary particles among the three lactose powders. Figure 4.13 shows the porosity of the primary particles for the three types of lactose. It is very clear that the non-agglomerated type of lactose (200M) showed the lowest porosity (almost zero) compare to the agglomerated types (21AN and SD). The SD lactose particles exhibited the highest porosity. As mentioned in Section 3.1.1, particles of 200M lactose consist of single crystals due to the slow crystallisation of supersaturated solution of lactose during the manufacturing process of this type of lactose. This resulted in producing particles with zero or very low porosity as shown in Figure 4.13. However, spraying of a supersaturated solution of lactose on a roller drier resulted in particles of 21AN lactose which consist of small crystals aggregated in a compacted structure. The aggregated structure of lactose 21AN resulted in particles with higher porosity compare to 200M as shown in Figure 4.13. The SD lactose is produced by spraying a suspension of lactose in a spray dryer, which resulted in crystals of lactose agglomerated in a highly porous structure.

It is worth mentioning that crystals of 200M lactose are expected to have zero porosity due to the slow crystallisation of supersaturated solution of lactose. However, in Figure 4.13, it can be seen that 200M particles have a porosity of ~ 0.01 . This is believed to be due to the limitation of the X-ray machine to scan very small particles.

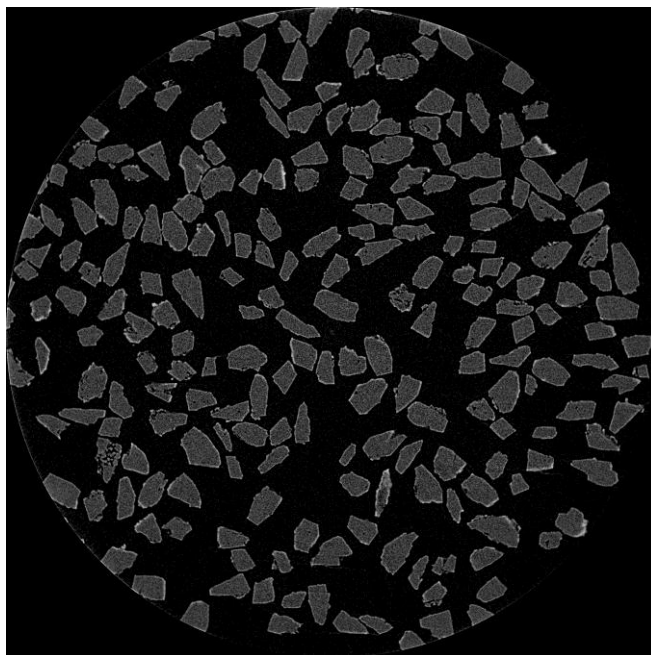


Figure 4.10: X-ray images of particles of lactose 200M.

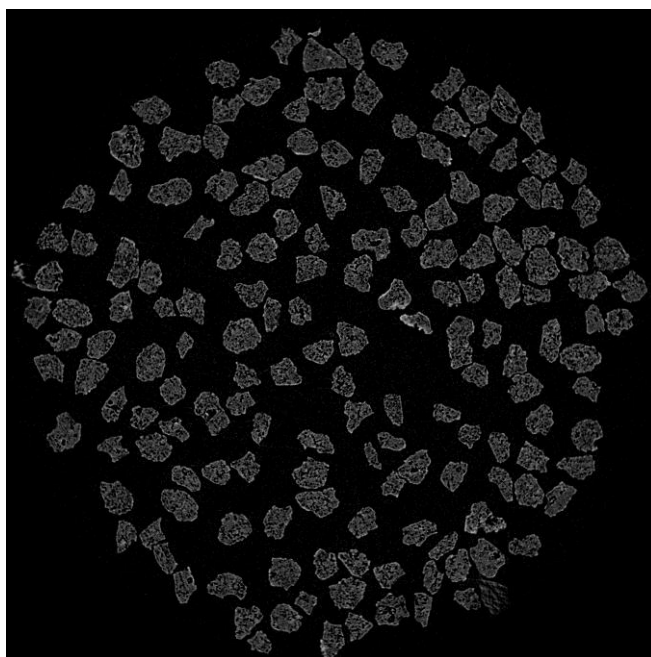


Figure 4.11: X-ray images of particles of lactose 21AN.

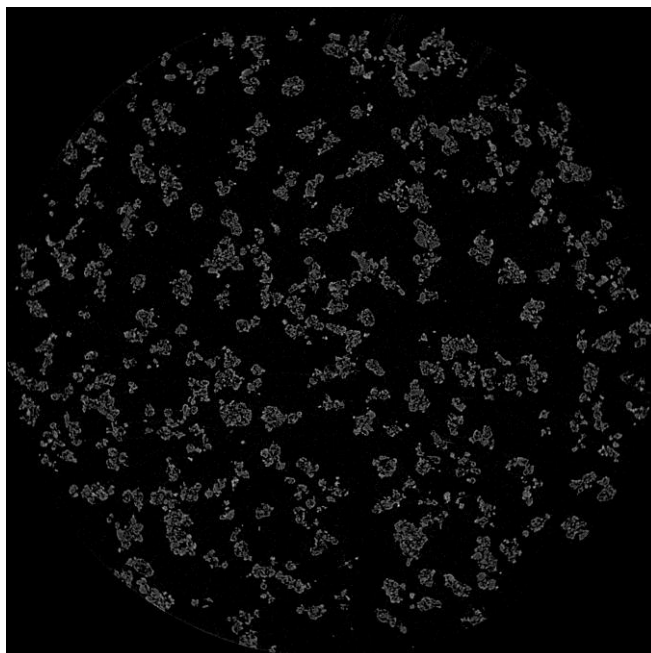


Figure 4.12: X-ray images of particles of lactose SD.

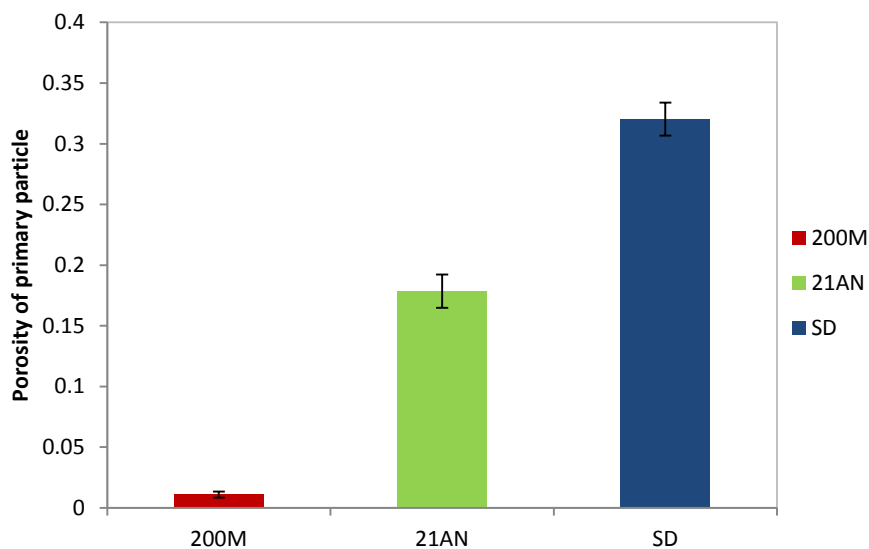


Figure 4.13: Porosity of the primary particles determined using X-ray tomography.

4.6 Single primary particle strength

The difference in the morphology and amorphous content of the primary particles, for the different types of lactose, is expected to have a significant effect on the particle strength. The strength of the primary particle for each type of lactose powder was measured using the Zwick-Roell testing machine. Figure 4.14 shows the Zwick-Roell setup which is used to measure the maximum force required to break a single particle.

Particles of size (212-300 μm) of each type of lactose were obtained by sieving using Retsch sieve shaker and used in the experiment. A single particle was placed on a transparent plate (8 mm thickness) which allowed the particle to be seen and recorded during the compression. The test was performed at the punch speed of 0.1 mm/min and the maximum force which the particle can resist before breakage was recorded. At least twenty particles were used for each type of lactose during the test and the average of them was presented. Figures 4.15- 4.17 show the force versus displacement curves of a single primary particle for the three types of lactose. It can be seen that the force increases gradually until it reaches maximum before the particle breaks then the force decreases suddenly. The maximum force at the breakage is different for the three types of lactose used. Particles of lactose 200M showed the highest force before the breakage, whereas lactose SD showed the lowest force.

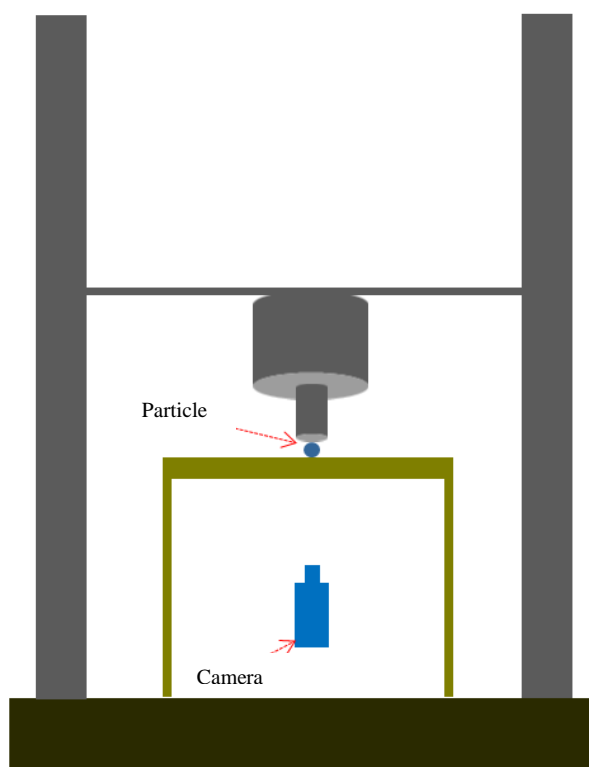


Figure 4.14: Zwick- Roell setup to measure the strength of a single primary particle.

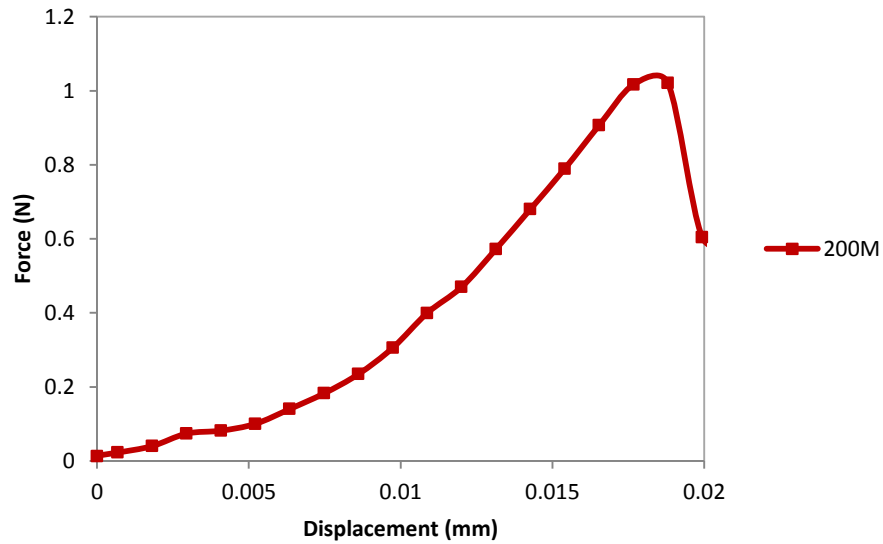


Figure 4.15: Force vs displacement curve for a single particle of 200M

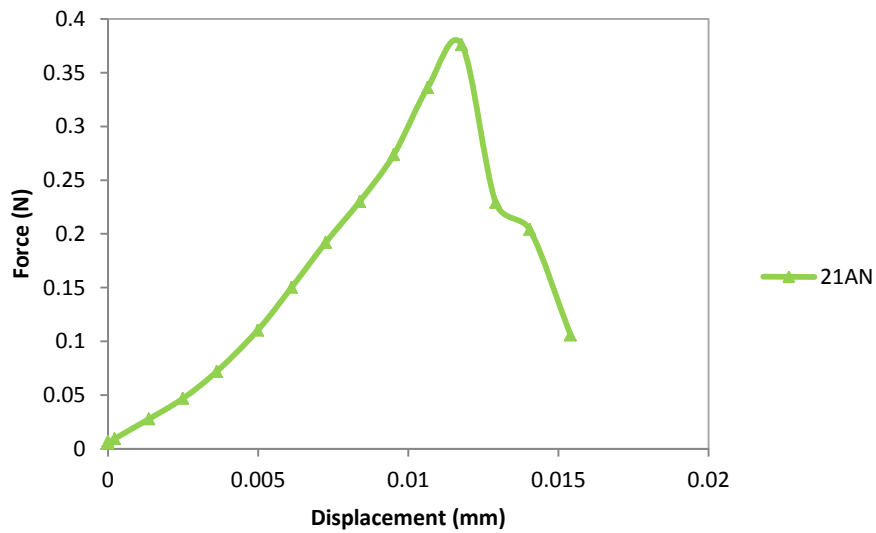


Figure 4.16: Force vs displacement curve for a single particle of 21AN.

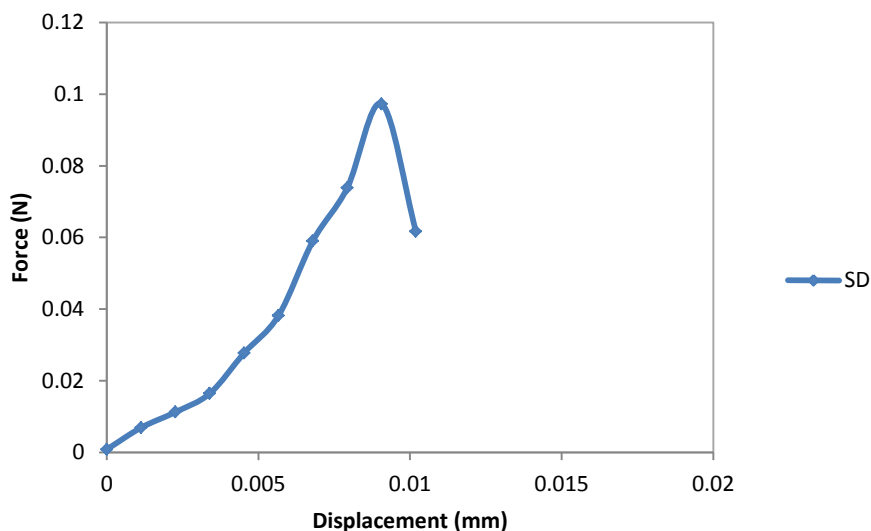


Figure 4.17: Force vs displacement curve for a single particle of SD

To be able to compare between the primary particles for the three types of lactose, the strength of the particles were determined. The strength of the particles was determined by dividing the maximum force recorded before breakage by the projection area of the particle, which was obtained from the camera. Figure 4.18 shows the average strength of the particle of each type of lactose. It can be seen that there is a significant difference in the strength of the primary particles between the different types of lactose.

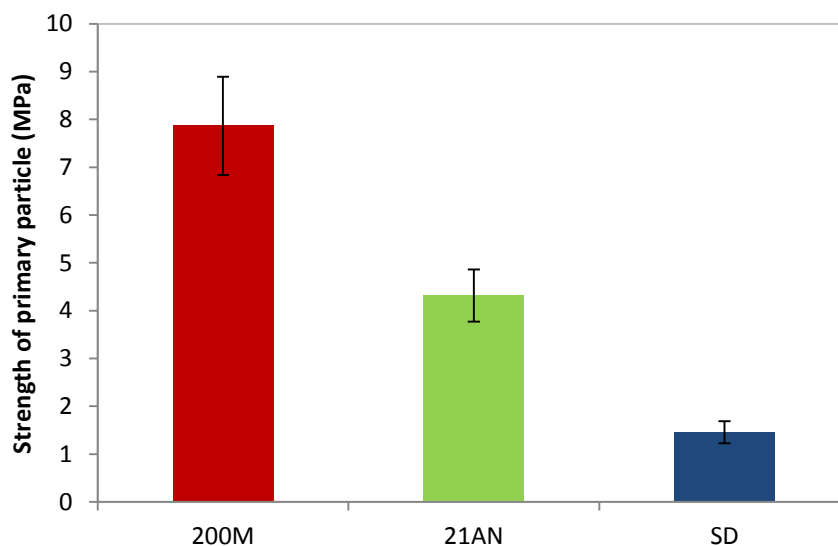


Figure 4.18: Strength of the primary particles of different types of lactose.

It is very clear that particles of lactose 200M showed the highest strength, whereas lactose SD exhibited the lowest strength. The difference in the strength of the primary particles of the powders is due to the difference in their morphology (internal structure). The agglomerated structure of particles of lactose 21AN and SD have a high porosity as shown in Figure 4.13, which then resulted in particles with low strength as shown in Figure 4.18. However, particles of lactose 200M are shown to have very low porosity (see Figure 4.13) due to their morphology as a single crystal, this was the reason of the high strength which was shown by particles of 200M as shown in Figure 4.18. This means that there is a relationship between the primary particle porosity and strength. Figure 4.19 shows the relationship between the primary particle porosity and strength for the three types of lactose. It can be seen that the higher the porosity of the primary particle the lower the strength of the particle.

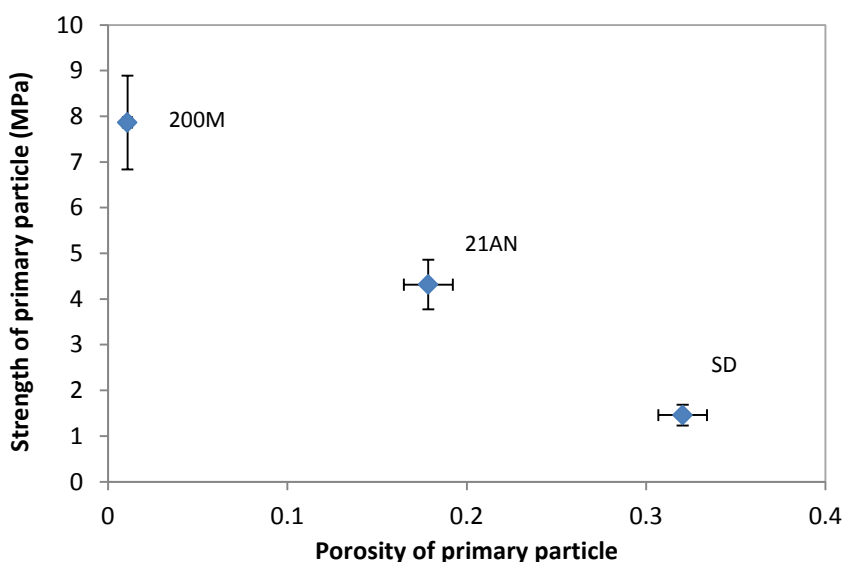


Figure 4.19: Relationship between the primary particle porosity and strength.

CHAPTER 5 EFFECT OF MORPHOLOGY AND AMORPHOUS CONTENT.

5.1 Introduction

The current chapter focuses on the investigation of the effect of the primary powder properties (morphology and amorphous content) on the roller compaction behaviour and ribbon properties [104]. Morphology is a property of a particle which describes the external feature and the internal structure of the primary particle including the size, shape, aspect ratio or crystal habit (plate, needle, equant, etc.). Particles can exist as a discrete entity or they associate with other particles in one structure. The bond of this association can be weak (i.e. agglomerate) or strong (i.e. aggregate) which then behaves as discrete particles. The morphology of the primary particle can have a significant effect on the behaviour of the powder during compression and on the compact properties. It affects the powder flowability, the packing behaviour and the consolidation during compression [9]. On the other hand, powders can exist in either crystalline or amorphous forms. Molecules in the crystalline material are highly organised and ordered with limited motion. The amorphous material, on the other hand, consists of disordered molecules or atoms which are distributed randomly in a matrix. During powder processing, e.g. compaction, different behaviour can be seen from these two types of material, due to their different structure [18, 113].

Three types of lactose powders were used; anhydrous SuperTab21AN, α -lactose monohydrate 200M, and spray dried lactose SuperTab11SD. The three lactose powders have different morphologies (internal structure) and contain different amount of amorphous lactose as illustrated in Chapter 4. The study in this chapter includes an online monitoring of ribbon temperature during roller compaction using the thermal camera. This is aimed to further understanding the behaviour of different lactose powders, and gain more information on the mechanisms taken place during roller compaction. Furthermore, the effect of the primary particle properties (morphology and amorphous content) on ribbon properties (tensile strength and porosity of the ribbon, fragment size distribution, the percentage of fines and ribbon structure) was also

examined. The properties of the ribbon produced from the different types of lactose will be correlated to the primary powder morphology and amorphous content.

5.2 Preparation of powders

As mentioned earlier in Section 4.1, the particle size distribution of the three types of lactose is different. In order to reduce the difference in the primary particle size and also reduce the effect of the primary particle size on the ribbon properties, all the lactose types were sieved. A sieve shaker (Retsch Technology, Germany) was used to sieve all types of lactose using an amplitude of 2 mm for 5 minutes. For all powders, a size class between 125-212 μm were chosen and used in the experiments.

After sieving, all powders with the same size class were conditioned in the climatic chamber to reduce the effect of powder moisture content on the product properties. Powders were stored in the chamber for equilibration at 20% RH and 25°C which was observed after 3 days as outlined in Section 4.3.1.

5.3 Scanning electron microscopy (SEM) of the primary powder

Figure 5.1 shows images of the primary powders using scanning electron microscopy at different magnification. It can be seen that different types of lactose have different morphologies, due to different manufacturing processes. Anhydrous lactose SuperTab21AN is produced from the crystallisation of a supersaturated solution of lactose above 93.5°C by roller drying; this crystallisation results in the aggregation of lactose microcrystals [33, 92] and produces anhydrous lactose with a rough surface as shown in Figure 5.1 (A and B). The slow crystallisation of a supersaturated lactose solution below 93.5°C results in single crystals of α -lactose monohydrate 200M. Crystals of α -lactose monohydrate are very hard and brittle with tomahawk-like shape [92] as illustrated in Figure 5.1 (C and D). Spray dried lactose SuperTab11SD is produced by spray drying a suspension of α -lactose monohydrate in a solution of lactose. Because of the very fast drying process, the product consists of small particles of α -lactose monohydrate connected with amorphous lactose [92]. Figure 5.1 (E and F) shows the spray dried lactose particles. It can be seen that particles of spray dried

lactose are more spherical than those of α -lactose monohydrate and anhydrous SuperTab21AN.

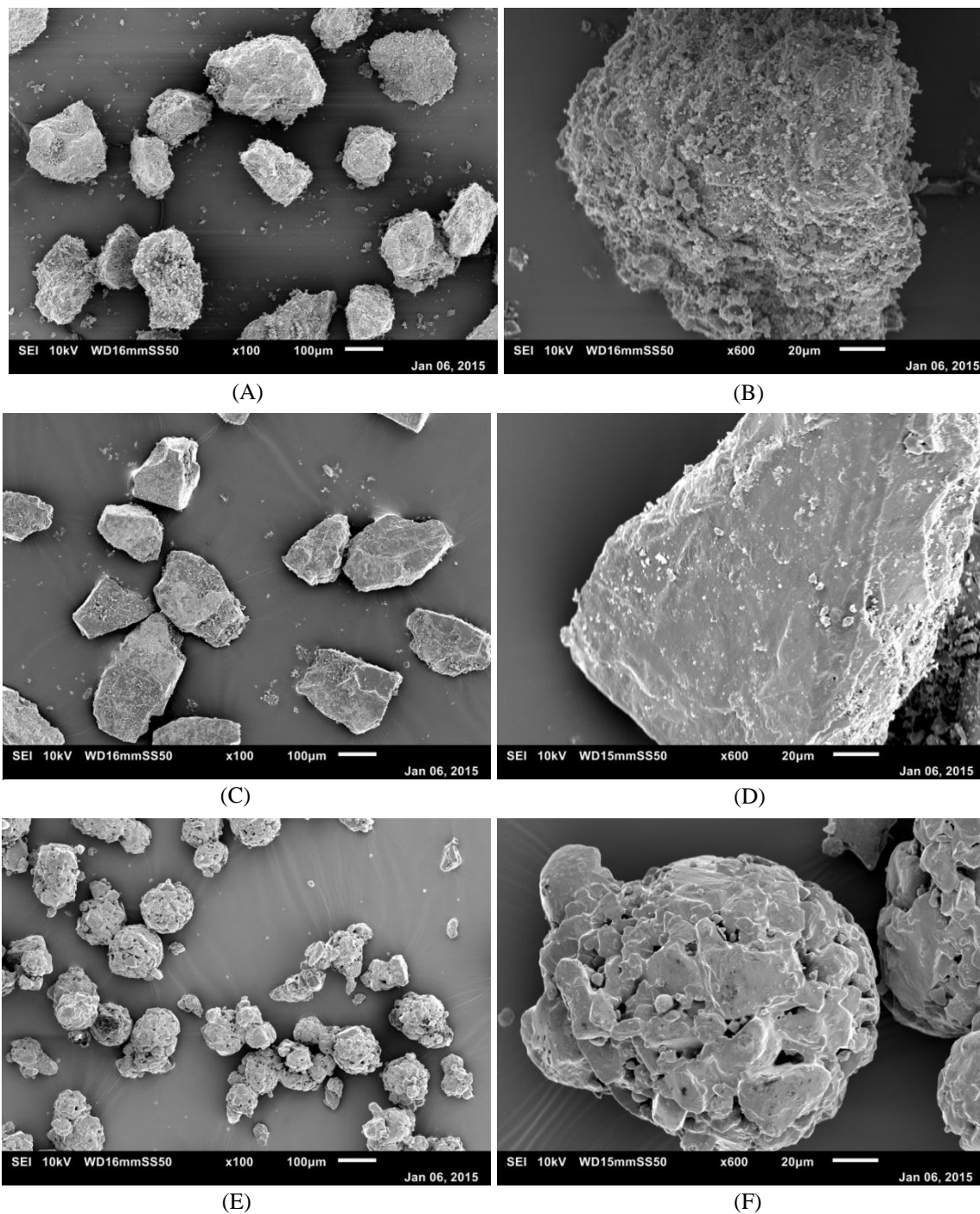


Figure 5.1: Scanning Electron Microscope images of sieved powders: 21AN (A, B), 200M (C, D), SD (E, F) at 100 \times magnifications (A, C, E) and 600 \times (B, D, F).

5.4 Production of ribbon

The powders were compressed into ribbons using an Alexanderwerk WP120 (Alexanderwerk, Germany) roller compactor, more details about the equipment can be found in Section 3.2.7. Hydraulic pressure of 30-100 bar range was used to compress the lactose powder and produce ribbon. The speed of the roller was kept constant at 3 rpm. The gap between the two rollers was also kept constant at 3 mm using the feedback system, which adjusts the feeder screw speed with changing the hydraulic pressure, to maintain a constant gap.

To eliminate the effect of humidity in the laboratory on the powder relative humidity a GenRH-A (London, UK) humidity generator was connected to the top of the hopper on the roller compactor as shown in Figure 3.6. The humidity generator was operated at the same conditions as the climatic chamber (20% RH); this ensured a constant humidity condition of the powder during roller compaction same as that used for the storage of the powder prior to compaction.

5.5 Effect of morphology and amorphous content

5.5.1 Stress applied on the powder during roller compaction

The maximum normal stress applied to the powder during the roller compaction can be determined theoretically using the mathematical model proposed by Johanson [7]. More details about Johanson's mathematical model can be found in Section 2.5.1. The model uses the roller dimensions (width, diameter), the gap between the two rolls and the material physical properties to predict the stress acting on the material during roller compaction. The main three physical properties used in the model are the effective angle of internal friction (δ), the angle of wall friction (ϕ_w) and the compressibility factor (K).

The effective angle of internal friction (δ) and the angle of wall friction (ϕ_w) were obtained for the three type of lactose using the shear cell tester RST-XS.s (Dr. Dietmar Schulze, Germany) as outlined in Section 3.2.5.1. The compressibility factor (K) can be obtained from the relationship between the uniaxial stress σ and the resulting bulk density using Equation 2.1 [7]. Powders of the same size class (125-212 μm),

conditioned in the chamber at 20% RH and 25°C, were compressed in a 12 mm die using Instron testing machine (Instron 3367- USA) as described in Section 3.2.6.

$$\frac{\sigma_1}{\sigma_2} = \left(\frac{\rho_1}{\rho_2}\right)^K \quad 2.1$$

The data of the effective angle of internal friction(δ), the angle of wall friction (ϕ_w) and the compressibility factor (K) for the three types of lactose are summarised in Table 5.1.

Table 5.1: Material friction properties and compressibility factor for different types of lactose, each measurement was repeated at least 6 times.

Powder type	Effective angle of internal friction(δ) (degrees)	Angle of wall friction (ϕ_w) (degrees)	Compressibility factor (K)
SuperTab21AN	37 ± 0	17.2 ± 0.49	7.6 ± 0.04
α -lactose monohydrate 200M	41.7 ± 0.49	20.7 ± 1.57	14.6 ± 0.04
SuperTab11SD	36.1 ± 0.38	16.4 ± 0.53	6.7 ± 0.03

The powder friction properties, the effective angle of internal friction(δ) and the angle of wall friction(ϕ_w), along with the powder compressibility factor (K) and the roller dimensions and settings were used to determine the nip angle. The nip angle is the angular position at which the powder transit from slip to the nip region and it is required for the maximum normal stress calculation in Johanson's theory [7]. The nip angle can be calculated by equating the pressure gradient equations for both the slip and the nip regions as shown in Equation 2.7. The calculations were carried out in MATLAB version R2014a. Table 5.2 shows the nip angle for the different types of lactose. It can be seen that the nip angle is different for various type of lactose due to the difference in the powder friction properties and compressibility factor as shown in Table 5.1.

$$\frac{4\left(\frac{\pi}{2} - \alpha - \nu\right) \tan \delta}{\frac{D}{2} \left[1 + \frac{S}{D} - \cos \alpha\right] [\cot(A - \mu) - \cot(A + \mu)]} = \frac{K \tan \alpha \left(2 \cos \alpha - 1 - \frac{S}{D}\right)}{\frac{D}{2} \left[\frac{d}{D} + \left(1 + \frac{S}{D} - \cos \alpha\right) \cos \alpha\right]} \quad 2.7$$

Table 5.2: Nip angle for the three types of lactose calculated using Equation 2.7.

Powder type	Nip angle (degrees)
SuperTab21AN	8.64
α -lactose monohydrate 200M	7.62
SuperTab11SD	8.73

Once the nip angle has been calculated, it can then be used to find the maximum normal stress applied on the powder during roller compaction using Equation 2.8 [7], having the roller force provided.

$$R_F = P_m W D F / 2 \quad 2.8$$

where R_F is the roll force, P_m is the maximum normal stress applied on the powder at the minimum gap, W and D are the roller width and diameter. The constant F was calculated from Equation 2.9 which was solved using the trapezoidal numerical integration function in MATLAB.

$$F = \int_{\theta=0}^{\theta=\alpha} \left[\frac{(d + S)/D}{d/D + (1 + S/D - \cos \theta) \cos \theta} \right]^K \cos \theta d\theta \quad 2.9$$

The roller force at different hydraulic pressure was provided by the manufacturer Alexanderwerk. Table 5.3 shows the relationship between the hydraulic pressure and the force applied by the roller.

Table 5.3: The conversion between the hydraulic pressure and the roller force provided by Alexanderwerk.

Hydraulic pressure (bar)	Roller force (KN)
30	12.44
50	20.74
80	33.17
100	41.47

The roller dimensions (width and diameter) along with the roller force in Table 5.3 were used to determine the maximum normal stress applied on the powder during roller compaction using Equation 2.8.

Table 5.4 show the maximum normal stress applied on the three types of lactose during the roller compaction at different hydraulic pressure. It can be seen that the maximum stress applied to the powder is different for the three types of lactose. Although the same hydraulic pressure was used during the roller compaction, the maximum stress applied to the non-agglomerated type of lactose (200M) was higher in comparison with the agglomerated lactose (21AN and SD). This is due to the difference in the primary powder properties (for example morphology and amorphous content). The maximum stress applied on the powder, calculated from Equation 2.8, is highly dependent on the powder compressibility factor K . The non-agglomerated structure of lactose 200M particles resulted in lower compressibility of the powder as shown in Table 5.1 (the higher the value of the compressibility factor K the lower the compressibility of the powder [7]). The low compressibility (high compressibility factor K) of lactose 200M resulted in an increase in the stress applied to the powder due to the resistance of the powder to the densification process. This is confirmed by the finding in Figure 4.18, which shows that particles of the non-agglomerated types of lactose (200M) require higher stress to break in comparison with the agglomerated type of lactose.

Table 5.4: Maximum normal stress applied to different types of lactose at different hydraulic pressure.

Hydraulic pressure (bar)	Maximum normal stress (MPa)		
	α -lactose monohydrate 200M	SuperTab21AN	SuperTab11SD
30	76.22	56.24	53.82
50	127.09	94.24	89.73
80	203.26	150.73	143.52
100	254.12	188.45	179.43

The agglomerated types of lactose (21AN and SD) are more compressible (lower values of compressibility factor K) in comparison to lactose 200M as shown in Table 5.1. This is due to their morphology as particles of the agglomerated types of lactose consist of small crystals aggregated in one structure (see Figure 5.1) which is easier to disassemble or break compare to the non-agglomerated lactose as shown in Figure 4.18. The high compressibility of the agglomerated type of lactose resulted in less stress being applied during the roller compaction as the powder is less resistant to the densification process. On the hand, the SD lactose has higher compressibility compared to the 21AN lactose which resulted in lesser stress being applied to the powder during the roller compaction. This is due to the fact that the SD lactose contains 10.32 % of amorphous lactose in a highly porous structure which affects the powder compressibility and, consequently, the stress applied during roller compaction.

5.5.2 Surface temperature and strength of the ribbon

The surface temperature of the ribbon was recorded using FLIR A655sc thermal camera. The setup of the online thermal camera is shown in Section 3.2.8.

Figure 5.2 shows a series of the thermal images taken for the three types of lactose during production at different hydraulic pressures. The lighter the colour in the image, the higher the temperature of the ribbon which is shown in the colour- temperature scale. It can be seen that the temperature of the ribbon is different for the three types of lactose and different hydraulic pressure.

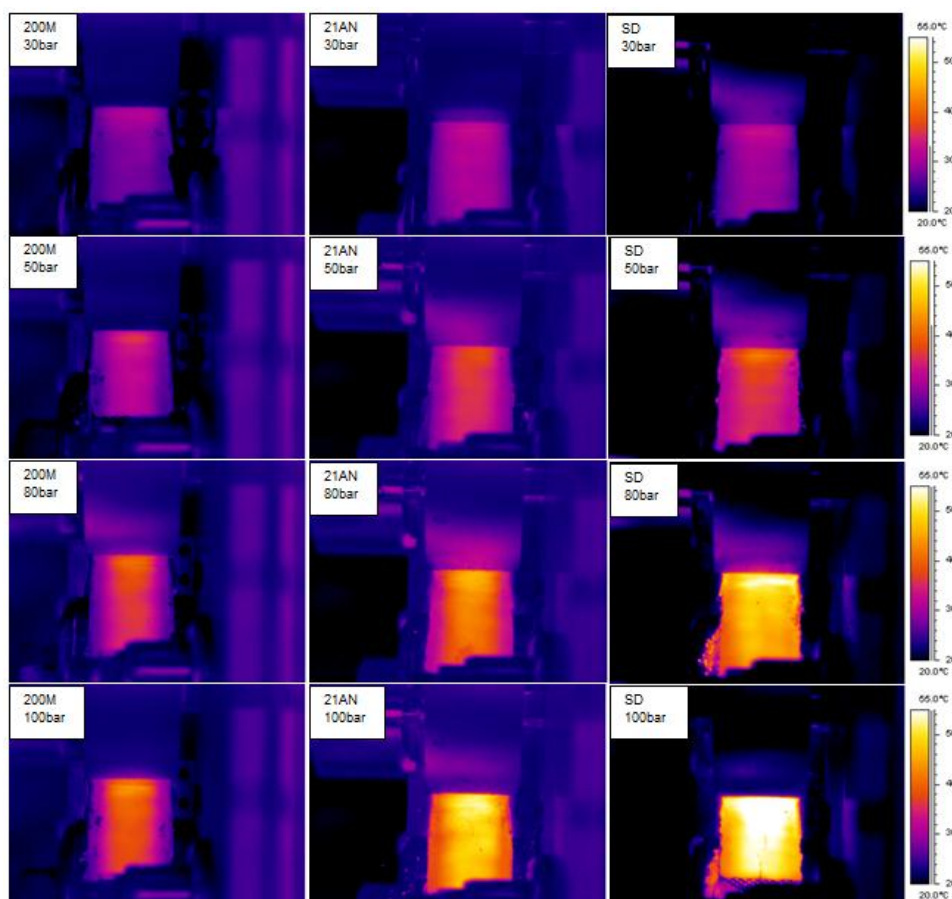


Figure 5.2: Thermal images of the three types of lactose at different compaction pressure.

The thermal images were analysed using FILR R&D software to determine the maximum temperature of the ribbon. Figure 5.3 shows the maximum temperature of ribbons during roller compaction for the three types of lactose. For all powders, the temperature of ribbon increased with increasing hydraulic pressure. Increasing the pressure increases the force and stress applied by the rollers on the powder. This brings the particles closer to each other, and increases their interaction and internal friction, therefore, increasing the surface temperature of the final ribbon [104]. This result is in agreement with what has been concluded in the literature using maltodextrin powder [51].

It can be seen that at low hydraulic pressure, there were very small differences in the surface temperature of ribbons produced from different types of lactose. While at high hydraulic pressure, the highest temperature recorded was for ribbons produced from the spray dried (SD) lactose, which contains the highest amorphous fraction (10.32%). Ribbons produced from monohydrate lactose 200M showed the lowest temperature. The

temperature of ribbon produced from anhydrous lactose (21AN) was lower than that of spray dried lactose (SD) and higher than that of α -lactose monohydrate 200M.

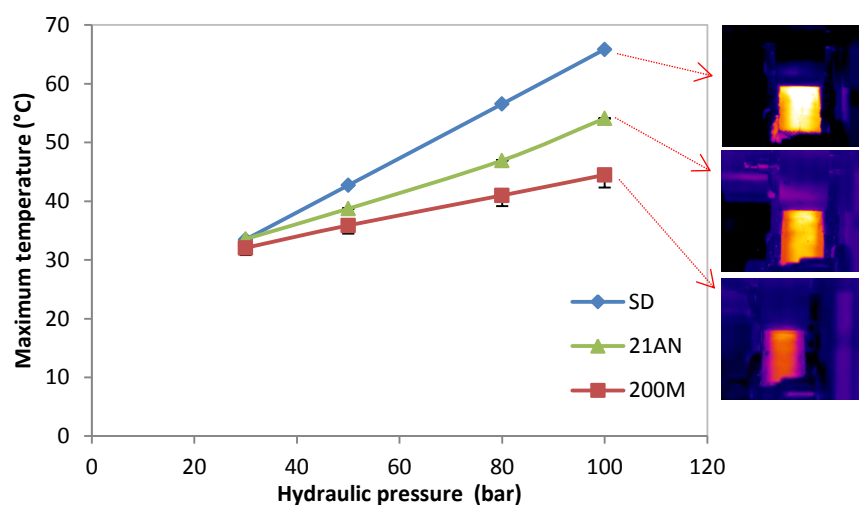


Figure 5.3: Ribbon maximum temperature at different hydraulic pressures.

The maximum force needed to break the ribbons and the tensile strength of all ribbons was determined using the three point bend test as mentioned in Section 3.2.10. Figure 5.4 shows the maximum force required to break ribbons produced from different types of lactose at different hydraulic pressures. The tensile strength of ribbon was determined by considering the maximum force, width and thickness of ribbon using equation 3.3. Figure 5.5 shows the tensile strength of ribbons produced at different hydraulic pressure using the three types of lactose. For all types of lactose, the force needed to break the ribbons and the tensile strength increased with increasing the hydraulic pressure. At low hydraulic pressure, 30 bar, there was a very small difference in the tensile strength for the different types of lactose. However, this difference increased with increasing the hydraulic pressure, and the biggest difference in strength between the different types of lactose was at 100 bar.

In Figure 5.4 and Figure 5.5 it can be seen that at high hydraulic pressure, the highest force and tensile strength recorded was for ribbons produced from the spray dried lactose (SD), which has the highest amorphous content (10.32%). The lowest force and tensile strength ribbon were obtained for α -lactose monohydrate 200M. The tensile strength of the ribbons produced from the anhydrous lactose (21AN) was lower than those of spray dried lactose (SD) and higher than those of α -lactose monohydrate 200M.

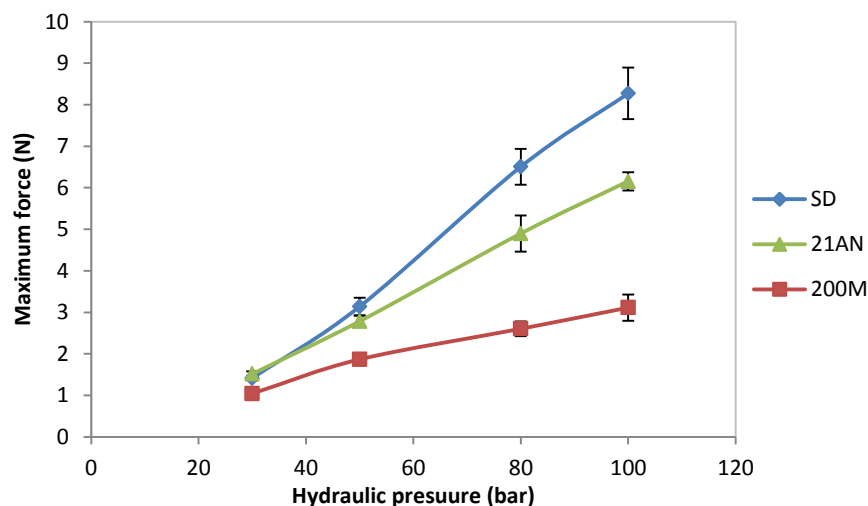


Figure 5.4: The Maximum force required to break ribbons produced from different types of lactose.

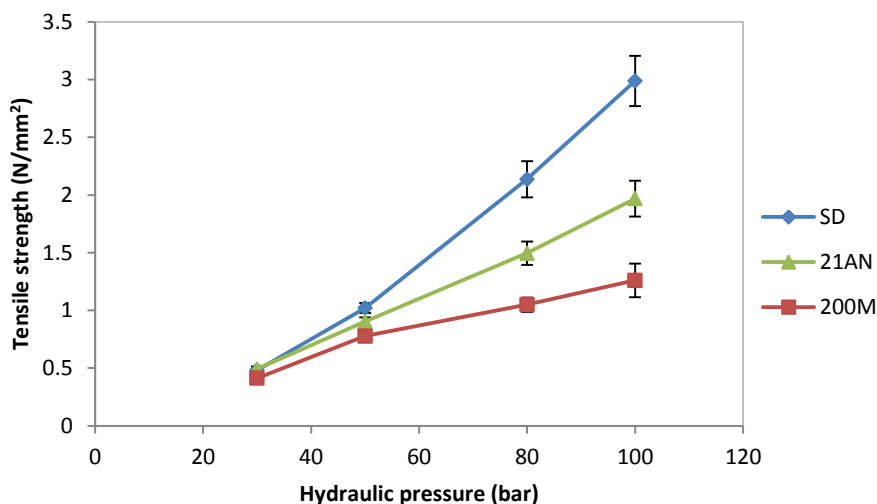


Figure 5.5: Tensile strength of ribbons produced from different types of lactose.

Ribbons from different types of lactose were also milled using the ball mill method. This method involves milling a sample of ribbon using a ball mill and then determine the fragment size distribution; a stronger ribbon gives a larger fragment size. A Retsch Planetary Ball Mill PM 100 (Retsch, Germany) was used to mill the ribbons, using three balls of 30 mm diameter in a 500 ml agate jar. For all types of lactose, only 2 g of ribbon was milled in the ball mill using same conditions. Ribbons were milled at a rotational speed of 215 rpm for 25 s [104]. The fragments produced from the ribbon after ball milling were analysed for their size using a QICPIC (Sympatec, Germany). This is an optical sizing technology provided with a high speed camera with a frequency

of up to 450 fps. The whole process was repeated at least five times for each ribbon produced under different conditions and from different types of lactose.

Figure 5.6, Figure 5.7 and Figure 5.8 show the cumulative size distribution of fragments from ribbons produced at different hydraulic pressures using 200M, SuperTab21AN and SuperTab11SD respectively. For all powders, the fragment size increased with increasing the pressure during production of the ribbons. This is represented by the shift of the curves from left to right. This indicates that ribbons produced at high pressure were stronger and, therefore, produced larger fragments. The fragment size distribution is different for the three types of lactose. The shift of the curves from left to right, with increasing the hydraulic pressure, is very small for the 200M. This indicates that the ribbons were weak even at a high pressure in comparison to the other two types of powder. For SD lactose, there is a big difference in the fragment size distribution of ribbon produced at different hydraulic pressure. The greater shift of the curve from left to right for the SD, compare to the other types of lactose, is a signature of stronger ribbon which resisted more during ball milling and resulted in larger fragment size.

The result of the fragment size distributions, for ribbons after milling, is in agreement with the result from the three point bend test, Figure 5.5, in that ribbon tensile strength increased with increasing hydraulic pressure. Increasing the hydraulic pressure increases the force and stress applied by the two rollers on the powder, which brings the particles close to each other and increases the bonding strength and, therefore, increases the tensile strength of the final ribbon. This result is in agreement with what has been concluded in the literature for maltodextrin powder [51].

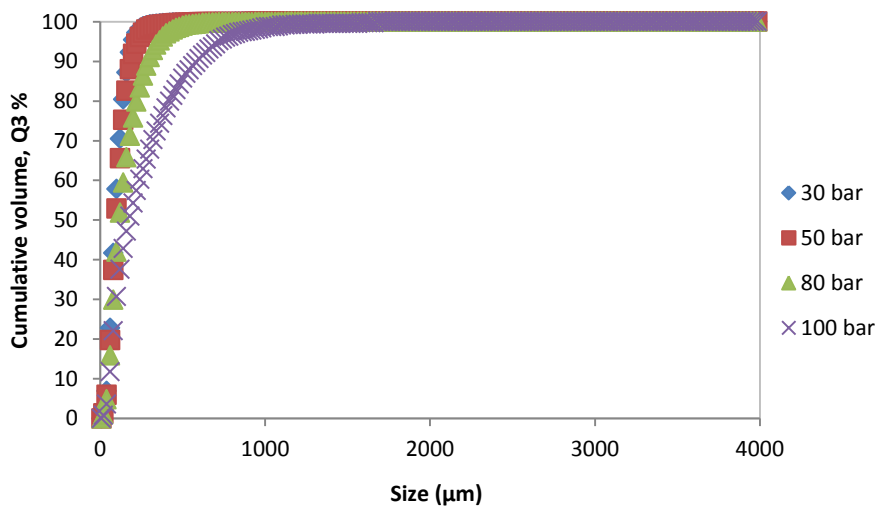


Figure 5.6: Cumulative size distribution of fragments of ribbons produced from α -lactose monohydrate 200M.

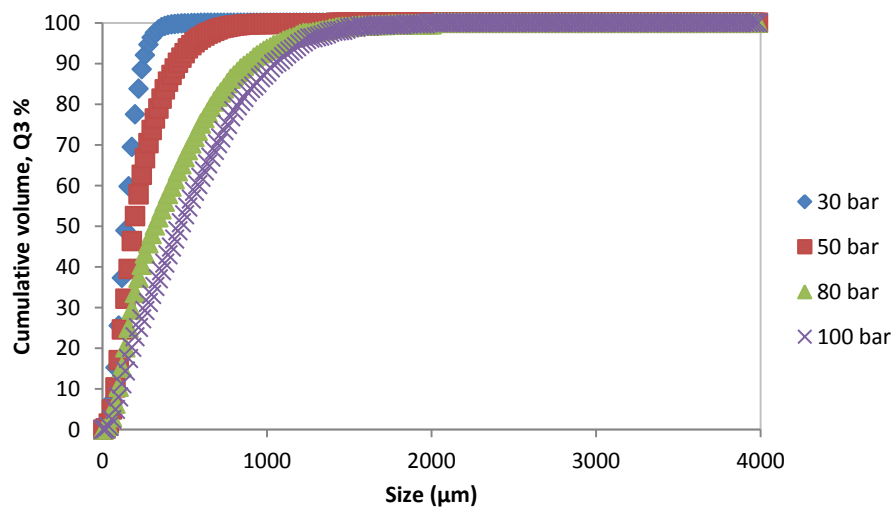


Figure 5.7: Cumulative size distribution of fragments of ribbons produced from anhydrous lactose SuperTab21AN.

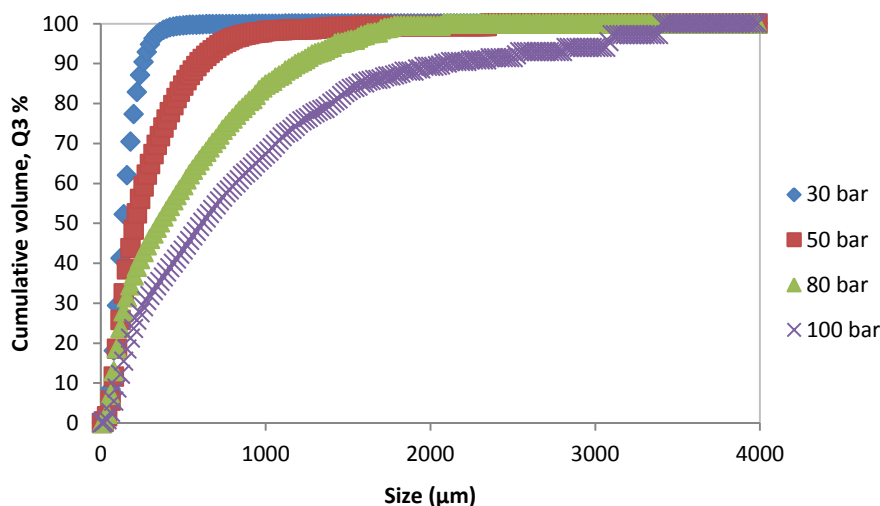


Figure 5.8: Cumulative size distribution of fragments of ribbons produced from spray dried lactose SuperTab11SD.

From the fragment size distribution, the fragment size (d_{50}) values at each hydraulic pressure and for all types of lactose were determined. Figure 5.9 shows the fragment size, d_{50} , of ribbons produced at different hydraulic pressure using the three types of lactose. It can be seen that fragment mean size increased with increasing the hydraulic pressure for all types of lactose. It can also be seen that at high hydraulic pressure, the larger d_{50} recorded was for ribbons produced from the spray dried lactose (SD), which has the highest amorphous content. Ribbons produced from anhydrous lactose (21AN) showed smaller fragment size d_{50} compared with the spray dried lactose. The smallest d_{50} was obtained for α -lactose monohydrate 200M. At low hydraulic pressure, there was a very small difference between the d_{50} of fragments of different types of lactose.

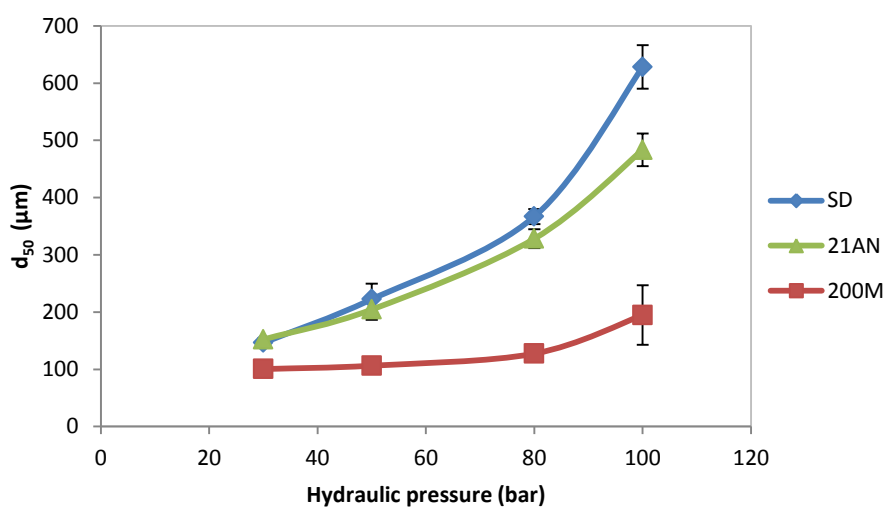


Figure 5.9: Fragment size of ribbons produced from different types of lactose.

The properties of the ribbon produced from the three types of lactose were different at different hydraulic pressure. At high hydraulic pressure, ribbon tensile strength (Figure 5.5) and fragment size (d_{50}) (Figure 5.9) were different for the three types of lactose. Ribbon surface temperature, recorded by the thermal camera, was also different for the lactose powders (Figure 5.3). SD lactose produced ribbons with the highest tensile strength, the highest temperature and the largest fragment size. Ribbons from the 200M showed the lowest strength, temperature and fragment size. These differences in properties of the ribbons of three types of lactose are due to the difference in the primary particle morphology (see Figure 5.1) and also to the difference in the amount of amorphous lactose present in the powders.

From the SEM images of the primary powders, shown in Figure 5.1, it can be seen that particles of 21AN consists of very small particles aggregated together in a compacted structure, 200M are single crystals and SD consists of small particles of lactose agglomerated in a highly porous structure (see Figure 4.13). Therefore, 21AN and SD can be considered as an agglomerated type of lactose, whereas the 200M is a non-agglomerated type of lactose.

In tableting, it has been reported that the main mechanism of consolidation in crystalline lactose is the fragmentation of the material [33, 114]. On the other hand, amorphous lactose was found to show more plastic deformation upon compression than crystalline lactose [21]. Therefore, the consolidation mechanism is different for the three types of lactose used in this study. The consolidation mechanism in crystalline 21AN lactose is mostly fragmentation of the aggregated structure of the particle. The single crystal of 200M is expected to show a limited amount of fragmentation due to the brittle fracture in addition to a small degree of plastic deformation by the amorphous fraction present. The porous structure of the SD particles has a significant effect on the powder consolidation mechanism during compaction. The structure of SD particle is believed to be disassembled to small crystals which will show further breakage upon applying an additional load, as well as plastic deformation due to the presence of the amorphous lactose [104].

Comparing the agglomerated form (21AN and SD) with the non-agglomerated form (200M), the high values of the tensile strength of the ribbon (Figure 5.5), surface temperature (Figure 5.3) and d_{50} (Figure 5.9) produced from the agglomerated form is

due to the morphology of the particles which is shown in the SEM images in Figure 5.1 [104]. The morphology of the primary particle of different types of lactose affects the single particle strength as shown in Section 4.6. Figure 4.18 shows the strength of the primary particles for the three types of lactose. It can be seen that there is a significant difference in the single particle strength of the different types of lactose. Particles of lactose 200M require the highest stress to break, whereas the structure of SD particle breaks down at the lowest stress in comparison with the other types of lactose. This means that at the same hydraulic pressure during roller compaction, the degree of fragmentation will be small for lactose 200M, high for lactose 21AN and the highest for lactose SD. Increasing the fragmentation of the particles during compaction results in an increase in the amount of the small particles, therefore, the number of the contact points will increase. The increase in the number of contact points between the small fragments and a decrease in the distance between them results in an increase in the Van der Waals forces [19]. This will result in a stronger bond between the particles and leads to a stronger ribbon. The strength of the ribbon after roller compaction can be related to the strength of the primary particles of each type of lactose. Figure 5.10 shows the relationship between the strength of the primary single particles and the tensile strength of the ribbon after roller compaction. It can be seen that the strength of the primary particle has a significant effect on the ribbon tensile strength; the lower the strength of the primary particles the higher the tensile strength of the produced ribbon (Figure 5.10). This could be then related to the morphology and the internal structure (porosity) of the primary particles and also to the different percentage of amorphous lactose present in the powder which resulted in different behaviour during compaction.

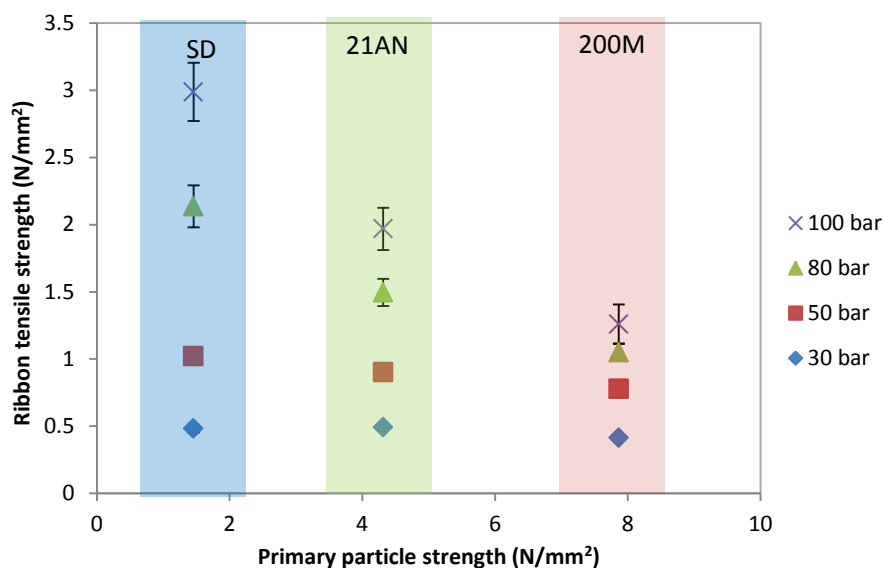


Figure 5.10: Relationship between the primary particle strength and ribbon tensile strength.

The higher temperature shown by the ribbons produced from the agglomerated forms of lactose is due to the fact that increasing the fragmentation of the material increases the amount of friction between the fragmenting particles, which increases the temperature of the ribbon during production.

The highest tensile strength of the ribbon (Figure 5.5), the highest temperature (Figure 5.3), and the larger fragment size (Figure 5.9) shown by the ribbons of SD lactose (compared with 21AN) is due to the morphology and the high amorphous content of the SD which had an effect on the compaction properties [104]. The amorphous lactose is believed to act as a binder and show more plastic deformation during compaction. This results in a larger bonding area and stronger bonds between particles, and consequently, a stronger ribbon when compared to the other two types of lactose. In tableting, it was found that spray dried lactose showed better binding capacity, and this was suggested to be due to the presence of an amorphous layer on the particle surface which acted as a binder during tablet production [21]. This was not the case with the 200M (2.67 % amorphous), which is due to the particle morphology of the powder as it is a non- agglomerated form of lactose (single crystal) as shown in the SEM images in Figure 5.1. In addition, the amorphous content was low in this type of lactose which may not improve the binding properties compared to the SD lactose.

At low hydraulic pressure (30 bar), there are very small differences in the tensile strength (Figure 5.5), temperature (Figure 5.3) and fragment size d_{50} (Figure 5.9) of

ribbons produced from the different types of lactose. This is due to the limited breakage and deformation of the primary particles as a result of insufficient operating pressure (applied by the rollers) [104]. In addition, the operating pressure was insufficient to significantly cause plastic deformation of the amorphous form of lactose present within the powders, which was causing the increase in strength of the ribbon produced from the SD lactose. It is believed that particle rearrangement is happening with a limited degree of fragmentation and deformation while compressing powders at low hydraulic pressure [13].

From Figure 5.3 and Figure 5.5, it can be noticed that there is a relationship between the tensile strength and surface temperature of the ribbon during production. Ribbon which showed higher temperature during production exhibited higher tensile strength. The SD lactose showed the highest temperature during production, therefore, it produced the strongest ribbon. Figure 5.11 shows the relationship between the maximum surface temperature of the ribbon during production and the tensile strength of the produced ribbon. It can be seen that the higher the temperature during roller compaction the higher the tensile strength of the ribbon. This means that the information from the online thermal camera can be used to predict the tensile strength of the produced ribbon regardless the types of the lactose used.

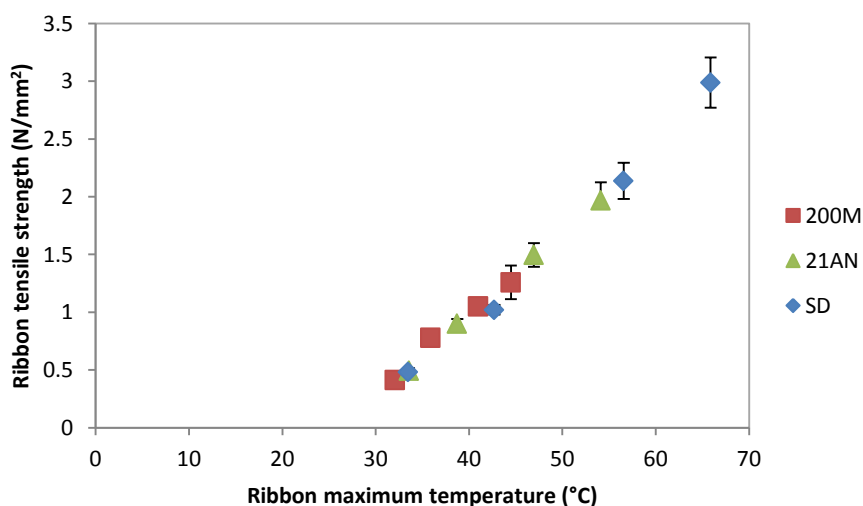


Figure 5.11: Relationship between ribbon temperature during production and ribbon tensile strength.

5.5.3 Scanning electron microscopy (SEM) for Ribbons

Figure 5.12 and Figure 5.13 show the SEM images of ribbons produced from anhydrous lactose SuperTab21AN, α -lactose monohydrate 200M, and spray dried lactose SuperTab11SD at 100 bar and 30 bar respectively. Images were taken at two different magnifications, low (100x) and high (600x). Ribbons were produced at the same operating conditions in the roller compactor 3 mm gap and 3 rpm roller speed. In addition, all powders were in the same size class and conditioned at the same relative humidity and temperature. It can be seen from Figure 5.12 that the ribbon structure is different for different types of lactose. Lactose 21AN and SD produced ribbons with a large amount of small fragments (Figure 5.12, A, B, E and F). The amount of small fragments is less in α -lactose monohydrate ribbon. The large amount of small fragments indicates a higher degree of fragmentation happened during compaction. The small amount of small fragments exhibited by the ribbon of 200M (Figure 5.12, C and D) indicates the lesser degree of fragmentation during compaction. This is in agreement with the finding in Figure 4.18, in that particles of lactose 200M requires the highest stress to break in comparison to the other types of lactose. Ribbons produced from the SD lactose (Figure 5.12, E and F) showed different features in comparison to other types of lactose. The surface of the SD ribbon was flatter and smoother compared to the surface of ribbon produced from the other two types of lactose. This was due to the presence of high amount of amorphous form in the SD lactose, which showed more plastic deformation upon compaction and resulted in flatter surfaces [104].

An increase in the temperature of amorphous powder results in softening the powder due to an increase in the free volume at the single particle level. Above the glass transition temperature, the free volume increases significantly, and the material transforms from its glassy state to the rubbery state. The increase in the free volume of the material increases the mobility of the molecules within the powder. This will help the atoms or molecules to diffuse into the gap between two particles and form bridges between each other [19, 51, 115]. This process is known as sintering, which may be occurring with the SD lactose and resulting in a stronger ribbon.

The temperature of the ribbon shown in Figure 5.3 was recorded during production at the exit of the roller, beyond the compaction zone. The temperature of the ribbon produced from the SD lactose at 100 bar is close to 70°C and this is outside the

compaction zone. It is believed that the temperature of the ribbon between the two rollers was much higher than that recorded by the thermal camera. The onset glass transition temperature of amorphous lactose is above 70°C which was measured using Differential Scanning Calorimetry (METTLER TOLEDO, Switzerland) at a heating rate of 10°C/min (see Figure 4.2). It is believed that the temperature of the ribbon in the compaction zone was in the same range as the glass transition temperature of amorphous lactose. This was the reason for the initiating the sintering process in the SD lactose and produce bridges between the particles. This is supported by the SEM images of the ribbon shown in (Figure 5.12, E and F) which illustrates that the ribbons produced from the SD lactose at 100 bar have smoother and flatter surfaces in comparison to the surface of the ribbons of the other types of lactose. The flat and smooth surface shown by these ribbons are believed to be due to the plastic deformation of the powder, which increased the temperature and initiated the sintering process between the particles [104].

Figure 5.13 shows some SEM images of ribbons produced from the different types of lactose at 30 bar. It confirms that there is little or no difference in the surface features of the ribbon for the three different types of lactose. This was, as mentioned before, due to the limited breakage and deformation of the primary particles as a result of insufficient operating pressure (30 bar).

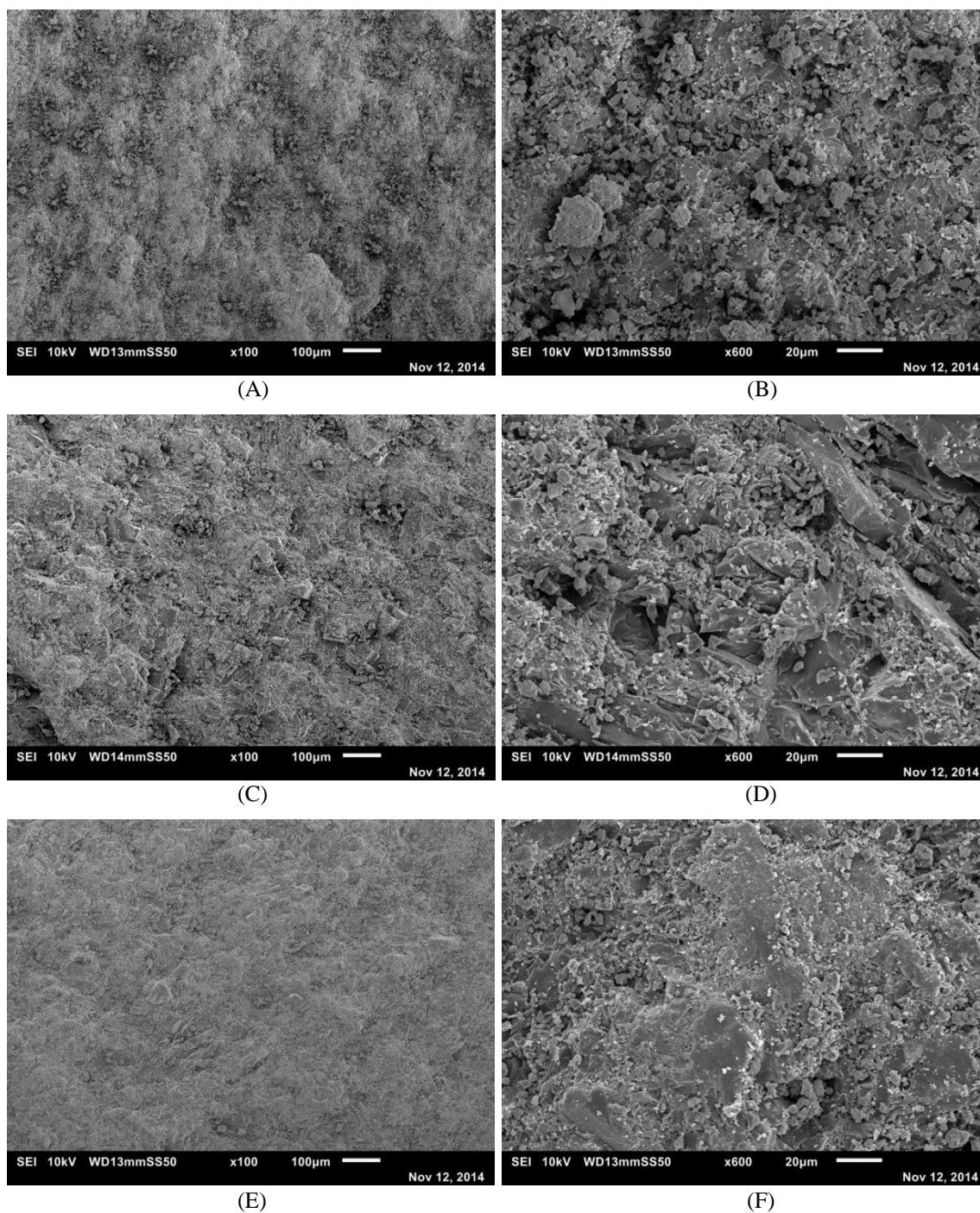


Figure 5.12: Scanning Electron Microscope images for ribbons produced at 100 bar from 21AN (A, B), 200M (C, D), and SD (E, F) at 100 \times magnifications (A, C, E) and 600 \times (B, D, F).

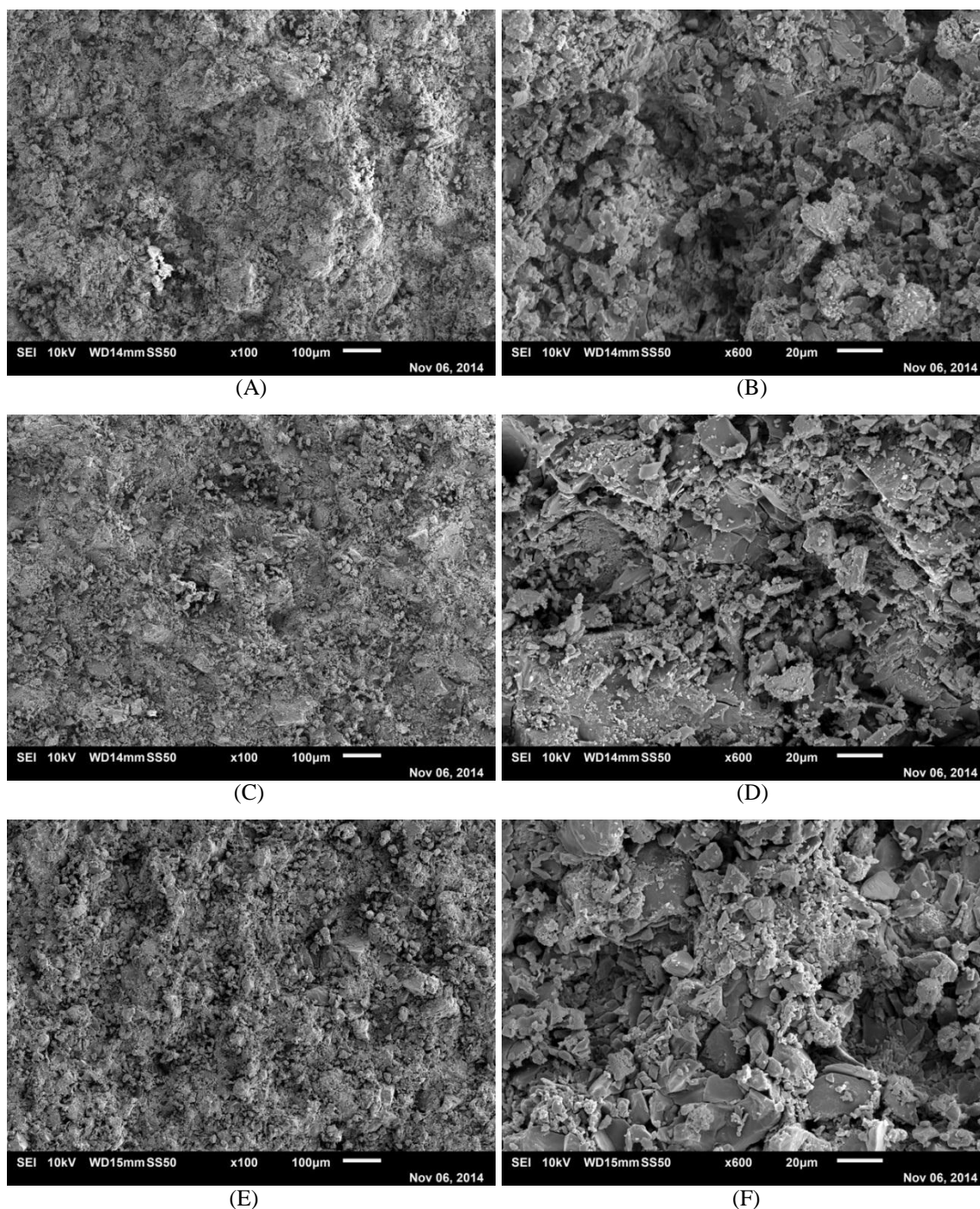


Figure 5.13: Scanning Electron Microscope images for ribbons produced at 30 bar from 21AN (A, B), 200M (C, D), and SD (E, F) at 100 \times magnifications (A, C, E) and 600 \times (B, D, F).

5.5.4 Percentage of fines and width of ribbon

The non-compacted powder, or the amount of fines, is a big disadvantage in dry granulation or roller compaction. A decrease in the amount of fines during roller compaction increases the overall yield and the efficiency of the process. The amount of fines in this study is the amount of non-compacted powder which is produced with the

ribbon during the roller compaction. The percentage of fines produced from each type of lactose during roller compaction at different hydraulic pressure was determined as described in Section 3.2.9. Figure 5.14 shows the percentage of fines at different hydraulic pressures for different types of lactose. It can be seen that the hydraulic pressure has a significant effect on the percentage of fine during roller compaction. The percentage of fines, for all types of lactose, decreased with increasing the hydraulic pressure due to better binding ability at high compaction pressures.

The percentage of fines in the product was high for the lactose 200M, low for the 21AN, and even lower for the SD lactose. This is again because of the more fragmentation, due to the morphology, of the agglomerated form of lactose (21AN and SD) compared with the 200M. This increases the bonding area between the particles which increases the Van der Waals forces and improves the binding ability, therefore resulting in a lower amount of fines [104]. The smaller percentage of fines in the product shown by the SD lactose is due to the higher amorphous content which affected the binding properties of the powder. The amorphous part improved the binding capacity of the powder, by showing more plastic deformation which increases the contact area between the particles and results in a reduction in the percentage of fines in the product.

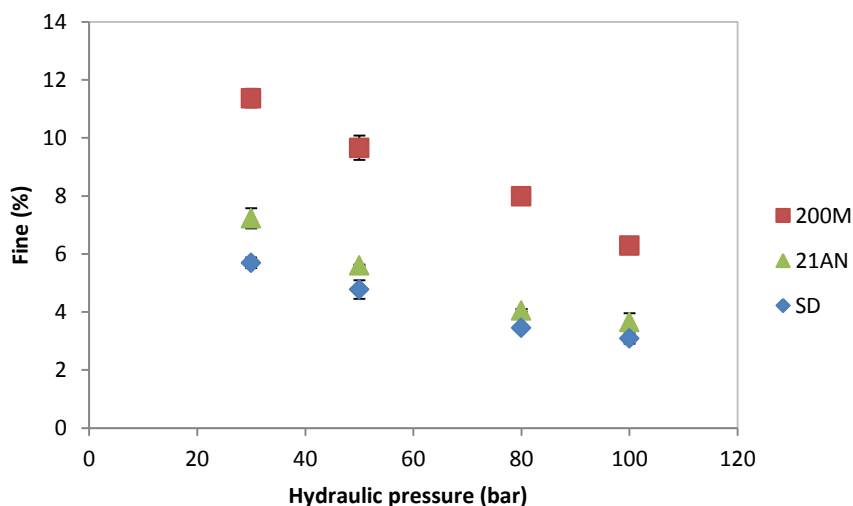


Figure 5.14: Fines weight percentage of different types of lactose at different hydraulic pressure.

The fines or the non-compacted powder usually comes from the edges of the ribbon, as the stress is lower. This means that the produced ribbon will have different width if the amount of fines is different. Figure 5.15 shows the width of ribbon produced from

different types of lactose at different compaction pressure. It can be seen that the hydraulic pressure during the roller compaction has a significant effect on the ribbon width; the higher the pressure during production the higher the width of the ribbon. The width of the ribbon is also different for the three types of lactose used. It was found that the SD lactose produced the widest ribbon in comparison with the other two types of lactose. The width of ribbon of lactose 21AN was higher than those of lactose 200M. The difference in the ribbon width is because of the difference in the powder binding ability which is due to the primary particle morphology. The better binding ability of lactose SD resulted in wider ribbon even at lower stress at the edges, which then resulted in lower fines percentage.

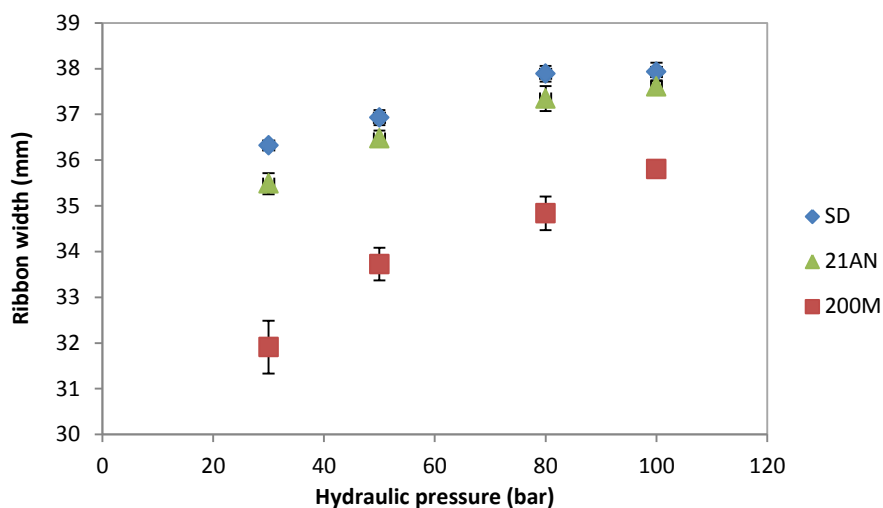


Figure 5.15: Width of ribbon of different types of lactose at different hydraulic pressure.

5.5.4.1 Relationship between the fine percentage and ribbon width

The result in Figure 5.14 and Figure 5.15 illustrate that there is a relationship between the width of the ribbon and the percentage of fines produced during the compaction process. The percentage of fines produced with each type of lactose was plotted against the width of the ribbon as shown in Figure 5.16. It is clear that there is a linear relationship between the fine percentage and the width of the ribbon regardless the type of lactose used during the compaction. The percentage of fines during production was found to decrease with increasing the width of the ribbon. The SD lactose produced ribbon with the least percentage of fines, therefore, resulted in the widest ribbon.

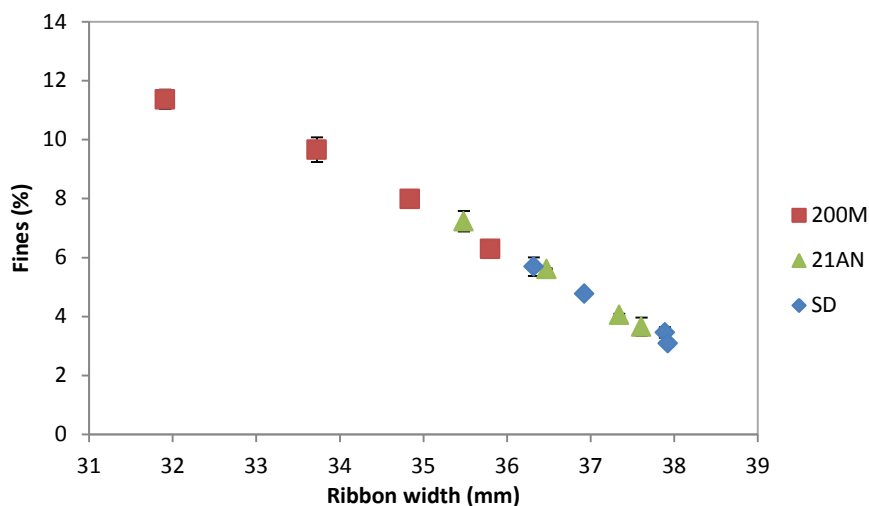


Figure 5.16: Relationship between the width of the ribbon and the percentage of fines during roller compaction.

5.5.4.2 Relationship between the fine percentage and ribbon temperature

As mentioned earlier, the non-compacted powder usually comes from the edges of the ribbon, due to the lower stress acting at the edge of the ribbon. Figure 5.2 supports this, in that the temperature is different across the width of the ribbon and also different for different types of lactose. As shown in Figure 5.2, the bright colour corresponds to a high temperature, which is seen at the centre of the ribbon, and the dark colour represents a low temperature, which is seen at the edges. The temperature at the edge of ribbon of SD lactose was relatively closer to the temperature at the centre of ribbon. This indicates that SD lactose has good binding properties even at low stresses which are present at the edge of the ribbon. This resulted in less non-compacted powder in the product of SD lactose as shown in Figure 5.14. For 21AN and 200M lactose, the temperature at the edge of the ribbon was much lower than that at the centre, which means that the stress at the edge of ribbon was not sufficient for the particles to show adequate binding. This results in a ribbon with weak edges, which increased the amount of non-compacted powder in the product.

From Figure 5.2 and Figure 5.14, it can be seen that there is a relationship between the temperature distribution of ribbon during production and the percentage of fines in the product. It was found that for all ribbons produced at the same pressure from different types of lactose, the largest area of the dark colour resulted in the greatest amount of fines in the product.

To investigate this, Image J software was used to analyse the images from the thermal camera. Firstly, the images were converted to RGB (Red, Green, and Blue) stacks. From the stacks, one of the colour components was used to calculate the grey scale profile along the width of the ribbon. From this information, using a minimum threshold of 100 on the grey scale, the length of the central region (grey scale 100 - 255) of the ribbon was calculated, which represents the white part at the centre of ribbon as seen on the right of Figure 5.17. Figure 5.17 shows an example of the original thermal images for ribbons produced at 100 bar, on the left (temperature range 20°C - 55°C), and the RGB stacks (showing one of the colour components) on the right. It can be seen that the spray dried lactose showed the greatest white region at the centre.

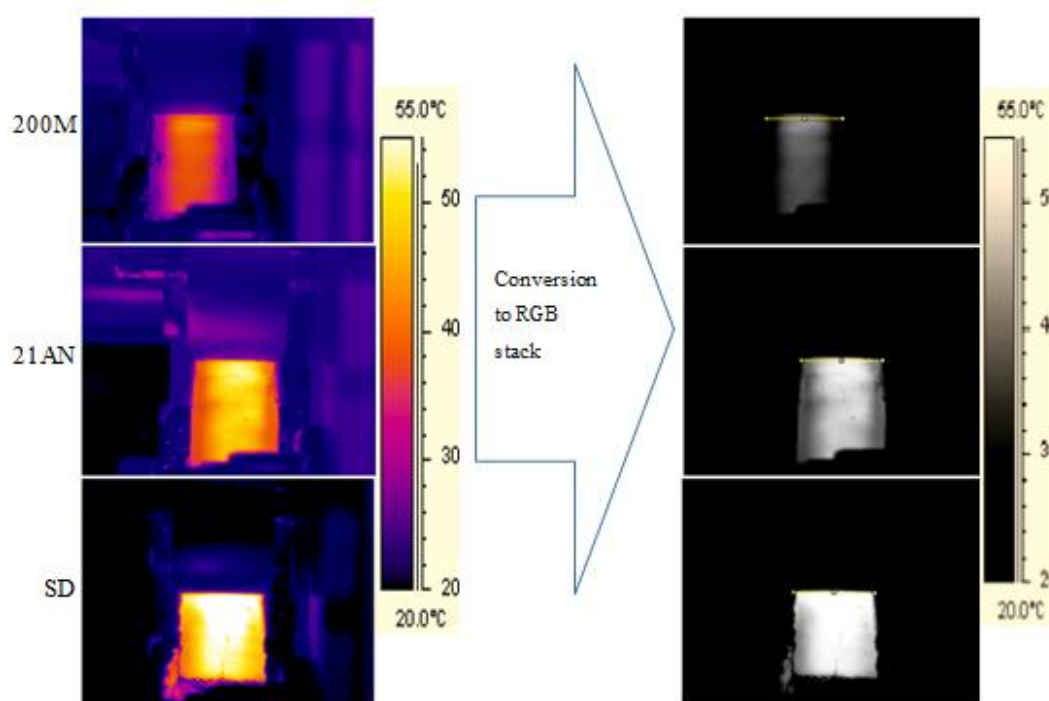


Figure 5.17: Example of the thermal images for ribbons produced at 100 bar (left), and the RGB stacks (right).

This procedure was repeated for the three other operating pressures (30, 50, 80 bar) using the same minimum threshold of 100. However, the temperature scale (range) in the thermal images was different. In Figure 5.17, the temperature scale for ribbons produced at 100 bar was 20°C - 55°C, while for other operating pressures the scale on the thermal images was as follows; 20°C - 50°C at 80 bar, 20°C - 40°C at 50 bar, and 20°C - 30°C at 30 bar. The reason for using different scales with lower operating

pressures was to be able to distinguish between the central region and the edges of the ribbon.

The ratio between the length of the central region and the width of the roller (40 mm) was then calculated and plotted against the percentage of fines produced for each type of lactose as shown in Figure 5.18. It was found that the amount of fines in the product decreased with increasing the length of the central region of the ribbon at all operating pressures. An increase in the length of the central region of the ribbon in the RGB stack images means an increase in the bright area in the thermal images, which was an indication of better binding properties. Therefore, the high value of the length of the central region shown by a ribbon of SD lactose resulted in the smallest percentage of fines in the product.

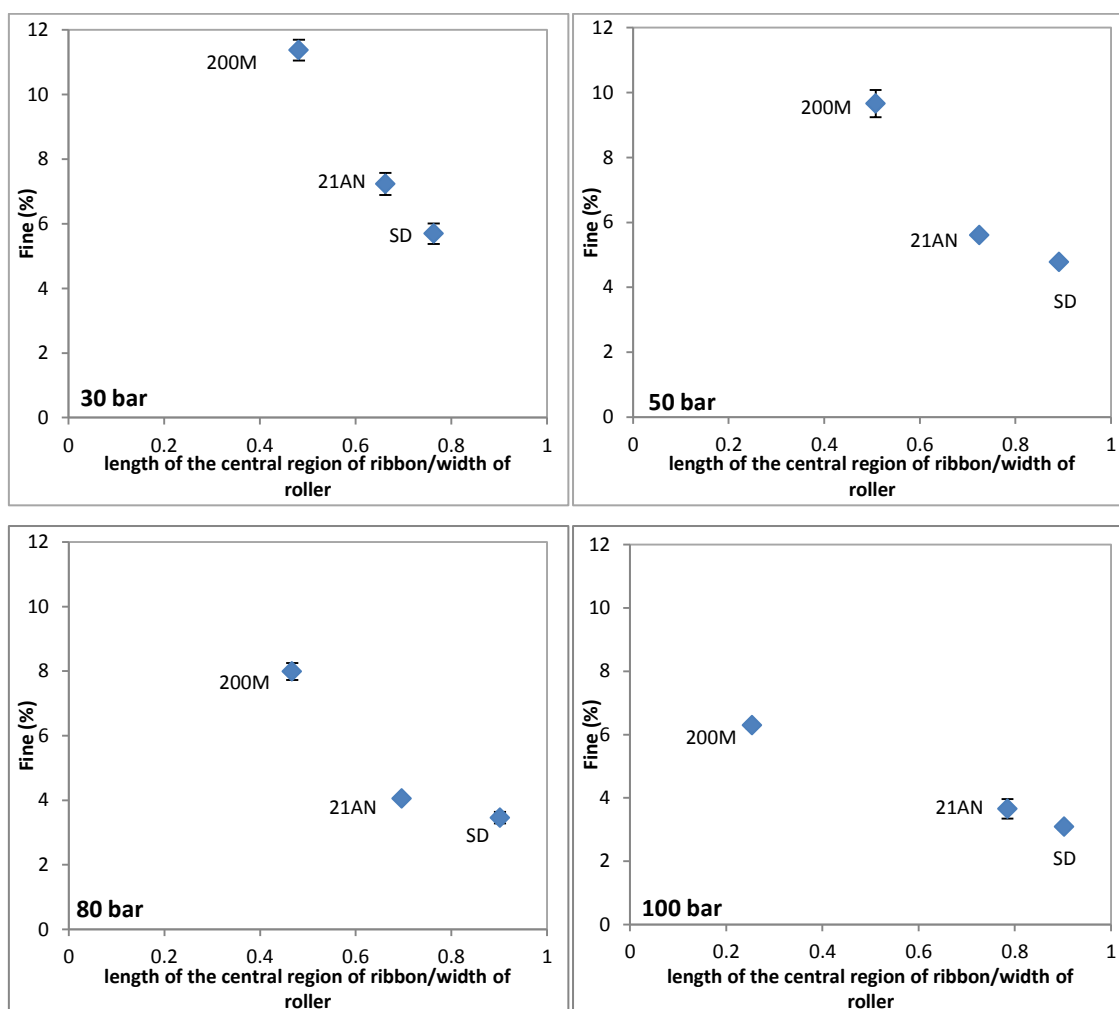


Figure 5.18: Fines percentage plotted against the ratio between the central region of ribbon and roller width, for different types of lactose at different hydraulic pressures.

5.5.5 Temperature distribution across the width of ribbon

As stated earlier, there is a difference in temperature across the width of the ribbons at all operating pressures. The thermal images were analysed using FLIR R&D software to determine the temperature distribution across the width of the ribbons. A line was drawn across the width of ribbon and close to the roller for all ribbons as shown in Figure 5.19. The temperature distribution was determined for the images which were extracted every 5 seconds from the video. The average value of these was plotted which can be seen in Figure 5.20, Figure 5.21 and Figure 5.22 for the different types of lactose.

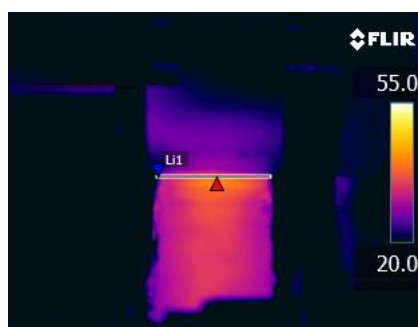


Figure 5.19: Example of the thermal image of SD ribbon produced at 50 bar with a line drawn across the width.

This procedure was repeated for different operating pressures and for all powders. Figure 5.20, Figure 5.21 and Figure 5.22 show the temperature profile across the width of ribbons for 200M, 21AN, and SD lactose respectively. Due to the difference in the width of ribbons produced at different pressures, all ribbon widths are shown in Figure 5.20, Figure 5.21 and Figure 5.22 have been normalised from 0 (one edge of ribbon) to 1 (the other edge of ribbon).

It can be seen that there is a difference in temperature between the centre of the ribbon and the edge. The difference in temperature between the centre and the edge of the ribbon is not the same for different types of lactose. The low temperature at the edge of the ribbon indicates that the powder has been compressed less than that at the centre of the ribbon, which is due to the low stresses applied to the powder at the edges.

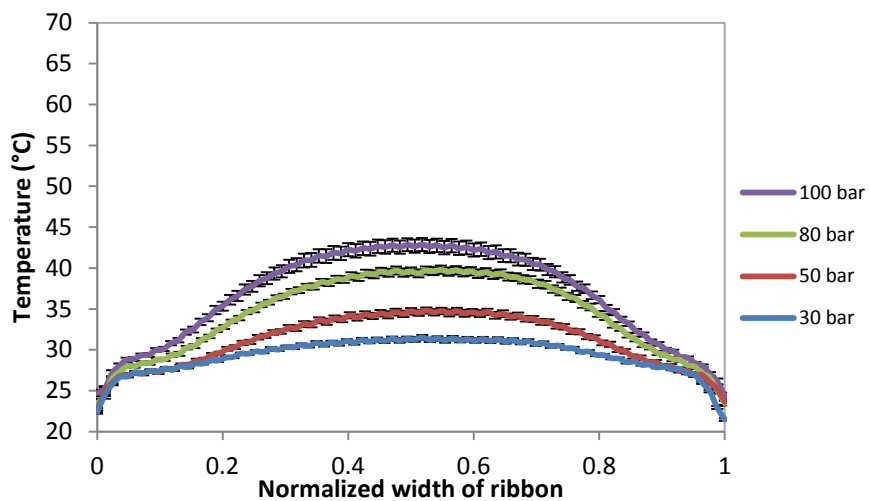


Figure 5.20: Temperature distribution across the width of ribbon produced from α -lactose monohydrate 200M at different hydraulic pressure.

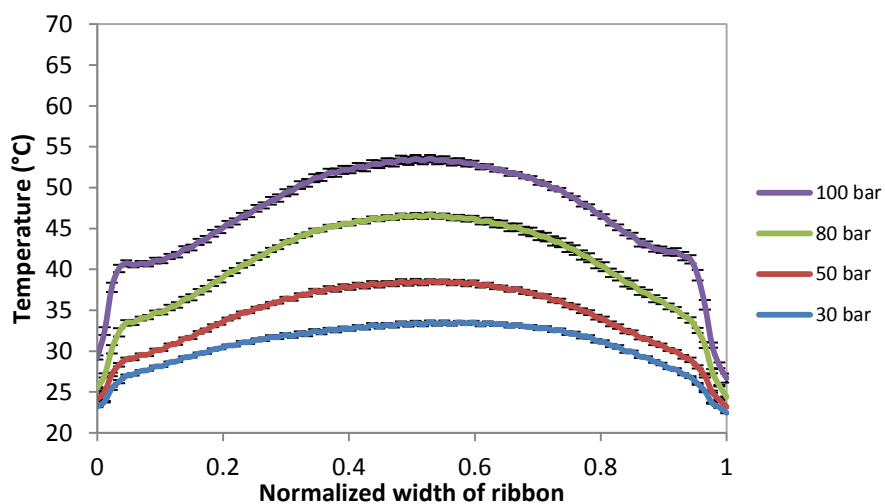


Figure 5.21: Temperature distribution across the width of ribbon produced from anhydrous 21AN lactose at different hydraulic pressure.

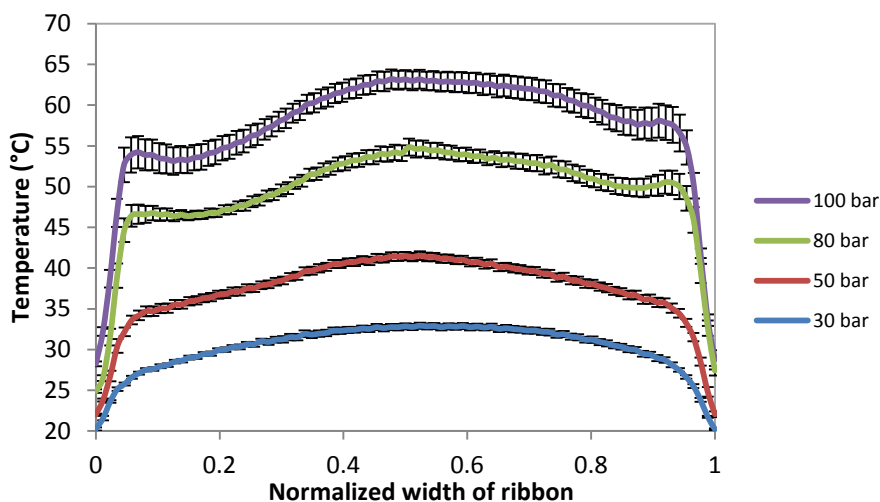


Figure 5.22: Temperature distribution across the width of ribbon produced from spray dried SD lactose at different hydraulic pressure.

The temperature of the ribbon during production increased with increasing the hydraulic pressure. This indicates that there is a relationship between the hydraulic pressure (stress applied by the roller) and the ribbon temperature during production. The higher temperature at the centre of the ribbon is an indication of a higher stress being experienced at the centre, and the low temperature at the edges indicates low stress. The difference in the stress experienced across the width of the ribbon results in a porosity distribution across the width of the ribbon (low porosity at the centre and high porosity at the edges). In the literature, works have been carried out to study the density distribution across the width of the ribbon [11, 12, 67, 76]. It was found that there is a difference in the density between the centre and edges of the ribbon, in which ribbon centre density was higher than that of edges. They attributed this result to the feeding system, which depends on the powder flow property and on the side seal system. Further investigation is required to understand the relationship between the applied stresses, the temperature of the ribbon during production and the porosity distribution across the ribbon width. This will be carried out in a separate study in Chapter 8

5.5.6 Ribbon porosity

The porosity of ribbon produced from different types of lactose was determined using X-ray tomography. In this method, X-ray tomography was used to obtain images of ribbon which was then analysed using Image J software as outlined in Section 3.2.11. Figure 5.23 shows some X-ray images at the centre of ribbons produced from the three types of lactose at 30 and 100 bar hydraulic pressure. It can be seen that there is a clear

difference in the internal structure of ribbons produced at different hydraulic pressure for the three types of lactose. Ribbons produced at 30 bar showed more porous structure, whereas, at 100 bar the structure of ribbons is more compacted. In addition, the structure of ribbon is different for the different types of lactose. Figure 5.24 shows the porosity at the centre of the ribbon of different types of lactose versus the hydraulic pressure.

From Figure 5.24, it can be seen that the porosity of ribbons produced from all types of lactose decreased with increasing the hydraulic pressure during the production. This was due to more force and stress applied on the powder with increasing hydraulic pressure, which brings the primary particles close to each other and decreases the porosity of the ribbon.

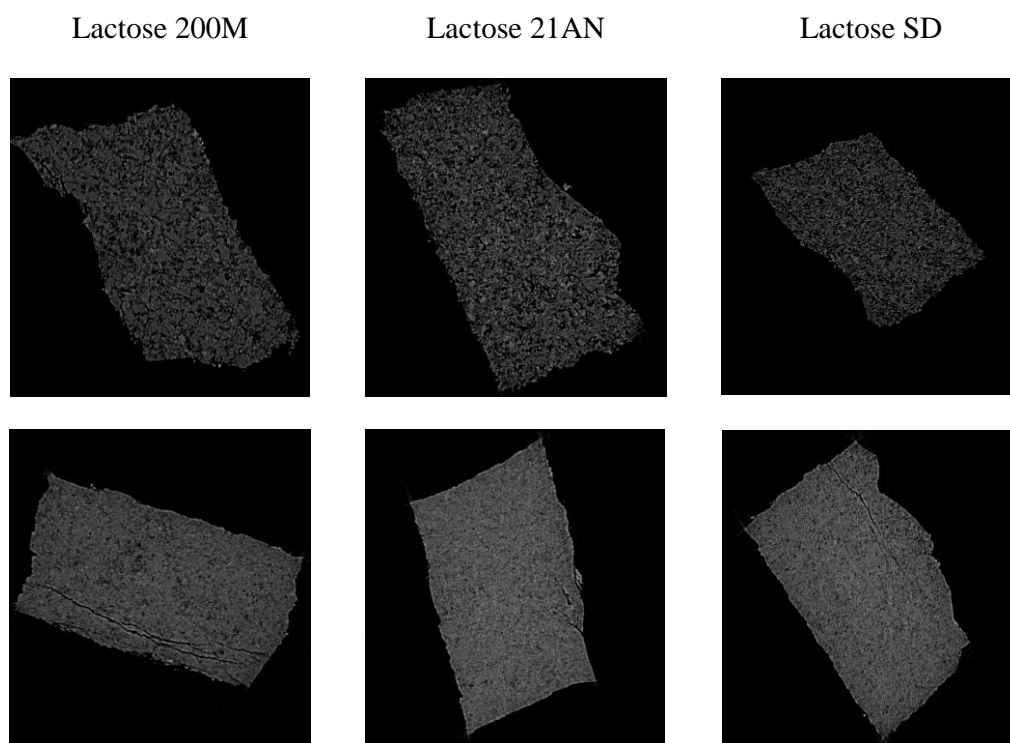


Figure 5.23: X-ray images for ribbon produced at 30 bar (top) and 100 bar bottom.

At a low hydraulic pressure of 30 bar, there is no significant difference in the porosity of different types of lactose. This is due to the low stress applied by the rollers which were insufficient to show significant breakage and plastic deformation of the particles within the powders. At high hydraulic pressure, there is a clear difference in the ribbon porosity for the three types of lactose. The porosity of ribbons produced from the SD and 21AN lactose was lower than those produced from the 200M lactose. This was due

to the structure of the primary particles as an agglomerated type. The particles in these types of powders break easily and produces a large amount of small fragments which leads to better interlocking and filling the gaps then results in a reduction in the ribbon porosity.

SD lactose produced ribbon with the lowest porosity. This is again due to the higher degree of fragmentation and the high amorphous content in the powder which is believed to show more plastic deformation and sintering during compaction. This will result in an increase in the contact area and a decrease in the distance between the particles, consequently, a decrease in the porosity.

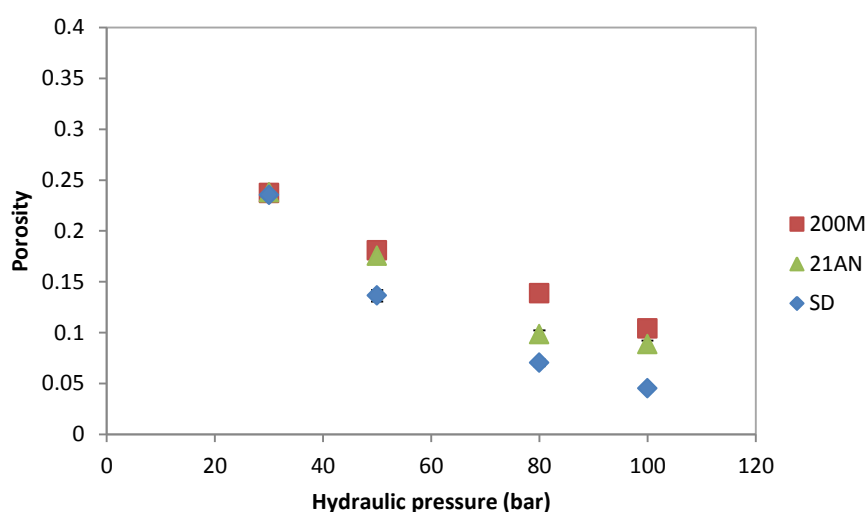


Figure 5.24: Porosity at the centre of ribbons of different types of lactose using X-ray.

It is worth mentioning that the result in Figure 5.24 is showing the porosity at the centre of the ribbon. However, it is expected that the porosity is not uniform across the width of the ribbon. This was confirmed by the thermal images which showed a difference in the temperature across the width of the ribbon. The temperature distribution in Figure 5.20, Figure 5.21 and Figure 5.22 indicate a difference in the stress applied by the roller across the width of the ribbon. The high temperature at the centre of the ribbon indicates a high stress applied during the roller compaction, while, the low temperature indicates low stress at the edges. This is expected to result in a low porosity at the centre of the ribbon and high porosity at the edges.

Figure 5.25 shows the porosity at the edge of the ribbon determined using the X-ray method. It is clear that the porosity at the edge of the ribbon in Figure 5.25 is higher than those at the centre of ribbon in Figure 5.24 for all types of lactose.

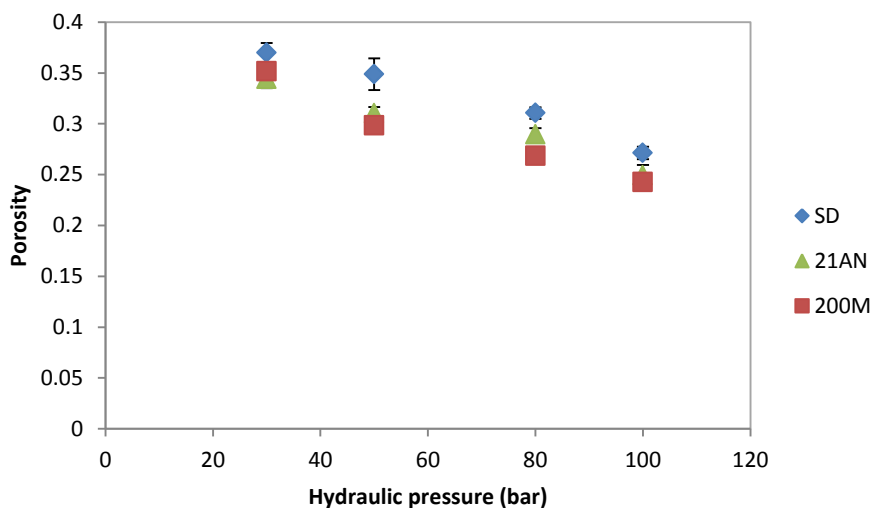


Figure 5.25: Porosity at the edge of ribbons of different types of lactose using X-ray.

5.6 Effect of amorphous content

The results in the previous section (Section 5.5) were discussing the effect of both the morphology and the amorphous content of the initial powder on ribbon properties. To eliminate the effect of the morphology and exclusively study the effect of the amorphous content, two experiments were conducted using both 200M and SD. The amorphous content of 200M and SD in the previous sections were 2.67% and 10.32% respectively. In this section, the powders were stored in a climatic chamber for one week at 70% RH and 25°C. This process will ensure the crystallisation of any amorphous fraction in the powder [25, 26, 116-118]. After one week, the conditions in the chamber changed to 20% RH and 25°C for another 3 days. The powders then roller compacted using the same settings as mentioned in Section 5.5. The results obtained from these experiments were compared with those in the previous section. The difference between the two sections will be the amorphous content of the powders. In Section 5.5, SD and 200M powders contain 10.32% and 2.67% amorphous respectively, whereas in this section they contain 0% amorphous.

Figure 5.26 and Figure 5.27 show the tensile strength of ribbon produced from SD and 200M lactose respectively, at different amorphous content. Figure 5.28 and Figure 5.29

illustrate the fine weight percentage which is produced with the ribbon during roller compaction of both the SD and 200M lactose respectively at different amorphous content.

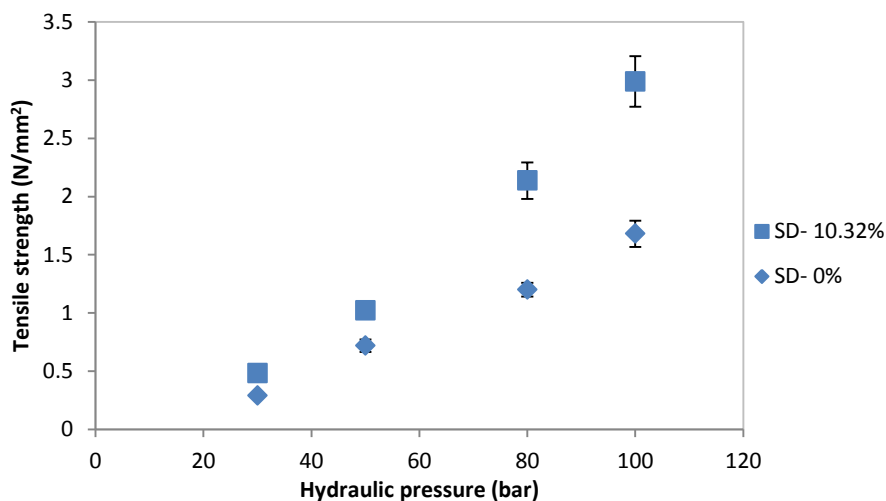


Figure 5.26: Tensile strength of ribbons produced from SD lactose containing different amorphous content.

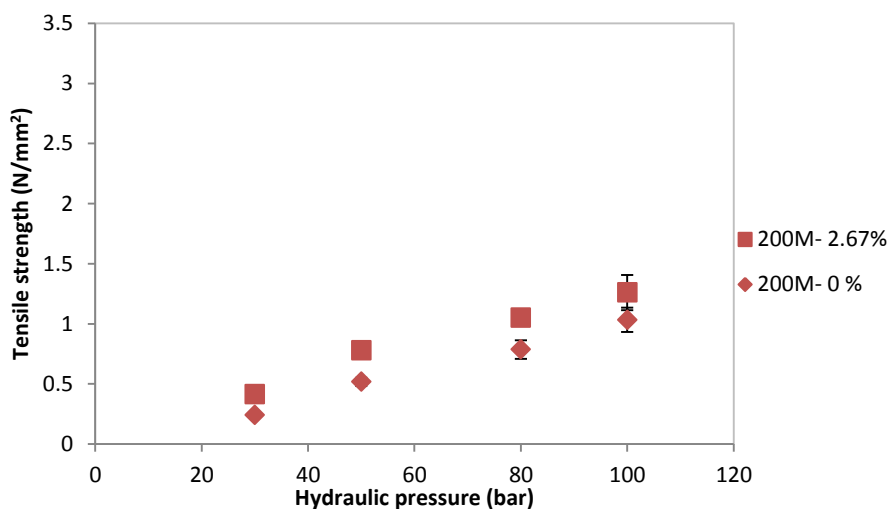


Figure 5.27: Tensile strength of ribbons produced from 200M lactose containing different amorphous content.

From these figures, it can be concluded that the higher the amorphous content of the lactose powder before compaction the better the binding properties during roller compaction. Powders with higher amorphous content produced ribbon with higher tensile strength and a lower percentage of fines. These results confirm that the existence of a fraction of amorphous lactose in the powder influences the binding properties of the powder during roller compaction. The amorphous lactose improves the binding

properties of the powder by showing more plastic deformation and sintering during compression which then have a significant effect on the final ribbon properties.

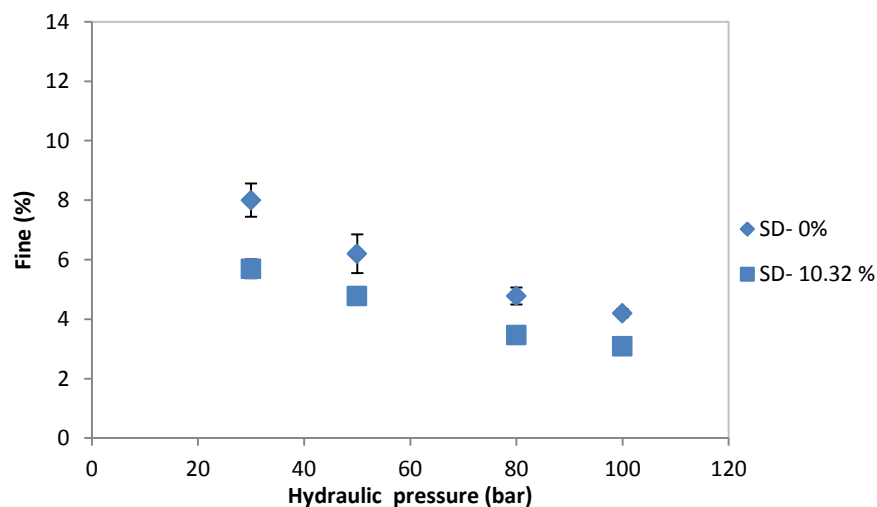


Figure 5.28: Fines weight percentage of SD lactose containing different amorphous content.

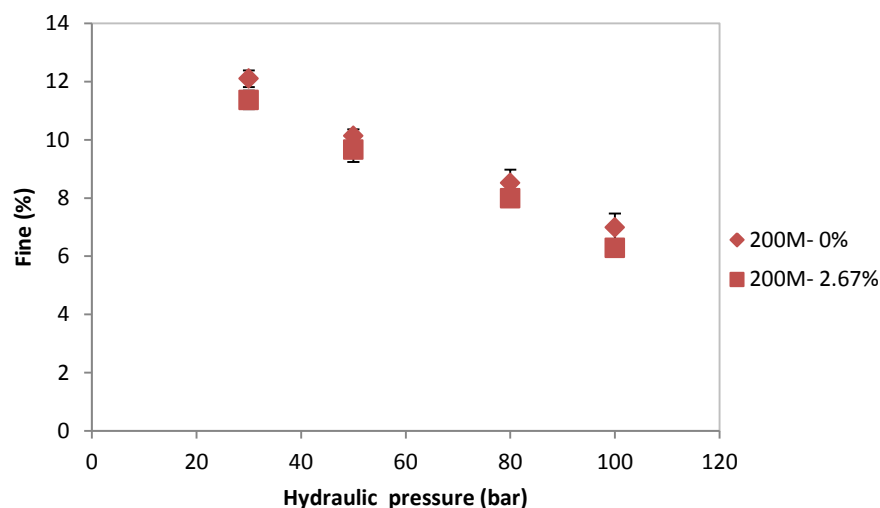


Figure 5.29: Fines weight percentage of 200M lactose containing different amorphous content.

It is worth noting that the difference in ribbon properties (tensile strength and fines percentage) is different for the SD lactose compared to lactose 200M. The difference in ribbon properties is more significant in SD lactose compared to 200M lactose. This is due to the higher amount of amorphous fraction in the SD lactose (10.32%) compare to lactose 200M which has 2.67%.

5.7 Effect of morphology

To eliminate the effect of the amorphous content in the powder and exclusively investigate the effect of the particle morphology, an experiment was conducted on the three types of lactose after removing any fraction of amorphous in the powder before compaction. The three types of lactose were stored in the chamber for one week at 70% RH and 25°C to remove the amorphous fraction in the powder, by doing so; the only difference between the powders will be the morphology of the particle. The powders then stored for another 3 days in the same chamber at 20% RH and 25°C. The powders then roller compacted using the same settings as mentioned earlier and the ribbons were tested for their temperature, fine percentage and tensile strength.

Figures (5.30- 5.32) show the temperature of the ribbon during production, the tensile strength of the ribbon and the fine percentage respectively. It can be seen that the binding properties are better for the lactose powders which consists of agglomerated particles (21AN and SD) in comparison to the non-agglomerated particle (200M). The agglomerated type of lactose produced ribbon with higher surface temperature, higher tensile strength and lower amount of fines during roller compaction. This confirms that the morphology of the primary particle of lactose powders plays an important role during roller compaction process and has a significant effect on the ribbon properties.

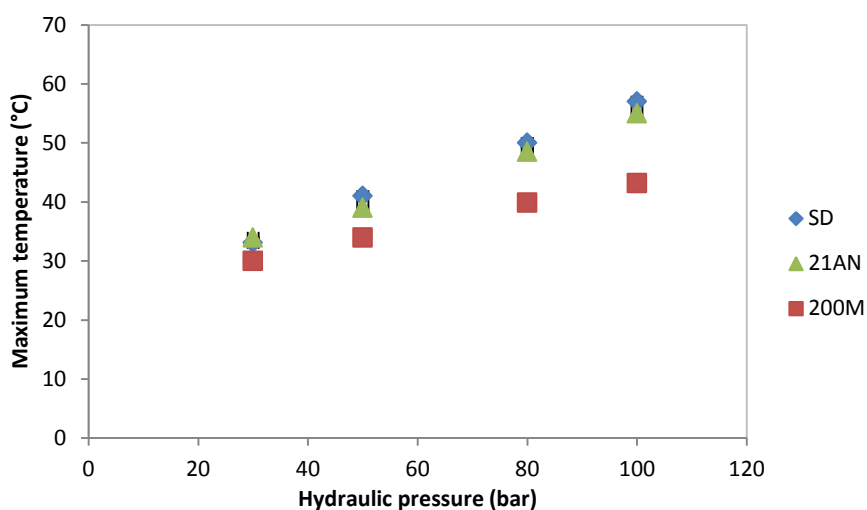


Figure 5.30: Surface temperature of ribbons of different types of lactose after removing the amorphous fraction.

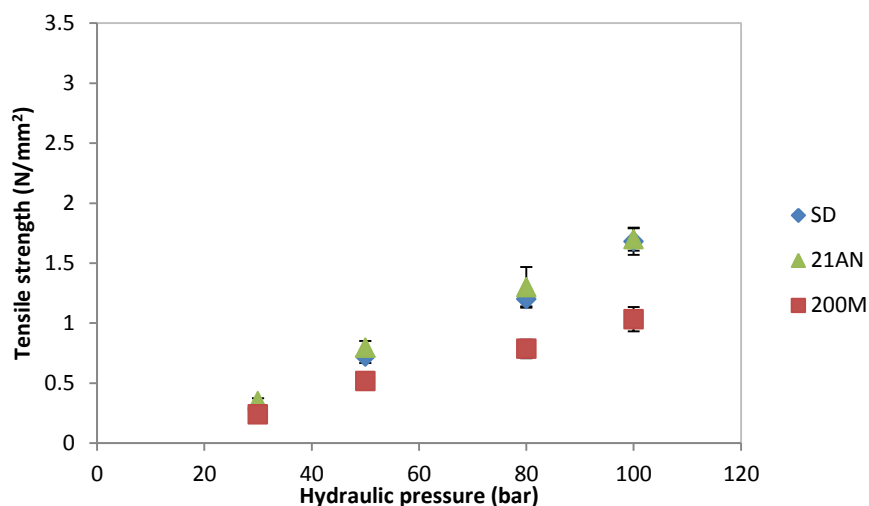


Figure 5.31: Tensile strength of ribbons of different types of lactose after removing the amorphous fraction.

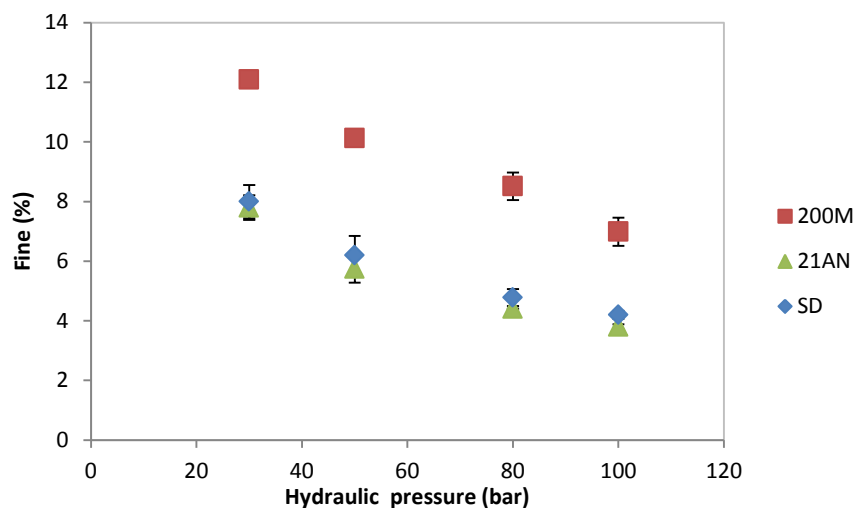


Figure 5.32: Fines weight percentage of different types of lactose after removing the amorphous fraction.

5.8 Conclusion

The work presented in this chapter investigated the effect of morphology and amorphous content of lactose powder on the properties of ribbons produced in a roller compaction. An online thermal imaging system was used during the experimental work to record the temperature of the ribbon during production.

The morphology and amorphous content of lactose powder were shown to have a significant effect on the single particle strength, the behaviour of powders during roller compaction and the ribbon properties. The maximum stress applied on the powder

during the compaction was determined using the Jonason's mathematical model. The maximum stress applied on lactose 200M was higher followed by lactose 21AN and the lowest stress was for lactose SD. This was due the difference in the primary particles morphology and the powder amorphous content which affected the powder compressibility, therefore the stress during the compaction. It was found that the agglomerated type of lactose (SD and 21AN) showed better binding capacity compare to the non- agglomerated type (200M). This was shown by the tensile strength, fragment size, ribbon temperature, ribbon porosity and the amount of fines in the product. The agglomerated type of lactose exhibited a higher degree of fragmentation during the roller compaction, which increased the number of small fragments and, therefore, increased the bonding area. The amount of non-compacted powder (fines) in the product was smaller for ribbons produced from the agglomerated type of lactose which had the highest amorphous content. It was found that there is a relationship between the strength of the primary particle and the final ribbon tensile strength. The stronger the primary particle of the initial powder the weaker the ribbon after the roller compaction.

There is also a relationship between the surface temperature of the ribbon during production and the tensile strength of the ribbon. It was concluded that, regardless the type of lactose, the higher the temperature of the ribbon during production the higher the tensile strength of the ribbon. This means that the information from the thermal camera can be used to predict the tensile strength of the produced ribbon. From the thermal images, it was found that the temperature of the ribbon during the production is not uniform across the width of the ribbon. The temperature is higher at the centre of the ribbon compare to the edges. This was believed to be due to the variation in the stress applied to the powder across the width of the roller, which resulted in temperature variation. This is then resulted in a non-uniform porosity along the width of the ribbon; low porosity at the centre and higher at the edges.

The effect of the powder amorphous content and particle morphology on the ribbon properties were also studied separately .It was shown that the powder amorphous content and the primary particle morphology (agglomerated, non-agglomerated) have a significant impact on the binding properties of the powder during compaction and on the ribbon quality.

CHAPTER 6 EFFECT OF THE RELATIVE HUMIDITY ON THE PRODUCT QUALITY

6.1 Introduction

During the storage or processing of powders, the particles in the powder bed can interact with water vapour. The interaction of powder with water vapour affects the powder moisture content which may have a significant effect on the powder flow properties, dissolution, stability and powder compaction behaviour [45-47]. Water can exist in food and pharmaceutical powders mainly in three forms: free, adsorbed and bound water [49, 50]. The existence of water in the material in different forms depends on the material structure (for example crystalline and amorphous). Due to the nature of the amorphous material, the water can absorb into the free volume within the material structure. This will influence the mobility of the molecules and the glass transition temperature of the material. The change in the glass transition temperature affects the state of the material (rubbery or glassy state), which will have an effect on the viscosity and the deformability of the powder. This will affect the interparticulate forces and promote the sintering process between the particles at the contact points and create solid bridges during compression [19, 51]. In crystalline material, moisture can be adsorbed onto the surface of the particle and create a monomolecular layer at low moisture content. This may help smoothen the irregularities on the particle surface and therefore decrease the distance between two particles and increase the contact area [47, 52]. The adsorption of the water on the crystal surface may also cause the particle to dissolve at the contact points and creating strong bonds after recrystallization/ solidification. On the other hand, an increase in the moisture content results in a multilayer of water molecules at the particle surface which may decrease the intermolecular forces and, therefore, decreases the bonding strength [47, 119].

The powder moisture content may have a significant effect on the properties of the powder during different processing for example tableting and roller compaction [47].

The relative humidity of the environment can affect the powder moisture content during storage. The humidity of the environment fluctuates significantly throughout the year everywhere in the world, resulting in varying product qualities. Therefore, it is important to investigate the effect of varying the relative humidity during storing of powders, on powder properties and processing.

The work in this chapter focuses on the investigation of the effect of storage at different relative humidity conditions, for various types of lactose, on roller compaction behaviour [120]. The study involves an investigation of the effect of the storage condition on the primary powder water content and flow properties before the roller compaction. The roller compaction behaviour and ribbon properties after the roller compaction will then be investigated and related to the storage condition. The study involves a Particle Image Velocimetry (PIV) technique to determine and examine the velocity of the powder during the compaction process. The knowledge created from such a study will help identify the optimum working conditions for roller compaction of different types of lactose.

6.2 Preparation of the powders

In this chapter, the three types of lactose were used as received from the supplier. The powders were conditioned in a climatic chamber (Binder KMF 240 climatic chamber, Germany) at 25°C and different relative humidity conditions (10, 20, 40 and 80% RH) for 3 days. Before the roller compaction, the powders were analysed to determine the moisture content and the flow properties at different RH conditions.

6.3 Production of ribbon

Powders conditioned at different storage RH were compressed into ribbons using hydraulic pressure of 20-100 bar range. The speed and the gap of the roller were kept constant at 3 rpm and 3 mm respectively.

To eliminate the effect of humidity in the laboratory on the powder relative humidity a GenRH-A (London, UK) humidity generator was connected to the top of the hopper on the roller compactor as shown in Figure 3.6. The humidity generator was operated at the same conditions as the climatic chamber; this ensured a constant humidity condition of

the powder during roller compaction same as that used for the storage of the powder prior to compaction.

6.4 Particle Image Velocimetry (PIV)

The velocity of the powder during the roller compaction process was measured using the Particle Image Velocimetry (PIV) method. Only one study has been conducted using PIV during the roller compaction of powder. Krok et al. [121] used PIV to measure the velocity of NaCl and wheat flour during roller compaction using a piston feeding system on a vertical roller compactor. The effect of the powder feeding stress on the velocity profile during roller compaction was investigated. The velocity profile was correlated to the powder properties (angle of wall friction and angle of internal friction). It was found that the wall and internal friction affects the mobility of the powder during compaction. They also measured the velocity of the powder in hoppers with different wall slopes.

In the current study, PIV experiments were carried out using a specially built transparent cheek plate which allows the powder during roller compaction to be seen optically [120]. For better tracking the movement of the particles during roller compaction, 5 wt. % of red-coloured lactose powder was added as a tracer. The tracer was prepared by dissolving lactose powder in distilled water and then mixed with a red dye (Erythrosine B; Acid red 51, Sigma-Aldrich). The solution was then dried in an oven at 100°C for 48 hrs. The coloured and dried material was then ball milled using a Retsch Planetary Ball Mill PM 100 (Retsch, Germany). A size class between 212-300 μm of the red particles was obtained after sieving, which was then used in the PIV experiments.

The movement of the powder before and in the compaction zone was recorded using a high-speed camera (Photron Fastcam 1024 PCI, Itronx Imaging Technologies, CA). A frame rate of 60 fps was used to capture images of the powder during motion at a resolution of (1024 pixels \times 1024 pixels). The camera was directed perpendicularly to the transparent check plate. The PIV experiments were conducted on powders conditioned at 20% and 80% RH and compacted at 100 bar hydraulic pressure. The camera recorded the powder motion with the full rotation of the roller, which resulted in approximately 1250 images.

Particle Image Velocimetry (PIV) is used to determine the surface velocity of particles in motion. This was carried out using the Cross Correlation Algorithm available in PIVlab package using MATLAB version R2014a. After importing the images into MATLAB, the area of interest needed to be defined. This ensured any undesired areas which are not of interest to be removed by creating a mask over these regions. To determine the real velocity, the images were calibrated against a known distance which calculates the number pixels present in 1 mm region.

The images were then divided into small interrogation areas of (32 pixels \times 32 pixels) which contain a set of pixels in X and Y directions. The velocity was calculated from the displacement of the interrogation areas between two consecutive images. The displacement of the interrogation areas was determined using the Cross Correlation Algorithm as shown in Equation 6.1 [122, 123].

$$C(m, n) = \sum_i \sum_j A(i, j) B(i - m, j - n) \quad 6.1$$

where A and B are the interrogation areas in the two consecutive images. The location of the maximum peak in the resulting correlation matrix $C(m, n)$ indicates the displacement of the particle from first to the second image [122, 123]. The velocity can be determined from the displacement and the capturing time interval of the two images. More details of the Cross Correlation Algorithm and the PIVlab can be found in the literature [122-125]. After analysing, the algorithm generates an array of velocity vectors over the images. Each of the vectors contains two components in the vertical and horizontal directions. From the vertical and horizontal velocity components, the resultant velocity of each vector was extracted as shown by the green arrows in Figure 6.1. The time averaged resultant velocity; every 32 pixels in X direction were calculated as shown in Figure 6.1. This gave the velocity at different angular positions starting from the point where the powder and the roller are in contact to the point where the two rollers have a minimum gap at angle 0° .

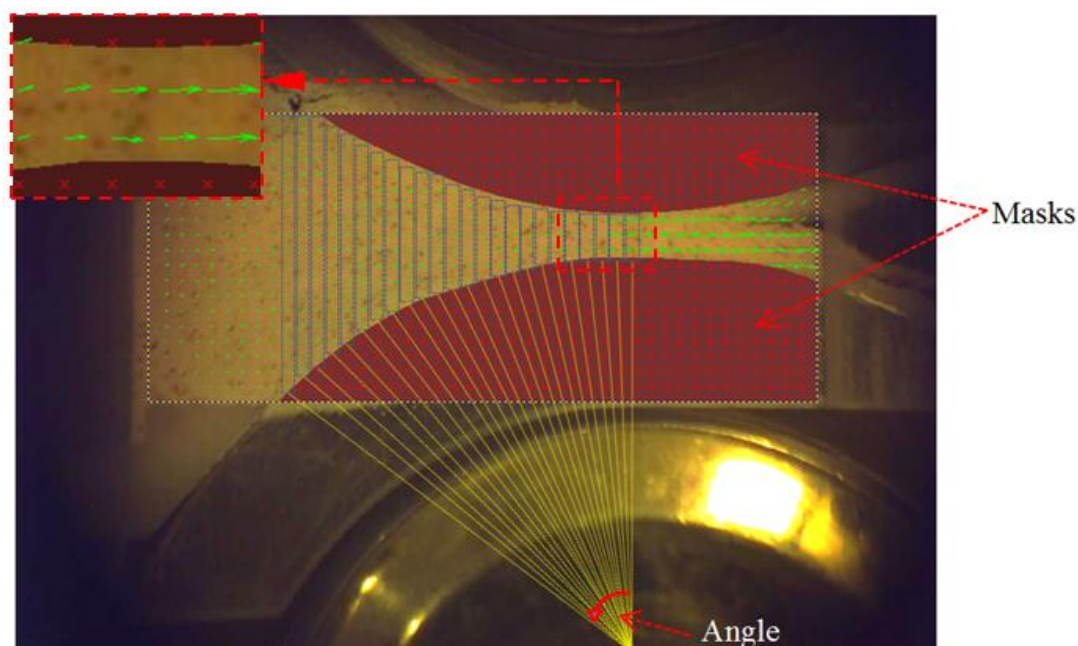


Figure 6.1: Representation of the area of investigation during PIV analysis.

6.5 Results and discussion

6.5.1 Powder water content

The moisture content of all powders was measured after conditioning in the climatic chamber for three days at 25°C and different humidity conditions. The powder moisture content was measured using Sartorius infrared moisture analyser (Sartorius, MA 35, Germany) as described in Section 3.2.4 [120]. Figure 6.2 shows the water content of the powders at different RH values. The water content of lactose 21AN increased gradually with increasing RH of the storage. The water content of 200M and SD lactose increased when the RH was increased from 10% to 40%. However, the increase in the storage condition from 40% to 80% RH did not show a significant change in the powder water content. This is believed to be due to the fact that these two types of lactose contain some amorphous lactose (see Table 4.2), which crystallise and desorb the water at 80% RH [25, 26, 116-118, 126]. It can be seen from Figure 6.2 that the powder absorbed water when the RH changed from 10% to 40% and then desorbed some of the water above 40% RH due to the solid-state crystallisation of the amorphous part of the powder. This resulted in a very minimal difference in the water content of powders stored at 40% and 80% RH. The water desorption after 40% RH results in an increase in the cohesiveness of the powder, thus, decreasing the flowability (see Figure 6.3).

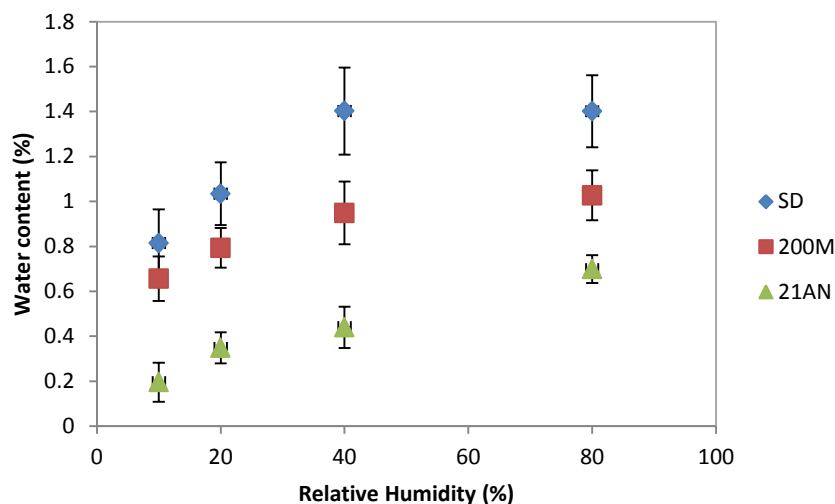


Figure 6.2: Water content of powders stored at different RH values.

6.5.2 Powder flow properties

Flowability is the ability of a material to flow, and it depends on both the material properties and the way the material is being stored, handled and processed in different equipment [96]. Flowability of a powder is difficult to be expressed as an absolute number, and it is always associated with the test method. The flow properties of powders stored at different relative humidity conditions were measured using different techniques as described in Section 3.2.5. The flowability of the powder was assessed by the flow function coefficient ffc using the shear cell tester, repose angle and compressibility index.

Figure 6.3 shows the flow function coefficients (ffc) for the three types of lactose at different RH conditions. Powders were initially conditioned in the climatic chamber for 3 days, and then the ffc value was measured as outlined in Section 3.2.5.1 [120]. It can be seen that the ffc values decreased slightly with increasing RH in the range of 10% to 40% RH and then decreased significantly at 80% RH. This indicates that the flowability of all types of lactose is decreasing with increasing the RH during storage.

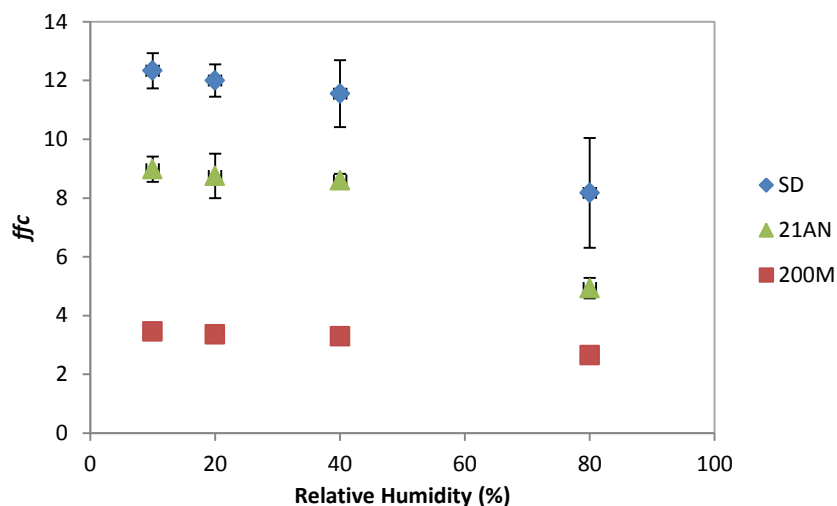


Figure 6.3: Powders flow function coefficient at different RH values, measured using the shear cell tester.

The shear cell tester was also used to calculate the effective angle of internal friction of lactose powders at different relative humidity conditions as shown in Figure 6.4. The effective angle of internal friction measures the resistance of the particle to flow and gives information about the friction occurred between the particles while flowing. The higher value of the effective angle of internal friction indicates lower powder flowability [127]. It can be seen (from Figure 6.4) that that effective angle of internal friction of the three types of lactose increased slightly with increasing the relative humidity condition during the powder storage. This means that the flowability of the powder is decreasing with increasing the relative humidity conditions during storage. This is in agreement with the finding in Figure 6.3 in that the increase in the powder moisture content with increasing the RH during the storage resulted in a decrease in the flowability of the powder.

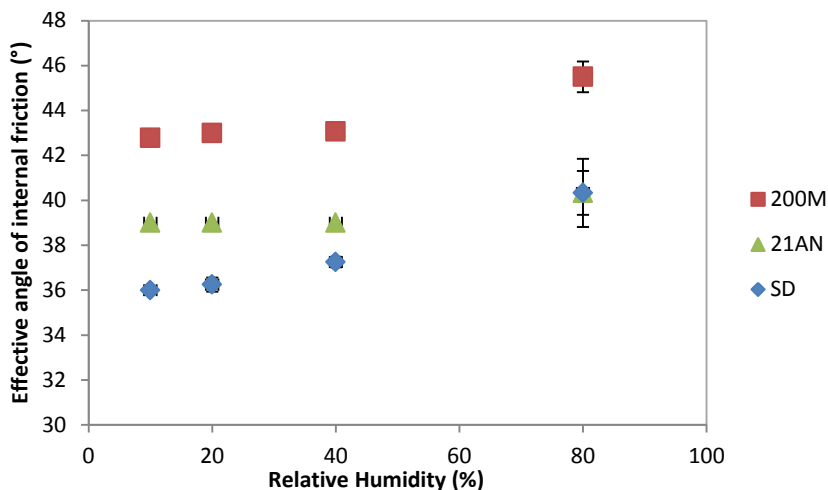


Figure 6.4: Effective angle of internal friction of powders at different relative humidity.

Figure 6.5 shows the angle of repose for the powders equilibrated at different relative humidity values which were measured as described in Section 3.2.5.2. Typically, the lower the value of repose angle the better the flowability of the powder [100, 102, 128]. It can be seen from Figure 6.5 that the angle of repose increases slightly with increasing the relative humidity during the powder storage. This was the case for all the three types of lactose used in this study. This result confirms that the powders become less flowable with increasing relative humidity. A similar result was found from the finding of the compressibility index of the powder as shown in Figure 6.6. The compressibility index of the powders at different storage conditions was measured as shown in Section 3.2.5.3. The lower the compressibility index the better the flowability of the powder [100]. From Figure 6.6 it can be seen that the compressibility index, for all types of lactose, was increasing with increasing the relative humidity of the powder during storage. This means that the flowability of the powder is decreasing with increasing the relative humidity of the powder during storage.

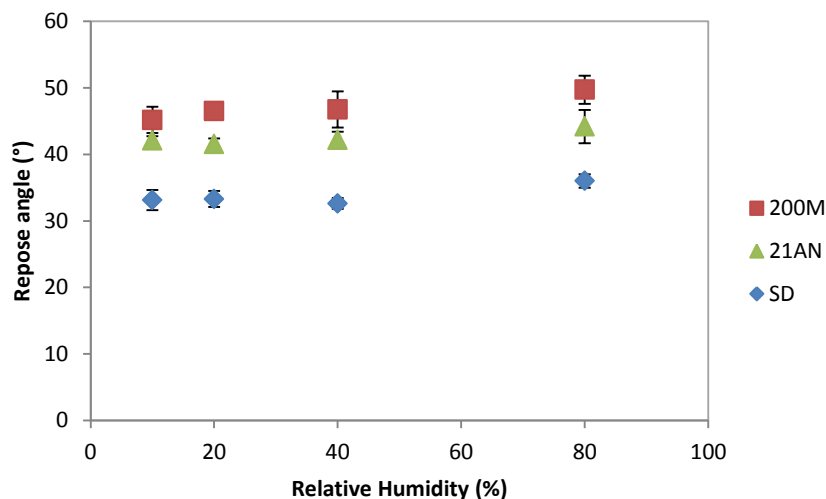


Figure 6.5: Repose angle of the powders equilibrated at different RH values.

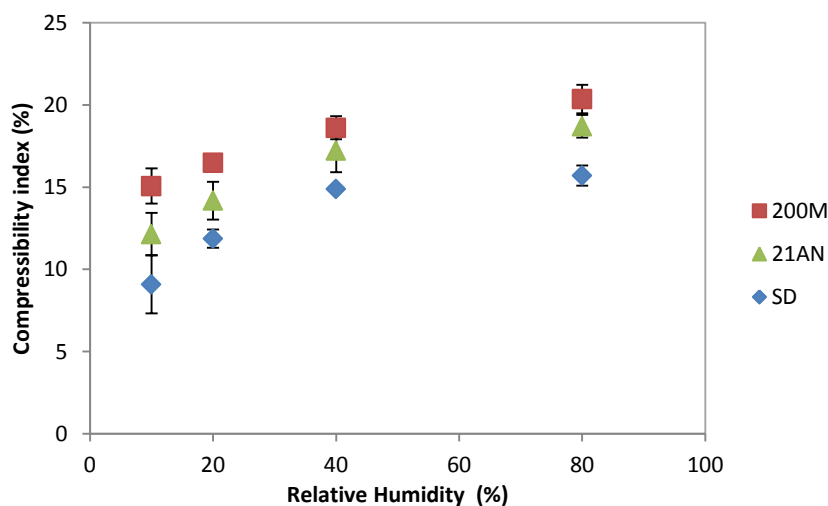


Figure 6.6: Compressibility index of the powders equilibrated at different RH values.

The result of the ffc values in Figure 6.3, the effective angle of internal friction (Figure 6.4), the angle of repose (Figure 6.5) and the compressibility index (Figure 6.6) are all in agreement and confirm that the powder flowability decreases with increasing the relative humidity of the storage.

The change in the relative humidity conditions during storage affects the properties of the material. Exposing a powder to a humid air or environment increases the powder moisture content as shown in Figure 6.2. The moisture content affects the cohesivity and frictional properties of the powder, which are important flow properties of a material [129]. Increasing the powder moisture content increases the powder cohesivity due to the formation of liquid bridges between the particles [102, 129-133]. The increase in the powder cohesivity results in a decrease in the powder flowability since

the cohesivity is the resistance to separation of particles in a material [129]. This was the reason for the reduction in the flowability of lactose powders with increasing the RH conditions during storage as shown in figures above. This result is in agreement and consistent with the finding in the literature, where the increase in the storage RH condition of MCC [131] resulted in an increase in the cohesivity of the powder, consequently, a decrease in the powder flowability.

It is worth noting that the flowability of the three types of lactose is different at the different relative humidity during storage. The SD lactose showed better flowability in comparison to the other two types of lactose. This is due to the difference in the shape and morphology of particles (see Figure 5.1) and also the difference in particle size of the powders (see Figure 4.1). The SD lactose particles are more spherical in shape in comparison to other types of lactose which makes them more flowable, due to reduced interlocking between particle surfaces. The sphericity of particles of 21AN lactose is better and the particles are larger than those of the 200M lactose; this was the reason of showing better flowability. The 200M lactose particles are smaller and have a tomahawk-like shape as can be seen in Figure 5.1. The size, shape and the morphology of particles of 200M affect the flow property of the powder and resulted in poor flowability in comparison to the other types of lactose.

6.5.3 Amount of fines in the product

Figures 6.7-6.9 show the percentage of fines produced with the ribbon at different relative humidity storage conditions using 21AN, 200M and SD lactose respectively. For the three types of lactose, the amount of fines associated with the ribbon during production decreased with increasing hydraulic pressure at all relative humidity conditions. This is due to the better binding ability of the powder at a higher pressure as more force and stress is being applied to the powder. The fines percentage decreased with increasing the relative humidity of the powder and increased again with a further increase in the relative humidity. The fines percentage in the product depends on both the powder moisture content (which affects the powder deformability) as well as the powder flowability during roller compaction [120].

The amount of fines produced from powders conditioned in the range of (10- 40% RH) is highly dependent on the moisture content of powders. At low relative humidity (10% RH) the powder contains the least amount of moisture, as can be seen in Figure 6.2.

This resulted in a reduction of the deformability of the powder. The low deformability of the powder at low relative humidity will affect the binding capacity between the primary particles during roller compaction. This is believed to be the reason for a high percentage of fines which is produced during the roller compaction of powders stored at low RH. Increasing the relative humidity of the storage increases the powder moisture content as seen in Figure 6.2. The increase in the powder moisture content is believed to improve the powder deformability at the edges of the roller. This resulted in a reduction in the fines percentages during roller compaction of powders stored at 20% RH and 40% RH compared to 10% RH.

The high percentage of fines produced from the powders stored at high relative humidity condition (80% RH) is due to the powder flowability. Increasing the relative humidity during storage of the powder increases the powder water content (see Figure 6.2) and, consequently, decreases the powder flowability (see Figures 6.3- 6.6). The decrease in powder flowability at high RH (80% RH) affects the powder flow and distribution between the two rollers in the compaction zone (resulting in ribbons with smaller width see Figures 6.14-6.16). This resulted in less powder presence at the edges of the rollers which reduced the stress being applied to the powder in this region. A lesser stress applied at the edges of the rollers resulted in weaker ribbons at the edges which increased the amount of non-compacted powder (fines) at high relative humidity (80% RH) as shown in Figures 6.7- 6.9.

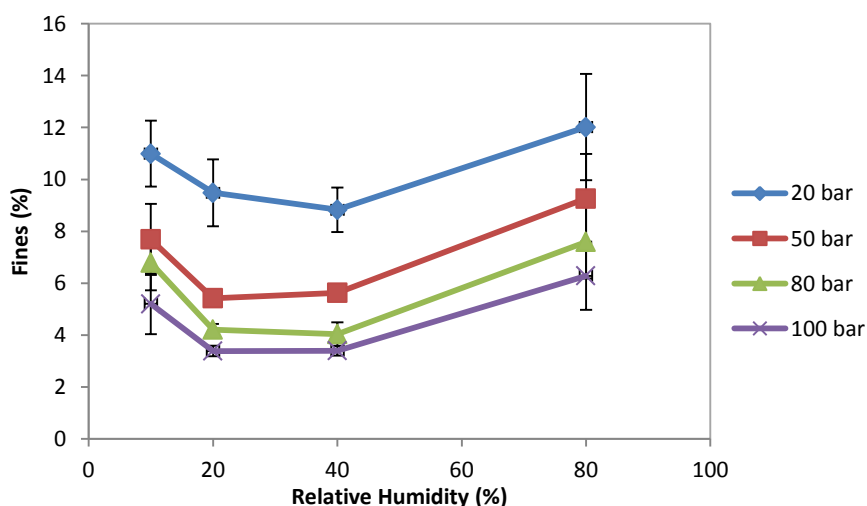


Figure 6.7: Fine percentage produced at different relative humidities for lactose 21AN.

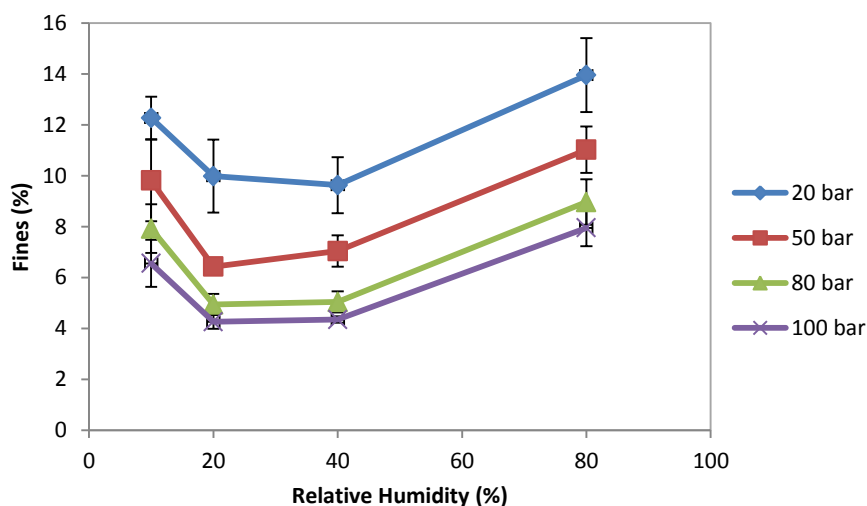


Figure 6.8: Fine percentage produced at different relative humidities for lactose 200M.

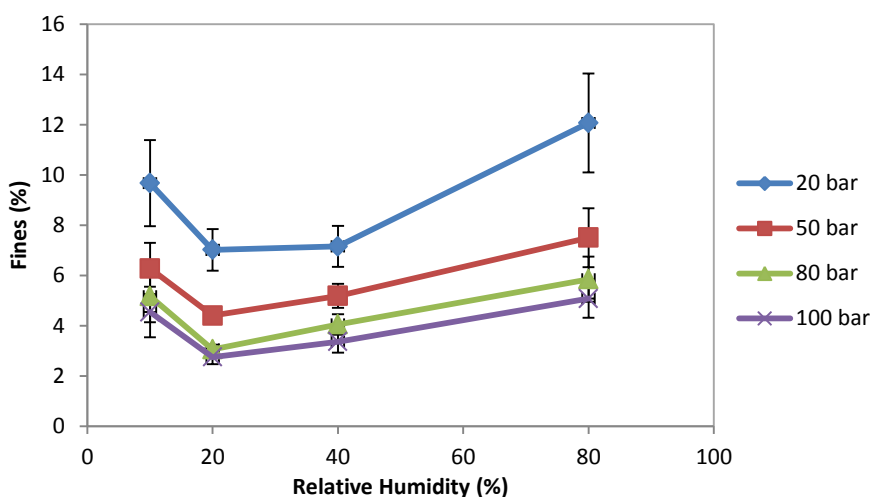


Figure 6.9: Fine percentage produced at different relative humidities for lactose SD.

6.5.4 Velocity of powders during roller compaction (PIV)

The velocity of powders during the production of ribbons in the roller compaction was also measured using the PIV technique [120]. The average surface velocity of each type of lactose was determined at a different angular position and different relative humidity as described in Section 6.4. Figures 6.10- 6.12 show the time averaged resultant velocity against the roll angular position for the three types of powders, conditioned at 20% and 80% RH. It can be seen that the powder velocity is constant in the region before the compaction zone then increases suddenly at a certain angular position (around 10°). The maximum powder surface velocity for all powders at all conditions was at angle zero which is the minimum gap between the two rollers. It can be seen that the velocity is

different for powders equilibrated at 20% and 80% RH. Powders conditioned at 20% relative humidity exhibited higher velocity than those conditioned at 80% RH. This is due to the decrease in the powder flowability at high relative humidity condition (80% RH). This is in agreement with the findings in Figures 6.3-6.6 in that the flowability of the bulk powder decreased with increasing the RH. The decrease in the powder flowability at 80% RH affected the powder surface velocity during the roller compaction.

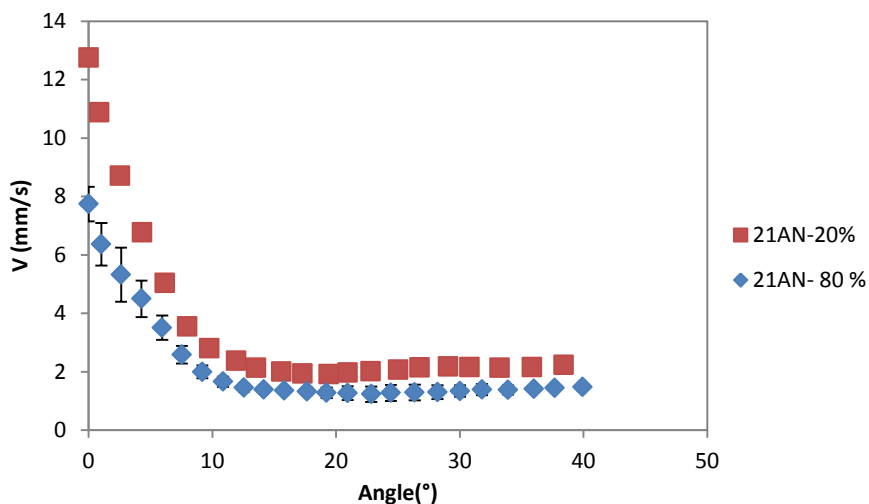


Figure 6.10: Velocity of 21AN lactose during roller compaction at different RH conditions.

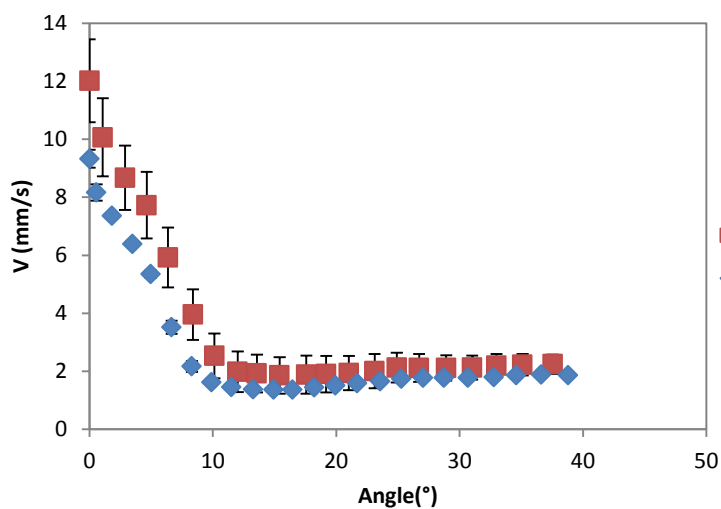


Figure 6.11: Velocity of 200M lactose during roller compaction at different RH conditions.

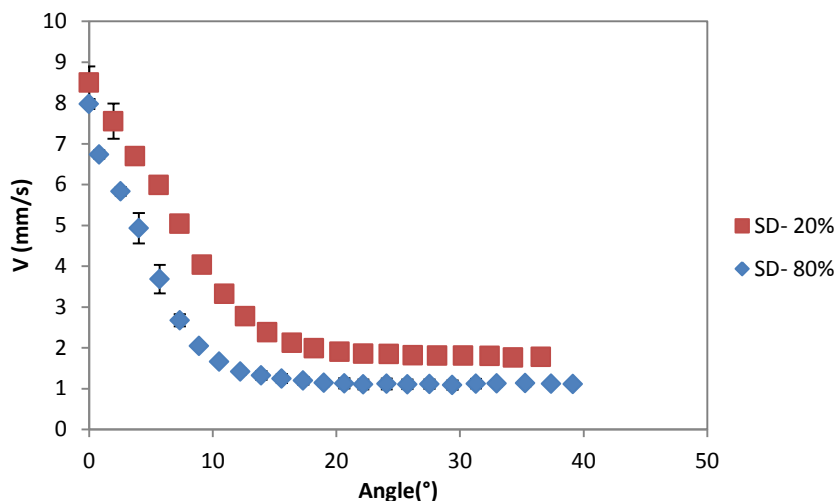


Figure 6.12: Velocity of SD lactose during roller compaction at different RH conditions.

It is worth mentioning that the powder surface velocity measured using the PIV technique represents the powder near the cheek plate which is at the edge of the rollers. The powder surface velocity measured by the PIV method is lower than the tip speed of the roller (18.8 mm/s).

Figure 6.13 shows images of the ribbon taken by the Keyence digital microscopy (Keyence VHX-5000, Japan) as an example to describe the surface of the ribbon across its width. It can be seen that there is a clear print of the roller surface on the ribbon; the rollers used in this work have a knurled surface. This will occur only if the powder is moving at the same velocity as the roller. The imprint of the roller surface onto the ribbon is very clear at the centre; however, when looking at the edges the imprint is not as clear in comparison to the central region. The clear print of the roller surface at the centre of the ribbon confirms that the powder at the centre was moving at the same speed as the roller tip speed. The magnified images in Figure 6.13 show that the surface at the edges of the ribbon is rougher in comparison to the centre, which indicates that the powder at the edges was not moving at the same speed as the roller. This agrees with the powder velocity which is measured using the PIV (Figures 6.10- 6.12). It can be concluded that there is a difference in powder velocity between the centre and the edges of the roller, with high velocity at the centre and lower at the edges.

The difference in the powder velocity across the width of the roller is due to the powder availability and distribution (less powder available at the edges of the roller). This is supported by the X-ray images in Figure 6.13 which illustrate that the ribbon is denser

at the centre in comparison to the edges. The less powder availability at the edges of the roller results in slipping the particles on the roll surface, therefore, resulting in a lower velocity of powder compared to the roller. The powder distribution across the width of the roller depends on the flow property of the bulk powder at different RH values [120]. The decrease in surface velocity of powder conditioned at 80% RH (Figures 6.10- 6.12), at the edges of the roller indicates less powder availability in the compaction zone compared to those conditioned at 20% RH. This resulted in ribbons with a smaller width as shown in Figures 6.14-6.16, therefore, producing a higher percentage of fines with the ribbons at 80% RH condition (Figures 6.7- 6.9).

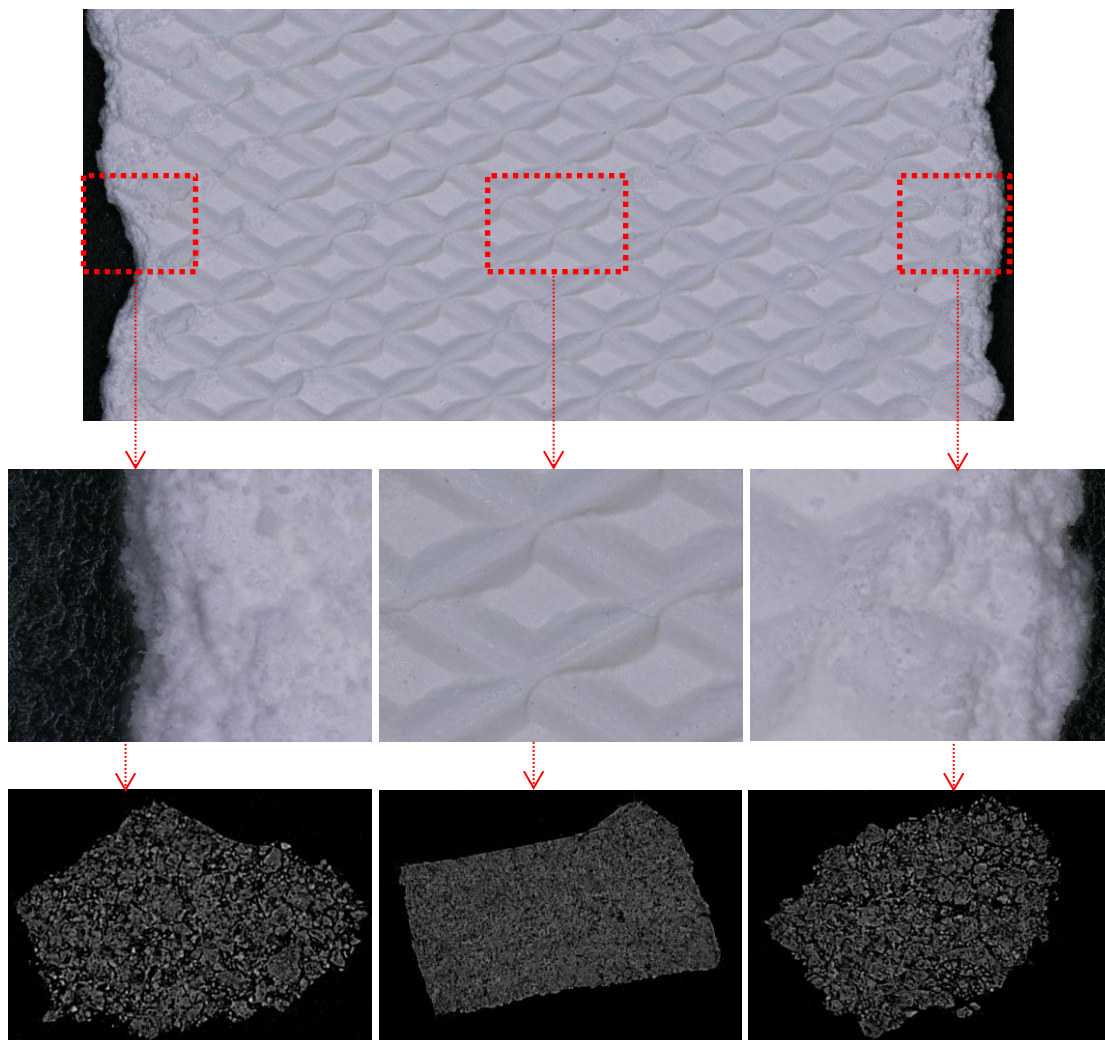


Figure 6.13: Microscope and X-ray Images of ribbon as an example to show the surface and structure across the width of the ribbon.

6.5.5 Width of the ribbon

The flow property of the powder plays an important role during roller compaction process, especially in the compaction zone. Powders with poor flowability cannot distribute evenly across the width of the roller, therefore, there will not be sufficient powder present at the edge of the roller. The lesser powder availability at the edges of the roller results in less stress being applied at the edges compared to the centre of the roller. This will affect the product quality and results in ribbons with different width and varied amount of fines. The width of ribbons produced from the lactose powders at different relative humidity conditions was determined and compared. Figures 6.14-6.16 show the width of the ribbons produced from different types of lactose at different relative humidity conditions. It can be seen that the relative humidity of the powder has a significant effect on the width of the ribbons produced from different types of lactose. The width of ribbon was found to increase slightly with increasing the RH, then decrease with further increase in the RH during powder storage. Powders stored at 80% RH condition produced ribbons with the smallest width. This explains the high percentage of fines produced from powders conditioned at 80% RH in Figures 6.7- 6.9. The fine produced during the ribbon production usually comes from the edges of the ribbon, as the stress is low due to the lesser powder being present at the edges of the roller. The wider ribbon was produced for powders stored in the range of 20% - 40% RH. At this range, the lowest amount of fines was produced from all types of lactose. This is believed to be due to the better binding ability of the primary particles as a result of the higher powder moisture content as shown in Figure 6.2. The increase in the powder moisture content in the range 20%- 40% RH improved the powder deformability, which resulted in better binding, and consequently, in wider ribbons with a lower amount of fines.

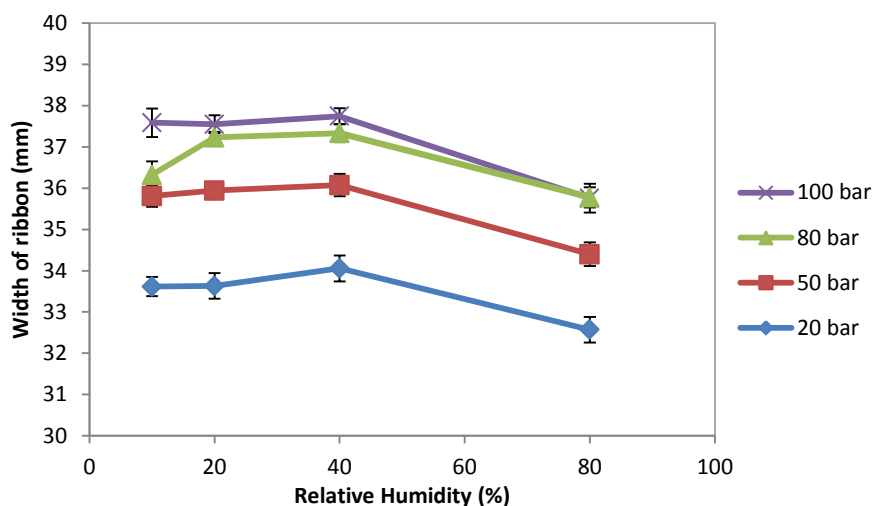


Figure 6.14: Width of the ribbon at different relative humidities for lactose 21AN.

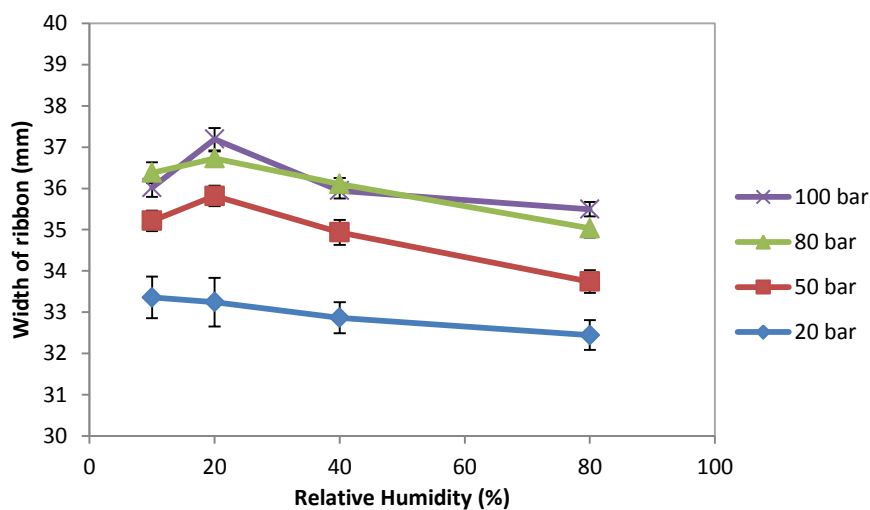


Figure 6.15: Width of the ribbon at different relative humidities for lactose 200M.

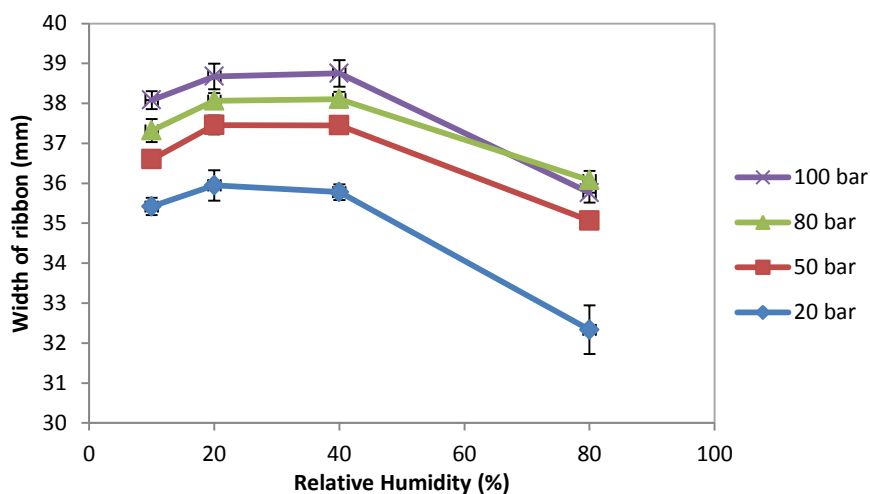


Figure 6.16: Width of the ribbon at different relative humidities for lactose SD.

6.5.6 Compressibility of the powders at different RH conditions

The compressibility factor of a material gives information on how the volume of a material changes under different stress levels. This was implemented to examine the behaviour of powder under different relative humidity conditions. The compressibility factor of the three types of lactose under different relative humidity conditions was determined using the relationship between the uniaxial stress and the resulting powder bed density. Powders of the same mass and equilibrated under different RH storage conditions were compressed using Instron testing machine and the compressibility factor was determined as described in Section 3.2.6. Figure 6.17 shows the compressibility factor for the three types of lactose stored at different relative humidity conditions. It was reported that the compressibility factor for a completely compressible material is $K=0$ and for an incompressible material $K=\infty$ [7]. It can be seen from Figure 6.17 that the storage under different RH values resulted in powders with different compressibility. For 200M and SD lactose the compressibility factor decreased with increasing the RH and then increased again with a further increase in the RH. The lowest compressibility factor was for powder stored at 40% RH which indicates the better compressibility of the powder. For lactose 21AN, the compressibility factor decreased gradually with increasing the RH value during storage, indicating that the higher the relative humidity of the powder during storage the better the compressibility of the powder.

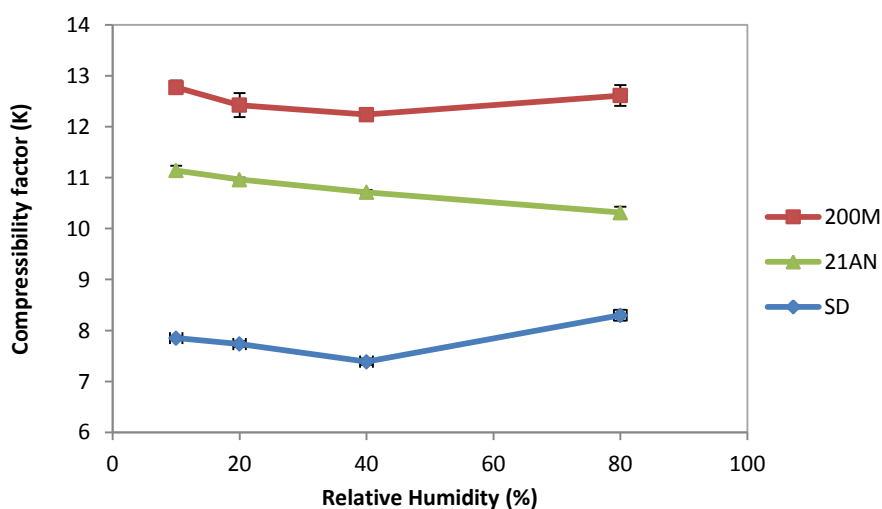


Figure 6.17: Compressibility factor (K) for the three types of lactose at different relative humidity conditions.

6.5.7 Ribbon tensile strength

Figures 6.18-6.20 show the tensile strength of the ribbon produced from different types of lactose at different relative humidity conditions (10% - 80% RH). From these results, it can be seen that the tensile strength of all types of lactose significantly affected by the hydraulic pressure applied on the powder during the roller compaction. Increasing the pressure during compaction increased the tensile strength of the ribbon at all RH conditions studied. This was due to the higher stress being applied on the powder with increasing the hydraulic pressure, which brings the primary particles closer to each other and decreases the distance between them. The decrease in the distance between the particles results in an increase in the Van der Waals forces [51, 104].

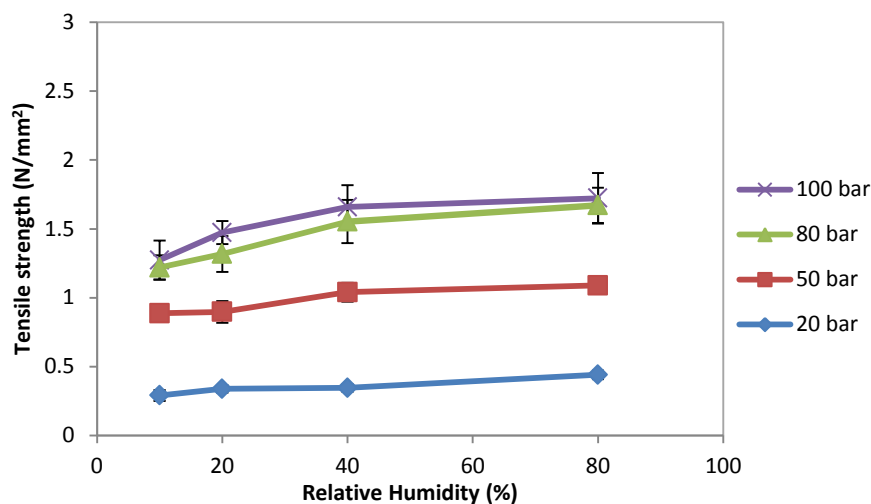


Figure 6.18: Tensile strength of the ribbon at different relative humidities for lactose 21AN.

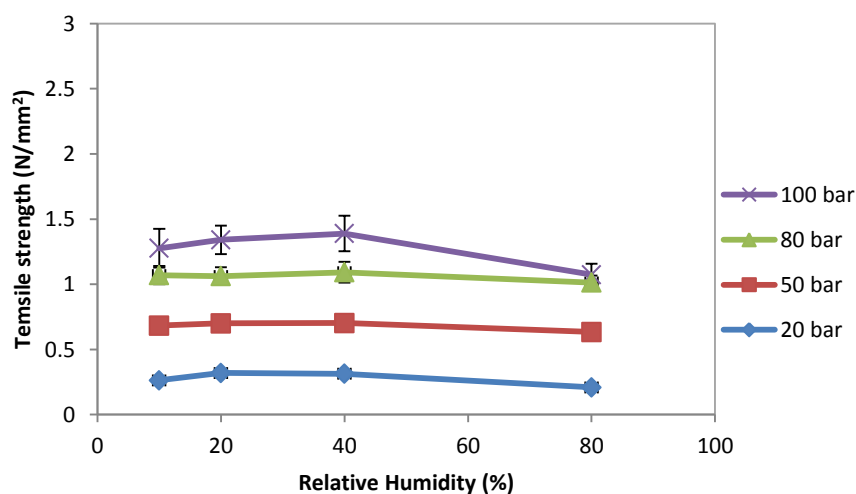


Figure 6.19: Tensile strength of the ribbon at different relative humidities for lactose 200M.

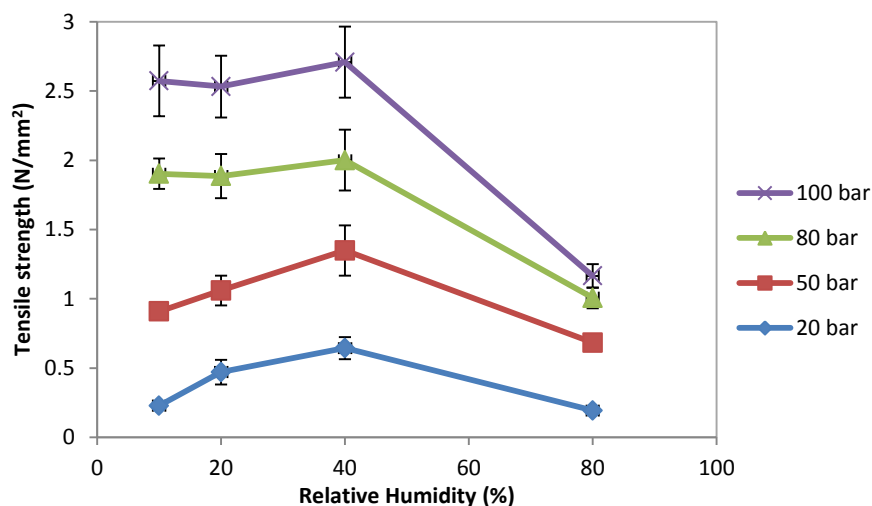


Figure 6.20: Tensile strength of the ribbon at different relative humidities for lactose SD.

The change in the storage RH condition was shown to have a minimal effect on the tensile strength of ribbon produced from lactose 21AN and 200M especially at low RH values. The tensile strength of ribbon produced from lactose 21AN increased slightly with increasing the RH value from 10% to 80% RH. The highest tensile strength for ribbons produced from 21AN lactose was at 80% RH, as can be seen in Figure 6.18. This is in agreement with the compressibility factor result in Figure 6.17, in that the lowest compressibility factor (highest compressibility) was shown for powder conditioned at 80% RH. The increase in the RH value during storage increases the powder moisture content (see Figure 6.2). The adsorption of a small amount of water at the particle surface, with increasing the RH value, is believed to dissolve and smoothen the irregularities on the particle surface. This results in decreasing the distance between the particles and therefore increasing the Van der Waals forces. The small amount of adsorbed water on the surface between two particles may also act as a binder after dissolving then solidifying during compression. This resulted in a slight increase in the tensile strength of ribbon produced from the 21AN lactose with increasing the RH value.

The increase in the compact strength with increasing the powder moisture content was reported during the tableting of different material. Nokhodchi et al. [119] revealed that the crushing strength of tablets of Ibuprofen increased with increasing the moisture content up to 2.5% w/w, while, moisture content above 3.5% w/w resulted in a reduction in tablet crushing strength. Increasing the moisture content of Paracetamol up to 6% w/w was also found to increase the tablet crushing strength [134]. These results

are in agreement with the result in Figure 6.18 in that the tensile strength of ribbon of 21AN lactose increased slightly with the increase in the storage RH since the water content of the powder was low (below 1% w/w) at all RH conditions.

The tensile strength of ribbon produced from 200M and SD lactose increased slightly (for some pressures) for powders stored at 40% RH as can be seen in Figure 6.19 and Figure 6.20. This is in agreement with the findings shown in Figure 6.17, where the lowest compressibility factor (high compressibility) was found for these two powders at 40% RH. The increase in compacts tensile strength with increasing the relative humidity and powder moisture content was reported in the literature [31, 51, 135]. Sebhatu and Alderborn [31] revealed that storing amorphous lactose at 22% RH condition resulted in tablets with a higher strength than that stored at 0% RH. This is in agreement with the result in Figure 6.19 and Figure 6.20, as the 200M and SD lactose contains a small amount of amorphous powder. The increase in the storage conditions to 40% RH increased the powder moisture content (see Figure 6.2). This will increase the powder compressibility and deformability (see Figure 6.17) which then increases the bonding area between the particles during roller compaction, therefore, results in slightly stronger ribbons.

From Figure 6.19 and Figure 6.20, it can be seen that the storage of powders at 80% RH condition resulted in ribbons with the lowest tensile strength, which is again in agreement with the findings in Figure 6.17 in that the powder (200M and SD) stored at 80% RH showed highest compressibility factor (lowest compressibility). This is believed to be due to the presence of amorphous lactose within the powder which affects the powder compressibility and deformability [120]. It is believed that at a high relative humidity of 80%, the amorphous lactose crystallises [116, 117], which results in a loss of the powder compressibility and deformability. The high compressibility factor (low compressibility) for 200M and SD lactose at 80% RH (see Figure 6.17) is due to the absence of amorphous lactose within the powder. The crystallisation of the amorphous part in the powder reduces the powder binding abilities which resulted in ribbons with the lowest tensile strength.

The crystallisation of the amorphous fraction in the powder at 80% RH was confirmed by the FT-NIR method for the SD lactose. Samples of the SD lactose were conditioned in the climatic chamber at 10% RH and 80% RH. These samples were kept in the

desiccator over silica gel for drying and remove the moisture as described in Section 3.2.2 [104, 120]. The FT-NIR was then used to obtain the second derivative of the NIR spectra for SD lactose conditioned at different RH as well as pure amorphous lactose as shown in Figure 6.21. It can be seen from Figure 6.21 that there is a clear difference in the absorbance of powders with varying amorphous content for a range of wave numbers. The most significant difference was seen at the wave number range between 5100-5290 cm^{-1} . It has been reported that the change in the structure of amorphous lactose, with increasing the RH, can be observed by changing the size of the NIR spectrum peak in the 1900-1950 nm region (corresponding to 5128-5263 cm^{-1}) [136]. In this region, the peak caused by the O-H group of water molecules appears. It is possible to recognise if the water is present as a hydrate, where the water molecules are organised in the crystal structure, or randomly arranged in the amorphous matrix by observing the peak size between 1900-1950 nm [111, 136]. It was found that increasing the crystallinity of lactose powder increases the sharpness of the peak in this region due to the change in the state of the water [111, 136]. Figure 6.21 shows that the two samples of the SD lactose exhibited sharper negative peaks in comparison to the pure amorphous lactose which showed a broader negative peak (negative peak in the second derivative corresponds to a positive peak in the original spectrum). The peak of the SD lactose which is conditioned at 80% RH is sharper in comparison to the powder conditioned at 10% RH indicating a higher crystallinity (lower amorphous content). This is in agreement with what have been reported in the literature [111, 136]. The conditioning of the powder at 80% RH resulted in the transformation of the amorphous fraction to crystalline lactose which increased the amount of water of crystallisation and resulted in a sharper peak as illustrated in Figure 6.21. This is in agreement with previous studies which stated that amorphous lactose begins to crystallise when stored at a relative humidity above 50% [116, 117].

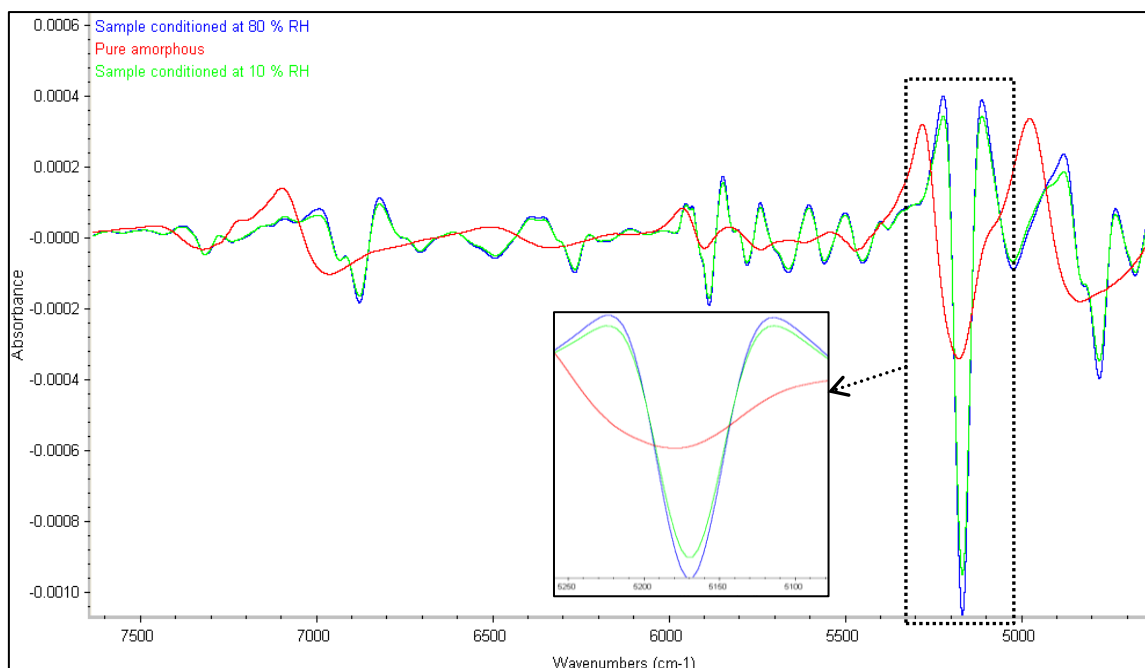


Figure 6.21: Second derivative of the spectra for the SD lactose conditioned at 10% and 80% RH and pure amorphous lactose.

6.5.8 Ribbon surface structure (SEM)

Figure 6.22 shows scanning electron microscopy (SEM) micrographs for ribbons produced at 100 bar from 21AN, 200M and SD lactose and different RH conditions. It can be seen that the surface of the ribbon seen by SEM images for powder conditioned at 20% RH and 80% RH are different for the three types of lactose. Figure 6.22 (A and B) shows the SEM images for ribbons produced at 100 bar using the 21AN lactose at 20% RH and 80% RH respectively. It can be seen that ribbons produced from powder stored at 80% RH have more flat surfaces in comparison to those at 20% RH. This is due to the fact that increasing the RH during storage results in adsorbing a small amount of water on the surface between two particles, which dissolves and smoothen the irregularities and decrease the distance between them. This resulted in an increase in the bonding area between the particles and consequently in stronger ribbons as shown in Figure 6.18.

Figure 6.22 (C, D, E, F) illustrate the difference in ribbon surface for 200M and SD lactose, conditioned at 20% RH and 80% RH. It can be seen that powders conditioned at 20% RH produced ribbon with a flatter surface in comparison to those produced at 80% RH. The flat surfaces which appear on the ribbon for powders conditioned at 20% RH (Figure 6.22 (C and E)) indicate a higher amount of plastic deformation during

compaction at 100 bar. This was not the case with powders conditioned at 80% RH, as the ribbon exhibited a rougher surface (Figure 6.22 (D and F)). The plastic deformation of 200M and SD lactose at 20%RH during compaction are believed to be due to the presence of an amorphous fraction in the powder. The amorphous lactose is known to deform in a more plastic manner in comparison to crystalline lactose [21, 31, 32]. Vromans et al. [21] reported that amorphous lactose is acting as a binder during compaction and shows more plastic deformation than crystalline lactose. Sebhatu and Alderborn [31] confirmed that amorphous lactose exhibited higher deformability during compression compared to crystalline lactose. The high deformability of amorphous lactose, during compression, increased the contact area between the particles which resulted in stronger inter-particle bonds in comparison to crystalline lactose.

The storage of 200M and SD lactose at 80% RH changed the powder properties. At 80% RH the amorphous fraction in the powder crystallised which resulted in a loss of the powder binding properties. The absence of the amorphous fraction in the powder at 80% RH resulted in a reduction in the powder deformability and compressibility, as shown in Figure 6.17. Furthermore, it produced ribbons with a less flat surface as illustrated in Figure 6.22 (D and F).

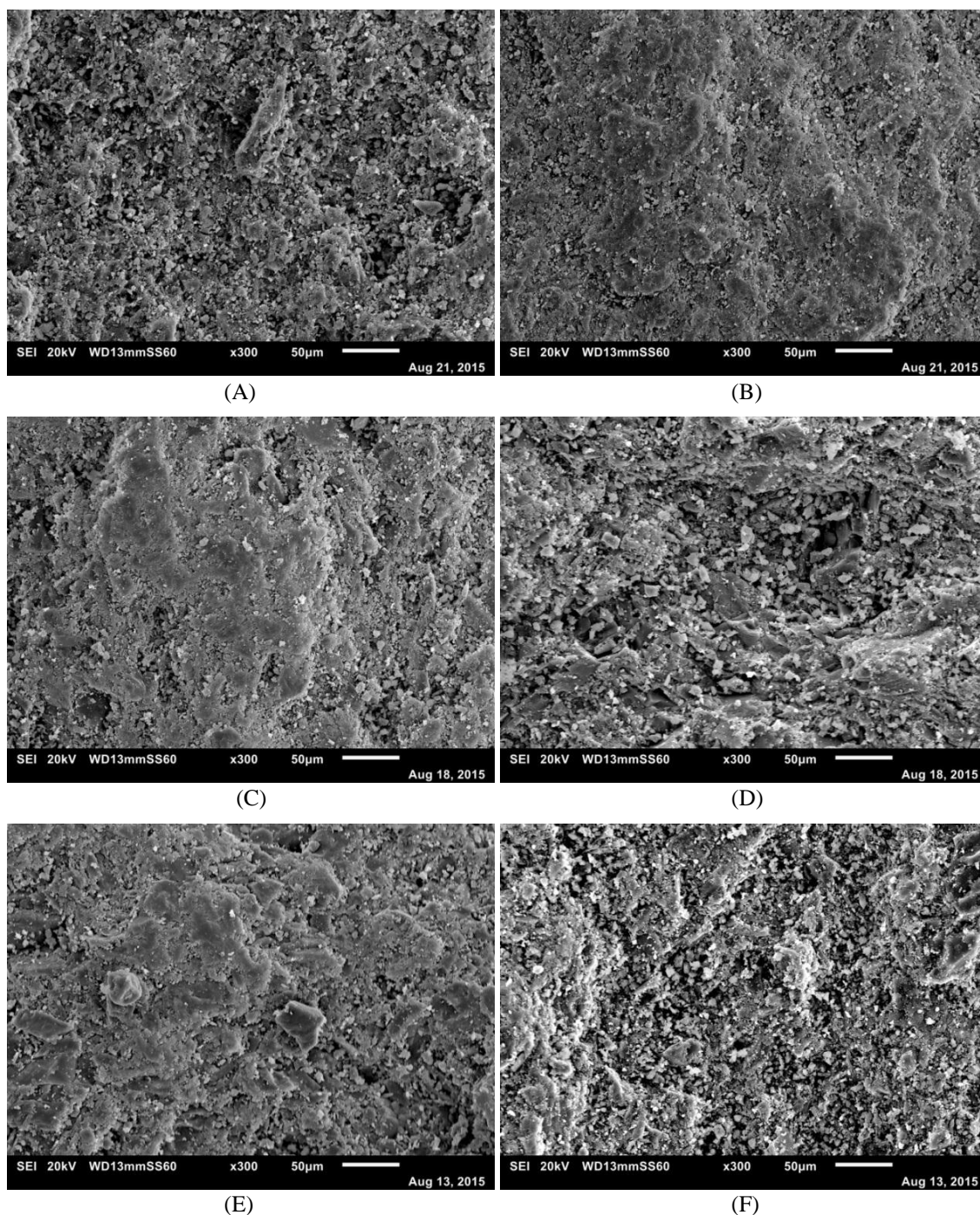


Figure 6.22: Scanning electron microscope images for ribbons produced at 100 bar from 21AN (A, B), 200M (C, D) and SD (E, F), at 20% RH (A, C, E) and 80% RH (B, D, F).

6.5.9 Porosity of ribbons

The porosity of the ribbon was determined using the X-ray technique as outlined in Section 3.2.11. Samples were taken from the centre of the ribbon and the X-ray was used to obtain images which were analysed for their porosity using the ImageJ software. Figures 6.23-6.25 show the porosity of ribbon produced from 21AN, 200M and SD lactose respectively at different relative humidity conditions. It can be seen that the

porosity of ribbon for all types of lactose decreased with increasing the hydraulic pressure during roller compaction. An increase in the hydraulic pressure increases the stress applied on the powder during the roller compaction. This will bring the particles close to each other and increase the particle fragmentation and deformation which results in filling the gap and decrease the porosity.

As regard to the RH during the storage of powder, ribbons with different porosity was exhibited by different powder at various RH conditions. The porosity of ribbon produced from lactose 21AN was decreasing gradually with increasing the RH value during storage as shown in Figure 6.23. The lowest porosity was shown for ribbon produced from powder stored at the highest RH condition 80%. The storage of powder at elevated RH conditions increases the powder moisture content (see Figure 6.2). As mentioned earlier, the small amount of the adsorbed water on the particle surface at elevated RH resulted in dissolving the irregularities between two particles which decreased the distance and resulted in ribbon with less porosity.

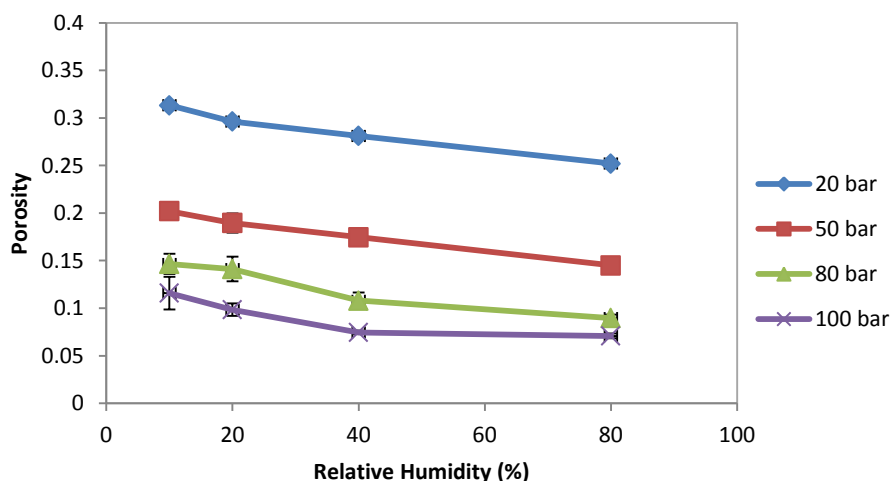


Figure 6.23: Porosity of ribbon of lactose 21AN at different RH condition.

The porosity of ribbon of 200M and SD lactose decreased with increasing the RH value during storage of powder up to 40% RH. Further increase in the storage RH condition (80%) resulted in an increase in the ribbon porosity as shown in Figure 6.24 and Figure 6.25. This is, as described earlier, due to the presence of a fraction of amorphous powder in 200M and SD lactose. The increase in the storage condition from 10% to 40% RH increased the powder moisture content (see Figure 6.2) while the amorphous fractions still exist. The increase in the powder moisture content increases the powder

compressibility and deformability (see Figure 6.17). This will result in a more plastic deformation and a decrease in the distance between the particles during compaction, therefore reduces the porosity of the ribbon. The increase in the porosity of ribbons produced from the powder stored at 80% RH is due to the absence of the amorphous fraction which crystallised at a relative humidity above 50% RH [116, 117]. The crystallisation of the amorphous fraction decreased the powder compressibility (see Figure 6.17). This then decreased the deformation of particles when powder stored at 80% RH, therefore, resulted in the higher porosity of ribbon during the roller compaction.

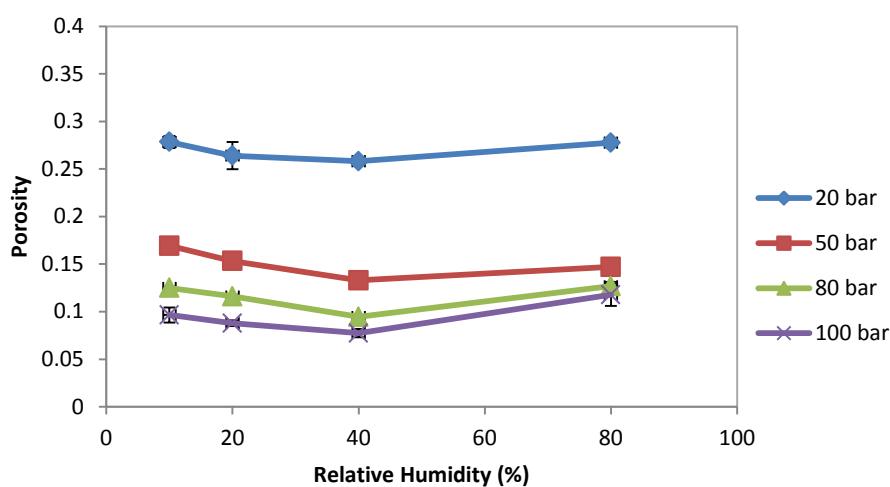


Figure 6.24: Porosity of ribbon of lactose 200M at different RH condition.

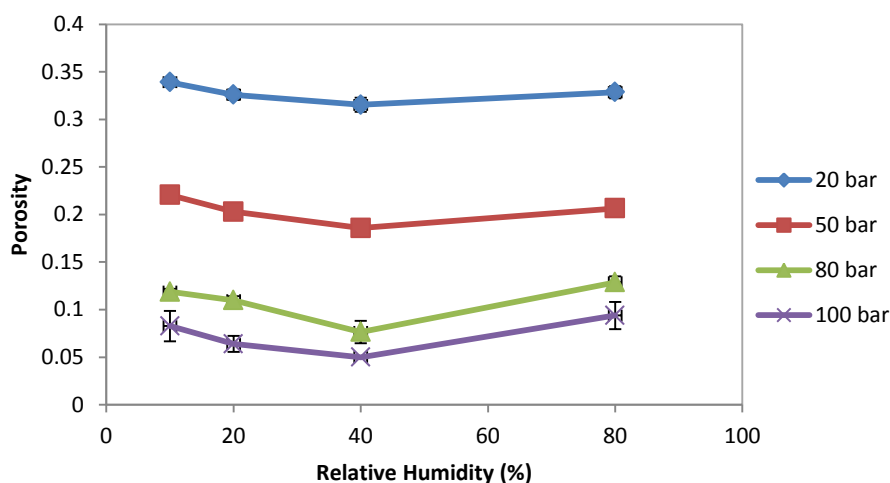


Figure 6.25: Porosity of ribbon of lactose SD at different RH condition.

6.6 Conclusion

The work in this chapter investigated the effect of the relative humidity during storage of lactose powders on properties of ribbon produced using roller compaction. Three types of lactose powders were used in this work, anhydrous lactose SuperTab21AN, α -lactose monohydrate 200M and spray dried lactose SuperTab11SD.

Powders were stored under different relative humidity conditions ranging from 10% to 80% RH. It was found that the relative humidity during storage of the powder has a significant effect on the roller compaction behaviour and on final ribbon properties. The percentage of fines in the product, which is a disadvantage in the roller compactor, decreased with increasing the relative humidity of the powder (from 10% to 40% RH) and increased again with a further increase in the relative humidity (80%). This was attributed to both the powder moisture content and powder flow property which changes by altering the relative humidity. The decrease in the percentage of fines with increasing the RH value (from 10% to 40% RH), was attributed to the better binding ability of the powder due to the increase in powder compressibility and deformability as the moisture increases. A further increase in the RH of the storage (80% RH) resulted in a significant decrease in powder flowability. The poor flowability of the powder at 80% RH affected the powder velocity during the roller compaction as shown in the PIV experiments. Powders stored at high RH value (80%) showed a lower velocity compared to those stored at 20% RH. This resulted in lesser powder availability at the edges of the rollers, which resulted in producing ribbons with a smaller width and increased the percentage of fines in the product. The relative humidity of the storage showed minimal effect on the ribbon tensile strength especially at low RH conditions (10 - 20%). At 80% RH, the tensile strength of ribbons produced from lactose 200M and SD was found to be the lowest. This was believed to be due to the presence of amorphous lactose within these two powders, which crystallised and reduced the powder compressibility and deformability. This was supported by SEM images which showed that ribbons produced at 20% RH contained more flat surfaces in comparison to those at 80% RH. The highest tensile strength of ribbons produced from lactose 21AN was for those conditioned at 80% RH. This was due to the high moisture content of the powder at 80% RH. This resulted in dissolving the irregularities between the particles which decreased the distance between them and resulted in stronger bonds. The porosity of the ribbon was

also found to be different at various storage conditions. The porosity of ribbons produced from lactose 200M and SD decreased with increasing the RH conditions up to 40% RH and then increased when the powder stored at 80% RH. The porosity of lactose 21AN was found to decrease gradually with increasing the RH value of the storage, and the lowest porosity was found for powder stored at 80% RH. It was concluded that the optimum processing conditions for all three types of lactose are in the range of 20% - 40% RH.

CHAPTER 7 ROLLER COMPACTION AT DIFFERENT PROCESS PARAMETERS

7.1 Introduction

In the previous Chapters, it was concluded that the properties of the starting material have a significant effect on both the roller compaction behaviour and the product quality. However, not only the properties of the primary powder will affect the product quality, but also the process parameter during the roller compaction. There are few process parameters in the roller compactor which could be altered during the production of compacts and granules. The compaction pressure, feeder screw speed, roller speed and the gap between the two rollers are the process parameters which affects the properties of ribbon and granules. Compaction pressure is one of the most important process parameters in the roller compaction. From the result in Chapter 5 and 6, it was found that the compaction pressure has a significant effect on the roller compaction behaviour and on the ribbon properties. Increasing the pressure during compaction increases the temperature of the ribbon during production, reduces the fines percentage, increases the ribbon width and tensile strength and decreases the porosity of the ribbon. However, during the work in the previous Chapters, other process parameters such as feeder screw speed, roller speed and the gap between the two rollers received very limited attention.

In this Chapter, the effect of the process parameter; feeder screw speed, roller speed and the gap between the rollers is investigated. The online thermal imaging camera was used to determine the temperature of the ribbon during production which was linked to the change in the process parameter. The percentage of fines produced during the roller compaction, width, tensile strength and porosity of the ribbon were employed to assess the product quality.

7.2 Preparation of the powders

The work in this Chapter was carried out using the three types of lactose as received from the supplier. The powders were conditioned in a climatic chamber (Binder KMF 240 climatic chamber, Germany) at 25°C and 20% relative humidity condition for 3 days.

7.3 Production of ribbon

A hydraulic pressure of 50 bar was used to compress the lactose powder and produce ribbon. Ribbons were produced at different roller speed, different feeder screw speed, and the different gap between the rollers.

To eliminate the effect of humidity in the laboratory on the powder relative humidity, a GenRH-A (London, UK) humidity generator was connected to the top of the hopper on the roller compactor as shown in Figure 3.6. The humidity generator was operated at the same conditions as the climatic chamber (20%); this ensured a constant humidity condition of the powder during roller compaction same as that used for the storage of the powder prior to compaction.

7.4 Result and discussion

7.4.1 Effect of the roller speed

The speed of the roller controls the dwell time of the powder between the two rollers and also the amount of powder between the rollers which may affect the strength of the ribbon. In order to examine the effect of the roller speed, the three types of lactose were compacted at a constant pressure of 50 bar, and using different speed of the roller as described in Table 7.1. The gap between the rollers was kept constant at 3 mm by using the automatic feedback system which alters the speed of the feeder screw to maintain a constant gap.

Table 7.1: Design of the experiment used during the investigation of the roller speed.

Hydraulic pressure (bar)	Roller speed (rpm)	Gap (mm)	Feeder screw speed (rpm)
50	3	3	Variable (due to the use of the gap controlling feedback system)
	4		
	5		
	6		

The surface temperature of the ribbon was determined using an online thermal camera during the roller compaction as described in Section 3.2.8. Figure 7.1 shows the maximum temperature of the ribbon during the production at a different roller speed of the three types of lactose. It can be seen that the temperature of the ribbon increased slightly with increasing the speed of the roller during production. The slight increase in the ribbon temperature with increasing the roller speed could be attributed to the increase in the internal friction of the powder as a result of increasing the speed of the powder while passing between the rollers. Another reason for the increase in the temperature could be the increase in the feeder screw speed (see Table 7.2) while attempting to maintain constant gap during ribbon production. This will increase the internal friction between the particles and increase the temperature of the ribbon. This is in agreement with the finding of Osborne [59] in that the temperature of ribbon of maltodextrin was found to increase slightly with increasing the roller speed in the range of (3-9 rpm).

Table 7.2: Feeder screw speed at different roller speed.

Roller speed (rpm)	Feeder screw speed (rpm)
3	59.5
4	69
5	76
6	81.3

It can be noted that the temperature of ribbon produced from SD lactose is higher than that produced from the other types of lactose. This is due to the difference in the particle morphology and the powder amorphous content as seen in Chapter 5.

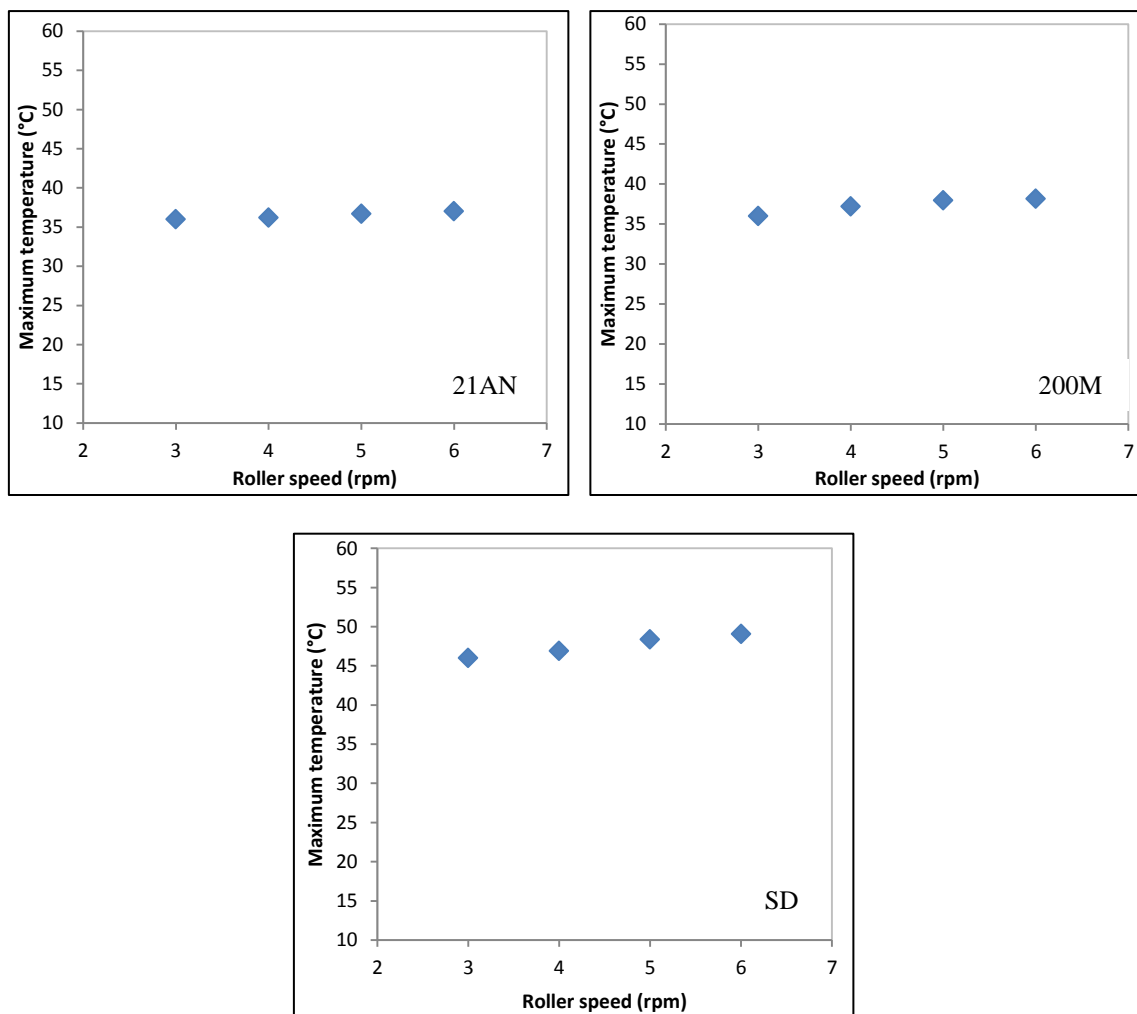


Figure 7.1: Surface temperature of the ribbon during the production at different roller speed.

The percentage of fines produced during the roller compaction at different roller speed was used to evaluate the product quality. The fine percentage was determined for each type of lactose as described in Section 3.2.9. Figure 7.2 shows the percentage of fines produced from the three types of lactose at different roller speed. The fines percentage was found to increase with increasing the speed of the roller during the roller compaction. The increase in the roller speed during the compaction increases the speed of the powder and decreases the time which the powder spends in the compaction zone. The higher the speed of the roller the lesser the time for powder in the compaction zone. This means that the powder will not have enough time to distribute evenly across the width of the roller. This will result in less powder availability at the edges which leads to a decrease in the stress applied on the powder at the edges consequently poor binding and a larger amount of fines at higher roller speed as shown in Figure 7.2.

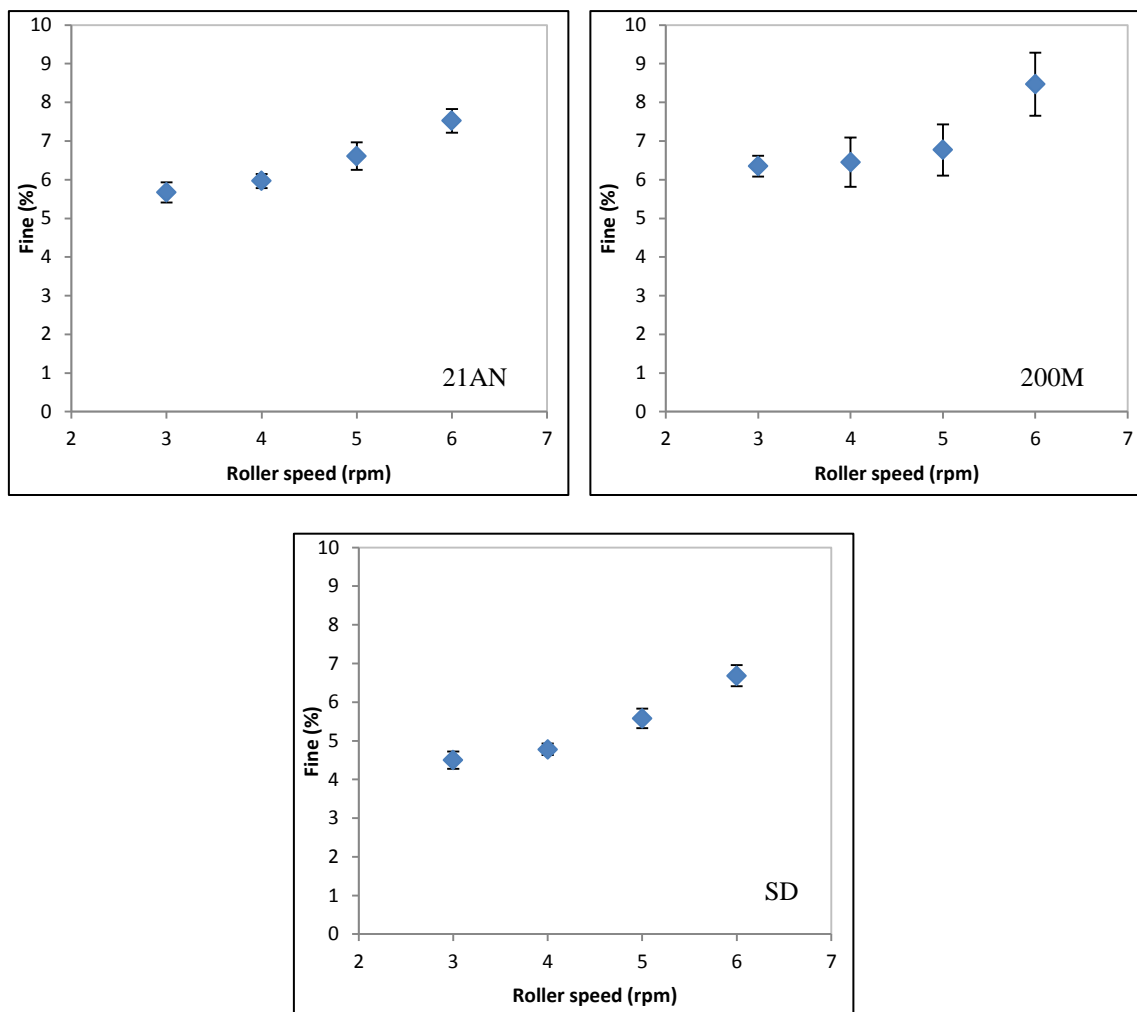


Figure 7.2: Fines percentage produced during the production of ribbon at different roller speed.

The poor distribution of the powder across the width of the roller at higher roller speed resulted in less powder being present at the edges which affected the width of the produced ribbon. Figure 7.3 shows the width of ribbon produced from the three types of lactose at different roller speed. It can be seen that the width of the ribbon is decreasing with increasing the speed of the roller during the production. Increasing the speed of the roller during the compaction decreases the amount of the powder at the edges. This will result in the larger amount of fines in the product (see Figure 7.2) and consequently in ribbons with smaller width as shown in Figure 7.3. This result is in agreement with the finding of Miguélez-Morán et al. [67], who reported that wider ribbons can be produced when lower roller speed used during the production of ribbon using MCC avicel PH102.

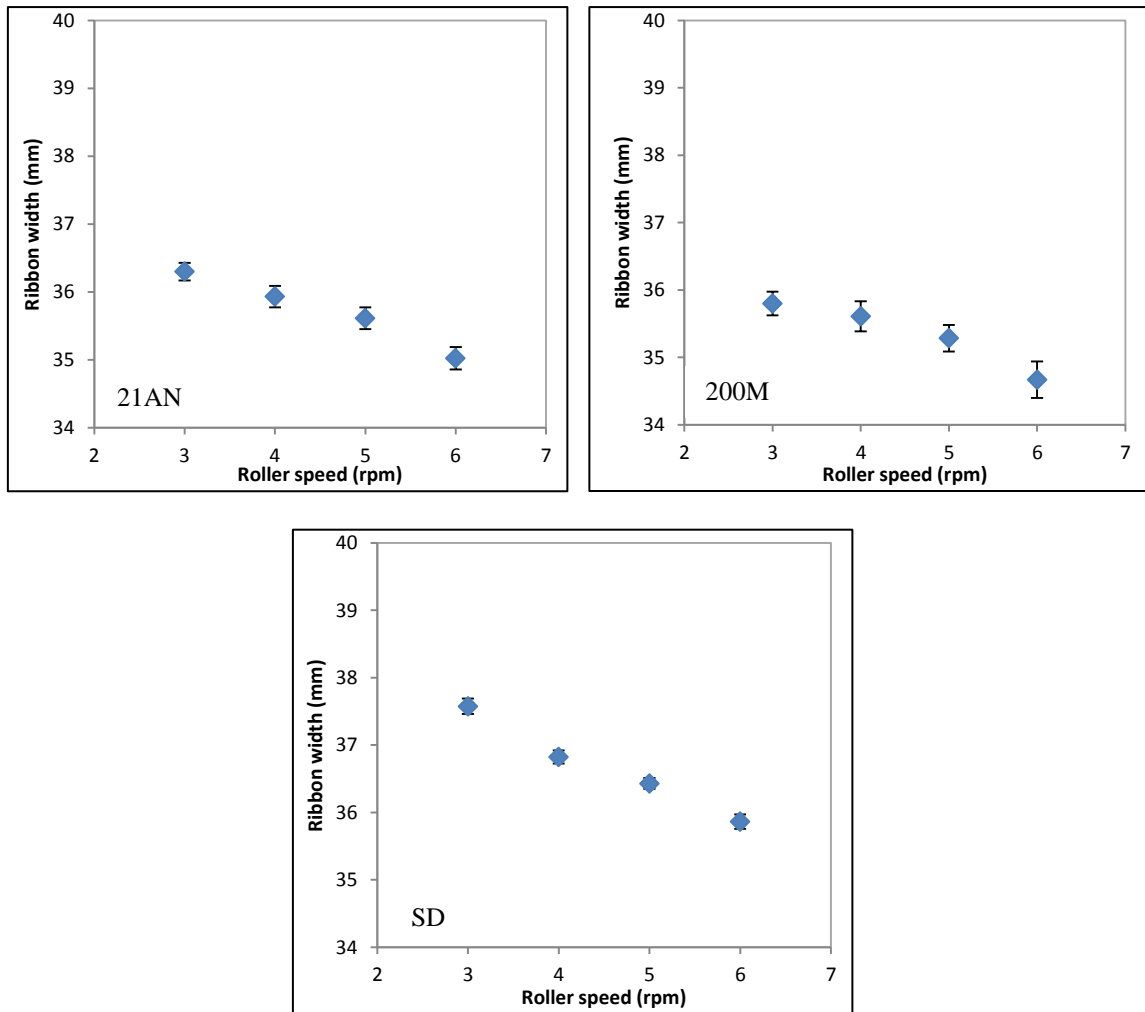


Figure 7.3: Width of ribbon produced from the three types of lactose at different roller speed.

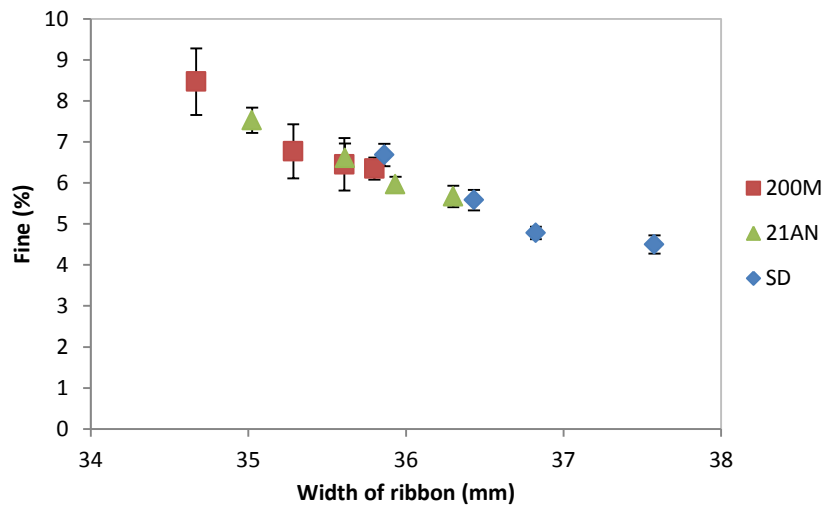


Figure 7.4: Relationship between the fine percentage and the width of the ribbon.

From Figure 7.2 and Figure 7.3, it can be concluded that the percentage of fines produced during the roller compaction are related to the width of the ribbon as shown in Figure 7.4. Regardless the types of the powder and the roller speed, it was found that the higher the width of the ribbon the lesser the percentage of fines in the product.

The increase in the roller speed was found to have an insignificant effect on the ribbon tensile strength. The tensile strength of ribbon of the three types of lactose was determined as described in Section 3.2.10 and plotted against the roller speed as shown in Figure 7.5. It can be seen that the ribbon tensile strength decreased very slightly with increasing the speed of the rollers during production. The slight and insignificant decrease in the ribbon strength could be attributed to the decrease in the dwell time (the time which the powder spends under compression) with increasing the roller speed.

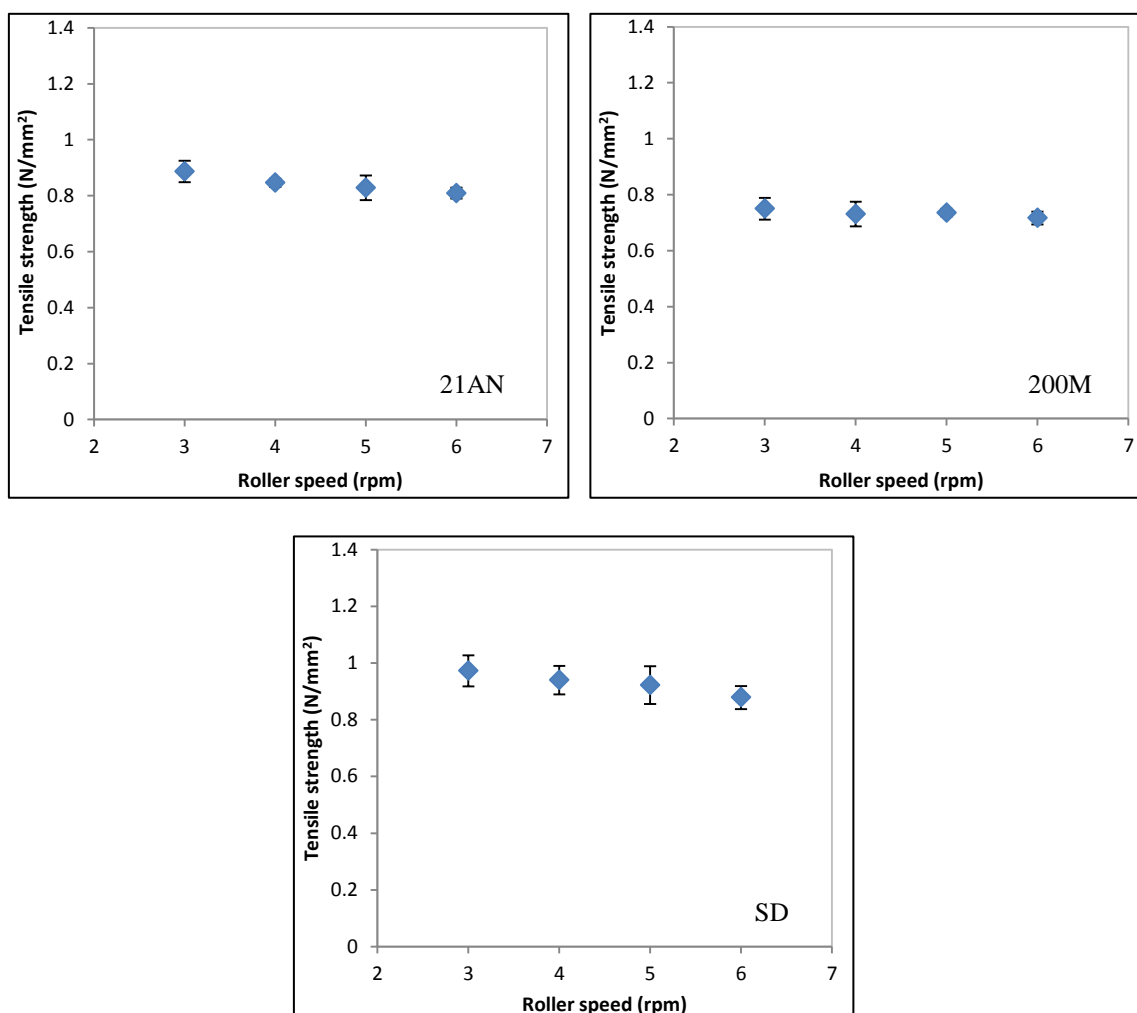


Figure 7.5: Tensile strength of ribbon produced from the three types of lactose at different roller speed.

The porosity of ribbon was determined using the X-ray tomography which is outlined in Section 3.2.11. The porosity of ribbon of the three powders was determined and plotted against the roller speed in Figure 7.6. It can be seen that the increase in the roller speed had no effect on the ribbon porosity. This result is supported by the finding in Figure 7.5 where roller speed was found to have an insignificant effect on the ribbon tensile strength. The minor effect of the roller speed on the ribbon tensile strength and porosity is in agreement with the findings in the literature [59, 61]. Osborne [59] reported that the increase in the roller speed during compaction has a minor effect on the tensile strength of ribbon produced from maltodextrin, microcrystalline cellulose (MCC) and sodium chloride. In the current work, the gap between the rollers was controlled using the automatic feedback system which adjusts the feeder screw speed. This means that the increase in the roller speed increases the feeder screw speed in order to feed more powder and maintain the gap. The constant gap between the rollers with increasing the roller speed resulted in ribbons with similar strength and porosity. This finding is interesting because it is suggesting that the production rate of ribbon of lactose powders could be increased by increasing the speed of the roller knowing that this will not affect the product strength and porosity.

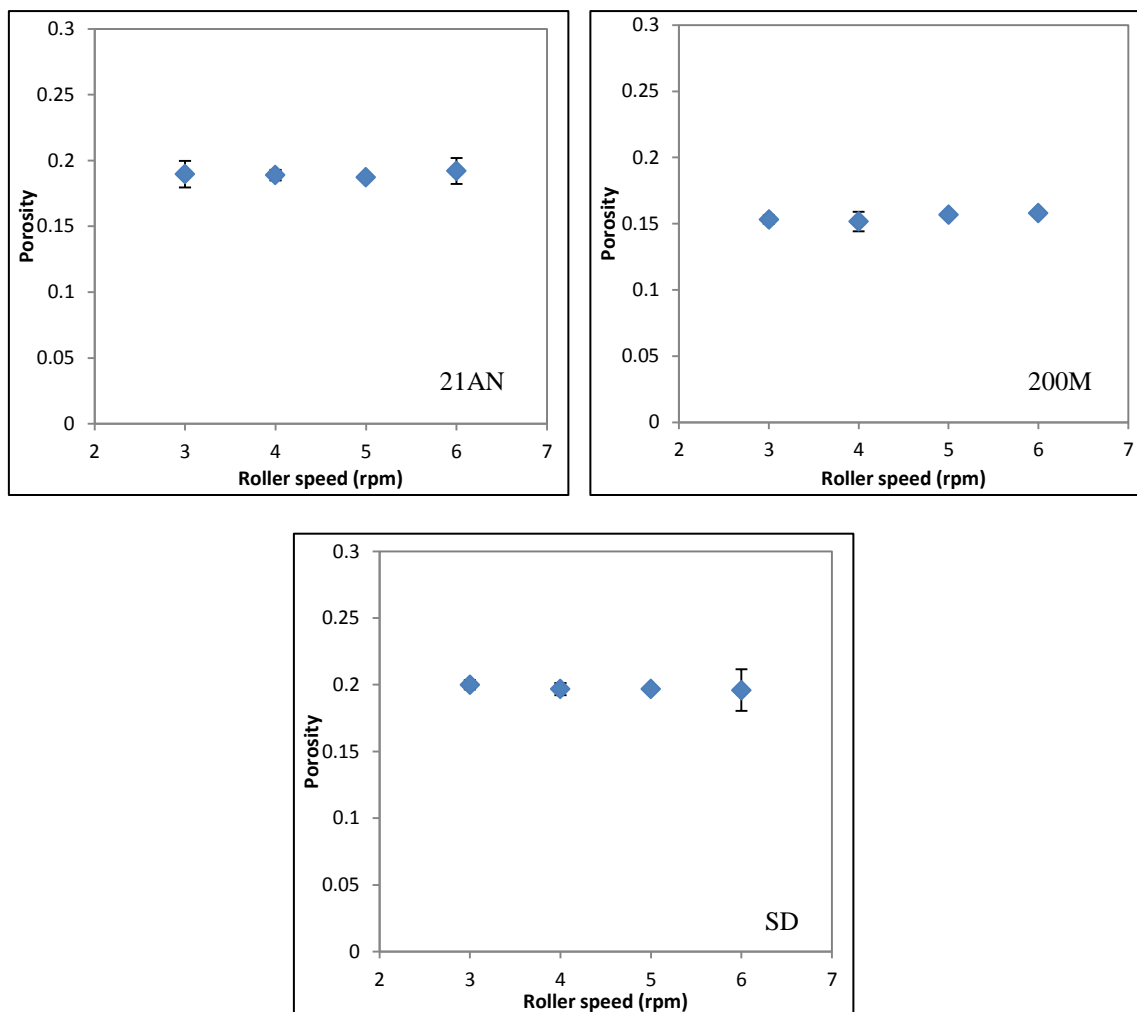


Figure 7.6: Porosity of ribbon produced from the three types of lactose at different roller speed.

7.4.2 Effect of the gap between the rollers

The gap between the two rollers is one of the process parameters which can be changed during the roller compaction. Increasing the gap during the production of ribbon increases the amount of powder between the rollers and results in thicker ribbon. The increase or decrease in the amount of powder between the two rollers may affect the stress applied on the powder at specific roller force. Previous work has been carried out to investigate the effect of the roller gap on the nip angle and the maximum pressure applied to the powder [65, 66]. It was found that the nip angle increased with increasing the roller gap during the roller compaction of MCC [66]. This may affect the properties of the produced ribbon.

In this Section, the effect of varying the roller gap on ribbon properties was studied using the three types of lactose. The powders have differences in their morphology, size

and amorphous content. The roller compactor was operated at a fixed hydraulic pressure of 50 bar and the roller speed was set to 3 rpm. To control the set gap, the feeder screw speed was varying automatically using the feedback system which adjusts the feeder speed to maintain the gap.

Table 7.3 shows the design of experiment used during the examination of the effect of the roller gap.

Table 7.3: Design of experiment during the investigation of the roller gap.

Hydraulic pressure (bar)	Roller speed (rpm)	Gap (mm)	Feeder screw speed (rpm)
50	3	1.5	Variable (due to the use of the gap controlling feedback system)
		2	
		3	
		4	

Figure 7.8 shows the maximum temperature of ribbon of different types of lactose during the production at different roller gap setting. It can be seen that the temperature of the ribbon during production increased with increasing the gap between the two rollers. The increase in the roller gap increases the speed of the feeder screw (see Figure 7.7) in order to deliver more material and fill the gap between the rollers. This is achieved by operating the roller compactor with the feedback system turned on, which adjusts the feeder screw speed according to the gap setting. The increase in the feeder screw speed, with increasing the roller gap, increases the internal friction between the particles and between the barrel wall and particles which increase the powder temperature. This was the reason for the increase in the ribbon surface temperature with increasing the roller gap. Another reason could be the higher heat accumulation in thicker ribbon which is produced at larger gap; thicker ribbon loses heat slower in comparison to thinner ribbon. This result is consistent with the finding of Osborne [59] who stated that there was an increase in the ribbon surface temperature when the roller gap increased from 2 mm to 4 mm during the roller compaction of maltodextrin.

From Figure 7.8 it can be noticed that the temperature of ribbon produced from the different types of lactose is not the same. The temperature of ribbon produced from the

SD lactose is higher (at larger roller gap) in comparison to the other two types of lactose. It is worth mentioning that the result in Figure 7.8 is the temperature of the exiting ribbon after the compaction of the powder. This means that the heat emitted by the ribbon (which is recorded by the thermal camera) is a combination of the heat from the friction due to the increase in the feeder screw speed and also from the deformation and fragmentation of particles due to the stress applied between the rollers. It was found in Chapter 5 that the temperature of ribbons produced from the SD lactose was higher than those of 21AN and 200M lactose. This was due to the difference in the particle morphology and the powder amorphous content.

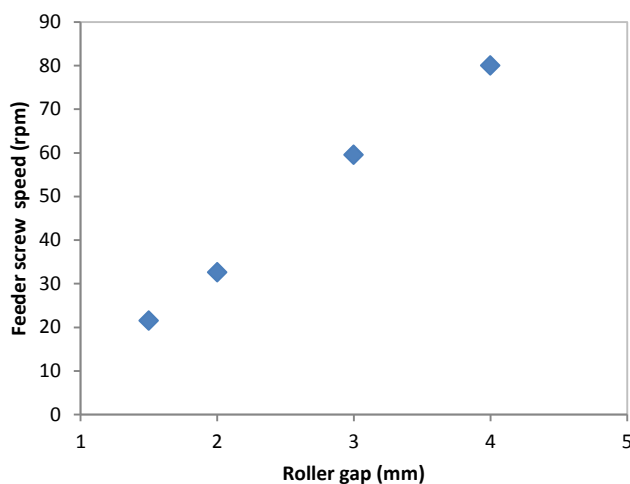


Figure 7.7: Feeder screw speed at different roller gap.

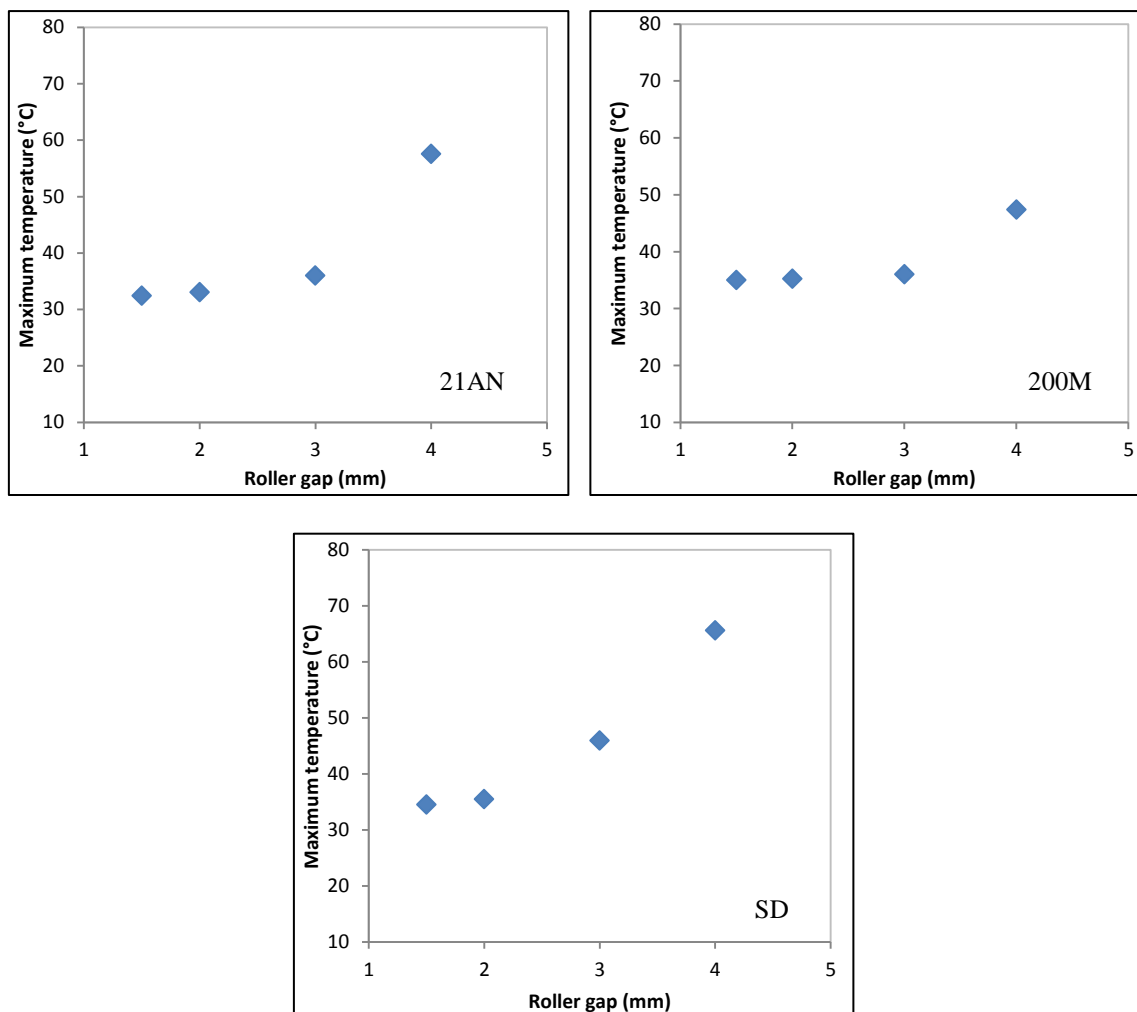


Figure 7.8: Maximum temperature of the ribbon during the production at different roller gap.

The quality of the product at different roller gap settings was also evaluated by determining the fines percentage in the product. As mentioned earlier, the fine is one of the main disadvantages of the roller compaction; therefore, decreasing the fines in the product increases the overall efficiency of the process. The fine percentage during the roller compaction of the three types of lactose were determined and plotted against the roller gap as shown in Figure 7.9. It can be seen that the increase in the roller gap during the compaction resulted in a significant decrease of the fine percentage in the product for all the lactose powders. This is supported by the finding in Figure 7.10, which shows the width of the ribbon produced from the different types of lactose at varying roller gap. It can be seen in Figure 7.10 that the width of the ribbon is increasing significantly with the increase in the roller gap during the production of ribbon. This confirms the result in Figure 7.9, as the fine is usually coming from the edges of the ribbon,

therefore, an increase in the width of the ribbon give an indication of a lower amount of fines in the product.

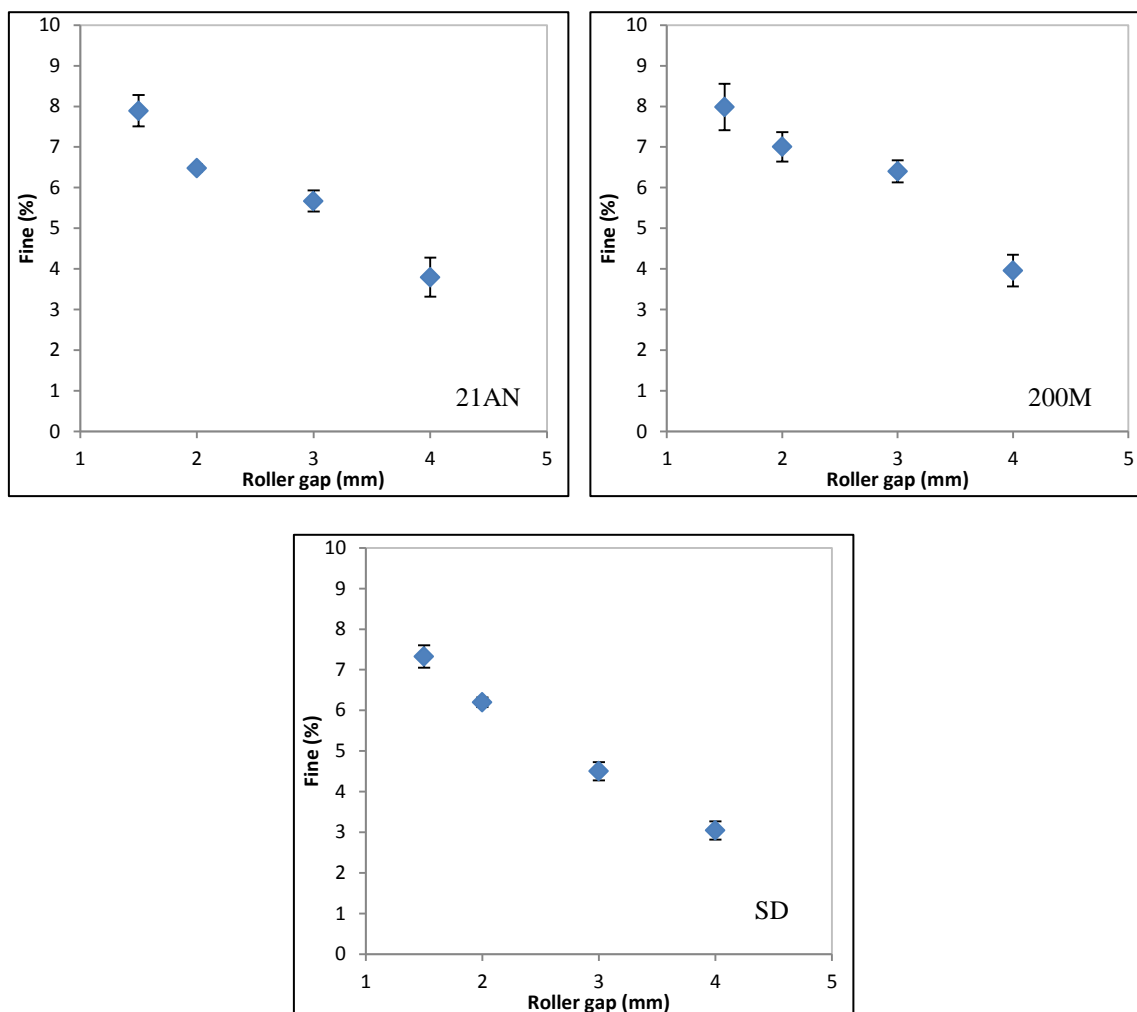


Figure 7.9: The percentage of fines produced with the ribbon during the production at different roller gap.

The lower percentage of fines and the wider ribbon produced at high roller gap is due to the powder distribution across the width of the roller. Increasing the gap size between the two rollers means more space for the powder to spread to the edges of the rollers. The better distribution of the powder to the edges at larger roller gap could improve the stress distribution across the width of the roller. The stress across the roller width is more uniform when larger gap size is used during the compaction. This results in a wider ribbon and therefore a lower percentage of fines in the product.

It is worth noting that SD lactose produced wider ribbons with the smaller fine percentage in comparison with the other two types of lactose. This is due to the

difference in the particle morphology and the powder amorphous content as seen in Chapter 5. The lower fine percentage of the SD lactose is also attributed to the better flowability of the SD lactose as seen in Chapter 6 which resulted in better powder distribution across roller width and produced wider ribbon in comparison to the other types of lactose.

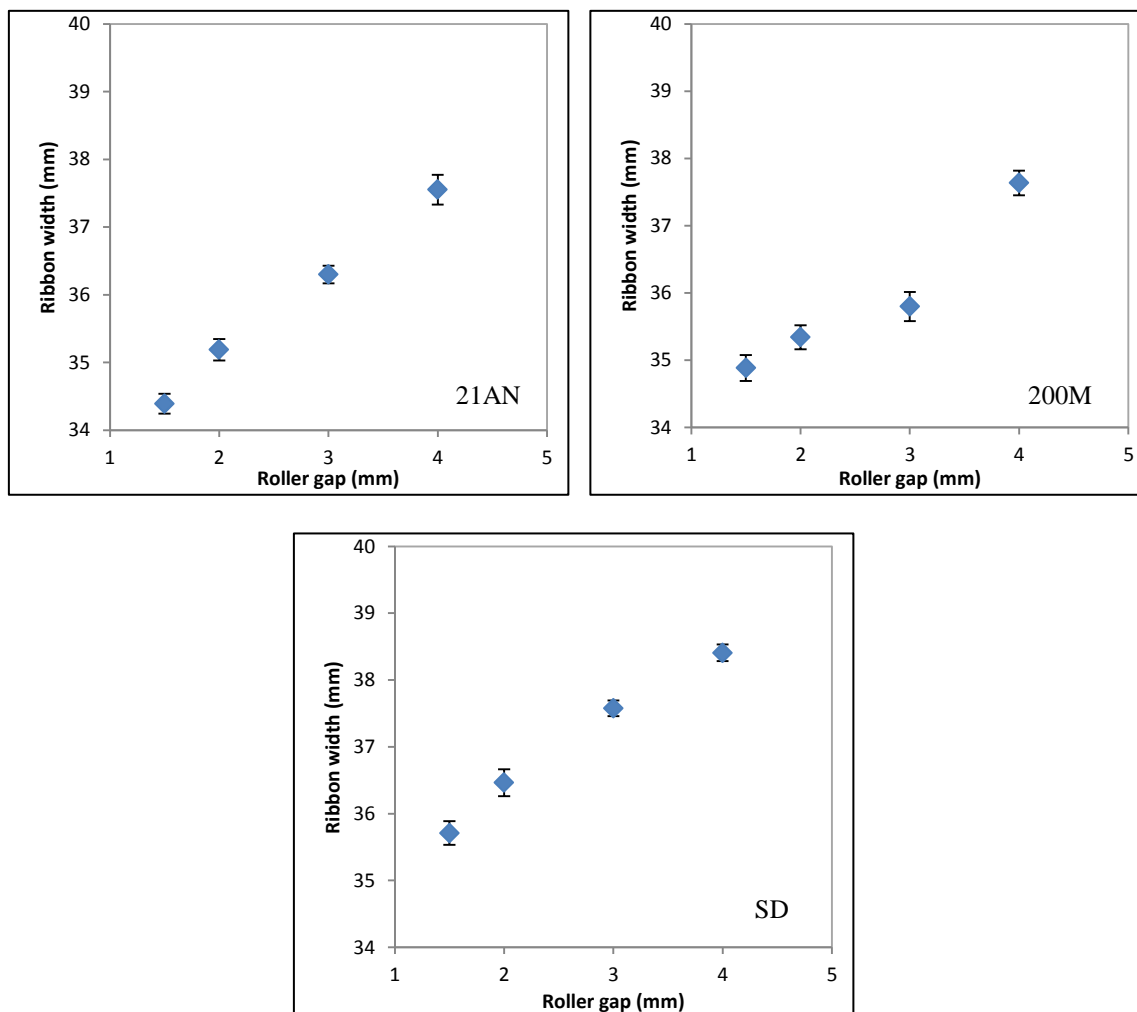


Figure 7.10: Width of ribbon produced from the three types of lactose at different roller gap.

The tensile strength and the porosity of ribbons produced from the three types of lactose at different roller gap are shown in Figure 7.11 and Figure 7.12 respectively. It can be seen that different types of lactose showed different tensile strength and porosity during the roller compaction at varying roller gap. The tensile strength of ribbons produced from lactose 21AN and 200M decreased and the porosity increased with increasing the roller gap. However, the tensile strength of ribbon produced from the SD lactose increased and porosity decreased with the increase in the roller gap during compaction.

The decrease in the tensile strength of ribbon produced from lactose 21AN and 200M is attributed to the fact that increasing the roller gap increases the amount of the powder between the two rollers. The higher amount of the powder at the gap between the rollers is believed to decrease the stress applied on the powder between the two rollers during the compaction. The decrease in the maximum stress applied on the powder with increasing the roller gap was reported previously by [65, 66, 81]. This was attributed to the fact that increasing the roller gap increases the amount of the powder between the rollers which resulted in distributing the force acting on the powder over a wider thickness, therefore, decreasing the stress. The decrease in the stress applied on the powder during the roller compaction, as a result of increasing the roller gap, resulted in ribbons with lower tensile strength (see Figure 7.11) and higher porosity (see Figure 7.12) for lactose 21AN and 200M. This is in agreement with the finding of [59, 65, 66] in that increasing the roller gap during the compaction decreases both the strength and the density of ribbon of MCC and sodium chloride.

The contradicting result showed by ribbons of the SD lactose is attributed to the different property of the primary powder. The SD lactose contains (10.32%) amorphous lactose which affects the powder behaviour during compression. The amorphous lactose is known to be sensitive to temperature. Increasing the temperature of an amorphous powder results in softening the powder and increases the mobility of the molecules [18, 19]. Compressing a powder at this stage will result in a formation of solid bridges due to the movements of molecules into the gap between particles. This process is known as sintering, which may be occurring with the SD lactose and resulting in a stronger ribbon [19].

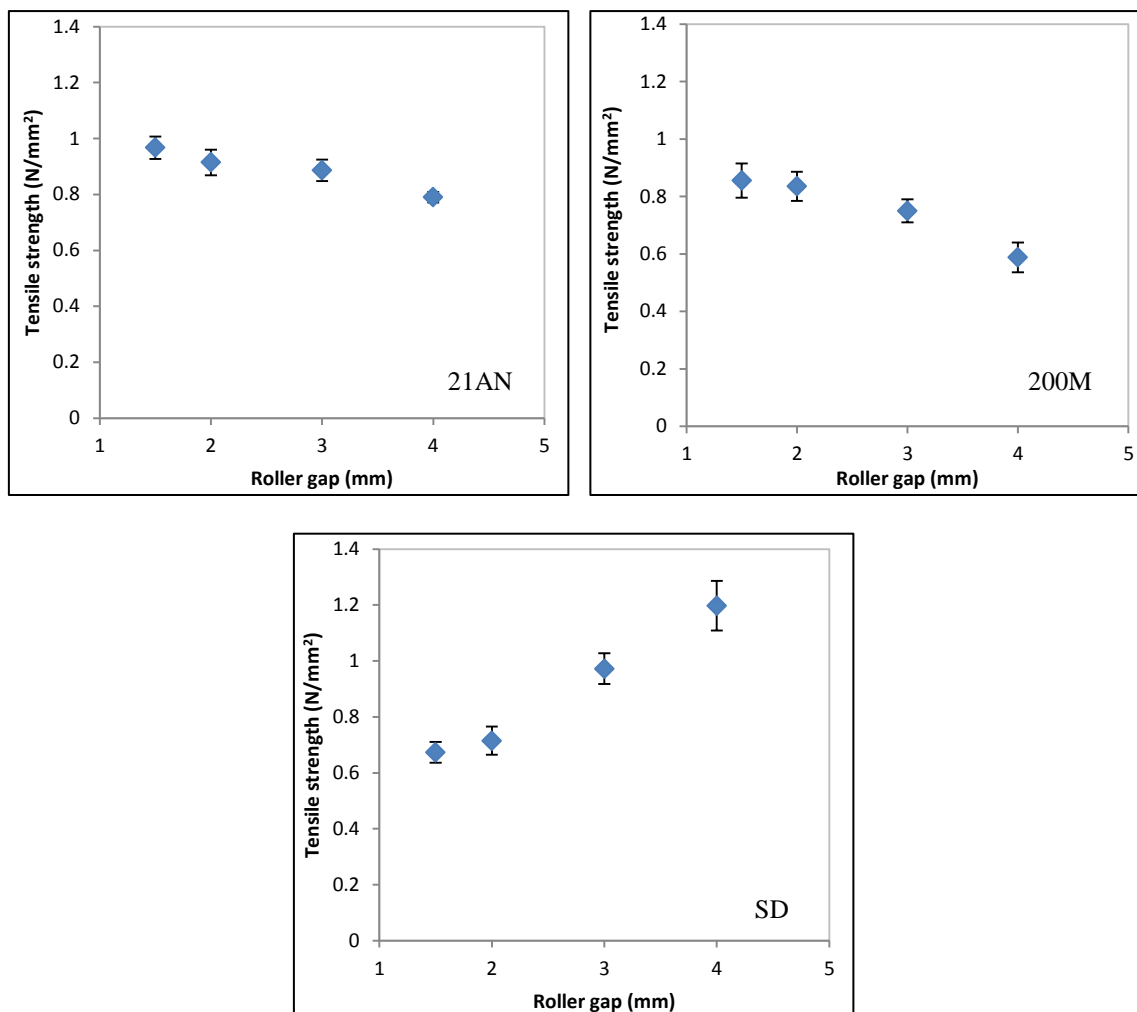


Figure 7.11: Tensile strength of ribbon produced from the three types of lactose at different roller gap.

From Figure 7.8 it can be seen that the temperature of the ribbon increased with increasing the roller gap. This was attributed to the increase in the internal friction of the powder due to the increase in the feeder screw speed. This means that the powder gained some heat while transporting by the feeder screw which resulted in an increase in the powder temperature before the compaction stage. The increase in the powder temperature before the rollers (compaction stage) softened the powder. This is then resulted in more deformation and sintering of particles while compacting by the rollers, which resulted in ribbons of SD lactose with higher tensile strength (see Figure 7.11) and lower porosity (see Figure 7.12) at larger gap size. This result is in agreement with the finding of Inghelbrecht et al. [8] who reported that the friability of granules of maize powder was decreasing with increasing the roller gap. The decrease in the granule friability with increasing the roller gap indicates stronger ribbon which is consistent

with the result of the SD lactose in that the ribbon tensile strength increased at large roller gap.

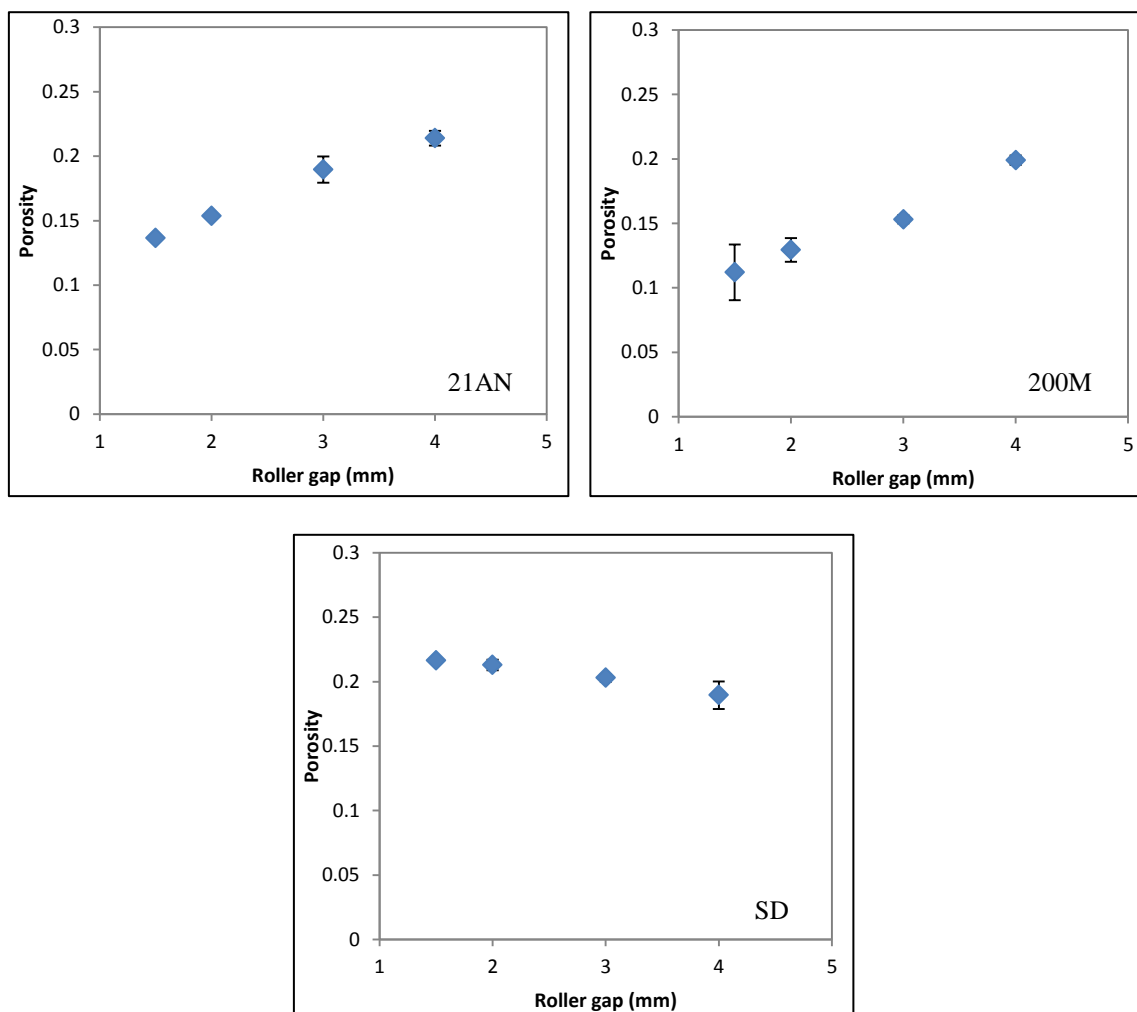


Figure 7.12: Porosity of ribbon produced from the three types of lactose at different roller gap.

7.4.3 Effect of temperature of the starting powder

In the previous Section, the high temperature of the ribbon at large roller gap was due to both the increase in internal friction of the powder as a result of increasing the feeder screw speed and also to the stress applied on the powder due to the compaction. In order to investigate the effect of the powder temperature before compaction on the ribbon properties, separate experiments were conducted to produce ribbon from powders conditioned at a different temperature. Moreover, to eliminate the effect of the process parameter (screw feeder speed, gap, roller speed and the hydraulic pressure), the roller compactor was operated at the same settings for all powders. The three types of lactose were stored in the climatic chamber for three days at 20% RH and different temperature

of 25, 35 and 45°C. Ribbons then produced from the powder with different temperature using 2 mm roller gap, 3 rpm roller speed and 50 bar hydraulic pressures.

Figure 7.13 shows the surface temperature during the production of ribbon of the three types of lactose at different starting temperatures. It can be seen that the temperature of the ribbon increased with increasing the temperature of the starting powder.

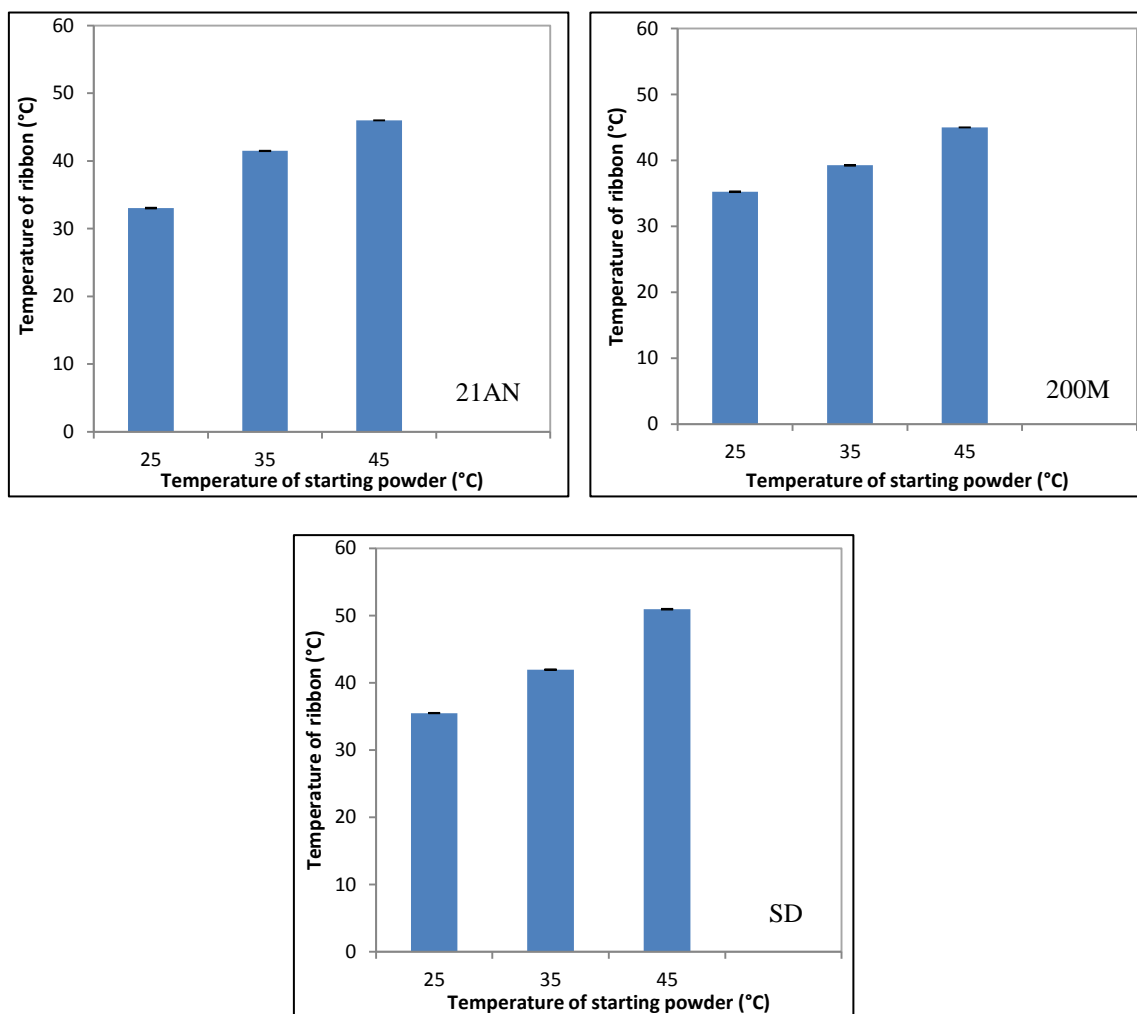


Figure 7.13: Surface temperature of ribbon produced from the three types of lactose at different temperature of the starting powder.

It can also be seen that the temperature of ribbon produced from the SD lactose is higher than those of the other two types of lactose, although the starting powder temperature was the same. This indicates that more heat is generated during the roller compaction which is due to the deformation of the particles, therefore, increased the temperature of the exit ribbon. The heat generated during the roller compaction depends on the powder

properties. The higher temperature of ribbon of the SD lactose is suggested to be due to the higher amount of plastic deformation which is showed by the amorphous fraction.

From Figure 7.13, it is worth noting that the roller compaction of powders stored at 45°C resulted in ribbons with similar temperature as the starting powder for (21AN and 200M) and a slightly higher temperature for ribbons of SD lactose. It is believed that the temperature of the powder decreased due to the heat lost while transferring the powder from the climatic chamber to the hopper of the roller compactor. The roller compaction experiment was conducted as quickly as possible to minimise the heat lost, as the temperature was not controlled in the hopper.

To examine the rate of heat loss of each type of lactose, the three types of lactose were kept in an electric oven for 24 hours at 60°C. The samples were then taken out of the oven and the temperature of each type of lactose was recorded using the thermal camera. The temperature of the samples was monitored for 15 minutes, and the average temperature of each sample was plotted against the time as shown in Figure 7.14. It can be seen that the rate of heat loss is higher at the beginning when the temperature is high. This is expected as the driving force (temperature difference between the sample and the laboratory) is higher. As the temperature of the sample decreases the rate of heat loss also decreases. This explains the small difference between the starting powder temperature and the temperature of ribbon produced from the powders stored at 45°C. It is believed that the temperature of the powder stored at 45°C decreased at a higher rate before the compaction stage; therefore, the surface temperature of ribbons after compaction did not show big difference compare to the temperature of the starting material.

Figure 7.14 also shows that the three types of lactose are losing heat at the same rate. This means that all powders had the same temperature before the compaction stage. However, the SD lactose which stored at 45°C resulted in ribbons with higher temperature compare to lactose 21AN and 200M. This confirms that the compaction of SD lactose resulted in generating more heat than the other two types of lactose, which was due to the high amorphous content.

Figure 7.15 and Figure 7.16 shows the fine percentage and width of ribbon produced from the three types of lactose at different powder starting temperature.

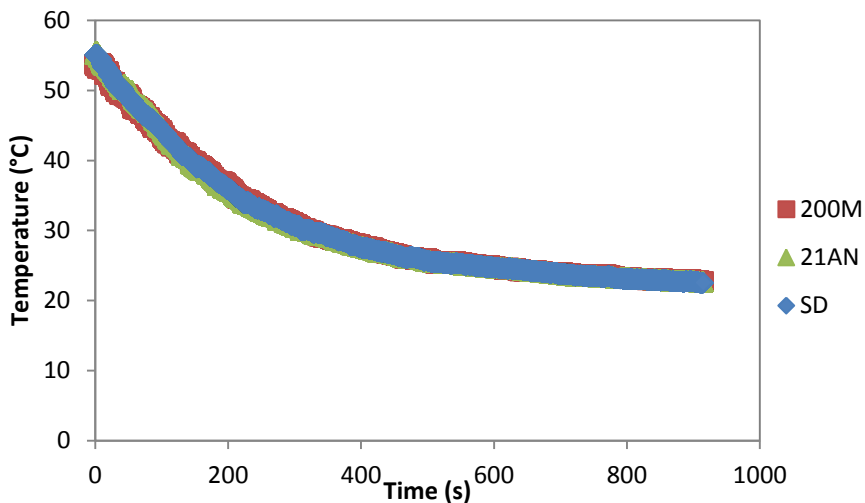


Figure 7.14: The rate of heat loss from the three types of lactose.

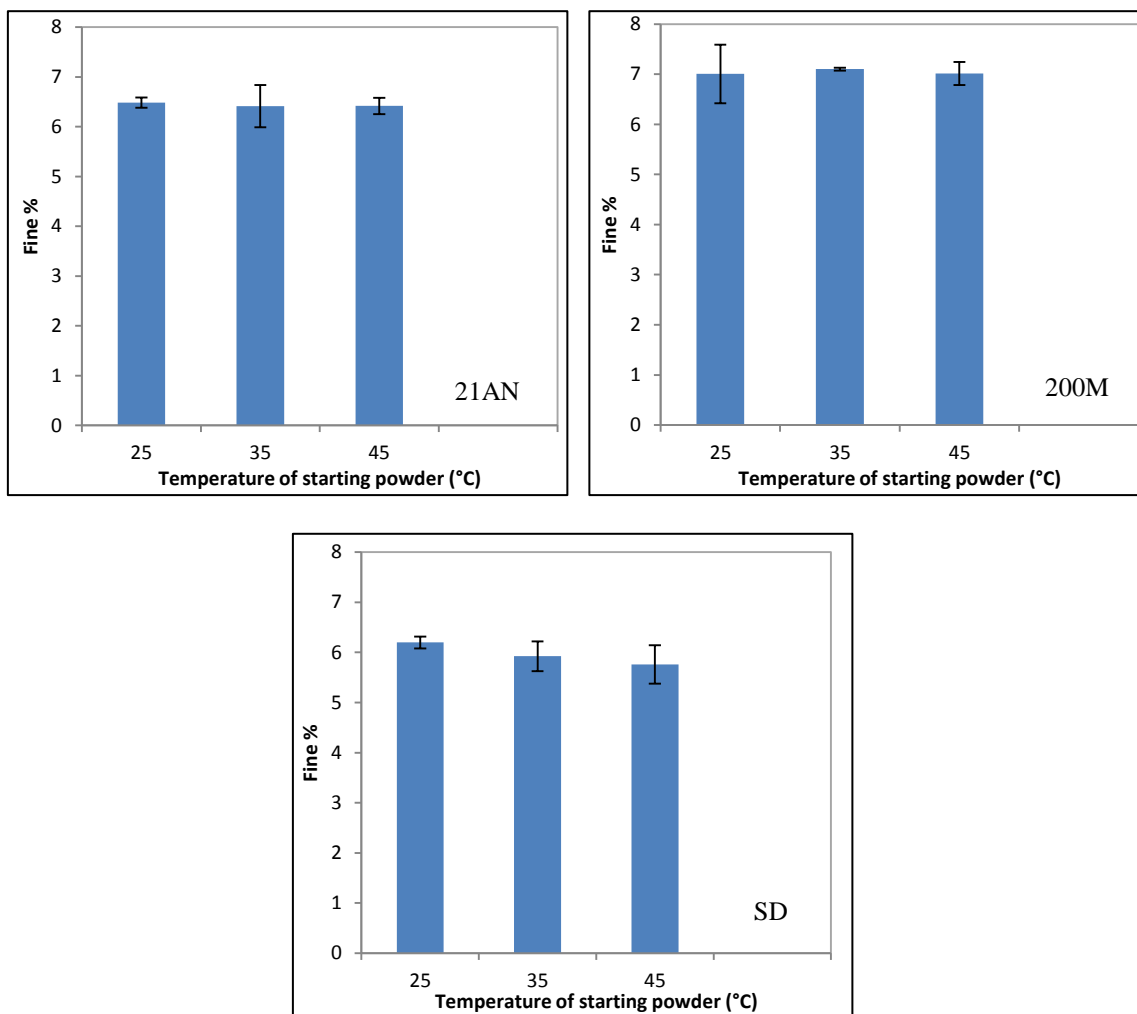


Figure 7.15: Percentage of fines produced from the three types of lactose at different temperature of the starting powder.

It can be seen that the temperature of the starting material has no effect on the fine percentage and width of the ribbon. Only SD lactose showed a very slight (insignificant) decrease in the fine percentage with increasing the temperature of the starting powder, which could be attributed to the better binding of the SD lactose at the edges.

The fine percentage and width of the ribbon are mainly depending on the powder distribution across the width. The temperature of the starting material is believed to have no influence on the powder distribution. This resulted in a minor effect of the starting powder temperature on the fine percentage and width of the ribbon as shown in Figure 7.15 and Figure 7.16.

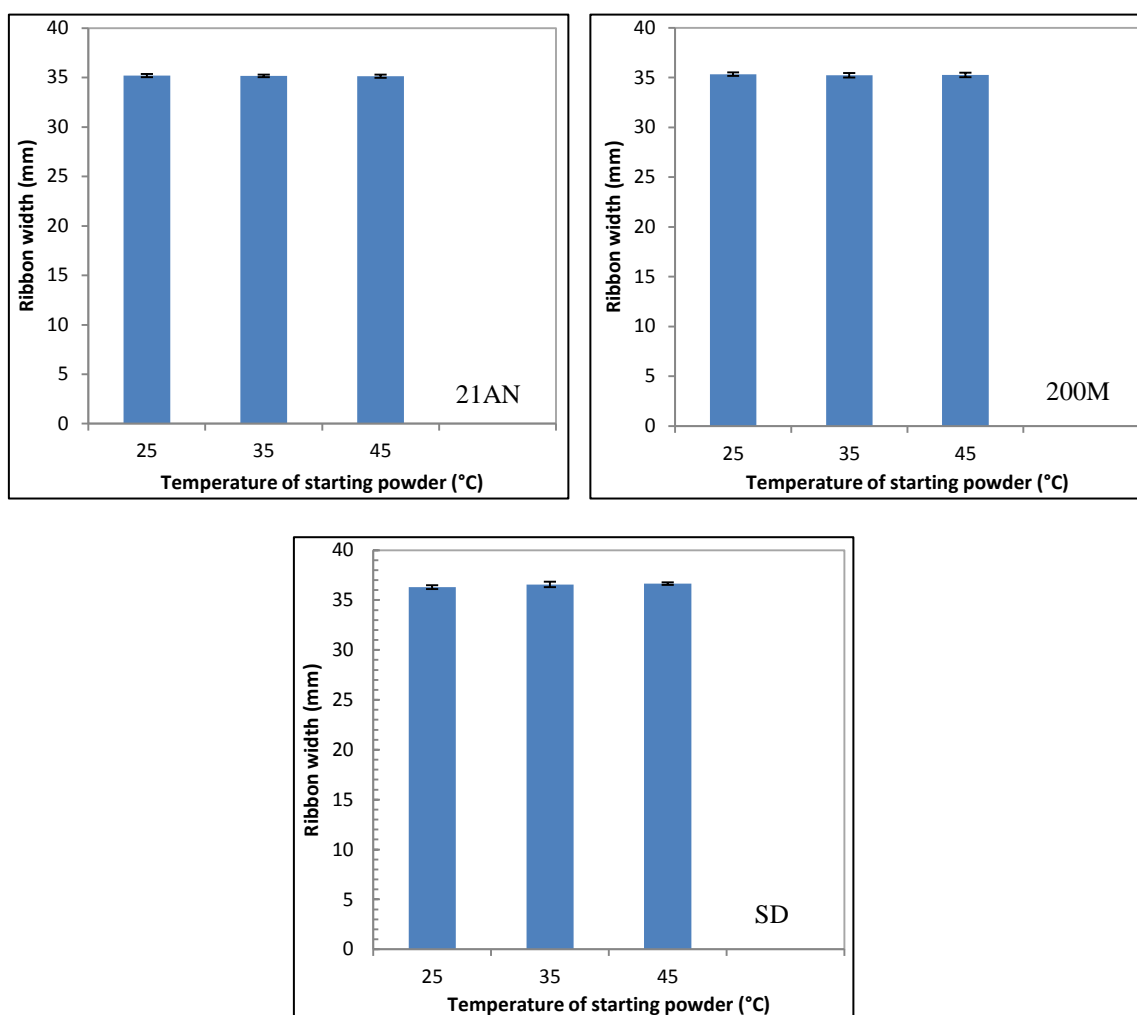


Figure 7.16: Width of ribbon produced from the three types of lactose at different temperature of the starting powder.

The tensile strength and the porosity of ribbons produced from the three types of lactose at different starting powder temperature are shown in Figure 7.17 and Figure 7.18 respectively. It can be seen that the tensile strength and porosity of ribbon produced from lactose 21AN and 200M were not affected by the increase in the starting powder temperature. However, the tensile strength of ribbon of SD lactose increased and the porosity decreased significantly with increasing the temperature of the starting material.

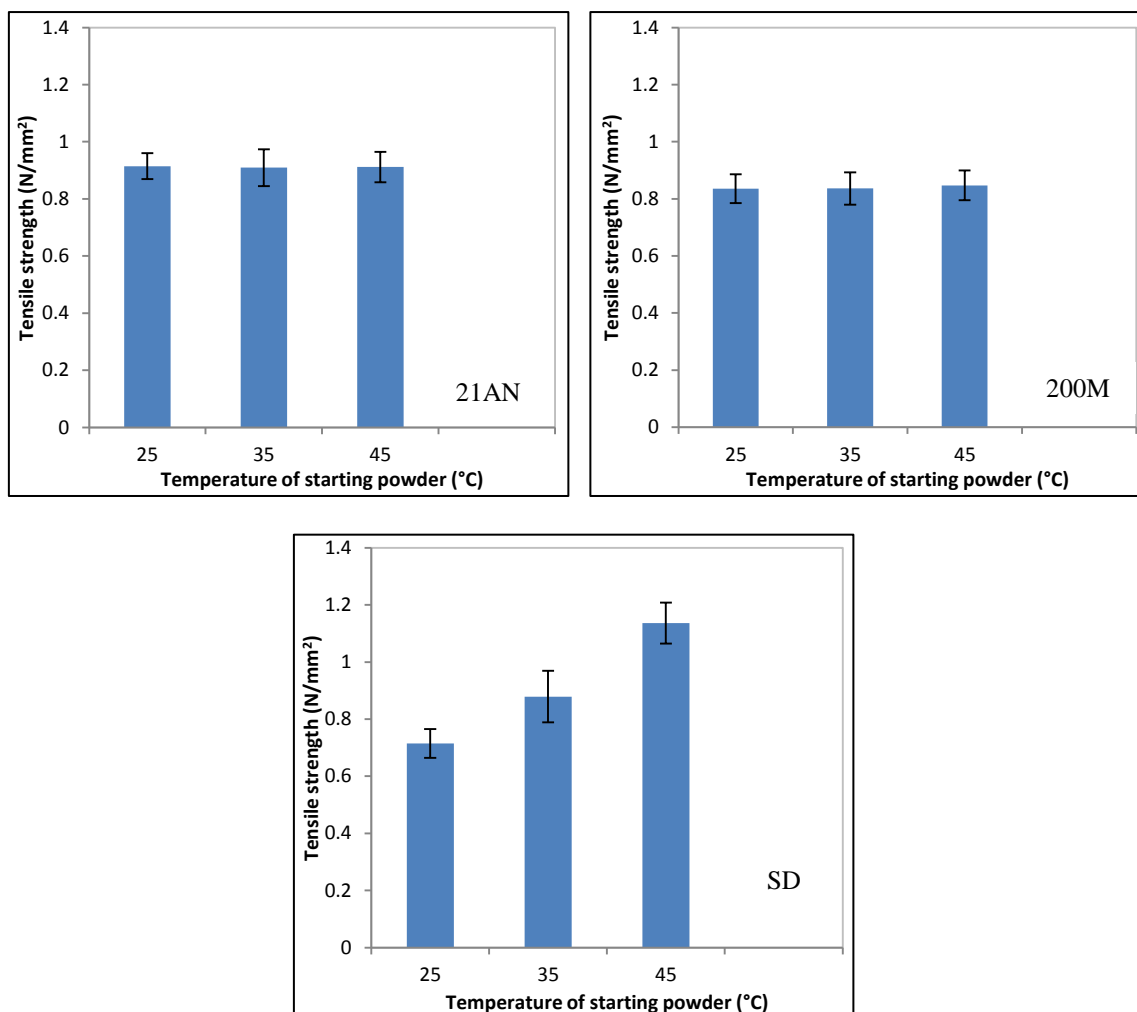


Figure 7.17: Tensile strength of ribbon produced from the three types of lactose at different temperature of the starting powder.

This is due to the high fraction of an amorphous powder which is present in the SD lactose. The increase in the temperature of amorphous lactose results in softening the powder and increases the mobility of molecules [18, 19]. This is increased the powder deformability and resulted in a formation of solid bridges because of the sintering

process during the roller compaction. This will result in ribbons with higher tensile strength (Figure 7.17) and lower porosity (Figure 7.18) for SD lactose.

From this Section, it can be concluded that lactose 21AN and 200M are not affected by the increase in the temperature of the starting material. It is only the SD lactose which is significantly affected by the increased in the temperature of the starting powder. This explains the difference in the ribbon tensile strength and porosity with increasing the roller gap in Section 7.4.2. The increase in the ribbon temperature had no effect on the properties of ribbon of 21AN and 200M, whereas the tensile strength and porosity of ribbon of SD lactose affected significantly by the temperature of the powder.

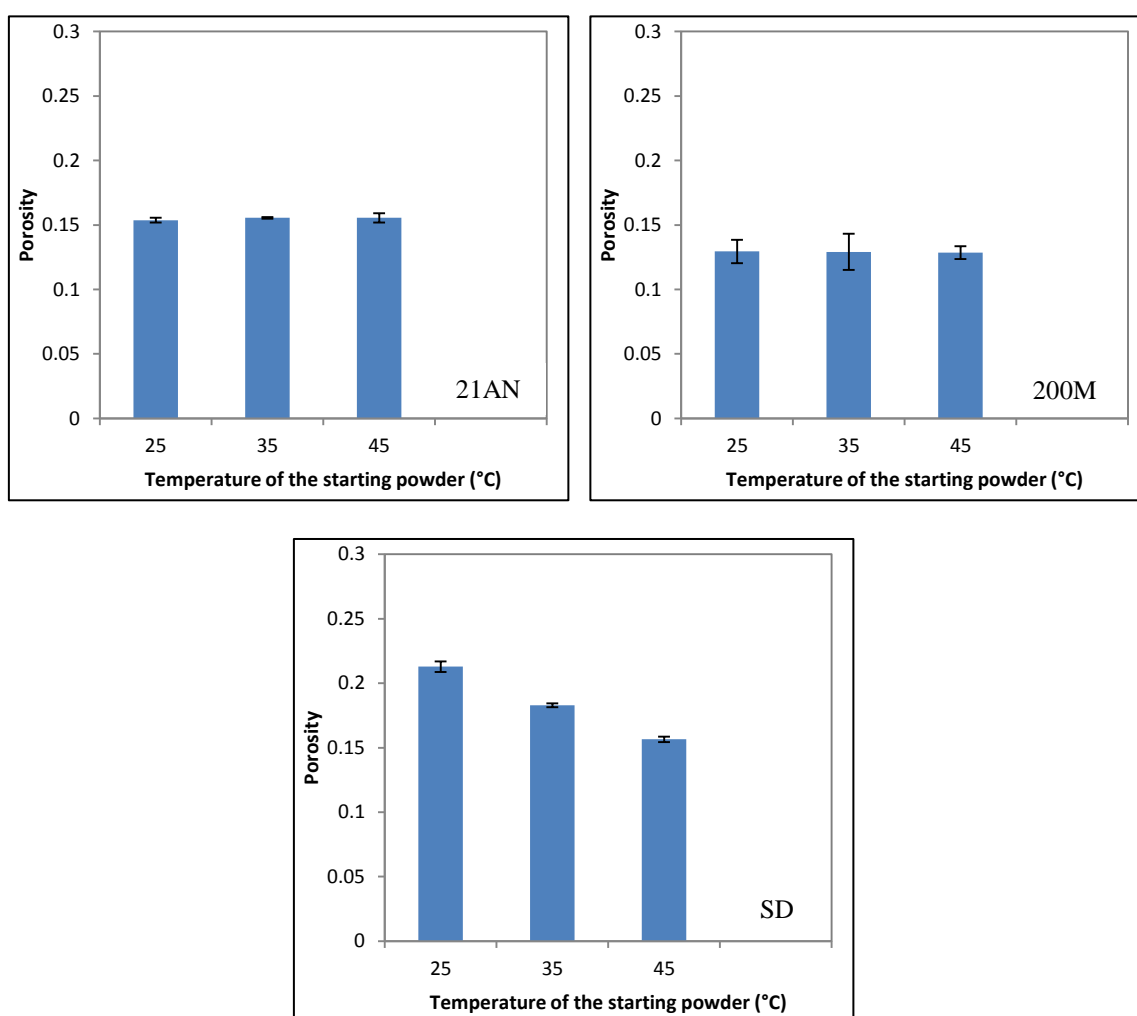


Figure 7.18: Porosity of ribbon produced from the three types of lactose at different temperature of the starting powder.

7.4.4 Effect of the feeder screw speed

In roller compaction, a screw feeder is used to transport the powder from the hopper to the compaction zone. A change in the feeder screw speed results in changing the gap between the rollers. In the previous sections the gap between the rollers was controlled using the automatic feedback system which adjusts the feeder screw speed to maintain the gap constant; therefore, the screw speed will change automatically. In order to investigate the effect of the feeder screw speed, the lactose powders were stored in the chamber for three days at 20% RH and 25°C. The powders then compacted using the settings shown in Table 7.4.

Table 7.4: Design of experiment during the investigation of the effect of the feeder screw speed.

Hydraulic pressure (bar)	Roller speed (rpm)	Gap (mm)	Feeder screw speed (rpm)
50	3	different	20
			40
			60
			80

An increase in the feeder screw speed results in an increase in the amount of powder in the compaction zone and then increases the gap between the rollers (at fixed roller speed). Therefore, it is expected that the feeder screw will have the same effect as the roller gap.

Figure 7.19 shows the surface temperature of the ribbon during the production at different feeder screw speed. The temperature of ribbon increased with increasing the feeder screw speed. This was because of the increase in the powder internal friction as a result of the increase in the screw speed. The Same result was found when increasing the roller gap since the increase in the gap increases the feeder screw speed due to the use of the automatic feedback system.

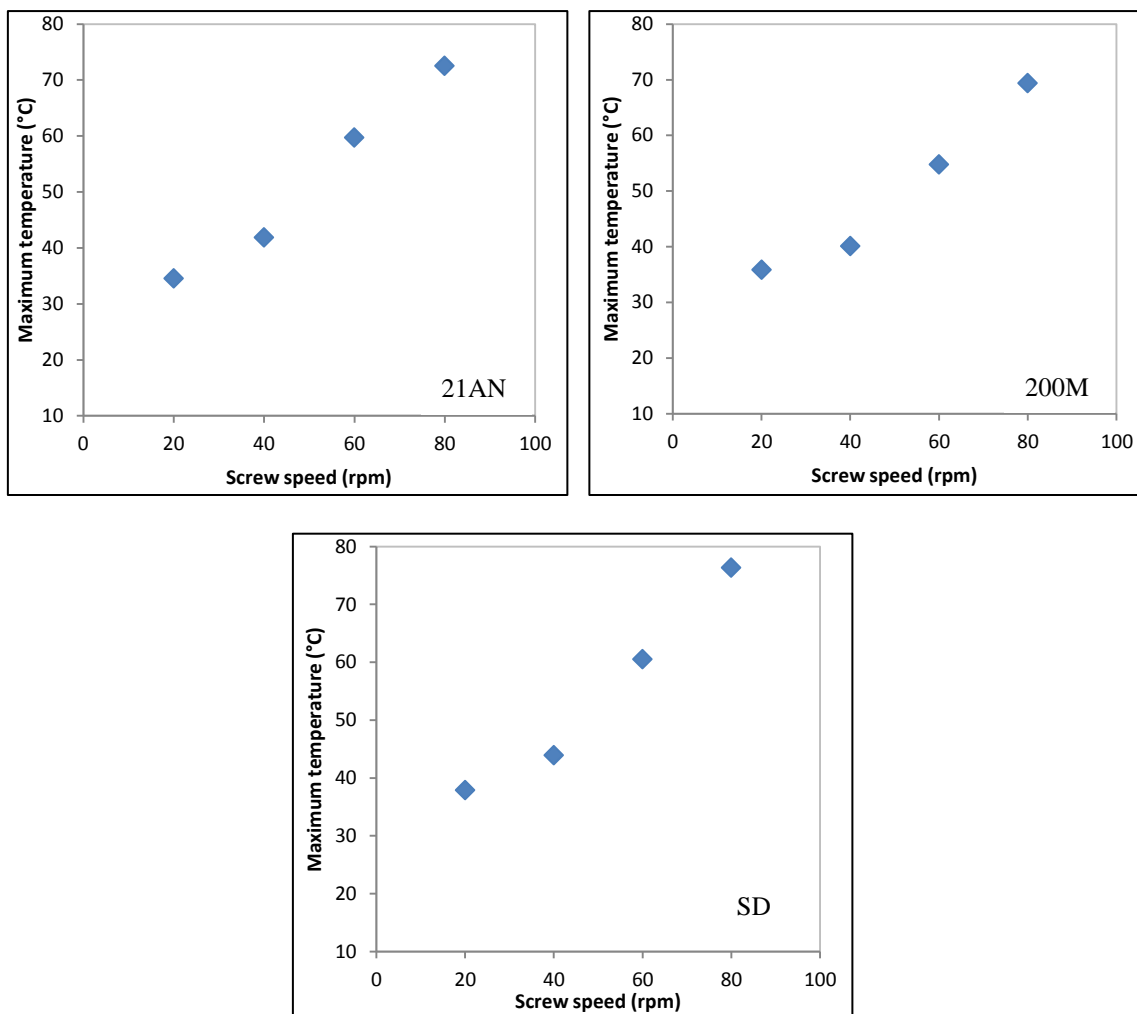


Figure 7.19: Surface temperature of ribbon produced from the three types of lactose at different feeder screw speed.

Figure 7.20 and Figure 7.21 show the fine percentage and the width of ribbon produced from the three types of lactose at different feeder screw speed. It can be seen that the fine percentage decreased and the width increased with increasing the speed of the feeder screw. As mentioned earlier, the increase in the feeder screw speed increases the roller gap.

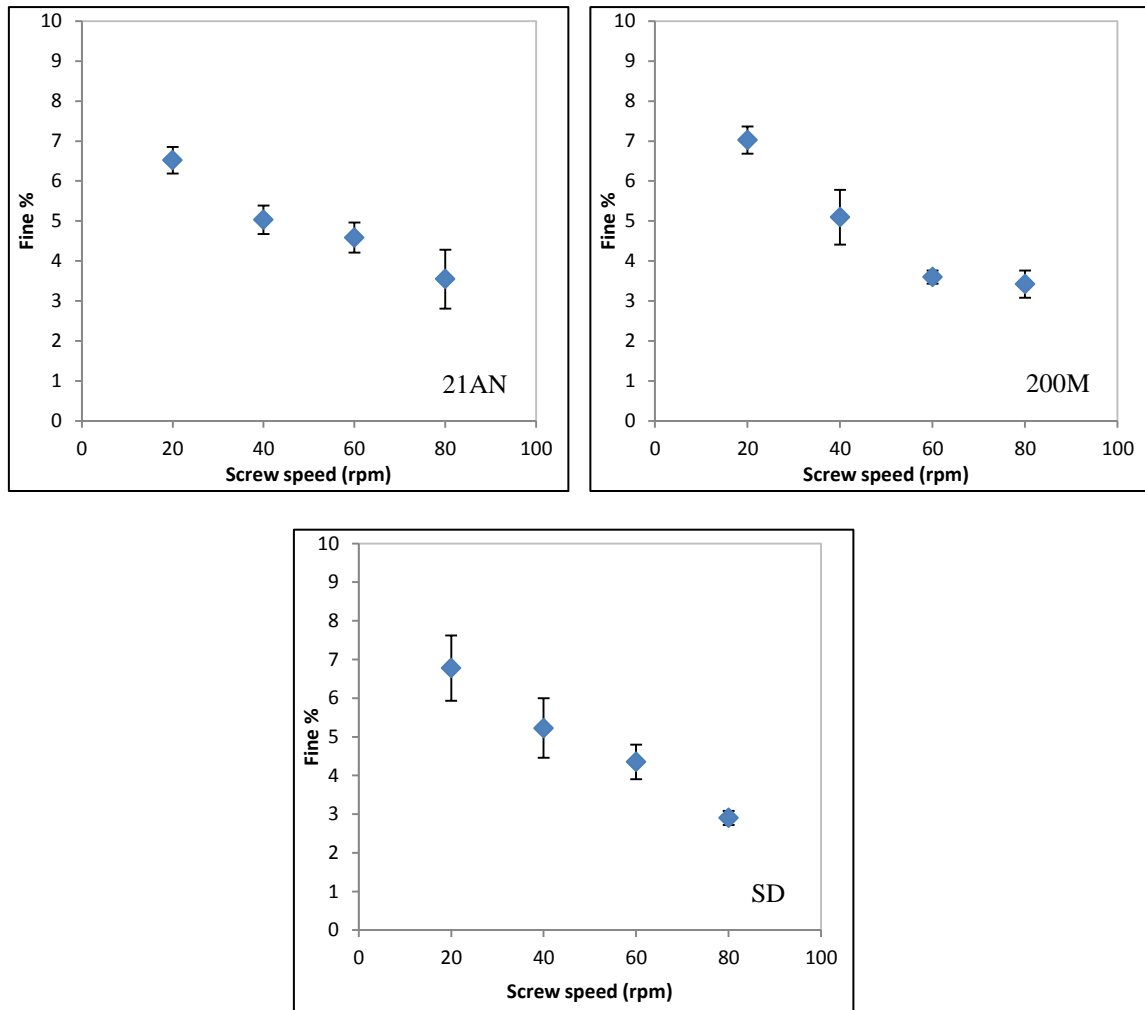


Figure 7.20: Percentage of fines produced from the three types of lactose at different feeder screw speed.

At a larger gap, the powder will have more space to distribute evenly across the width of the roller. The uniform distribution of the powder across the width of the roller is believed to result in a uniform stress being applied on the powder across the roller width. This will result in ribbons with a higher width (see Figure 7.21) and reduce the percentage of the fines in the product (see Figure 7.20).

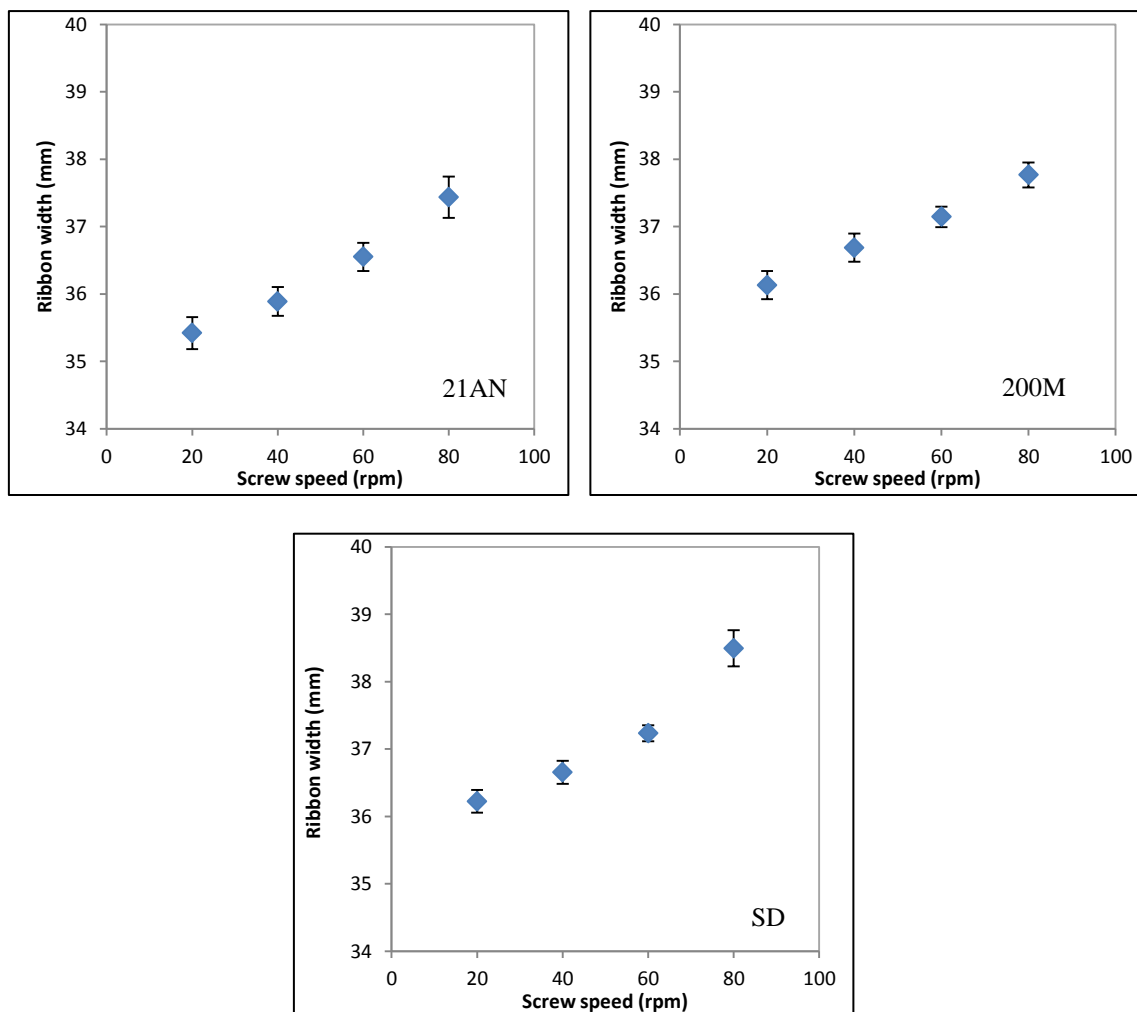


Figure 7.21: Width of ribbon produced from the three types of lactose at different feeder screw speed.

The tensile strength and the porosity of ribbon produced from the three types of lactose at different feeder screw speed are shown in Figure 7.22 and Figure 7.23 respectively. The effect of the feeder screw speed on the ribbon tensile strength and porosity was different for the three types of lactose. For lactose 21AN and 200M, the tensile strength decreased and the porosity increased with increasing the feeder screw speed. However, the increase in the screw speed resulted in increasing the tensile strength and decreasing the porosity of ribbons produced from the SD lactose.

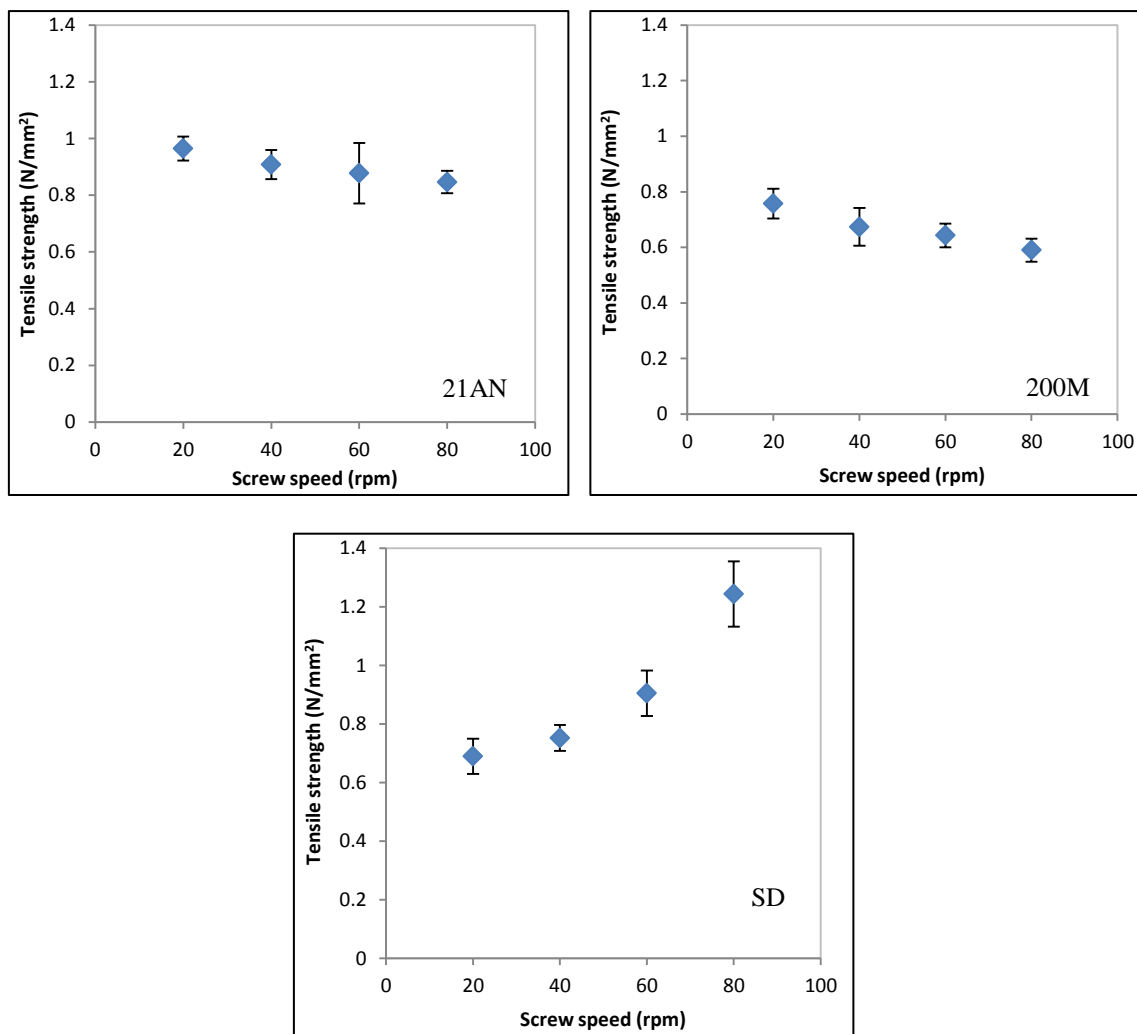


Figure 7.22: Tensile strength of ribbon produced from the three types of lactose at different feeder screw speed.

The result in Figure 7.22 and Figure 7.23 are similar to the finding in Figure 7.11 and Figure 7.12 respectively since the increase in the roller gap has the same effect as increasing the feeder screw speed. The decrease in the tensile strength and the increase in porosity of ribbon of 21AN and 200M with increasing the feeder screw speed are due to the higher amount of powder between the rollers at higher screw speed. The presence of a large amount of powder between the rollers decreases the stress applied on the powder [65, 66, 81]. This will then decrease the ribbon tensile strength and increase the porosity of ribbon. The opposite trend for the SD lactose is attributed to the high amorphous fraction in the powder which improves the powder deformability with increasing the temperature of the powder as a result of increasing the screw speed. More

details of the effect of the screw speed as a result of increasing the roller gap can be found in Section 7.4.2 and 7.4.3.

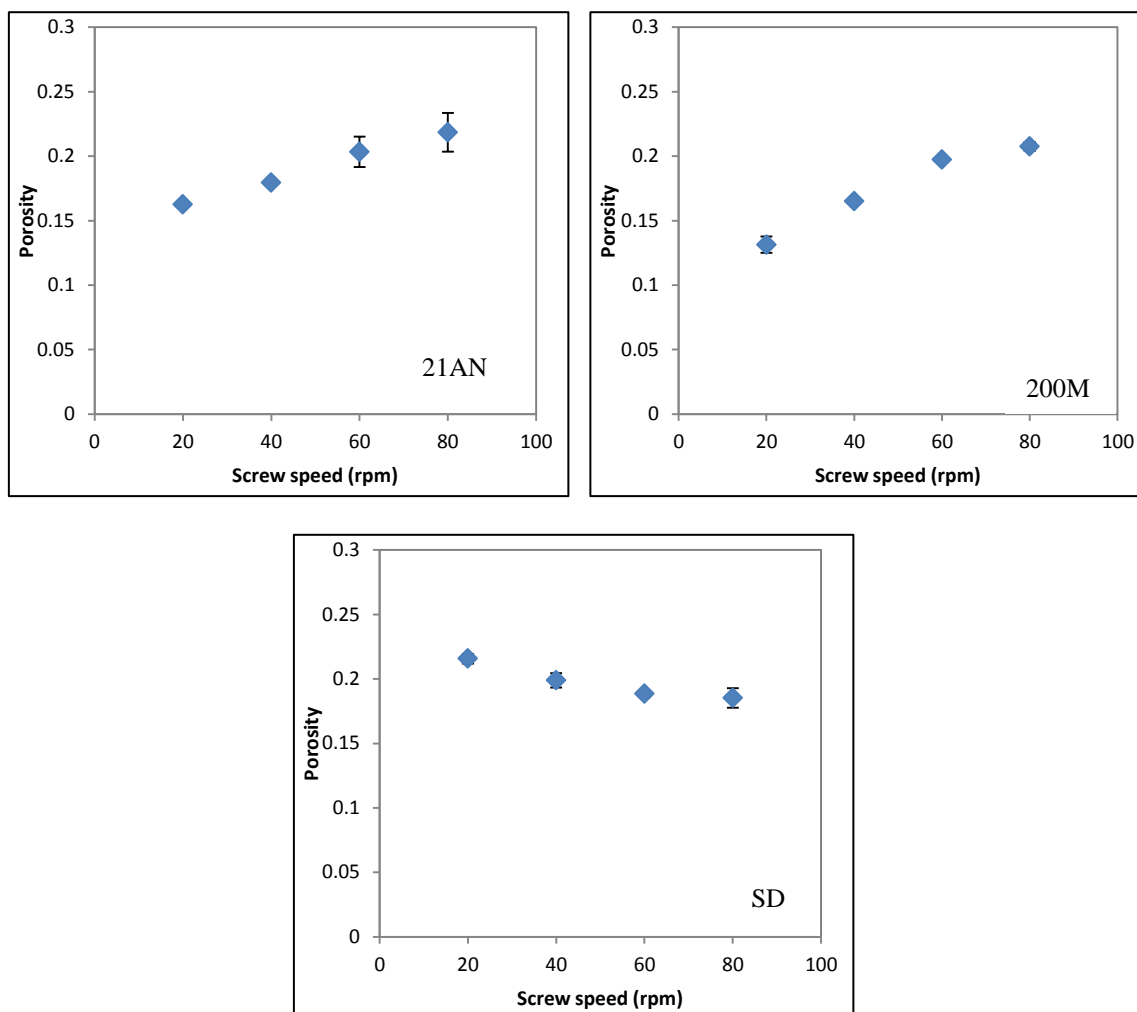


Figure 7.23: Porosity of ribbon produced from the three types of lactose at different feeder screw speed.

7.5 Conclusion

In this Chapter, the effect of the process parameters of the roller compaction was investigated. An online thermal imaging was employed to determine the maximum temperature of the ribbon during production at various process variables. The amount of fines, width, strength and porosity of ribbon were used to evaluate the product quality. It was found that increasing the roller speed during the roller compaction decreases the width of the ribbon, which consequently increases the fine percentage in the product. However, the speed of the rollers was found to have a minor effect on the tensile

strength and porosity of the ribbon. This is an attractive finding, as it proposes the possibility of increasing the production rate of ribbon of lactose powders with increasing the roller speed, knowing that this will not affect the ribbon strength and porosity.

The gap between the two rollers was also found to affect the powder compaction behaviour and ribbon properties. The temperature of the ribbon during production was found to increase with increasing the gap size between the rollers. This was due to the increase in the feeder screw speed with increasing the roller gap in order to deliver more material and fill the gap between the rollers. The increase in the feeder screw speed increased the powder internal friction which increases the temperature of the powder. An increase in the roller gap means more space for the powder to move and distribute across the width of the rollers. The better distribution of the powder across the width of the roller at larger gap size resulted in wider ribbons and, consequently, a lower percentage of fines. The change in tensile strength and porosity of the ribbon with changing the gap was different for the three types of lactose. The tensile strength of ribbon of lactose 21AN and 200M decreased and the porosity increased with increasing the roller gap, whereas for SD lactose the tensile strength increased and porosity decreased with increasing the roller gap. The opposite result for the SD lactose was attributed to the high amorphous fraction in the powder which affects the powder compaction behaviour at elevated temperature. The higher temperature generated from the screw feeder at larger gap influenced the powder compaction and resulted in a different result of SD powder.

The effect of the temperature of the starting material on the powder compaction behaviour was conducted separately at constant process parameter settings. It was found that lactose 21AN and 200M are not affected by the temperature of the starting material. However, the temperature of the powder was found to have a significant effect on the compaction behaviour of the SD lactose.

The feeder screw speed was found to have a similar effect as the roller gap since the increase in the gap during the roller compaction increased the feeder screw speed due to the use of the automatic feedback system.

CHAPTER 8 INHOMOGENEITY OF RIBBON ACROSS THE WIDTH

8.1 Introduction

In Chapter 5, it was found that the temperature of the ribbon during production was increasing with increasing the hydraulic pressure. The increase in the hydraulic pressure during the roller compaction increases the stress applied on the powder and therefore increases the temperature of the ribbon. This means that the temperature of the ribbon during production can be used as a signature of stress applied to the powder during the compaction. It was shown in Section 5.5.5 that there is a difference in temperature across the width of the ribbon. The temperature was higher at the centre in comparison with the edges of the ribbon. The higher temperature at the centre of the ribbon indicates higher stress being applied to the powder and vice versa at the edges. The different stress applied on the powder across the width of the roller resulted in different porosity along the ribbon width. The result in Section 5.5.6 in Chapter 5 showed that the porosity is higher at the edges of the ribbon compared to the centre. This was due to the less stress applied to the powder at the edges of the roller, which was confirmed by the temperature profile across the width of the ribbon during the online temperature measurements. The difference in the stress applied across the width of the ribbon has been reported in the literature [80, 81]. It was stated that the stress applied at the centre of the roller is higher than that at the edges, which resulted in ribbons with high density at the centre and lower at the edges [67, 75]. The variation of stress and density across the roller width was attributed to the feeding of the powder, which depends on the powder flow property and also to the side seal system.

Rimmed rollers are offered by several roller compactors nowadays, and it can be used instead of the cheek plates to help to reduce the side seal friction. A comparison between rimmed rollers and ordinary cheek plates have been made by Mazor et al. [76] in order to investigate the effect of the sealing system design on ribbon density distribution across the width using microcrystalline cellulose. They revealed that the use of the cheek plate sealing system resulted in a non-uniform density across the width of

the ribbon. The density at the centre of the ribbon was higher in comparison to the edges. However, more uniform density across ribbon width was obtained when using the rimmed rollers.

The rimmed rollers showed a potential to overcome the issue of the side seal friction and could be useful for certain materials. However, when the issue is the powder distribution and availability across the width of the roller due to the poor flowability, the rimmed rollers might not be an appropriate approach to overcome the non-uniformity of stress along the width of the roller.

In this Chapter, a novel approach will be presented in order to obtain a uniform stress applied on the powder during roller compaction and produce ribbon with homogenous properties across the width [137]. This will ensure the consistency and quality of the final product, as the quality of the ribbon has a direct impact on the final product properties. In the current approach, a new roller with a novel curved surface has been designed at the University of Sheffield. The roller with the curved surface will be compared with the standard flat surface roller. The thermal camera will be used to record the temperature of the ribbon during production which will be then analysed to obtain the temperature profile across the width of the ribbon. The temperature, stress, fine percentage, porosity and local strength across the width of the ribbon will be employed to examine the potential of the new curved roller in producing ribbons with homogenous properties across the width.

8.2 Powder preparation

The three types of lactose were used to examine the potential of the new curved roller. The powders were conditioned in a climatic chamber at 25°C and 20% relative humidity for 3 days.

8.3 Production and characterisation of ribbon

The powders were compressed into ribbons using a hydraulic pressure in the range of 20-100 bar, fixed roller speed of 3 rpm, and the gap between the rollers was set to 2.5 mm, using the automatic feedback system.

A GenRH-A (London, UK) humidity generator was connected to the top of the hopper on the roller compactor as shown in Figure 3.6. The humidity generator was operated at the same conditions as the climatic chamber (20% RH); this ensured a constant humidity condition of the powder during roller compaction same as that used for the storage of the powder prior to compaction.

The temperature of ribbon was recorded during production (online). The fines produced during the roller compaction were collected and the fines weight percentage was determined. SEM was used to investigate the structure of the ribbon and X-ray tomography was used to determine ribbon porosity. The results for lactose 200M are shown comprehensively in this Chapter, whereas the results for lactose 21AN and lactose SD are shown in Appendix B.

8.3.1 The novel design of the curved roller

In order to obtain a uniform stress applied to the powder during the roller compaction, a new roller with a concave surface geometry was designed. The new roller has the same diameter and width as the standard flat roller, 120 mm and 40 mm respectively. The roller has a curved surface which can be defined by an arc with a radius of 101 mm. This will give a surface with 2 mm difference between the centre and the edges of the roller along the width as shown in Figure 8.1. The curved surface of the new roller will improve the stress applied on the powder at the edges as the gap between the two rollers will be smaller in comparison to the centre. The smaller gap between the two rollers will compensate the lesser powder at the edges which was the reason of a non-uniform stress across the roller width.

The setup of the rollers during the experiments is shown in Figure 8.2. In one set of experiment, two standard flat knurled rollers were used as shown in Figure 8.2-(A); this was then compared with the other set of experiment using the new curved roller on the top and a standard roller at the bottom as shown in Figure 8.2-(B). In the case of setup B in Figure 8.2, the gap between the two rollers is smaller at the edges compared to the centre due to the curved design of the new roller.

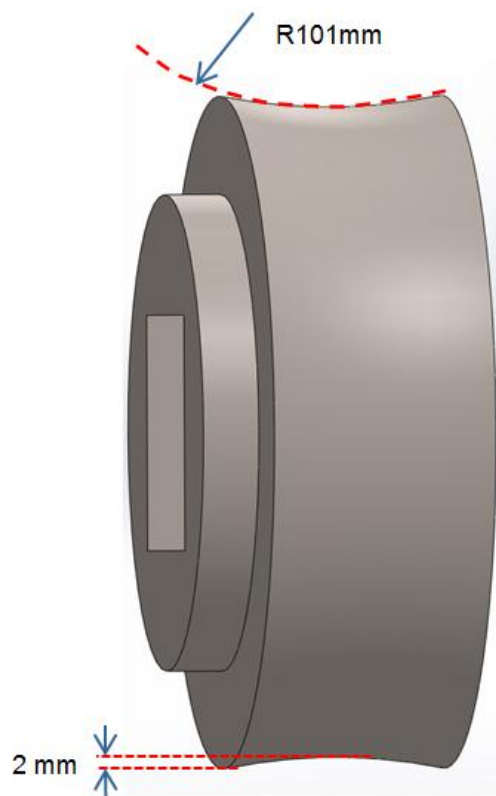


Figure 8.1: The geometry of the new curved roller.

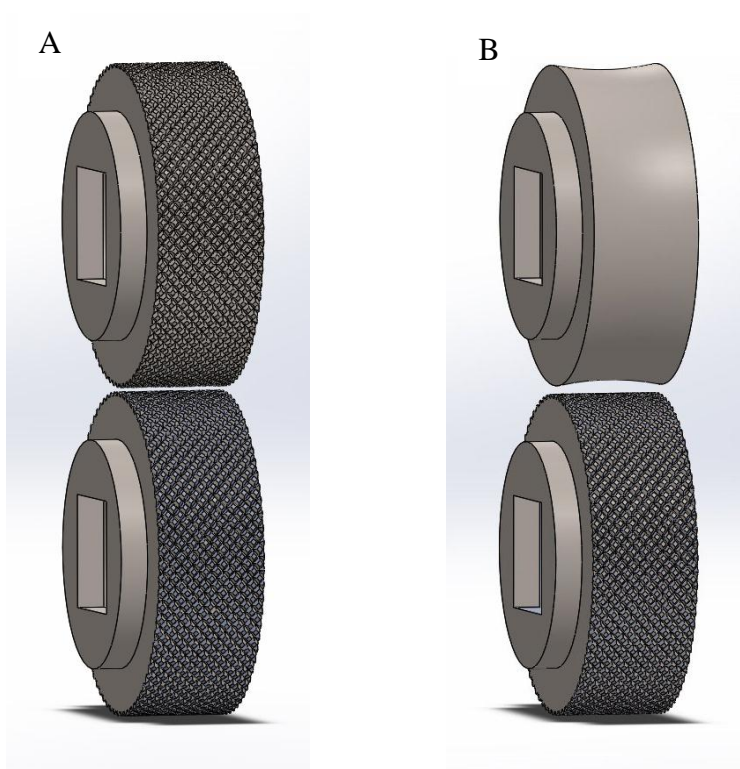


Figure 8.2: The setup of the rollers during the experiments using: (A) the standard flat rollers and (B) the new curved roller.

8.4 Result and discussion

8.4.1 Temperature profile across roller width

The images from the thermal camera were analysed using FILR R&D software to determine the temperature distribution across the width of the ribbons. This was done by drawing a line along the ribbon width then determining the temperature across this line as described in Section 5.5.5. This procedure was repeated for all types of lactose using both the standard flat roller and the new curved roller. Figure 8.3 show the temperature profile across the width of ribbon produced using the flat roller (A) and the curved roller (B) for lactose 200M. The temperature profile across the width of ribbon of lactose 21AN and SD are presented in Appendix B. The vertical axis (in Figure 8.3) is the average temperature of the ribbon which was extracted every 5 seconds from the video, and the horizontal axis is the normalised width of the ribbon. In all cases, the temperature of the ribbon during production increased with increasing the hydraulic pressure. This was due to the higher stress being applied to the powder at a higher hydraulic pressure; which increases the amount of deformation, fracture and friction between the particles, consequently, increases the ribbon temperature.

For the standard flat roller Figure 8.3 (A), it can be seen that the temperature is not uniform along the ribbon width; the temperature is higher at the centre compared to the edges. The difference in the temperature between the centre and the edge of the ribbon indicates that there was a variation in stress applied across the width of the roller during compaction. The higher temperature at the centre of the ribbon is an indication of a high stress and the low temperature at the edges indicates low stress.

The use of the new curved roller (setup B in Figure 8.2) resulted in different temperature profile across the ribbon width as shown in Figure 8.3 (B). It can be seen that the temperature profile along the width of ribbon produced from the curved roller is more uniform compared to that of the flat roller. The uniform temperature distribution along the width of ribbon produced from the curved roller is an indication of a uniform stress. It is believed that the surface geometry of the curved roller affected the stress distribution along the width of the roller. The difference in the gap along the width of the two rollers (see setup B in Figure 8.2) resulted in a uniform overall stress to be applied across the width, therefore, a uniform temperature distribution.

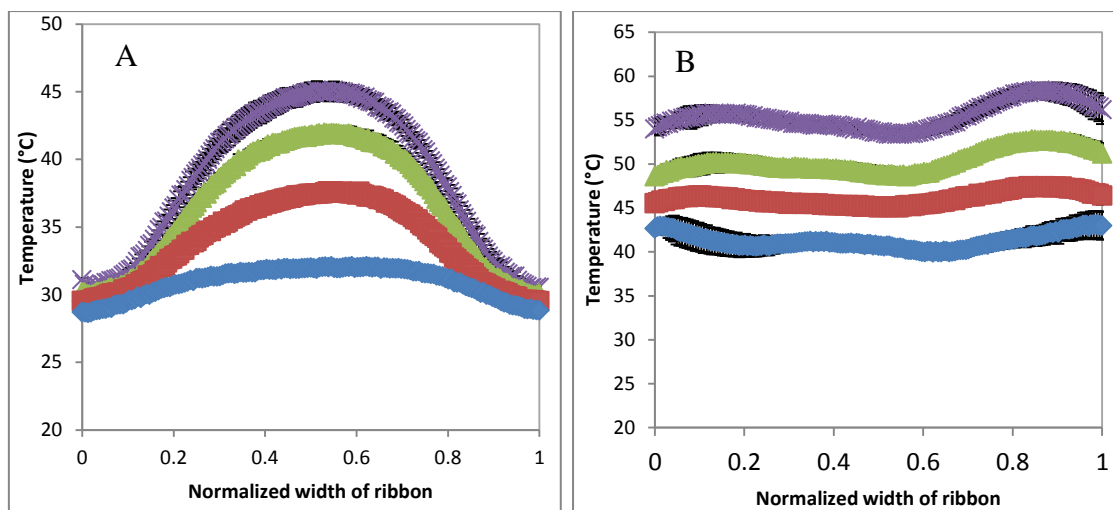


Figure 8.3: Temperature profile across the width of ribbon of lactose 200M during the roller compaction using the flat roller (A) and the curved roller (B) (◆ 20 bar, ■ 50 bar, ▲ 80 bar, × 100 bar).

8.5 Measurements of the stress during the roller compaction

The actual normal stress applied to the powder during the roller compaction process was measured using a prescale pressure film (Fujifilm, UK). The film used in this study was the super high-pressure film which is a mono-sheet type. The film is composed of a polyester base on which the colour developing material is coated, with the micro-encapsulated colour-forming material layered on top as shown in Figure 8.4.

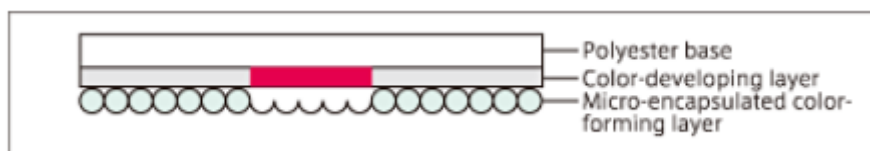


Figure 8.4: The design of the Fujifilm pressure film.

When pressure is applied on the film, the microcapsules start to break and the colour-forming material reacts with the colour developing material which results in the appearance of red patches on the film. The density of the red colour changes with changing the pressure level applied to the film. The actual stress applied on the film can be determined from the relationship between the colour density and the stress which is provided as a standard chart by Fujifilm (see Figure 8.5).

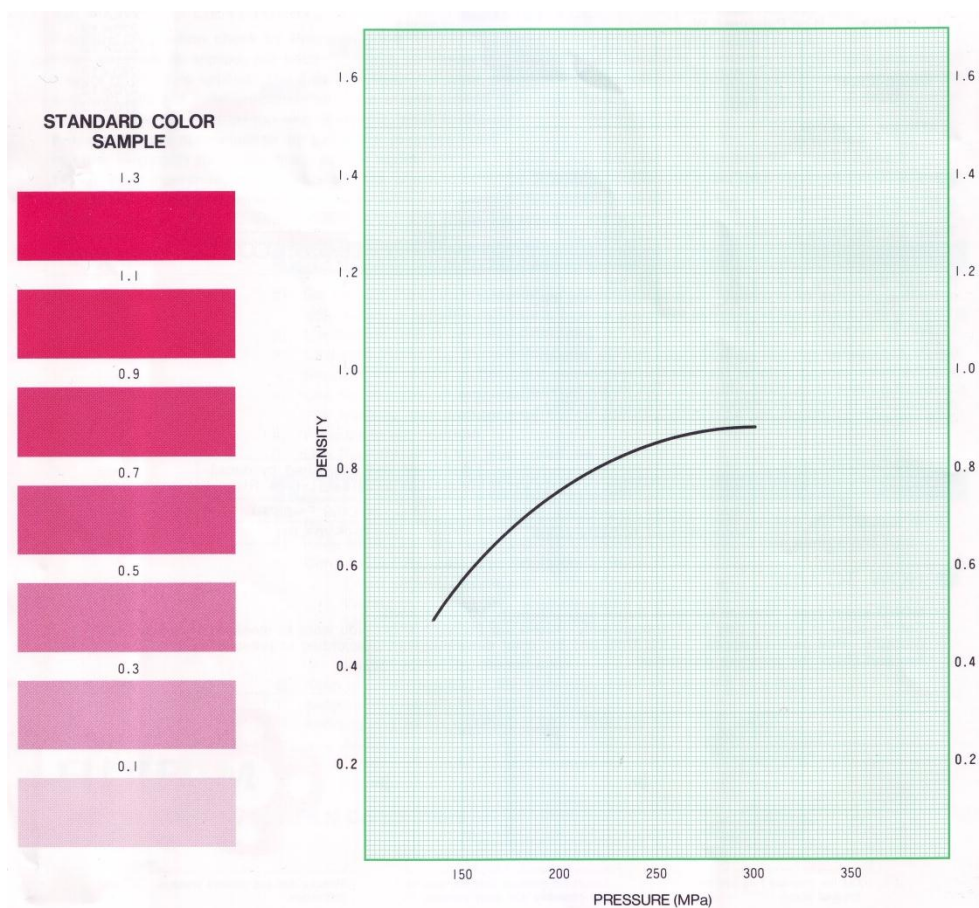


Figure 8.5: Relationship between the density of the colour and the stress applied on the film (Fujifilm 2014).

8.5.1 Calibration of the pressure film

Before using the prescale pressure film in the roller compactor, it was important to obtain a calibration curve using the standard colour samples and the standard chart in Figure 8.5. This will ensure accuracy and consistency of stress measurements using the pressure films. Firstly, the images of the standard coloured samples in Figure 8.5 were imported using a flatbed scanner (Canon, CanoScan LiDE 25) at a resolution of 1200 dpi. Image J was then used to process and convert the coloured images into a grey scale image, which was then converted to a black and white image using a certain threshold value [59] as shown in Figure 8.6.

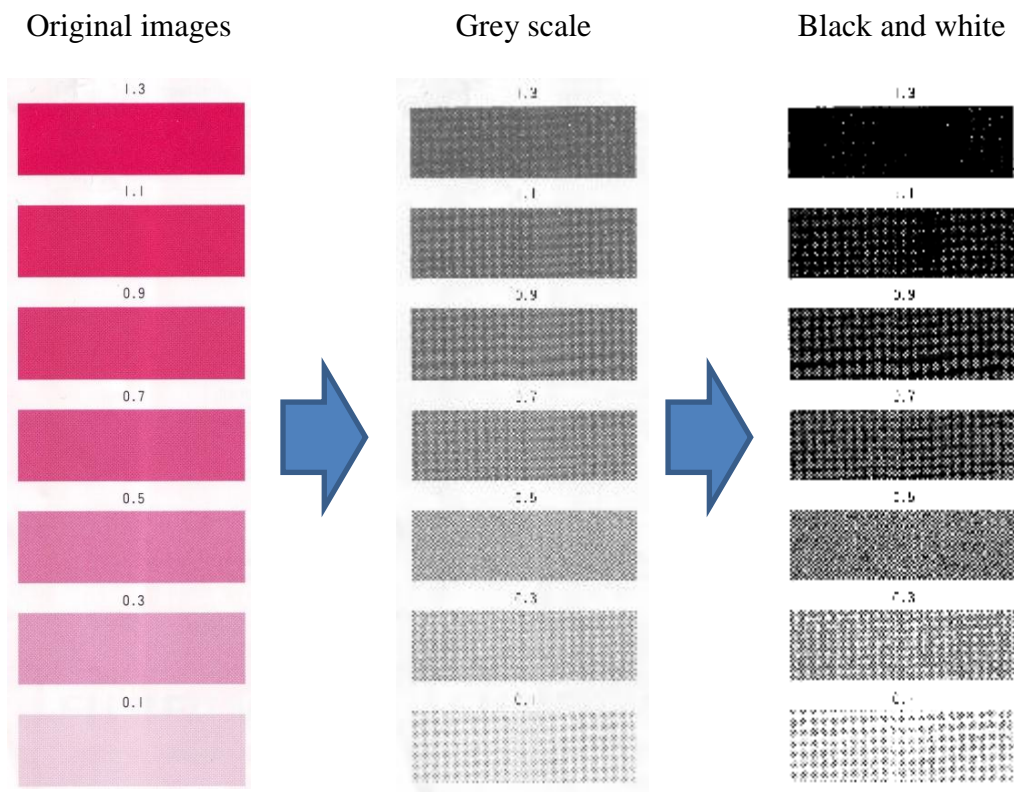


Figure 8.6: Images of the standard coloured samples before and after processing.

From the black and white images, the mean grey scale value (i.e. the ratio of the black to white pixels) was extracted using the Image J software. The mean grey scale value of each image was then plotted against the corresponding colour density of the original standard images, see Figure 8.7.

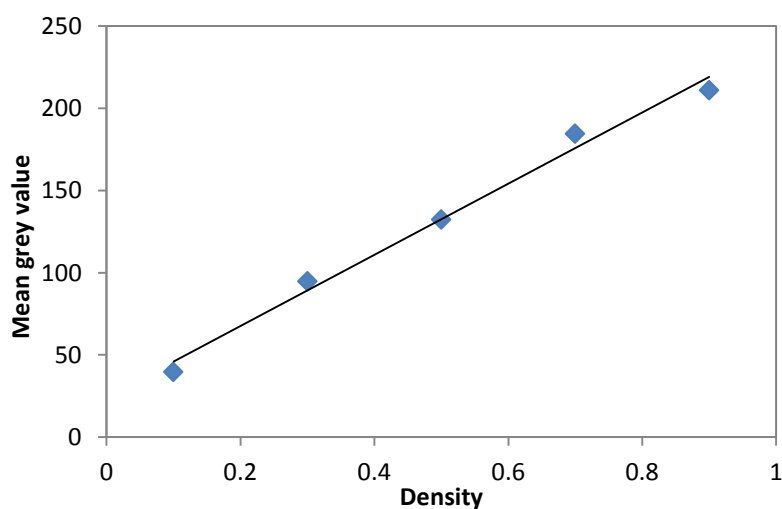


Figure 8.7: Relationship between the density of the colour and the mean grey scale value.

The standard chart provided by Fujifilm (in Figure 8.5) along with the information in Figure 8.7 were used to obtain a direct relationship between the grey scale value of an image and the stress applied to the film as shown in Figure 8.8. This figure can be used as a calibration curve to convert the mean grey scale value obtained from a film to the normal stress applied to the film.

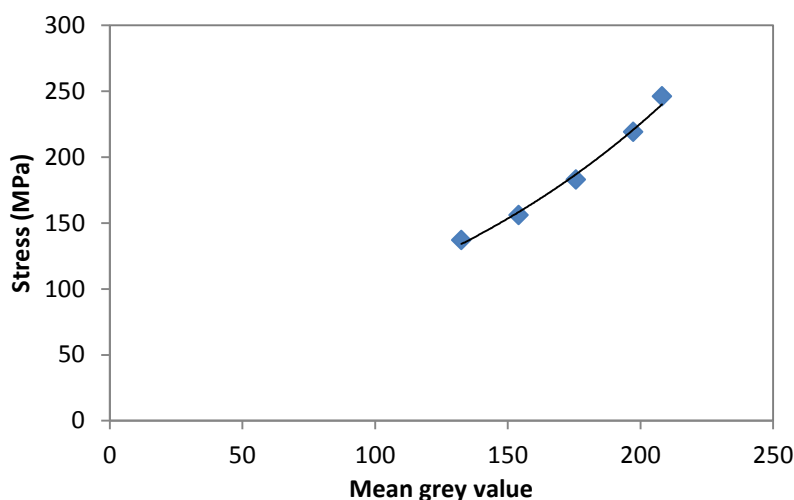


Figure 8.8: Calibration curve showing the relationship between the mean grey scale value and the applied stress.

8.5.2 Determination of the stress profile across roller width

The Prescale pressure film was used during the roller compaction of the different types of lactose using both the standard flat rollers (see Figure 8.2 -A) and the new curved roller (see Figure 8.2- B). The idea was to determine the stress applied on the powder along the width of the roller during compaction, then compare the stress profile for the flat and the curved roller.

During the roller compaction and after the hydraulic pressure and the gap reached steady state, the prescale pressure film was passed through the rollers while compacting the powder. The pressure film was then collected and images of the films were imported using the Canon scanner and the same setting which is used during importing images of the standard samples as described in Section 8.5.1. Figure 8.9 shows the images of the pressure film after passing through both the flat and the curved rollers while compacting the powder.

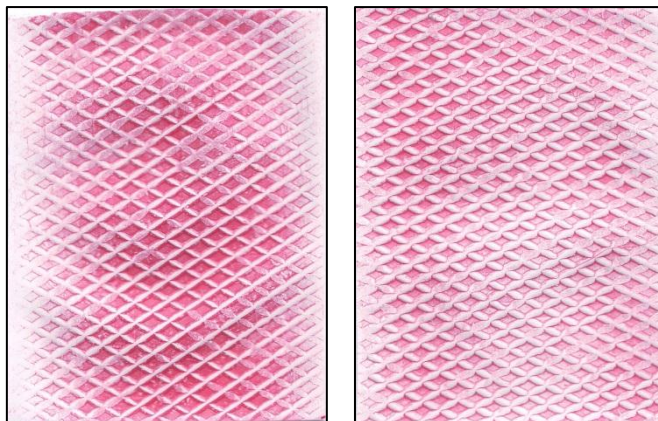


Figure 8.9: Images of the pressure film after compaction at 50 bar using the standard flat roller (left) and the new curved roller (right).

Image J was then used to convert the coloured images into a grey scale image as shown in Figure 8.10. The grey scale images were then converted to black and white images (see Figure 8.11) using the same threshold value which is used during the pressure film calibration as described in Section 8.5.1.

From Figure 8.9, it can be seen that the red colour density is not uniform across the width of the film. The density of the colour is higher at the centre compared to the edges when the standard flat roller used during the compaction. This indicates that the stress applied at the centre of the film during the compaction was higher than that at the edges. However, the density of the colour is more uniform across the width of the film when the new curved roller was used during the compaction, which indicates a more uniform stress across the width of the roller compare to the flat roller. The difference of the colour density along the width of the film can be noticed more easily in the black and white image in Figure 8.11. The higher the density of the red colour in the original images in Figure 8.9 the higher the amount of the black pixels in the black and white images in Figure 8.11. It can be seen that the centre of the film is blacker than the edges when using the flat roller, whereas the black pixels are distributed in more uniform manner across the width of the roller when the curved roller was used.

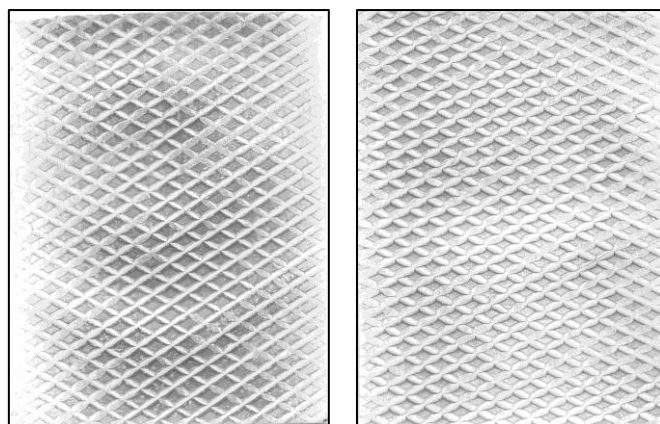


Figure 8.10: Grey scale images of the pressure film after compaction at 50 bar using the standard flat roller (left) and the new curved roller (right).

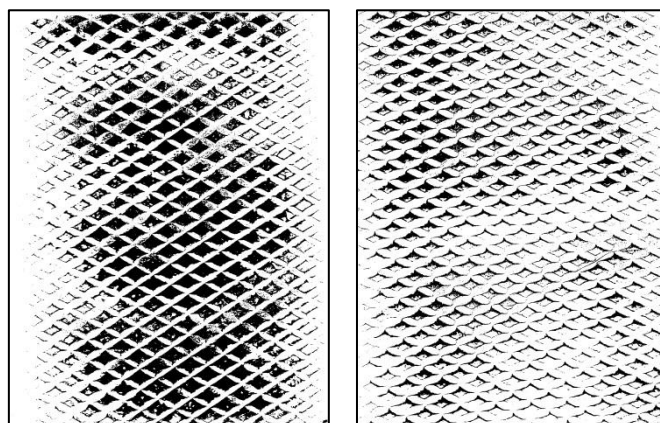


Figure 8.11: Black and white images of the pressure film after compaction at 50 bar using the standard flat roller (left) and the new curved roller (right).

From the black and white images (in Figure 8.11) the mean grey scale value was obtained and then used to determine the normal stress using the calibration curve shown in Figure 8.8. The mean grey scale value was extracted every 2-2.5 mm along the width of each film and related to the normal stress using Figure 8.8. This resulted in stress profile across the width of the film which is the stress applied to the powder along the width of the roller during the roller compaction. This procedure was applied to all the films compacted at different hydraulic pressure. Figure 8.12 shows the stress profile across the width of the flat roller (A) and the curved roller (B) for lactose 200M compacted at different hydraulic pressure (the result of other types of lactose are shown in Appendix B). It can be seen (from Figure 8.12) that the stress applied on the film/powder increased with increasing the hydraulic pressure during the compaction using both the flat and the curved rollers.

It can be seen that there is a non-uniform stress distribution across the width of the roller when using a standard flat roller. The stress applied at the centre of the film is higher than that applied at the edges. This is due to the variation in the powder distribution along the width of the roller, which results in less powder being present at the edges of the roller. The less powder availability at the edges of the roller results in less stress being applied to the powder. The difference in the stress between the centre and the edges of the roller was reported by [80, 81] using an instrumented roller provided with three pressure sensors along the width. It was reported that the stress recorded by the sensor at the middle was higher than that at the edges. They attributed their result to the non-uniformity of the feeding pressure which was caused by the last flight of the feeding screw and this has been reported previously in [78, 79].

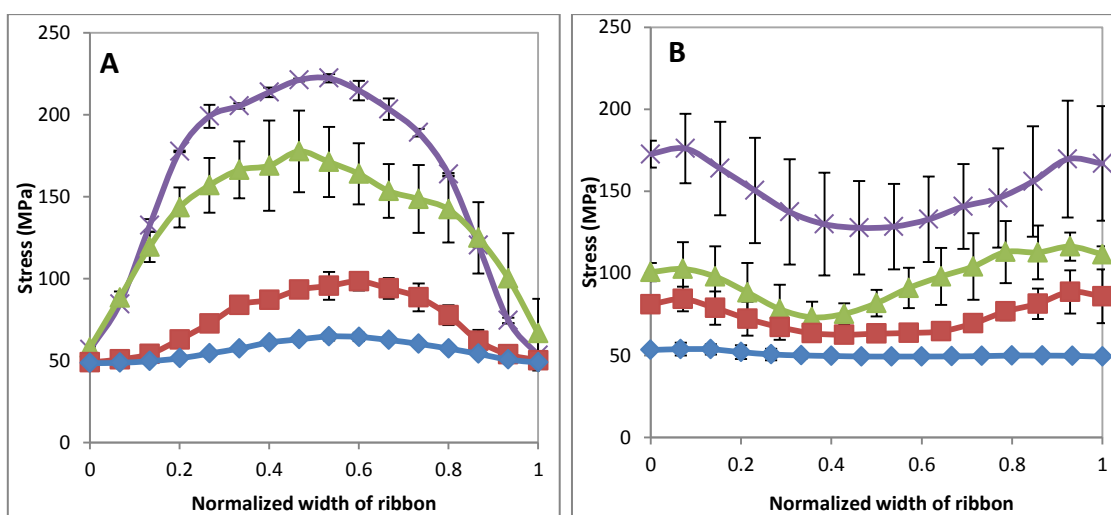


Figure 8.12: Stress distribution across the width of the flat roller (A) and the curved roller (B) during roller compaction of lactose 200M (◆ 20 bar, ■ 50 bar, ▲ 80 bar, × 100 bar).

The stress profile across the width of the film using the flat roller was compared with that obtained using the curved roller at each hydraulic pressure as shown in Figure 8.13. At all hydraulic pressures, it can be seen that the new curved roller resulted in more uniform stress across the width of the film in comparison to the flat roller. This means that the stress applied on the powder during the roller compaction was almost uniform along the width of the curved roller. As mentioned earlier, the lower stress at the edges of the flat roller was due to the less powder availability which resulted in less stress being applied at the edges. With the new curved roller, the less powder availability at the edges was compensated by a larger roller displacement due to the curvature of the roll surface. The surface of the new roller was designed in a way which results in a large

gap in the centre and smaller towards the edges. The large gap at the centre of the rollers decreases the stress applied on the powder and this stress increased with decreasing the gap towards the edges. Compared to the stress applied by the flat roller, the curved roller decreased the stress at the centre and increased it at the edges, consequently, resulting in a uniform overall stress across the whole width. The uniform stress applied on the powder along the width of the roller resulted in a uniform temperature distribution across the width of the ribbon as shown in Figure 8.3. This means that the temperature of the ribbon is an indication of the stress applied to the powder, and the online thermal camera can be used as a successful tool to monitor the stress applied on the powder in real time.

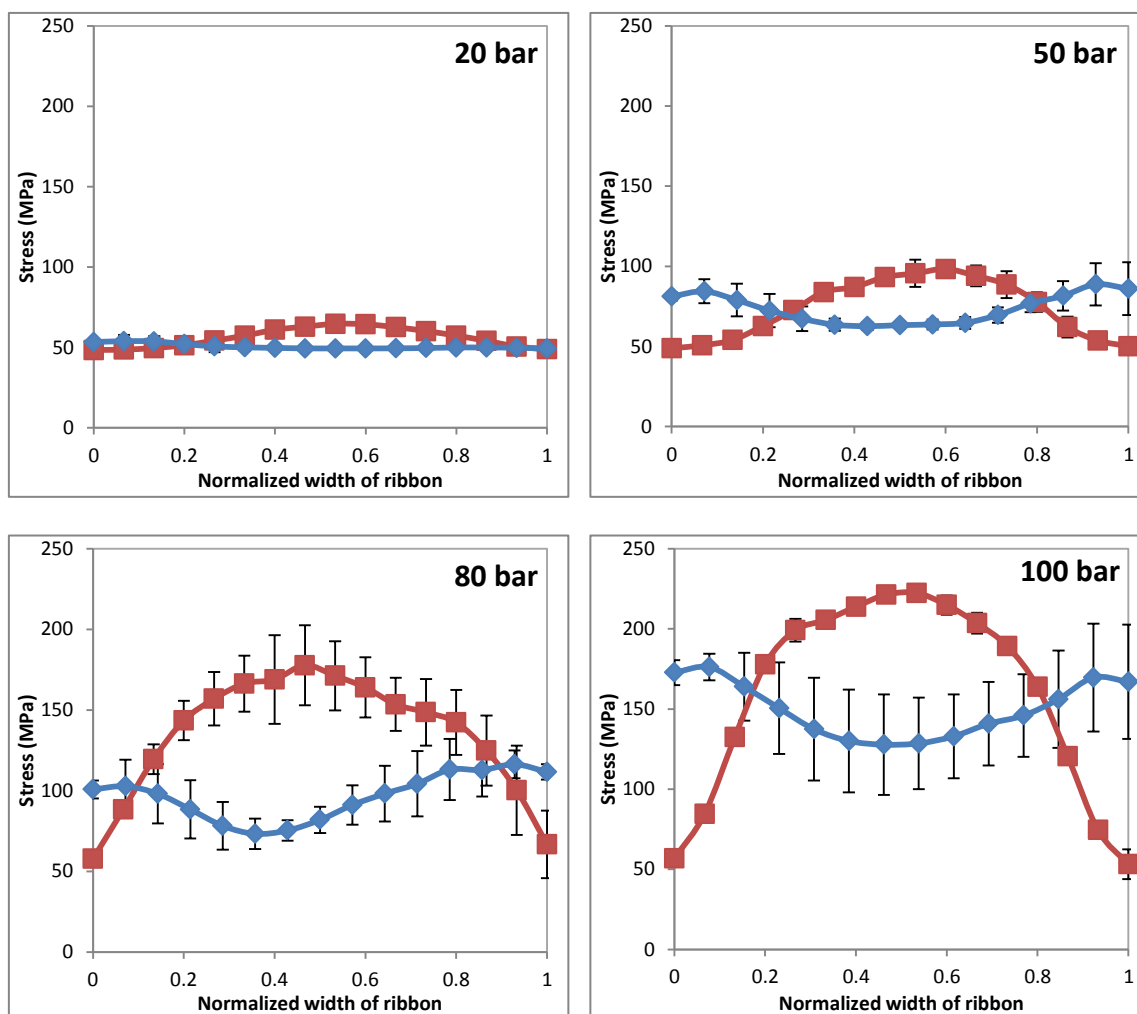


Figure 8.13: Stress distribution of the flat vs the curved roller using lactose 200M (◆ curved roller, ■ flat roller).

8.6 Fines percentage and width of ribbon

The fine is the uncompacted powder which is produced during the roller compaction. It is one of the main disadvantages of dry granulation using the roller compaction. The percentage of fines was used to evaluate the product quality and it was determined as described in Section 3.2.9. Decreasing the amount of fines in the product increases the overall efficiency of the process. Figure 8.14 shows the percentage of fines produced during compaction of lactose 200M using both the standard flat roller and the new curved roller (see appendix B for other types of lactose). It can be seen that the fine percentage decreased with increasing the hydraulic pressure. In addition, the use of the new curved roller resulted in a significant reduction in the fine percentage.

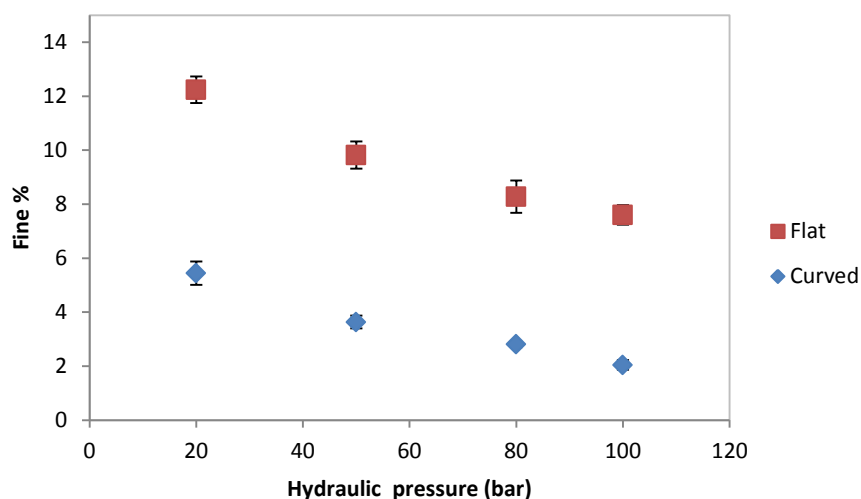


Figure 8.14: Percentage of fines produced from lactose 200M using the standard flat roller and the new curved roller.

Figure 8.15 shows the width of ribbon produced from lactose 200M at different hydraulic pressure using both the flat and the curved roller. The width of the ribbon increased with increasing the hydraulic pressure during compaction of the powder. It can be seen that ribbon produced using the roller with the curved surface is wider than that produced using the flat roller.

The higher fines percentage and the smaller width of ribbon produced during the roller compaction using the standard flat roller was due to the lower stress at the edges of the roller (see Figure 8.12) which resulted in lower temperature (see Figure 8.3). The

decrease in the fine percentage (Figure 8.14) and the increase in the ribbon width (Figure 8.15) are as a consequence of using the new roller with the curved surface. The use of the curved roller resulted in a uniform stress to be applied across the roller width (Figure 8.12) which resulted in uniform temperature distribution of ribbon during production (see Figure 8.3). The higher stress applied at the edges of the curved roller, compared to the flat roller, improved the binding ability between the particles and consequently increased the width of ribbon and reduced the percentage of fines in the product.

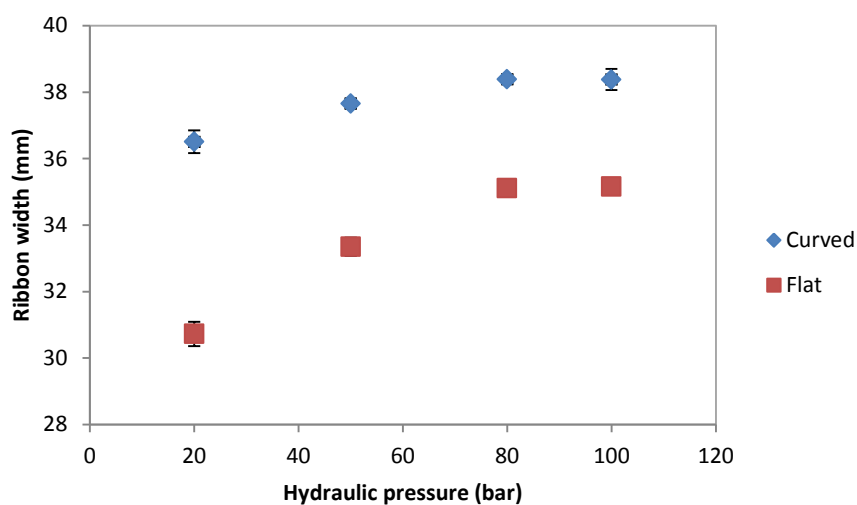


Figure 8.15: Width of ribbon of lactose 200M produced using the standard flat roller and the new curved roller.

From Figure 8.14 and Figure 8.15, it can be noticed that the fine percentage was lower for wider ribbons and higher for the narrower ribbon. This means that there is a relationship between the width of the final ribbon and the percentage of fines produced during the roller compaction. Figure 8.16 shows the relationship between the width of the ribbon and the fine percentage. It can be seen, regardless the roller types, that the higher the width of the final ribbon the lower the fine percentage during the roller compaction.

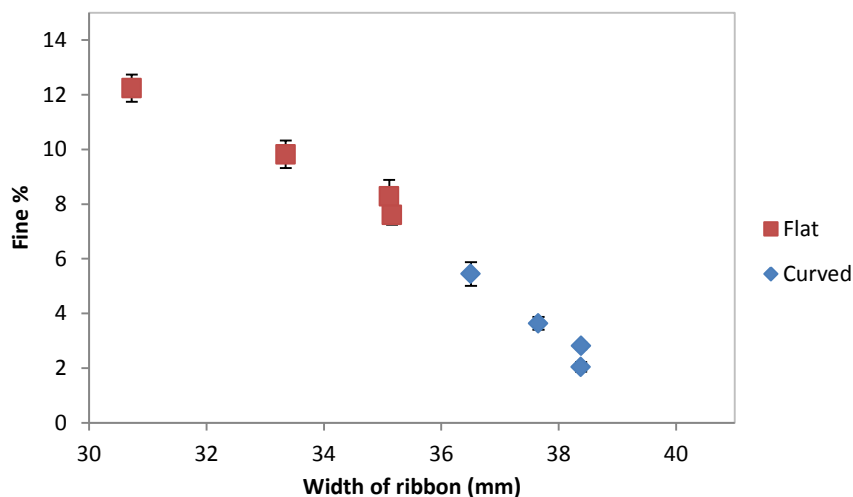


Figure 8.16: Fine percentage vs width of ribbon of lactose 200M.

8.7 Local strength across the width of the ribbon

The local strength of the ribbon across the width was assessed by the indentation method using the Zwick/Roell Z 0.5 (Zwick/Roell, Germany). The ribbon was cut to three equal pieces (centre and two edges) as shown in Figure 8.17. The local strength of each piece was measured using a ball indenter of 2.5 mm in diameter. The test speed was set to 0.05 mm/min and the force and penetration depth was recorded during the measurement. The maximum force and the corresponding penetration depth was extracted from the data and used to determine the local strength. The strength was determined by dividing the maximum force by the corresponding cross-sectional area which was calculated using the penetration depth. This procedure was repeated for all ribbons produced at different hydraulic pressures using both the flat and curved rollers.

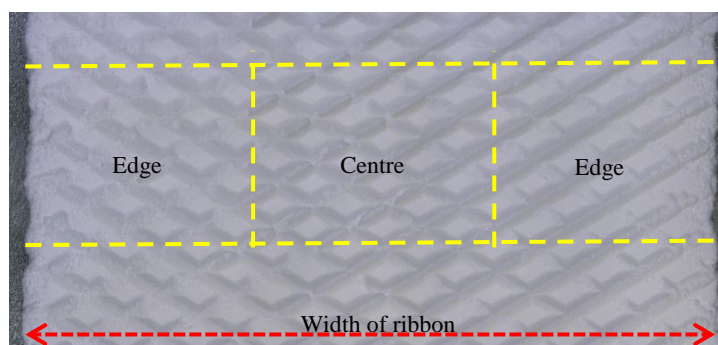


Figure 8.17: Example of ribbon sectioning method.

Figure 8.18 show the local strength of ribbon at the edges and centre of ribbon produced from lactose 200M at different hydraulic pressure using both the standard flat (A) and the new curved roller (B) (for lactose 21AN and SD, the result are presented in Appendix B). It can be seen that the local strength of the ribbon increased with increasing the hydraulic pressure for both roller setups. For the standard flat roller, the strength of ribbon at the centre was higher in comparison to the strength at the edges. However, the strength at the centre of ribbons produced using the curved roller was similar to that at the edges. The difference in strength between the centre and edges of ribbon produced using the flat roller is due to the variation in stress applied by the roller across the width as shown in Figure 8.12 (A). The stress applied at the centre of the roller was higher compared to the stress at the edges. This was due to the lesser powder being present at the edges of the roller as a result of non-uniformity of powder distribution across the roller width. This can also be observed from the online thermal camera which showed a difference in ribbon temperature along the width of the ribbon (see Figure 8.3).

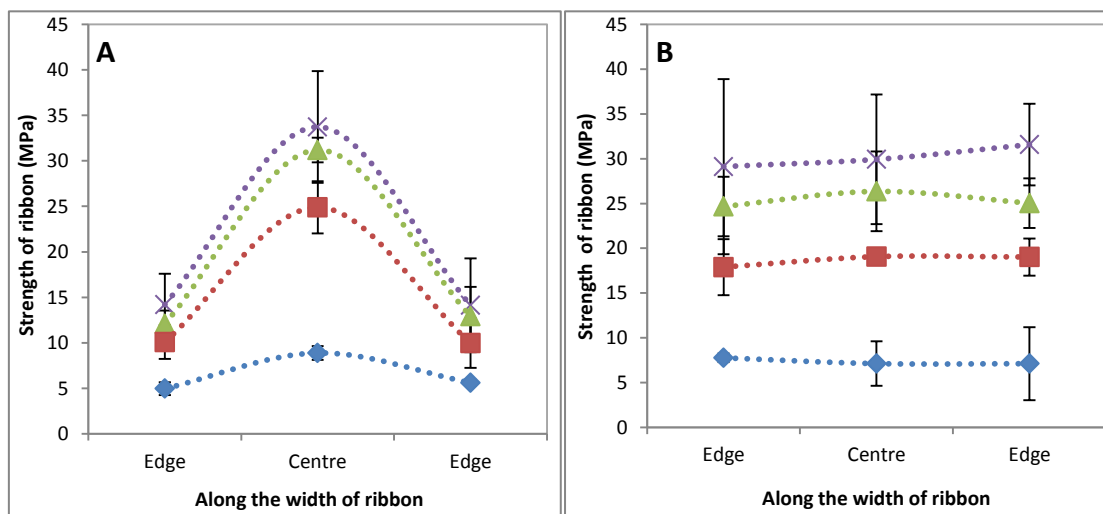


Figure 8.18: Local strength across the width of ribbon of 200M using the flat roller (A) and the curved roller (B) (◆ 20 bar, ■ 50 bar, ▲ 80 bar, × 100 bar).

Figure 8.19 shows a comparison of local strength along the width for ribbon produced using both the flat and the curved roller at each hydraulic pressure. At all hydraulic pressures, it can be seen that the use of the new curved roller enhanced the strength across the width of the ribbon. The difference in strength between the centre and edges of ribbon produced from the flat roller is disappeared when the curved roller was used. The lesser powder at the edges of the roller (which was the reason of low strength at the

edges) was compensated by the higher roller displacement using the new curved roller. The design of the curved roller increased the stress applied on the powder at the edges, therefore, increased the local strength. Overall, the new curved roller resulted in a uniform strength across the width of the ribbon.

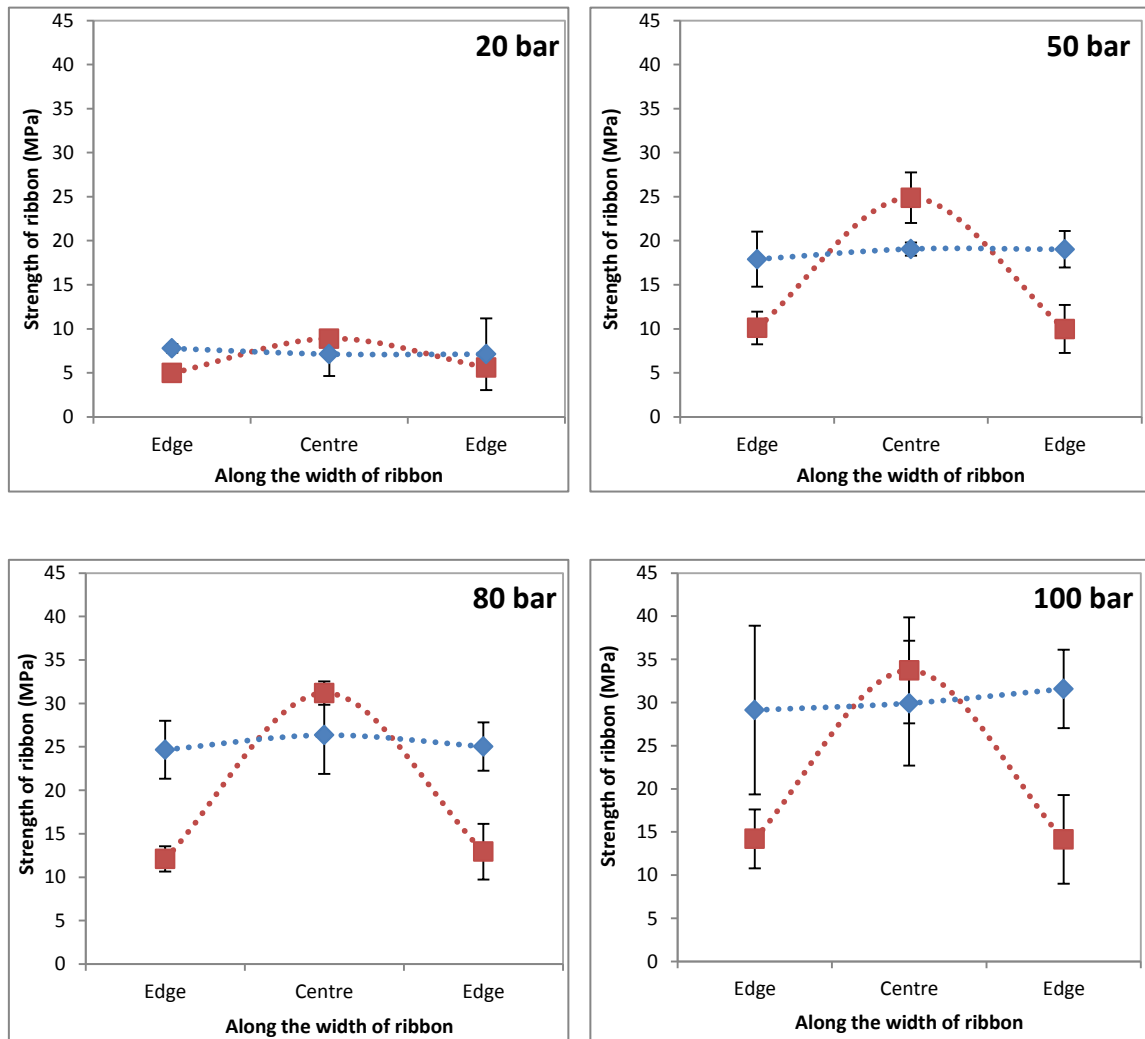


Figure 8.19: Local strength across the width of ribbon produced from 200M using the curved roller ◆, and the flat roller ■.

8.8 Ribbon surface structure

Scanning electron microscopy (SEM) was used to investigate the structure of the ribbon produced using both the flat and the curved roller. Pieces of ribbon were cut from the centre and the edges of the ribbon in order to investigate the surface structure across the width of the ribbon. JEOL JSM- 6010LA scanning electron microscopy was used to obtain the micrographs at different magnifications. Figure 8.20 shows the SEM images of centre and edges of ribbon produced from lactose 200M at 100 bar using the standard flat roller. Images at different magnifications show that there is a significant difference in the surface structure between the centre and the edges of the ribbon. It can be seen that the surface of ribbon at the centre is flatter than that at the edges. The flatter surface appeared at the centre of the ribbon is due to the higher stress applied on the powder (see Figure 8.12 and Figure 8.13). The lower stress applied at the edge of the flat roller resulted in a rough surface of ribbon at the edges as shown in Figure 8.20 (B, D, F). It is believed that the stress at the edges of the roller was not enough to show significant breakage and deformation of the particles, and particles can easily be distinguished from the SEM images. The difference in the ribbon surface structure between the centre and the edges resulted in variation in ribbon strength of along the width (see Figure 8.18). The flat and compacted structure at the centre of the ribbon (Figure 8.20 A, C, E) resulted in higher ribbon strength at the centre and the rough surface at the edges resulted in weak ribbon.

Figure 8.21 shows the SEM images at the centre and the edges of the ribbon produced from lactose 200M at 100 bar using the new curved roller. It can be seen that the use of the new curved roller reduced the difference in the surface structure between the side and the centre of the ribbon. This was due to the uniform stress which was applied by the curved roller on the powder during the compaction (Figure 8.12). The surface geometry of the new curved roller improved the stress distribution across the roller width, therefore produced ribbon with similar surface structure along the width (Figure 8.21). This was the reason of a uniform local strength across the width of ribbon produced using the curved roller (see Figure 8.18 and Figure 8.19).

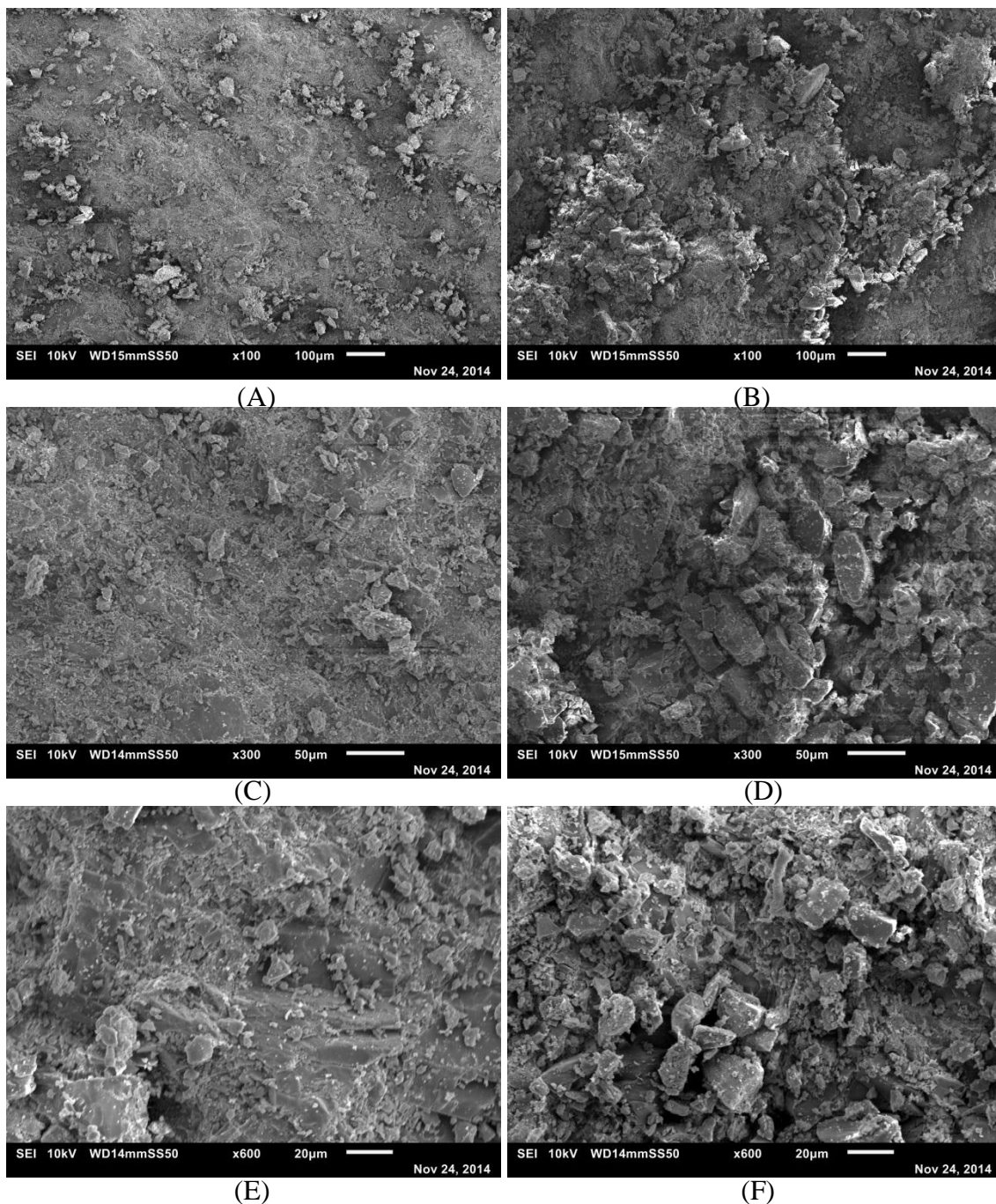


Figure 8.20: SEM images for ribbons produced from lactose 200M at 100 bar using the flat rollers; centre of ribbon (A, C, E) and edges of the ribbon (B, D, F), at 100 \times magnification (A, B), 300 \times (C, D), and 600 \times (E, F).

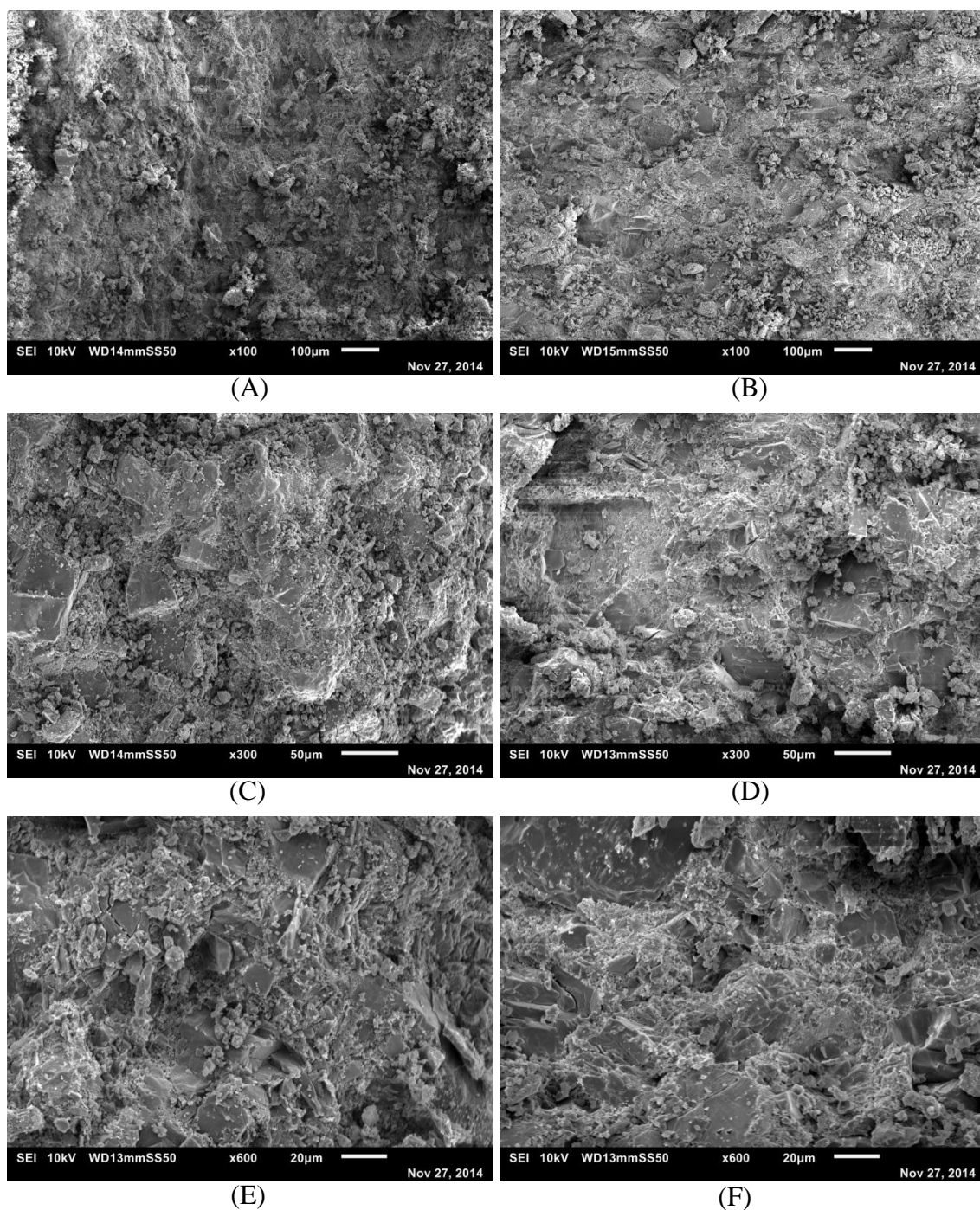


Figure 8.21: SEM images for ribbons produced from lactose 200M at 100 bar using the curved rollers; centre of ribbon (A, C, E) and edges of the ribbon (B, D, F), at 100 \times magnification (A, B), 300 \times (C, D), and 600 \times (E, F).

8.9 X-ray

X-ray tomography was used to investigate the internal structure of ribbon produced from the different types of lactose using both the flat and the new curved roller. Samples were taken from the centre and edge of the ribbon in order to determine the porosity along ribbon width. This was repeated for all ribbons produced from the different types of lactose using the standard flat roller and the new curved roller.

The difference in porosity and internal structure between the centre and the edge of ribbon produced from the flat roller can be seen in the X-ray images in Figure 8.22. The centre of the ribbon is more compacted and contains less air in the structure than that at the edges. This is in agreement with the ribbon surface structure as shown in the SEM images in Figure 8.20. Figure 8.23 shows the X-ray images of centre and edge of ribbon produced from lactose 200M using the new curved roller. It can be seen that the centre of ribbons produced using the new curved roller has a similar internal structure in comparison to the edge. Similar phenomena can be seen for the ribbon surface structure as shown in the SEM images in Figure 8.21, which illustrates that there is no significant difference in the surface structure between the centre and the edge of the ribbon.

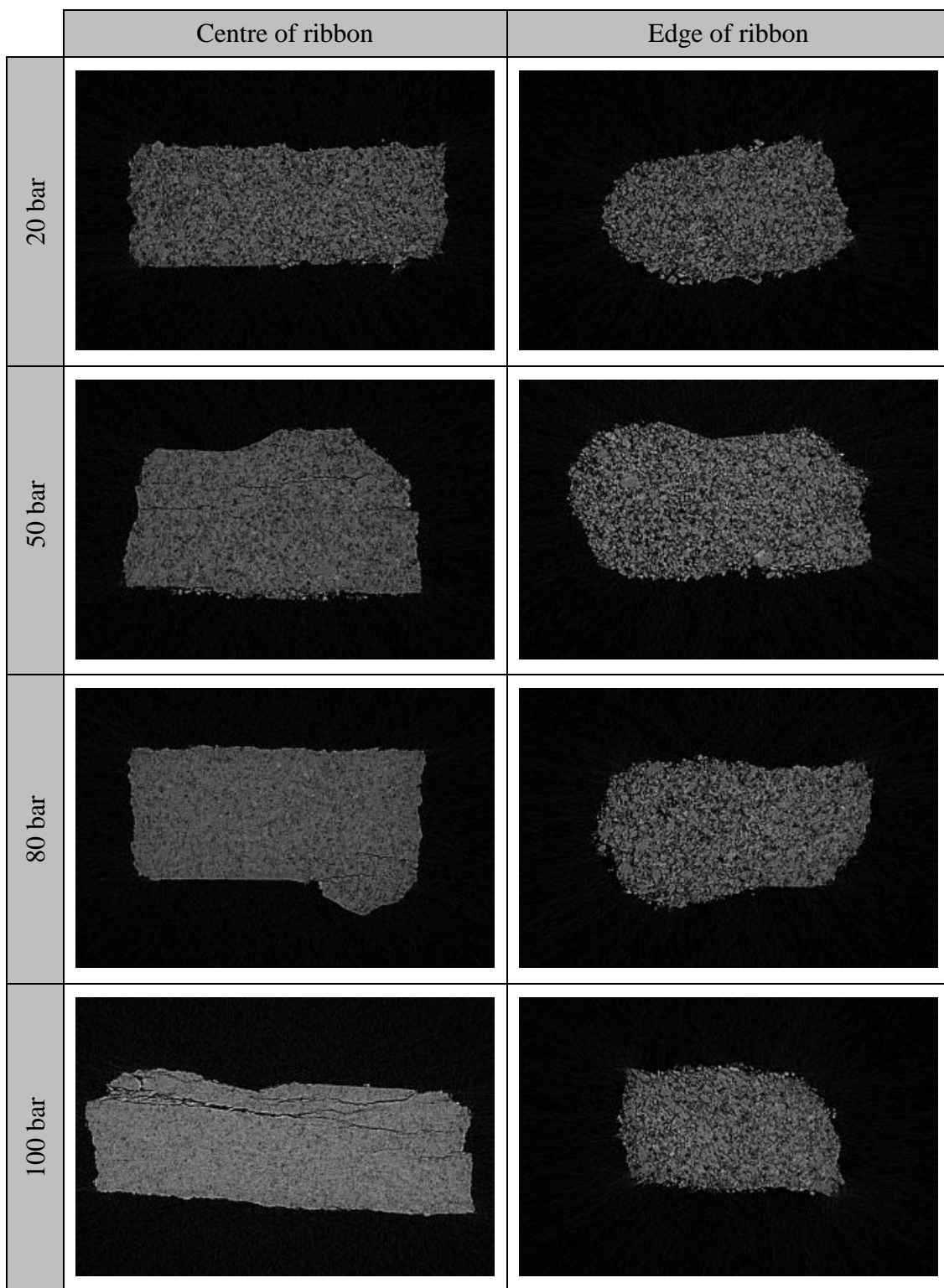


Figure 8.22: X-ray images for ribbon produced from lactose 200M using the flat rollers.

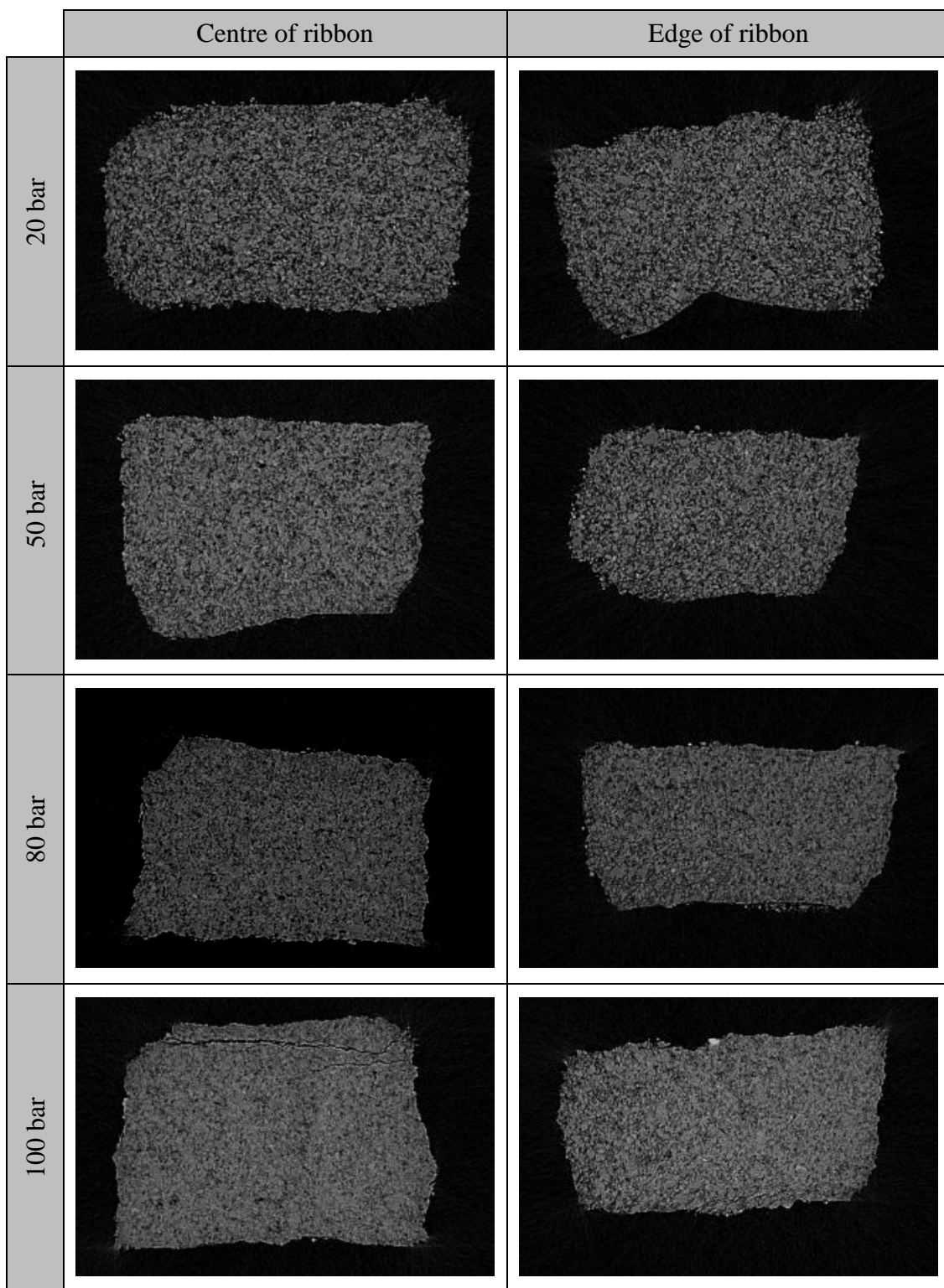


Figure 8.23: X-ray images for ribbon produced from lactose 200M using the curved roller.

The porosity of the ribbon was determined by analysing the X-ray images using Image J software as described in Section 3.2.11. Figure 8.24 shows the porosity at the edge and the centre of the ribbon produced from lactose 200M at different hydraulic pressure using the flat roller (A) and the curved roller (B), (for lactose 21AN and SD, the result are presented in Appendix B). For both rollers, the porosity decreased with increasing the hydraulic pressure during compaction. It can be seen that ribbons produced from the flat roller showed a significant variation in porosity between the centre and the edge. The porosity at the centre of the ribbon was lower than that at the edges. However, the porosity of ribbon produced using the new curved roller was almost uniform along the ribbon width as shown in Figure 8.24 (B). The difference in the porosity profile between the flat and the curved roller is due to the different stress applied across the width of the rollers during the compaction. The stress applied during the compaction using the flat roller was higher at the centre and low at the edges (see Figure 8.12 (A)). This resulted in ribbon with low porosity at the centre and higher at the edges.

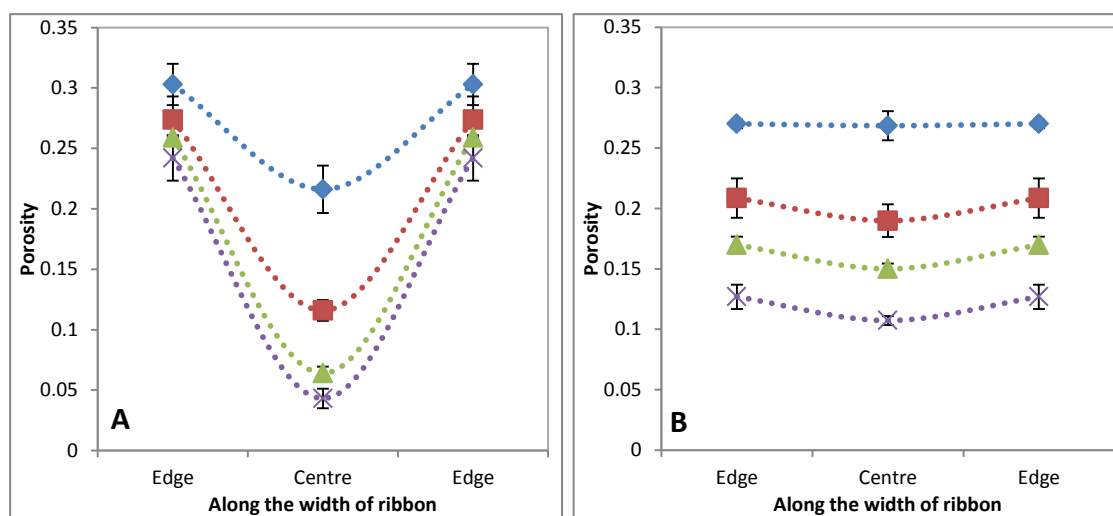


Figure 8.24: Porosity across the width of ribbon of 200M using the flat roller (A) and the curved roller (B) (◆ 20 bar, ■ 50 bar, ▲ 80 bar, × 100 bar).

The uniform porosity along the width of ribbon produced from the curved roller Figure 8.24 (B) is due to the uniform stress which is applied by the roller during compaction (see Figure 8.12 (B)). Figure 8.25 shows a comparison between the porosity profile of ribbon produced from the flat and the curved roller at each hydraulic pressure. It is very clear that the curved roller produced ribbon with more uniform porosity across the width than that produced from the flat roller. This was due to the curvature design of the new roller which resulted in applying a uniform stress across the roller width. This

was then the reason for producing ribbon with similar porosity at the centre and the edges.

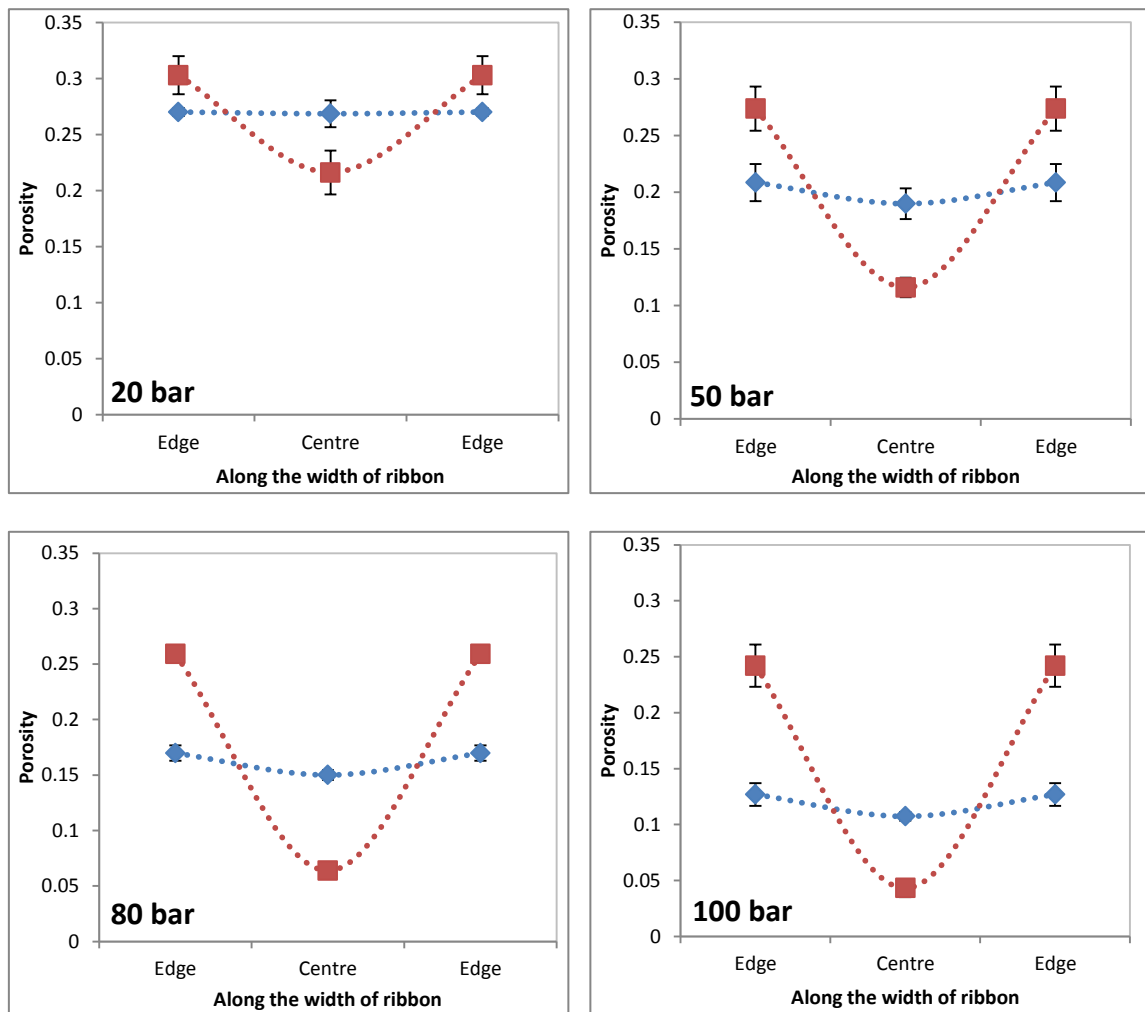


Figure 8.25: Porosity across the width of ribbon produced from 200M using the curved roller ◆, and the flat roller ■.

8.10 Conclusion

In this Chapter, the powder compaction behaviour across the width of the roller was investigated. The compaction of powder was not uniform across the width of the standard flat roller. This was initially observed from the non-uniformity of ribbon temperature across the width which was obtained from the online thermal imaging during the production of ribbon. The non-uniformity of ribbon temperature was found to be due to the non-uniform stress which is applied by the standard flat roller along the width. The stress applied at the centre of the flat roller was higher than that at the edges.

The higher stress at the centre of the roller resulted in higher temperature and the low stress at the edges resulted in low temperature. The non-uniform stress applied along the width of the standard roller affected the local porosity and strength of the ribbon along the width. Ribbon produced from the standard roller was found to be strong with low porosity at the centre, whereas, the edges of the ribbon were weaker and more porous than the centre.

To overcome the non-uniformity of the stress along the roller width and to produce ribbon with homogenous properties across the width, a new roller with a novel surface geometry was designed at the University of Sheffield [137]. The surface of the new roller has a curvature design which aims to apply a uniform stress during the powder compaction. It was found that the new curved roller improved the powder compaction across the roller width. The temperature of the ribbon during the production was more uniform across the ribbon width in comparison to the standard flat roller. This was due to the uniform stress which is applied across the width of the curved roller as shown by the pressure films. This means that the temperature of the ribbon is an indication of the stress applied during compaction, and the thermal camera can be used as a successful tool to monitor the stress applied on the powder in real time. The uniform stress applied by the new curved roller along the width resulted in a significant reduction in the amount of fines in the product and also increased the ribbon width. In addition, the porosity and the local strength of ribbon produced using the new curved roller were uniform across the width.

Overall, the use of the new curved roller resulted in a significant improvement in the compaction behaviour across the roller width and also resulted in homogenous properties along the width of the ribbon.

CHAPTER 9 CONCLUSION AND FUTURE WORK

9.1 Conclusion

In this research, the behaviour of different types of lactose during the roller compaction was investigated in a comprehensive perspective. The work focused on the effect of the morphology of the primary particle and the powder amorphous content on the quality of ribbon produced in the roller compactor. Three types of lactose were used in this study; anhydrous lactose SuperTab21AN (0.2% amorphous) and spray dried lactose SuperTab11SD (10.32% amorphous) which are agglomerated types of lactose and α -lactose monohydrate 200M (2.67% amorphous) is a non-agglomerated type of lactose.

The morphology and amorphous content of lactose powder were found to have a significant effect on the strength of a single particle, the behaviour of powders during roller compaction and the ribbon properties. It was found that the strength of a single particle of the non-agglomerated type of lactose (200M) is higher than that of the agglomerated types (21AN and SD). This was due to the morphology of the particle of 200M lactose as a single crystal which required a higher force to break than particles of 21AN and SD. During the roller compaction, it was found that the agglomerated type of lactose (21AN and SD) showed better binding capacity compare to the non-agglomerated type (200M). This was shown by the tensile strength, fragment size, ribbon temperature, ribbon porosity and the amount of fines in the product. The difference in the properties of ribbon of the three types was due to the different morphology and amorphous content. It was found that there is a relationship between the strength of the primary particle and the final ribbon tensile strength. The stronger the primary particle of the initial powder the weaker the ribbon after the roller compaction. There was also a relationship between the surface temperature of the ribbon during production and the tensile strength of the ribbon. It was concluded that, regardless the type of lactose, the higher the temperature of the ribbon during production the higher the tensile strength of the ribbon. This means that the temperature of the ribbon which is measured during production can be used to predict the tensile strength of the produced ribbon.

The effect of storage of powder at different relative humidity conditions on both the roller compaction behaviour and ribbon properties was also investigated. The three types of lactose were conditioned at different relative humidity conditions ranging from (10% to 80% RH). It was found that the relative humidity of the storage has a significant effect on both the roller compaction behaviour and the product quality. The percentage of fines in the product decreased with increasing the relative humidity of the powder from 10% to 40%, and increased again with a further increase in the relative humidity to (80%). The flowability of the powder at different RH values affected the powder velocity during the roller compaction as shown by the PIV experiments. In the compaction zone, the velocity of powders conditioned at 80% RH was lower than that conditioned at 20% RH. This resulted in lesser powder being present at the edges of the rollers for powder conditioned at 80% RH, which resulted in ribbons with a smaller width and increased the percentage of fines in the product. The relative humidity of the storage was found to have minimal effect on the ribbon tensile strength at low RH conditions (10% - 20%). However, at 80% RH, lactose 21AN produced ribbon with the highest tensile strength, whereas lactose 200M and SD produced ribbon with the lowest tensile strength. This was believed to be due to the crystallisation of the amorphous fraction within lactose 200M and SD, which reduced the powder compressibility and deformability. It was concluded that the optimum processing conditions for all three types of lactose are in the range of 20% - 40% RH.

The online thermal imaging was found to be a useful technique to describe and explain the difference in ribbon properties at various process parameters in the roller compactor. The process parameter of the roller compactor was found to have an effect on the ribbon properties. For all powder, the increase in the roller speed had minimal effect on the ribbon strength and porosity. This is useful information which suggests that the production rate can be increased, by increasing the roller speed, without having an influence on the ribbon strength and porosity of lactose powders. The roller gap and the feeder screw speed were found to have the same effect on the ribbon properties. Increasing the gap increases the feeder screw speed in order to deliver more powder. This will increase the internal friction between the particles and results in increasing the temperature of the ribbon during production. The fines percentage decreased and ribbon width increased with increasing the roller gap. The increase in the gap had a different effect on the tensile strength and porosity of ribbon of the three types of lactose. Lactose

SD showed different behaviour at higher gap compare to the other types of lactose. This was due to the high amorphous content in the powder which influenced by the temperature and resulted in different trend.

During the online thermal imaging of ribbon during production, it was found that the temperature is not uniform across the width of the ribbons. The temperature at the centre of the ribbons was higher in comparison to the edges. This indicates that the powder at the edges has been compressed less compared to the centre of the ribbons. The variation in the stress during powder compaction resulted in a non-uniform porosity along the width of the ribbon; low porosity at the centre and higher at the edges.

An improvement in the powder compaction across the roller width and a homogenous property along the width of the ribbon were obtained using a new roller with a novel curved design. The curved roller successfully applied more uniform stress on the powder along the width of the roller during compaction. This resulted in more uniform temperature distribution across the width of the ribbon during production. It was concluded that the online thermal camera can be used as a successful tool to monitor the stress applied on the powder in real time. Moreover, the new curved roller resulted in a significant reduction in the percentage of fines in the product as well as a uniform strength and porosity along the ribbon width.

9.2 Future work

1. The work in this thesis investigated the effect of particle morphology and powder amorphous content of different types of lactose on ribbon properties. It is also of interest to investigate the effect of powder amorphous content with particles of the same morphology. This could be achieved by using spray drying process, for instance, to produce lactose powder with similar morphology and varying amorphous content and then use it in the roller compaction to produced ribbon.

2. The main aim of roller compaction is to convert powders with poor flow property to free flowing granules, which are then used in different applications. Tableting is one of the most important applications used in various industries. The study in this work concerned with the effect of morphology, amorphous content and process parameters on the quality and properties of ribbon. In roller compaction, ribbons are the intermediate

product which is usually need to be milled to granules and finally compressed into tablets. The knowledge created from the current study can be employed to investigate the properties of granules and tablet after crushing the ribbon and link this to the morphology and amorphous content of lactose powder as well as the process parameters.

3. The velocity of particles of different types of lactose during the roller compaction was successfully measured using the PIV technique. Further information can be extracted from images of particles in movements during the process such as the velocity profile along the gap between the two rollers and in the rolling direction. Such information will give more understanding about the compression behaviour of different types of powders, for example, determining the nip angle optically.

4. Present work has been conducted on using a thermal camera to record the temperature of ribbons just outside the rollers. To gain more information about the compaction zone, it is important to know the temperature between the two rollers where the powder is compacted. This can be achieved by using a special cheek plate which is transparent to the infrared frequencies. Materials such as Calcium Fluoride (CaF_2) and Germanium (Ge) are usually used in lens systems for the thermal imaging due to their ability to pass infrared frequencies. Using a cheek plate made from such materials helps to record the temperature of powder/ ribbon before and at the compaction stage. However, extra care needs to be taken while using a glass material as a cheek plate on moving rollers under high pressure.

5. The novel design of the roller surface successfully improved the stress distribution across the roller width and resulted in uniform properties along the width of ribbon of different types of lactose. It is also of interest to use rollers of different surface curvature for a wide range of materials. This will help to better understand the relationship between the ribbon properties with both the properties of the starting material and the roller surface geometry, and link them in a mathematical model.

REFERENCES

1. Miller, R.W., *Roller compaction Technology*, in *Handbook of Pharmaceutical Granulation Technology*, D.M. Parikh, Editor. 1997, Marcel Dekker, New York, pp. 99-150.
2. Miller, R.W., *Roller compaction Technology*, in *Handbook of Pharmaceutical Granulation Technology*, D.M. Parikh, Editor. 2010, Informa Healthcare, New York USA. pp. 163-182.
3. Dhenge, R.M., et al., *Twin screw wet granulation: Granule properties*. Chemical Engineering Journal, 2010. **164**(2-3): p. 322-329.
4. Osborne, J.D., et al., *Binder addition methods and binder distribution in high shear and fluidised bed granulation*. Chemical Engineering Research and Design, 2011. **89**(5): p. 553-559.
5. Kleinebudde, P., *Roll compaction/dry granulation: pharmaceutical applications*. European Journal of Pharmaceutics and Biopharmaceutics, 2004. **58**(2): p. 317-326.
6. Guigon, P., et al., *Chapter 5 Roll pressing*, in *Handbook of Powder Technology*. 2007, Elsevier Science B.V. p. 255-288.
7. Johanson, J.R., *A Rolling Theory for Granular Solids*. Journal of Applied Mechanics, 1965. **32**(4): p. 842-848.
8. Inghelbrecht, S., et al., *Instrumentation of a roll compactor and the evaluation of the parameter settings by neural networks*. International Journal of Pharmaceutics, 1997. **148**(1): p. 103-115.
9. Carlson, G.T. and B.C. Hancock, *A Comparison of Physical and Mechanical Properties of Common Tableting Diluents*, in *Excipient Development for Pharmaceutical, Biotechnology, and Drug Delivery Systems*, A. Katdare and M.V. Chaubal, Editors. 2006, Informa Healthcare New York USA, Inc. p. 127-153.
10. Sheskey, P.J., et al., *Use of roller compaction in the preparation of controlled-release hydrophilic matrix tablets containing methylcellulose and hydroxypropyl methylcellulose polymers*. Pharmaceutical Technology, 1994. **18**(9): p. 132-150.
11. Cunningham, J.C., et al., *Understanding variation in roller compaction through finite element-based process modeling*. Computers & Chemical Engineering, 2010. **34**(7): p. 1058-1071.
12. Michrafy, A., et al., *Experimental and numerical analyses of homogeneity over strip width in roll compaction*. Powder Technology, 2011. **206**(1-2): p. 154-160.
13. Fuhrer, C., *Interparticulate Attraction Mechanisms*, in *Pharmaceutical Powder Compaction Technology*, G. Alderborn and C. Nyström, Editors. 1996, Marcel Dekker, New York. p. 1-15.
14. Buckton, G., *Intermolecular bonding forces: where materials and process come together*, in *Pharmaceutical powder compaction technology*, M. Celik, Editor. 2011, Informa Healthcare, London. p. 1-8.
15. Nyström, C. and P.-G. Karehill, *The Importance of Intermolecular Bonding Forces and the Concept of Bonding Surface Area*, in *Pharmaceutical Powder Compaction Technology*, G. Alderborn and C. Nyström, Editors. 1996, Marcel Dekker, New York. p. 17-53.

16. Pietsch, W., *Roll pressing*. 1976: Heyden & Son Ltd, London.
17. Rumpf, H., *The strength of granules and agglomerates*, in *Agglomeration*, W.A. Knepper, Editor. 1962, Interscience, New York. p. 379-414.
18. Palzer, S., *The relation between material properties and supra-molecular structure of water-soluble food solids*. Trends in Food Science & Technology, 2010. **21**(1): p. 12-25.
19. Palzer, S., *Chapter 13 Agglomeration of dehydrated consumer foods*, in *Handbook of Powder Technology*, A.D. Salman, M.J. Hounslow, and J.P.K. Seville, Editors. 2007, Elsevier Science B.V. p. 591-671.
20. Bronlund, J. and T. Paterson, *Moisture sorption isotherms for crystalline, amorphous and predominantly crystalline lactose powders*. International Dairy Journal, 2004. **14**(3): p. 247-254.
21. Vromans, H., et al., *Studies on tableting properties of lactose. VII. The effect of variations in primary particle size and percentage of amorphous lactose in spray dried lactose products*. International Journal of Pharmaceutics, 1987. **35**(1-2): p. 29-37.
22. Vollenbroek, J., et al., *Determination of low levels of amorphous content in inhalation grade lactose by moisture sorption isotherms*. International Journal of Pharmaceutics, 2010. **395**(1-2): p. 62-70.
23. Willart, J.F., et al., *Athermal character of the solid state amorphization of lactose induced by ball milling*. Solid State Communications, 2004. **132**(10): p. 693-696.
24. Buckton, G. and P. Darcy, *The use of gravimetric studies to assess the degree of crystallinity of predominantly crystalline powders*. International Journal of Pharmaceutics, 1995. **123**(2): p. 265-271.
25. Gombás, Á., et al., *Quantitative determination of crystallinity of alpha-lactose monohydrate by Near Infrared Spectroscopy (NIRS)*. International Journal of Pharmaceutics, 2003. **256**(1-2): p. 25-32.
26. Gombás, Á., et al., *Quantitative Determination of Crystallinity of α -Lactose Monohydrate by DSC*. Journal of Thermal Analysis and Calorimetry, 2002. **68**(2): p. 503-510.
27. Hogan, S. and G. Buckton, *The Application of Near Infrared Spectroscopy and Dynamic Vapor Sorption to Quantify Low Amorphous Contents of Crystalline Lactose*. Pharmaceutical Research, 2001. **18**(1): p. 112-116.
28. Murphy, B.M., et al., *Measurement of lactose crystallinity using Raman spectroscopy*. Journal of Pharmaceutical and Biomedical Analysis, 2005. **38**(1): p. 186-190.
29. Saunders, M., et al., *The potential of high speed DSC (Hyper-DSC) for the detection and quantification of small amounts of amorphous content in predominantly crystalline samples*. International Journal of Pharmaceutics, 2004. **274**(1-2): p. 35-40.
30. Lehto, V.-P., et al., *The comparison of seven different methods to quantify the amorphous content of spray dried lactose*. Powder Technology, 2006. **167**(2): p. 85-93.
31. Sebhatu, T. and G. Alderborn, *Relationships between the effective interparticulate contact area and the tensile strength of tablets of amorphous and crystalline lactose of varying particle size*. European Journal of Pharmaceutical Sciences, 1999. **8**(4): p. 235-242.
32. Cal, S., et al., *Comparison of a spray-dried α -lactose monohydrate with a fully hydrated roller-dried β -lactose*. International Journal of Pharmaceutics, 1996. **136**(1-2): p. 13-21.

33. Vromans, H., et al., *Studies on tableting properties of lactose: Part 2. Consolidation and compaction of different types of crystalline lactose*. Pharmaceutisch Weekblad, 1985. **7**(5): p. 186-193.
34. Sebhatu, T., et al., *The effect of moisture content on the compression and bond-formation properties of amorphous lactose particles*. International Journal of Pharmaceutics, 1997. **146**(1): p. 101-114.
35. Ziffels, S. and H. Steckel, *Influence of amorphous content on compaction behaviour of anhydrous alpha-lactose*. International Journal of Pharmaceutics, 2010. **387**(1-2): p. 71-8.
36. Nyström, C., et al., *Studies on direct compression of tablets II. The influence of the particle size of a dry binder on the mechanical strength of tablets*. International Journal of Pharmaceutics, 1982. **10**(3): p. 209-218.
37. Adolfsson, Å. and C. Nyström, *Tablet strength, porosity, elasticity and solid state structure of tablets compressed at high loads*. International Journal of Pharmaceutics, 1996. **132**(1-2): p. 95-106.
38. Busignies, V., et al., *Compaction of crystallographic forms of pharmaceutical granular lactoses. II. Compacts mechanical properties*. European Journal of Pharmaceutics and Biopharmaceutics, 2004. **58**(3): p. 577-586.
39. Gupta, A., et al., *Influence of ambient moisture on the compaction behavior of microcrystalline cellulose powder undergoing uni-axial compression and roller-compaction: A comparative study using near-infrared spectroscopy*. Journal of Pharmaceutical Sciences, 2005. **94**(10): p. 2301-2313.
40. Gupta, A., et al., *Effect of the variation in the ambient moisture on the compaction behavior of powder undergoing roller-compaction and on the characteristics of tablets produced from the post-milled granules*. Journal of Pharmaceutical Sciences, 2005. **94**(10): p. 2314-2326.
41. Chikosha, S., et al., *Effect of particle morphology and size on roll compaction of Ti-based powders*. Powder Technology, 2014. **264**(0): p. 310-319.
42. Bacher, C., et al., *Improving the compaction properties of roller compacted calcium carbonate*. International Journal of Pharmaceutics, 2007. **342**(1-2): p. 115-123.
43. Freitag, F. and P. Kleinebudde, *How do roll compaction/dry granulation affect the tableting behaviour of inorganic materials? Comparison of four magnesium carbonates*. European Journal of Pharmaceutical Sciences, 2003. **19**(4): p. 281-289.
44. Inghelbrecht, S. and J.P. Remon, *The roller compaction of different types of lactose*. International Journal of Pharmaceutics, 1998. **166**(2): p. 135-144.
45. Airaksinen, S., et al., *Role of Water in the Physical Stability of Solid Dosage Formulations*. Journal of Pharmaceutical Sciences, 2005. **94**(10): p. 2147-2165.
46. Sandler, N., et al., *Effect of Moisture on Powder Flow Properties of Theophylline*. Pharmaceutics, 2010. **2**(3).
47. Nokhodchi, A., *Effect of moisture on compaction and compression*. Pharmaceutical Technology, 2005. **6**: p. 46-66.
48. Gerhardt, A.H., *Moisture effects on solid dosage forms--formulation, processing, and stability*. Journal of GXP Compliance, 2009. **13**(1): p. 58-67.
49. Figura, L.O. and A.A. Teixeira, *Water Activity, in Food Physics: Physical Properties - Measurement and Applications*. 2007, Springer: Berlin, Heidelberg. p. 1-39.

50. Reh, C., et al., *Determination of water content in powdered milk*. Food Chemistry, 2004. **86**(3): p. 457-464.
51. Osborne, J.D., et al., *Investigating the influence of moisture content and pressure on the bonding mechanisms during roller compaction of an amorphous material*. Chemical Engineering Science, 2013. **86**(0): p. 61-69.
52. Eaves, T. and T.M. Jones, *Effect of Moisture on Tensile Strength of Bulk Solids I: Sodium Chloride and Effect of Particle Size*. Journal of Pharmaceutical Sciences, 1972. **61**(2): p. 256-261.
53. Ollet, A.L., et al., *A comparative study of the effects of water content on the compaction behaviour of some food materials*. Powder Technology, 1993. **75**(1): p. 59-65.
54. Mollan, M.J. and M. Celik, *The effects of humidity and storage time on the behavior of maltodextrins for direct compression*. International Journal of Pharmaceutics, 1995. **114**(1): p. 23-32.
55. Gupta, A., et al., *Real-time near-infrared monitoring of content uniformity, moisture content, compact density, tensile strength, and young's modulus of roller compacted powder blends*. Journal of Pharmaceutical Sciences, 2005. **94**(7): p. 1589-1597.
56. Wu, C.Y., et al., *Roller compaction of moist pharmaceutical powders*. International Journal of Pharmaceutics, 2010. **391**(1-2): p. 90-97.
57. Sun, C.C., *Mechanism of moisture induced variations in true density and compaction properties of microcrystalline cellulose*. International Journal of Pharmaceutics, 2008. **346**(1-2): p. 93-101.
58. Inghelbrecht, S. and J.P. Remon, *Reducing dust and improving granule and tablet quality in the roller compaction process*. International Journal of Pharmaceutics, 1998. **171**(2): p. 195-206.
59. Osborne, J., *Bonding Mechanisms Involved in the Roller Compaction of an Amorphous Food Material, Thesis*, in Department of Chemical and Biological Engineering, The University of Sheffield, 2013.
60. Inghelbrecht, S. and J.P. Remon, *Roller compaction and tableting of microcrystalline cellulose/drug mixtures*. International Journal of Pharmaceutics, 1998. **161**(2): p. 215-224.
61. Gupta, A., et al., *Nondestructive measurements of the compact strength and the particle-size distribution after milling of roller compacted powders by near-infrared spectroscopy*. Journal of Pharmaceutical Sciences, 2004. **93**(4): p. 1047-1053.
62. Mansa, R.F., et al., *Using intelligent software to predict the effects of formulation and processing parameters on roller compaction*. Powder Technology, 2008. **181**(2): p. 217-225.
63. Miguélez-Morán, A.M., et al., *The effect of lubrication on density distributions of roller compacted ribbons*. International Journal of Pharmaceutics, 2008. **362**(1-2): p. 52-59.
64. Yu, S., et al., *A comparative study of roll compaction of free-flowing and cohesive pharmaceutical powders*. International Journal of Pharmaceutics, 2012. **428**(1-2): p. 39-47.
65. Bindhumadhavan, G., et al., *Roll compaction of a pharmaceutical excipient: Experimental validation of rolling theory for granular solids*. Chemical Engineering Science, 2005. **60**(14): p. 3891-3897.
66. Yu, S., *Roll compaction of pharmaceutical excipients, Thesis*, in School of Chemical Engineering, The University of Birmingham, 2012.

67. Miguélez-Morán, A.M., et al., *Characterisation of density distributions in roller-compacted ribbons using micro-indentation and X-ray micro-computed tomography*. *European Journal of Pharmaceutics and Biopharmaceutics*, 2009. **72**(1): p. 173-182.
68. Souihi, N., et al., *A quality by design approach to investigate the effect of mannitol and dicalcium phosphate qualities on roll compaction*. *International Journal of Pharmaceutics*, 2013. **447**(1-2): p. 47-61.
69. Dumarey, M., et al., *Combining experimental design and orthogonal projections to latent structures to study the influence of microcrystalline cellulose properties on roll compaction*. *International Journal of Pharmaceutics*, 2011. **416**(1): p. 110-119.
70. Shlieout, G., et al., *Dry granulation with a roller compactor Part I: The functional units and operation modes*. *Pharmaceutical Technology Europe*, 2000. **12**(11): p. 24-35.
71. Samanta, A.K., et al., *Cone milling of compacted flakes: Process parameter selection by adopting the minimal fines approach*. *International Journal of Pharmaceutics*, 2012. **422**(1-2): p. 17-23.
72. Samanta, A.K., et al., *Energy-based analysis of cone milling process for the comminution of roller compacted flakes*. *International Journal of Pharmaceutics*, 2014. **462**(1-2): p. 108-114.
73. Bultmann, J.M., *Multiple compaction of microcrystalline cellulose in a roller compactor*. *European Journal of Pharmaceutics and Biopharmaceutics*, 2002. **54**(1): p. 59-64.
74. Wagner, C.M., et al., *Roll compaction of mannitol: Compactability study of crystalline and spray-dried grades*. *International Journal of Pharmaceutics*, 2013. **453**(2): p. 416-422.
75. Muliadi, A.R., et al., *Validation of 3-D finite element analysis for predicting the density distribution of roll compacted pharmaceutical powder*. *Powder Technology*, 2013. **237**(0): p. 386-399.
76. Mazor, A., et al., *Effect of roll compactor sealing system designs: A finite element analysis*. *Powder Technology*, 2016. **289**: p. 21-30.
77. Akseli, I., et al., *A Quantitative Correlation of the Effect of Density Distributions in Roller-Compacted Ribbons on the Mechanical Properties of Tablets Using Ultrasonics and X-ray Tomography*. *AAPS PharmSciTech*, 2011. **12**(3): p. 834-853.
78. Guigon, P. and O. Simon, *Roll press design—influence of force feed systems on compaction*. *Powder Technology*, 2003. **130**(1-3): p. 41-48.
79. Simon, O. and P. Guigon, *Correlation between powder-packing properties and roll press compact heterogeneity*. *Powder Technology*, 2003. **130**(1-3): p. 257-264.
80. Nesarikar, V.V., et al., *Instrumented roll technology for the design space development of roller compaction process*. *International Journal of Pharmaceutics*, 2012. **426**(1-2): p. 116-131.
81. Souihi, N., et al., *Roll compaction process modeling: Transfer between equipment and impact of process parameters*. *International Journal of Pharmaceutics*, 2015. **484**(1-2): p. 192-206.
82. Funakoshi, Y., et al., *The use of a Novel Roller Compactor with a Concavo-Convex Roller pair to Obtain Uniform Compacting Pressure*. *Drug Development and Industrial Pharmacy*, 1977. **3**(6): p. 555-573.
83. Jenike, A.W. and R. Shield, *On the plastic flow of Coulomb solids beyond original failure*. *Journal of Applied Mechanics*, 1959. **26**(81): p. 599-602.

84. Reynolds, G., et al., *Practical application of roller compaction process modeling*. Computers & Chemical Engineering, 2010. **34**(7): p. 1049-1057.
85. Yusof, Y.A., et al., *Roll compaction of maize powder*. Chemical Engineering Science, 2005. **60**(14): p. 3919-3931.
86. Muliadi, A.R., et al., *Modeling the powder roll compaction process: Comparison of 2-D finite element method and the rolling theory for granular solids (Johanson's model)*. Powder Technology, 2012. **221**(0): p. 90-100.
87. Katashinskii, V.P., *Analytical determination of specific pressure during the rolling of metal powders*. Soviet Powder Metallurgy and Metal Ceramics, 1966. **5**(10): p. 765-772.
88. Katashinskii, V. and M. Shtern, *Stressed-strained state of powder being rolled in the densification zone. I. Mathematical model of rolling in the densification zone*. Powder Metallurgy and Metal Ceramics, 1983. **22**(11): p. 882-885.
89. Dec, R.T., et al., *Comparison of various modeling methods for analysis of powder compaction in roller press*. Powder Technology, 2003. **130**(1-3): p. 265-271.
90. Peter, S., et al., *Roller compaction/Dry granulation: Use of the thin layer model for predicting densities and forces during roller compaction*. Powder Technology, 2010. **199**(2): p. 165-175.
91. Michrafy, A., et al., *Analysis of strain stress state in roller compaction process*. Powder Technology, 2011. **208**(2): p. 417-422.
92. DFEpharma. *Lactose: Some basic properties and characteristics*. 2013; Available from: <http://www.dfepharma.com/en/search-results.aspx?search=Some+basic+properties+and+characteristics>.
93. Kamat, M., et al., *Near-Infrared Spectroscopic Determination of Residual Moisture in Lyophilized Sucrose Through Intact Glass Vials*. Pharmaceutical Research, 1989. **6**(11): p. 961-965.
94. PANalytical. *Crystallinity determination - Quantification of low amounts of amorphous material in a crystalline matrix and vice versa*. 2013; Available from: <http://www.panalytical.com/Application-notes/Crystallinity-determination-Quantification-of-low-amounts-of-amorphous-material-in-a-crystalline-matrix-and-vice-versa.htm>.
95. *United States Pharmacopeia and National Formulary, (USP28-NF23)*, in *NF Monograph*. p. 3024.
96. Prescott, J.K. and R.A. Barnum, *On powder flowability*. Pharmaceutical Technology, 2000. **24**(10): p. 60-85.
97. Schulze, D., *Powders and bulk solids: behavior, characterization, storage and flow*. 2008: Springer, Verlag Berlin Heidelberg.
98. Jenike, A.W., *Storage and flow of solids, bulletin no. 123*. Bulletin of the University of Utah, 1964. **53**(26).
99. Schulze, D., *Powders and Bulk Solids: Behavior, Characterization, Storage and Flow*. 2010: Springer, Berlin Heidelberg.
100. Carr, R.L., *Evaluating flow properties of solids*. Chemical Engineering, 1965. **72**: p. 163-168.
101. Geldart, D., et al., *Characterization of powder flowability using measurement of angle of repose*. China Particuology, 2006. **4**(3-4): p. 104-107.

102. Ganesan, V., et al., *Flowability and handling characteristics of bulk solids and powders – a review with implications for DDGS*. Biosystems Engineering, 2008. **101**(4): p. 425-435.
103. Haririan I, et al., *Determination of mechanical strength of different material double-layer rectangular tablets*. DARU Journal of Pharmaceutical Sciences, 2000: p. 22.27.
104. Omar, C.S., et al., *Roller compaction: Effect of morphology and amorphous content of lactose powder on product quality*. International Journal of Pharmaceutics, 2015. **496**(1): p. 63-74.
105. BS-2782-10, *Method 1005: Determination of flexural properties - Three point method, in British Standard Methods of Testing*. 1977.
106. ASTM-D790-10, *Standard Test Methods for Flexural Properties of Unreinforced and Reinforced Plastics and Electrical Insulating Materials*, in ASTM International. 2010, West Conshohocken: PA.
107. Farber, L., et al., *Unified compaction curve model for tensile strength of tablets made by roller compaction and direct compression*. International Journal of Pharmaceutics, 2008. **346**(1–2): p. 17-24.
108. Miguélez-Morán, A.-M., *Roller compaction of pharmaceutical ingredients, Thesis*, in Ruperto-Carola University of Heidelberg, Germany, 2009.
109. Farrenkopf, J., *Relevant Aspects of Roller Compaction Covering the Impact of Excipients, Milling Devices, Fines and Feasibility Prediction, Thesis*, in Ruperto-Carola University of Heidelberg, Germany, 2009.
110. Nørgaard, L., et al., *Multivariate near-infrared and Raman spectroscopic quantifications of the crystallinity of lactose in whey permeate powder*. International Dairy Journal, 2005. **15**(12): p. 1261-1270.
111. Savolainen, M., et al., *Determination of amorphous content in the pharmaceutical process environment*. Journal of Pharmacy and Pharmacology, 2007. **59**(2): p. 161-170.
112. FLIR. *Thermal imaging guidebook for industrial applications*. 2013; Available from: <http://www.flircameras.co.uk/pdf/thermal-imaging-handbook.pdf>.
113. Grant, D.J., *Theory and origin of polymorphism*. Drugs and the Pharmaceutical Sciences, 1999. **95**: p. 1-33.
114. Boer, A.H., et al., *Studies on tableting properties of lactose: Part III. The consolidation behaviour of sieve fractions of crystalline α -lactose monohydrate*. Pharmaceutisch Weekblad, 1986. **8**(2): p. 145-150.
115. Hartmann, M. and S. Palzer, *Caking of amorphous powders — Material aspects, modelling and applications*. Powder Technology, 2011. **206**(1–2): p. 112-121.
116. Buckton, G. and P. Darcy, *Water mobility in amorphous lactose below and close to the glass transition temperature*. International Journal of Pharmaceutics, 1996. **136**(1–2): p. 141-146.
117. Briggner, L.-E., et al., *The use of isothermal microcalorimetry in the study of changes in crystallinity induced during the processing of powders*. International Journal of Pharmaceutics, 1994. **105**(2): p. 125-135.
118. Sebhatu, T., et al., *Assessment of the degree of disorder in crystalline solids by isothermal microcalorimetry*. International Journal of Pharmaceutics, 1994. **104**(2): p. 135-144.
119. Nokhodchi, A., et al., *The effect of moisture on the properties of ibuprofen tablets*. International Journal of Pharmaceutics, 1995. **118**(2): p. 191-197.

120. Omar, C.S., et al., *Roller compaction: Effect of relative humidity of lactose powder*. European Journal of Pharmaceutics and Biopharmaceutics 2016. **106**: p. 26-37.
121. Krok, A., et al., *Using the DPIV optical technique to measure the velocity of powder material in the space between the rollers in a roll compactor*. Powder Technology, 2014. **262**(0): p. 131-141.
122. Huang, H., et al., *On errors of digital particle image velocimetry*. Measurement Science and Technology, 1997. **8**(12): p. 1427.
123. Thielicke, W. and E.J. Stamhuis, *PIVlab—Towards user-friendly, affordable and accurate digital particle image velocimetry in MATLAB*. Journal of Open Research Software, 2014. **2**(1): p. e30.
124. Dhenge, R.M., et al., *Twin screw granulation using conveying screws: Effects of viscosity of granulation liquids and flow of powders*. Powder Technology, 2013. **238**(0): p. 77-90.
125. Raffel, M., et al., *Particle image velocimetry: a practical guide*. 2007: Springer,Verlag Berlin Heidelberg.
126. Listiohadi, Y., et al., *Moisture sorption, compressibility and caking of lactose polymorphs*. International Journal of Pharmaceutics, 2008. **359**(1–2): p. 123-134.
127. Thomson, F.M., *Storage and flow of particulate solids*, in *Handbook of Powder Science & Technology*, M.E. Fayed and L. Otten, Editors. 1997, Springer Science+Business Media Dordrecht p. 389-486.
128. Geldart, D., et al., *Characterisation of dry powders*. Powder Technology, 2009. **190**(1–2): p. 70-74.
129. Dawoodbhai, S. and C.T. Rhodes, *The Effect of Moisture on Powder Flow and on Compaction and Physical Stability of Tablets*. Drug Development and Industrial Pharmacy, 1989. **15**(10): p. 1577-1600.
130. Moreyra, R. and M. Peleg, *Effect of Equilibrium Water Activity on the Bulk Properties of Selected Food Powders*. Journal of Food Science, 1981. **46**(6): p. 1918-1922.
131. Sun, C.C., *Quantifying effects of moisture content on flow properties of microcrystalline cellulose using a ring shear tester*. Powder Technology, 2016. **289**: p. 104-108.
132. Faqih, A.M.N., et al., *Effect of moisture and magnesium stearate concentration on flow properties of cohesive granular materials*. International Journal of Pharmaceutics, 2007. **336**(2): p. 338-345.
133. Fitzpatrick, J.J., et al., *Flow property measurement of food powders and sensitivity of Jenike's hopper design methodology to the measured values*. Journal of Food Engineering, 2004. **61**(3): p. 399-405.
134. Garr, J.S.M. and M.H. Rubinstein, *The influence of moisture content on the consolidation and compaction properties of paracetamol*. International Journal of Pharmaceutics, 1992. **81**(2): p. 187-192.
135. Vromans, H., et al., *Studies on tableting properties of lactose. VI. Consolidation and compaction of spray dried amorphous lactose*. Acta pharmaceutica Suecica, 1986. **23**(4): p. 231-40.
136. Buckton, G., et al., *The use of near infra-red spectroscopy to detect changes in the form of amorphous and crystalline lactose*. International Journal of Pharmaceutics, 1998. **168**(2): p. 231-241.
137. Salman, A.D., Omar, C. S. & AL-Asady, R. B., *Roller compactor: Improving the roller stress distribution along the roller width*. 2016.

APPENDIX A: NIR spectra for lactose 21AN and 200M

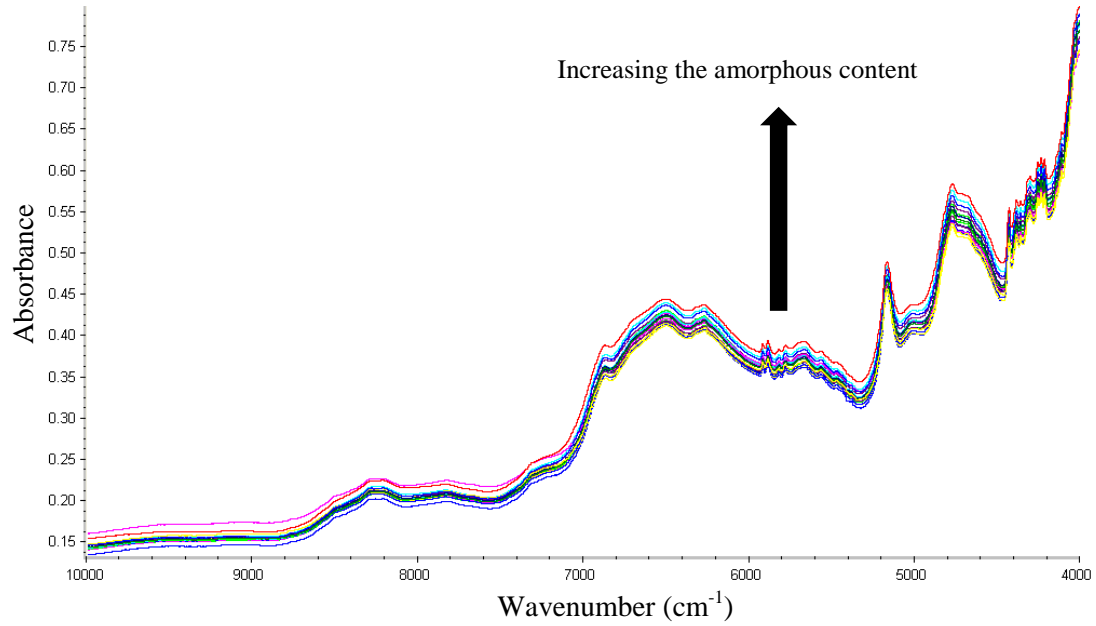


Figure A.1: NIR spectra of lactose 200M with difference amorphous content.

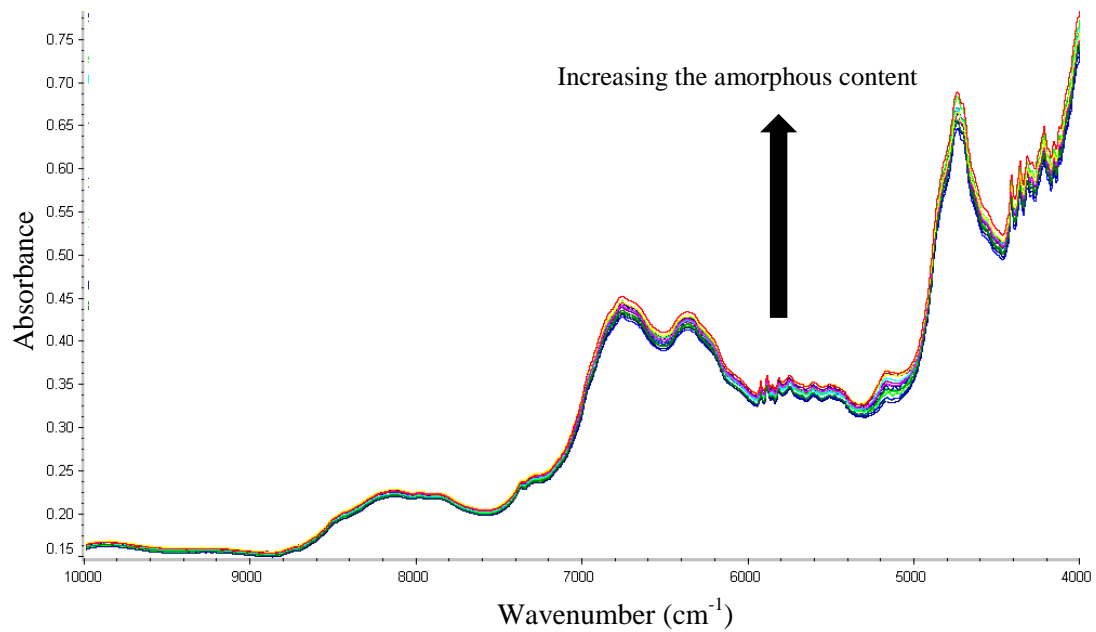


Figure A.2: NIR spectra of lactose 21AN with difference amorphous content.

APPENDIX B: Inhomogeneity of ribbon property across the width (lactose 21AN and lactose SD)

The result in this Appendix is related to the work presented in Chapter 8. It is basically the comparison between the standard flat roller with the new curved roller for lactose 21AN and SD.

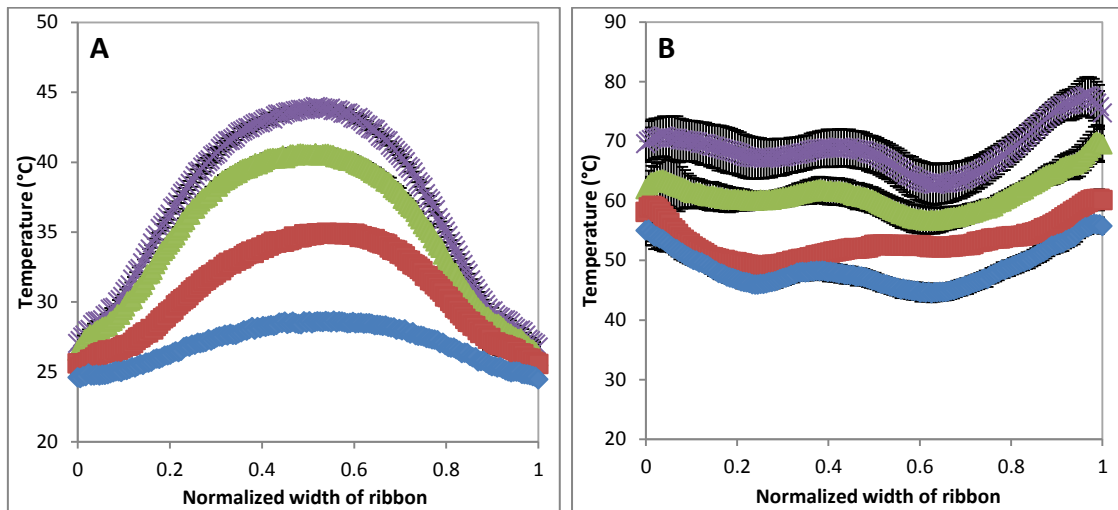


Figure B.1: Temperature profile across the width of ribbon of lactose 21AN during the roller compaction using the flat roller (A) and the curved roller (B) (◆ 20 bar, ■ 50 bar, ▲ 80 bar, × 100 bar).

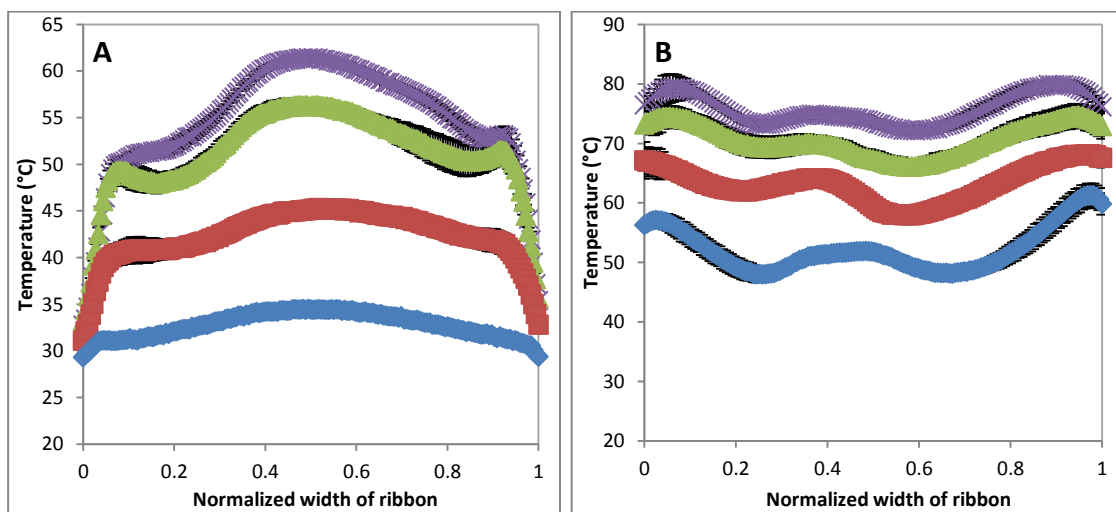


Figure B.2: Temperature profile across the width of ribbon of lactose SD during the roller compaction using the flat roller (A) and the curved roller (B) (◆ 20 bar, ■ 50 bar, ▲ 80 bar, × 100 bar).

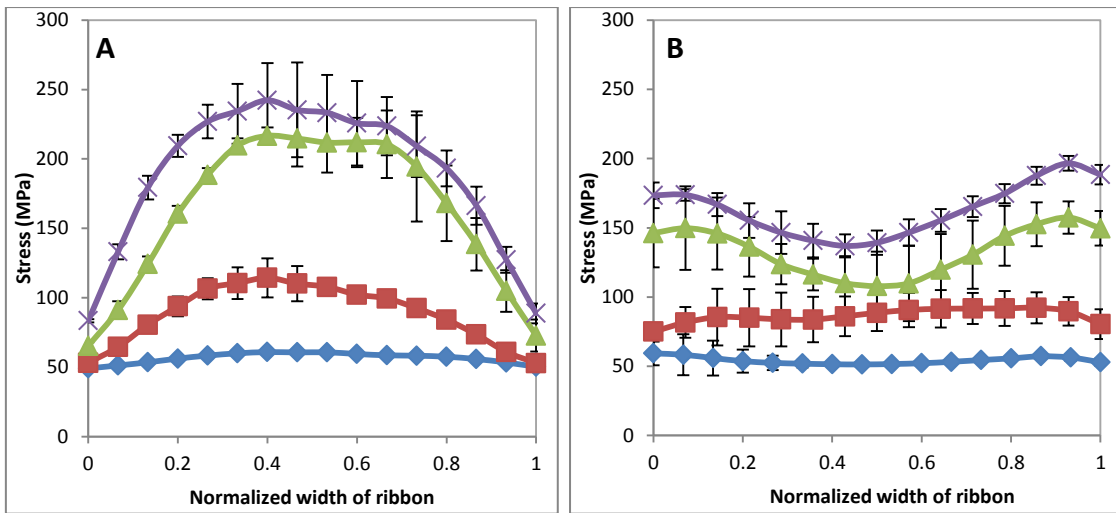


Figure B.3: Stress distribution across the width of the flat roller (A) and the curved roller (B) during roller compaction of lactose 21AN (◆ 20 bar, ■ 50 bar, ▲ 80 bar, × 100 bar).

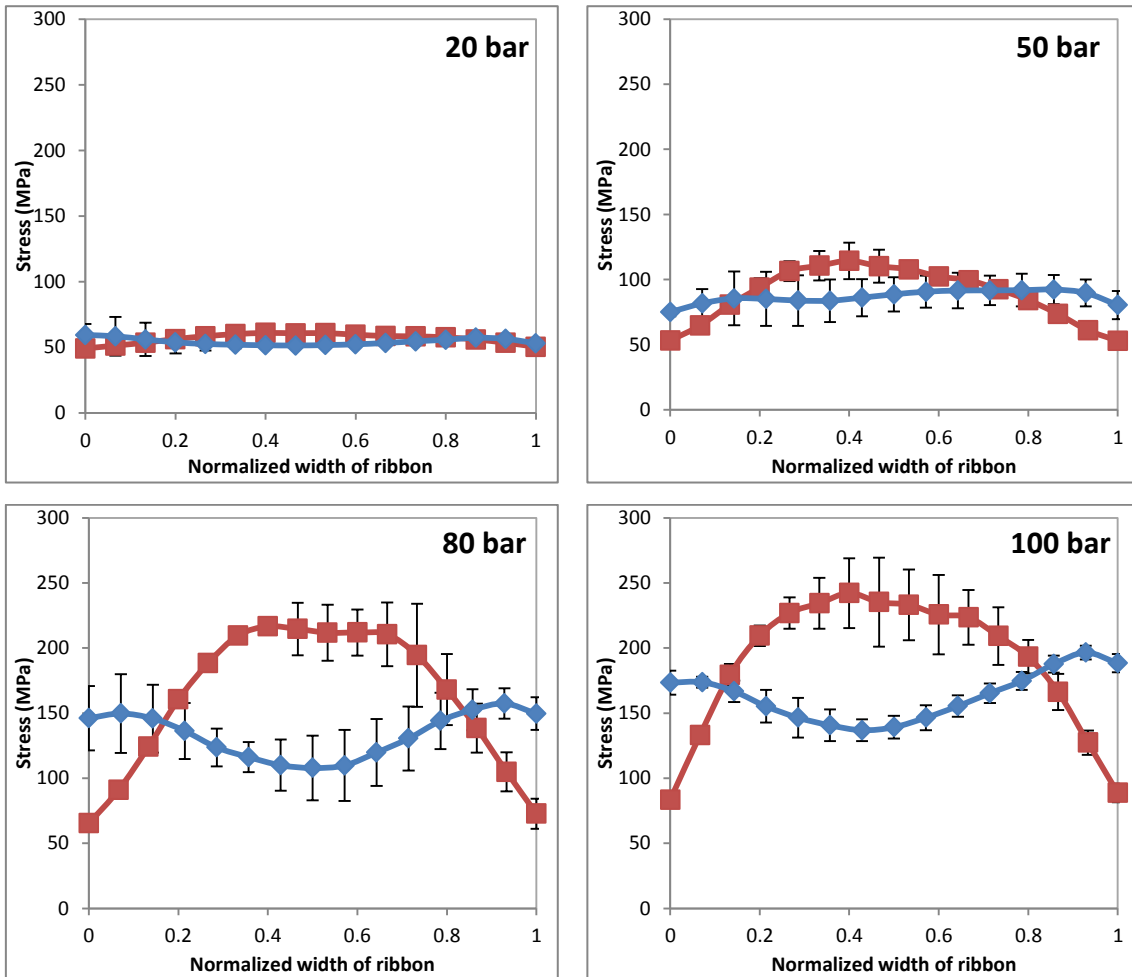


Figure B.4: Stress distribution of the flat vs the curved roller using lactose 21AN (◆ curved roller, ■ flat roller).

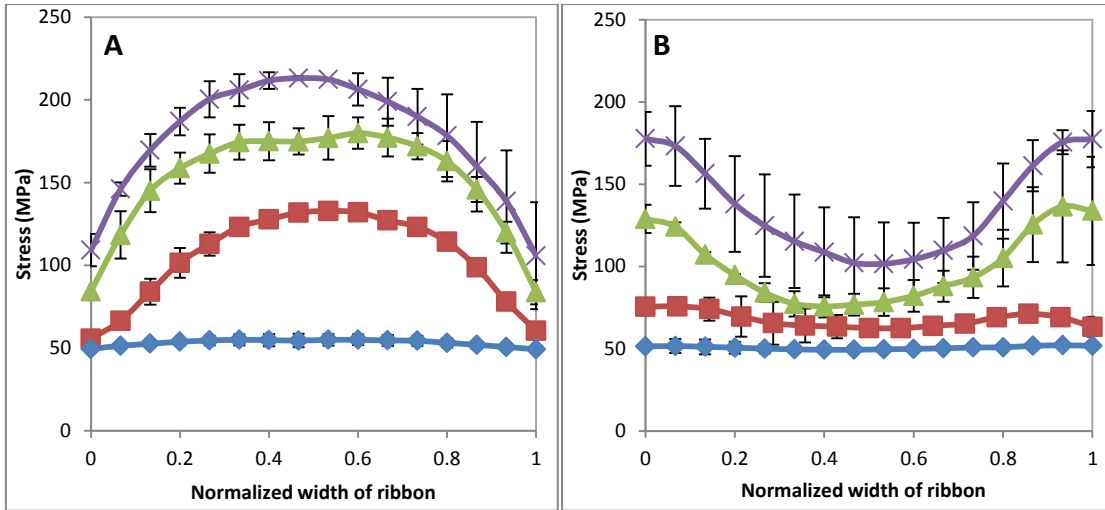


Figure B.5: Stress distribution across the width of the flat roller (A) and the curved roller (B) during roller compaction of lactose SD (◆ 20 bar, ■ 50 bar, ▲ 80 bar, × 100 bar).

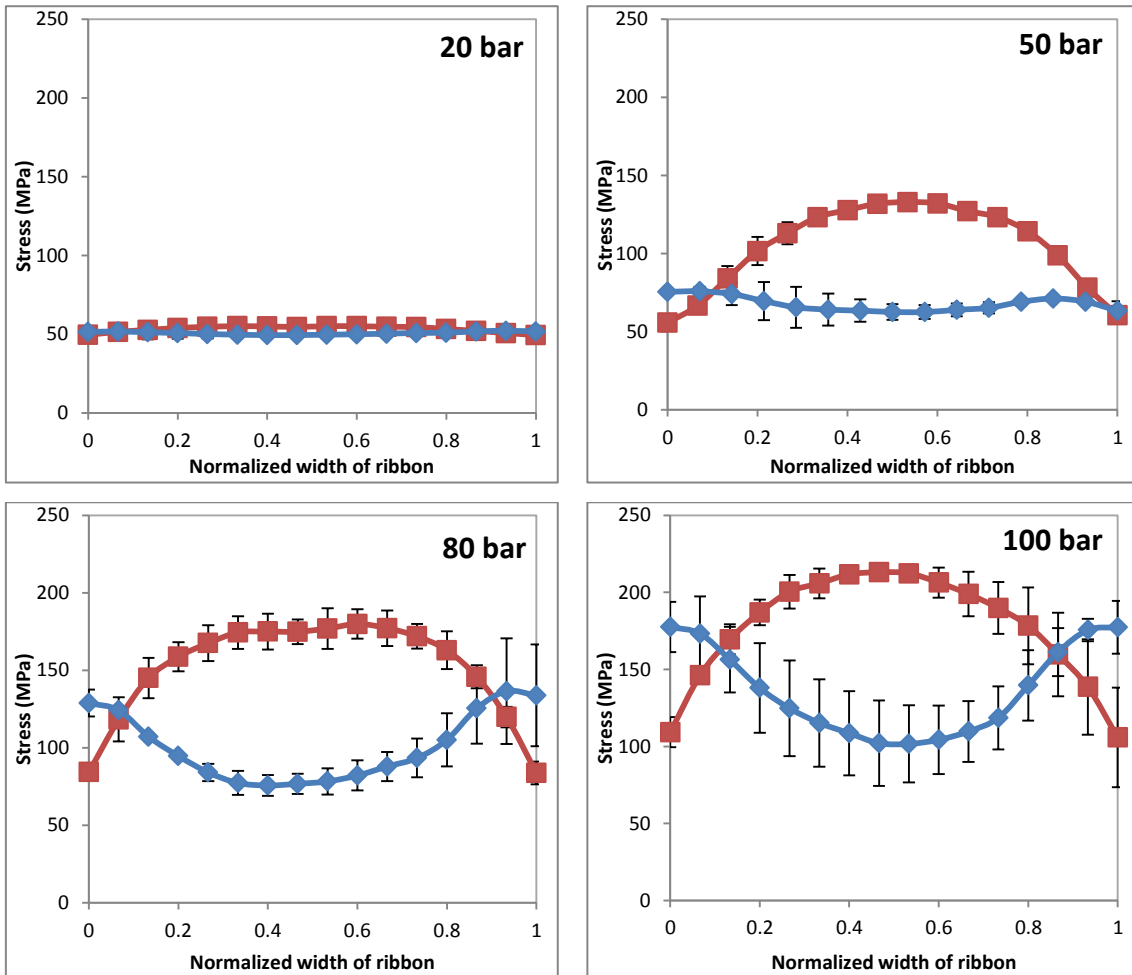


Figure B.6: Stress distribution of the flat vs the curved roller using lactose SD (◆ curved roller, ■ flat roller).

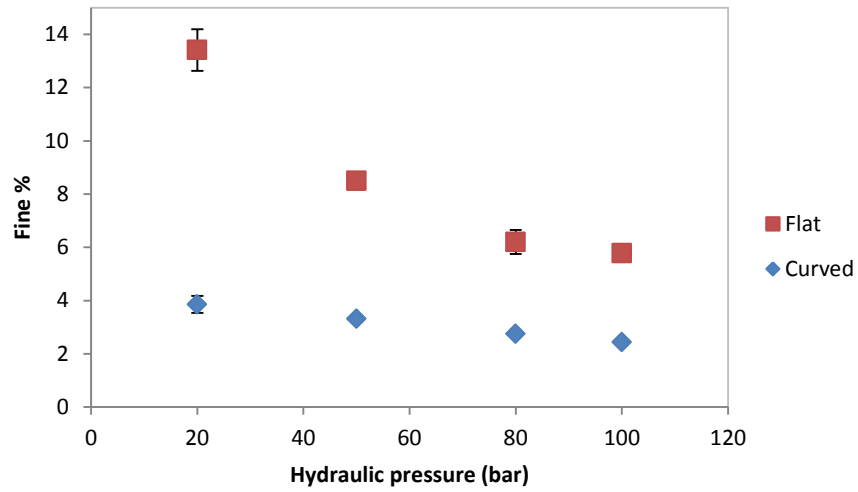


Figure B.7: Percentage of fines produced from lactose 21AN using the standard flat roller and the new curved roller.

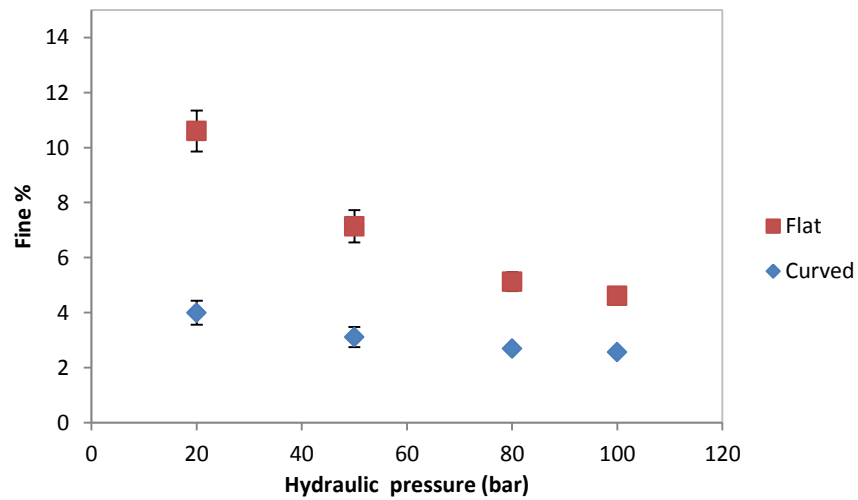


Figure B.8: Percentage of fines produced from lactose SD using the standard flat roller and the new curved roller.

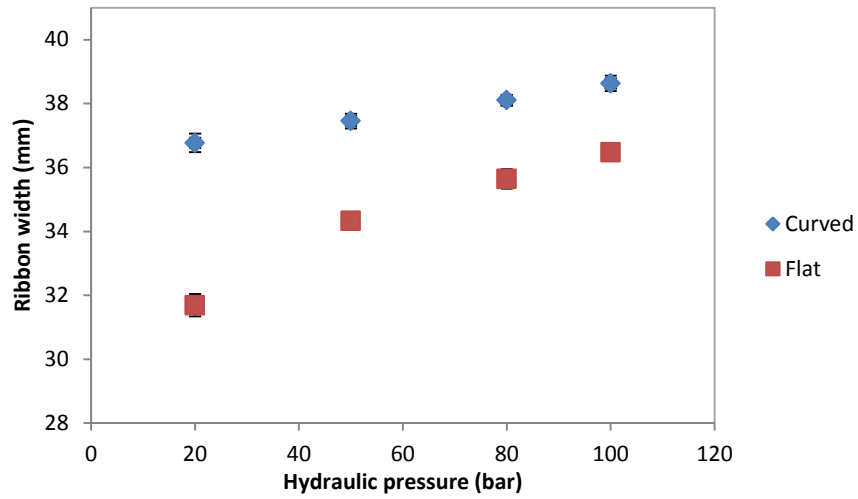


Figure B.9: Width of ribbon of lactose 21AN produced using the standard flat roller and the new curved roller.

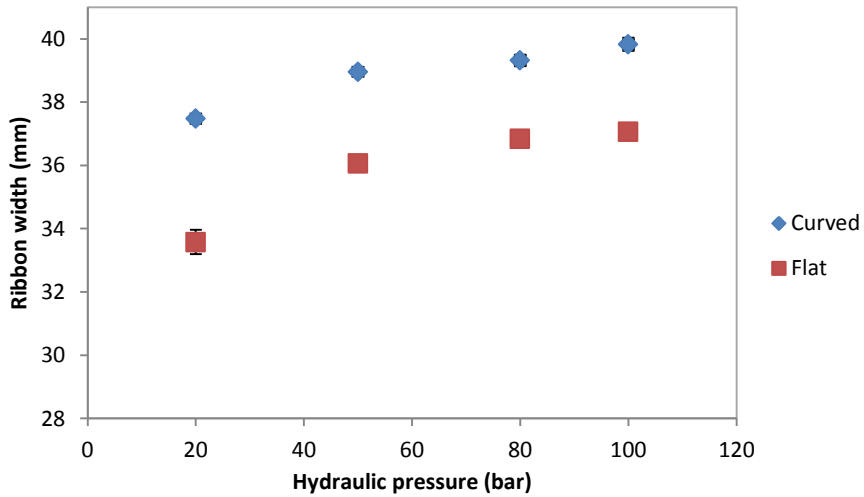


Figure B.10: Width of ribbon of lactose SD produced using the standard flat roller and the new curved roller.

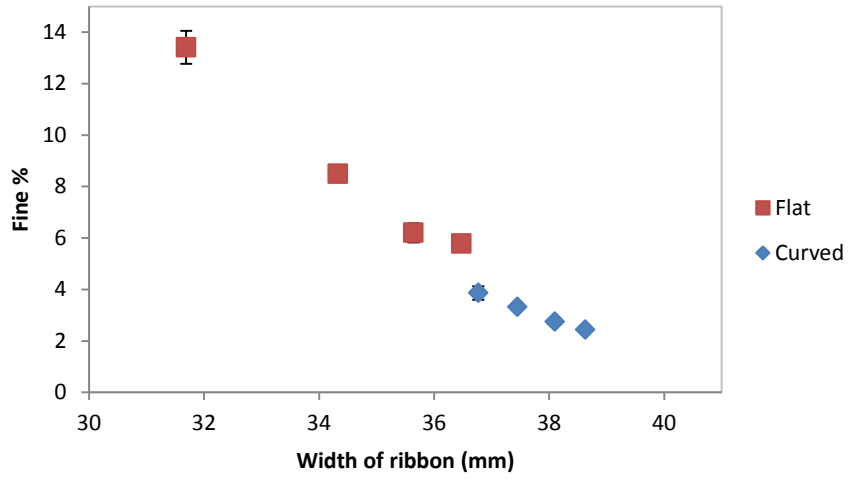


Figure B.11: Fine percentage vs width of ribbon of lactose 21AN.

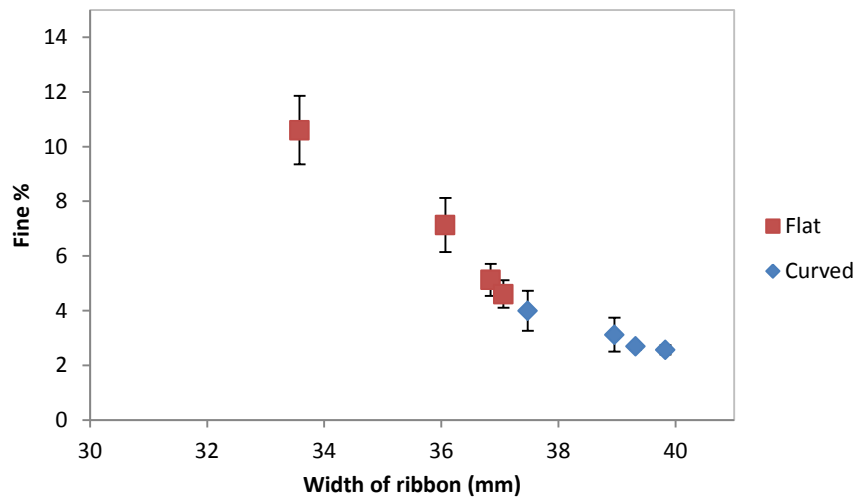


Figure B.12: Fine percentage vs width of ribbon of lactose SD.

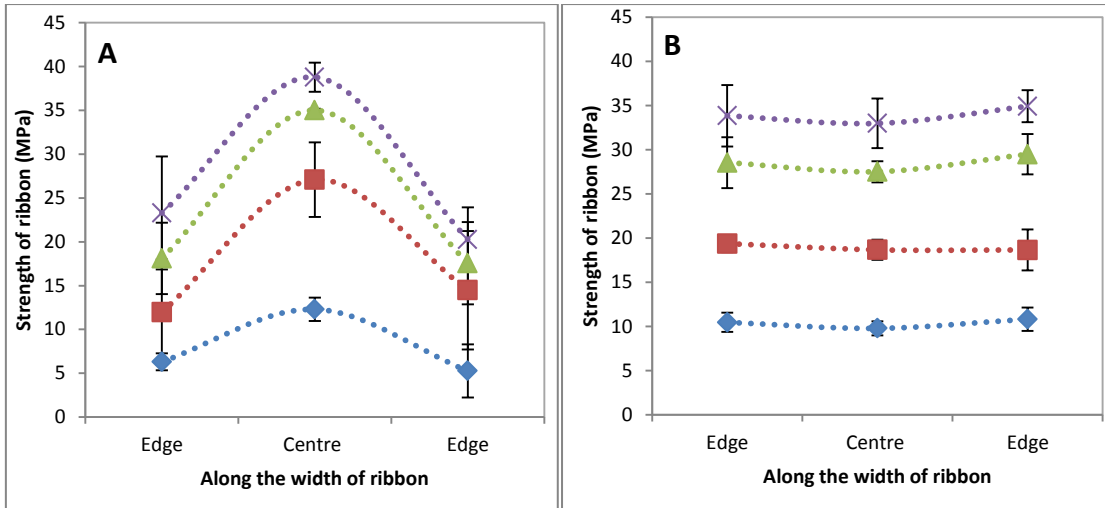


Figure B.13: Local strength across the width of ribbon of 21AN using the flat roller (A) and the curved roller (B) (◆ 20 bar, ■ 50 bar, ▲ 80 bar, × 100 bar).

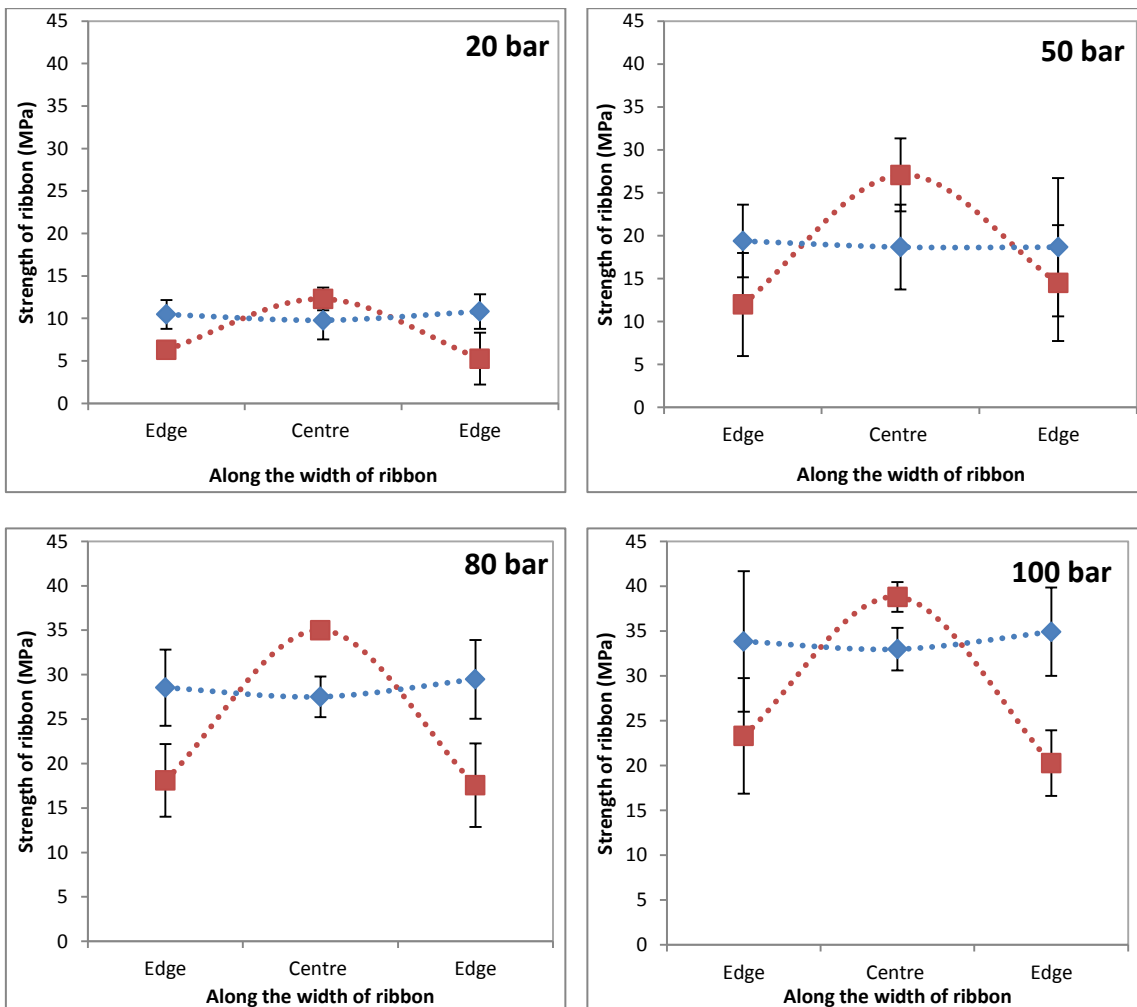


Figure B.14: Local strength across the width of ribbon produced from 21AN using the curved roller ◆, and the flat roller ■.

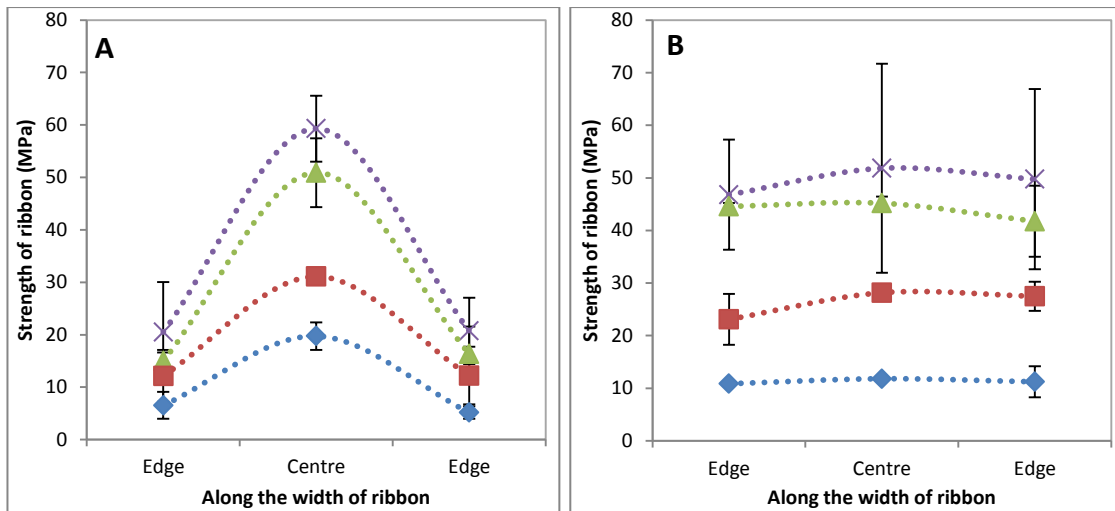


Figure B.15: Local strength across the width of ribbon of SD using the flat roller (A) and the curved roller (B) (◆ 20 bar, ■ 50 bar, ▲ 80 bar, × 100 bar).

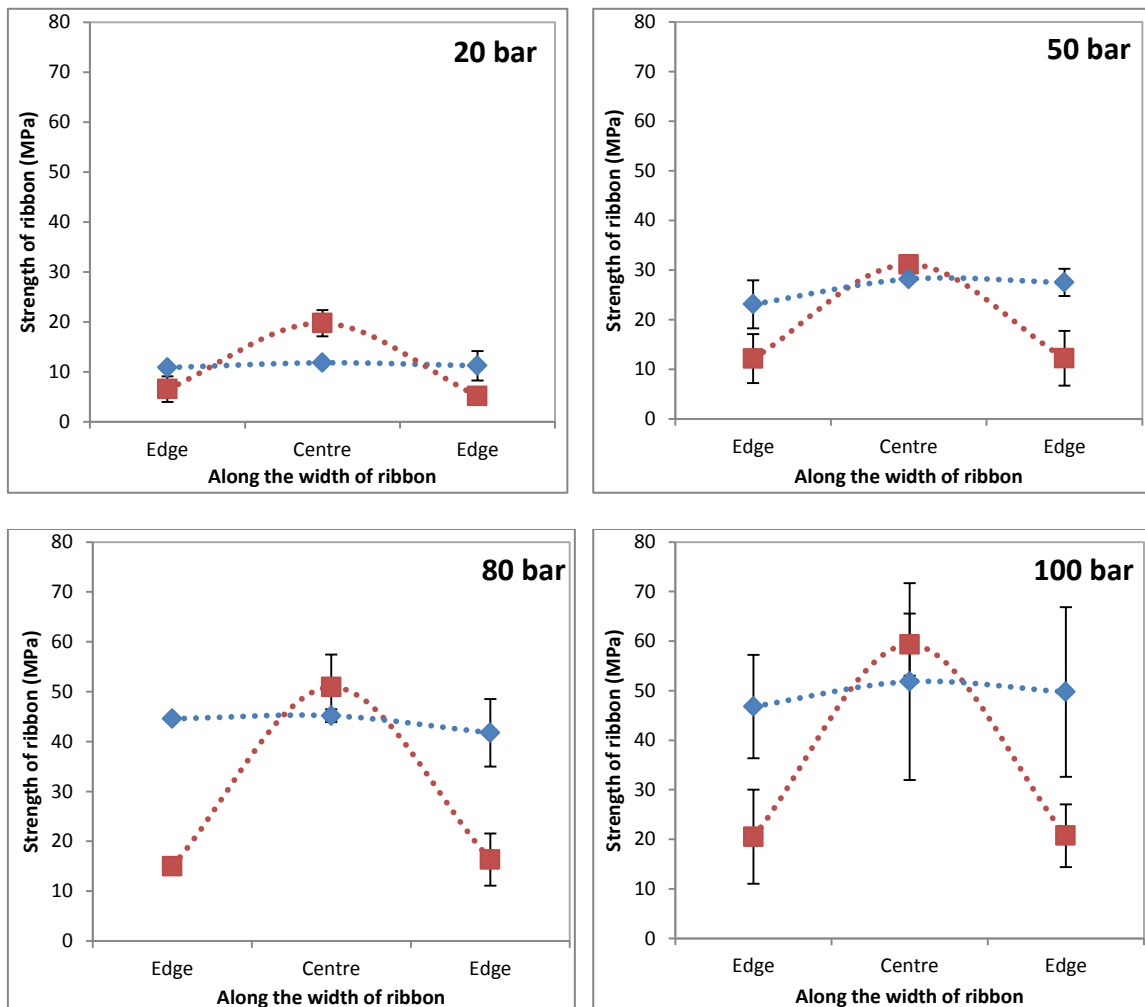


Figure B.16: Local strength across the width of ribbon produced from SD using the curved roller ◆, and the flat roller ■.

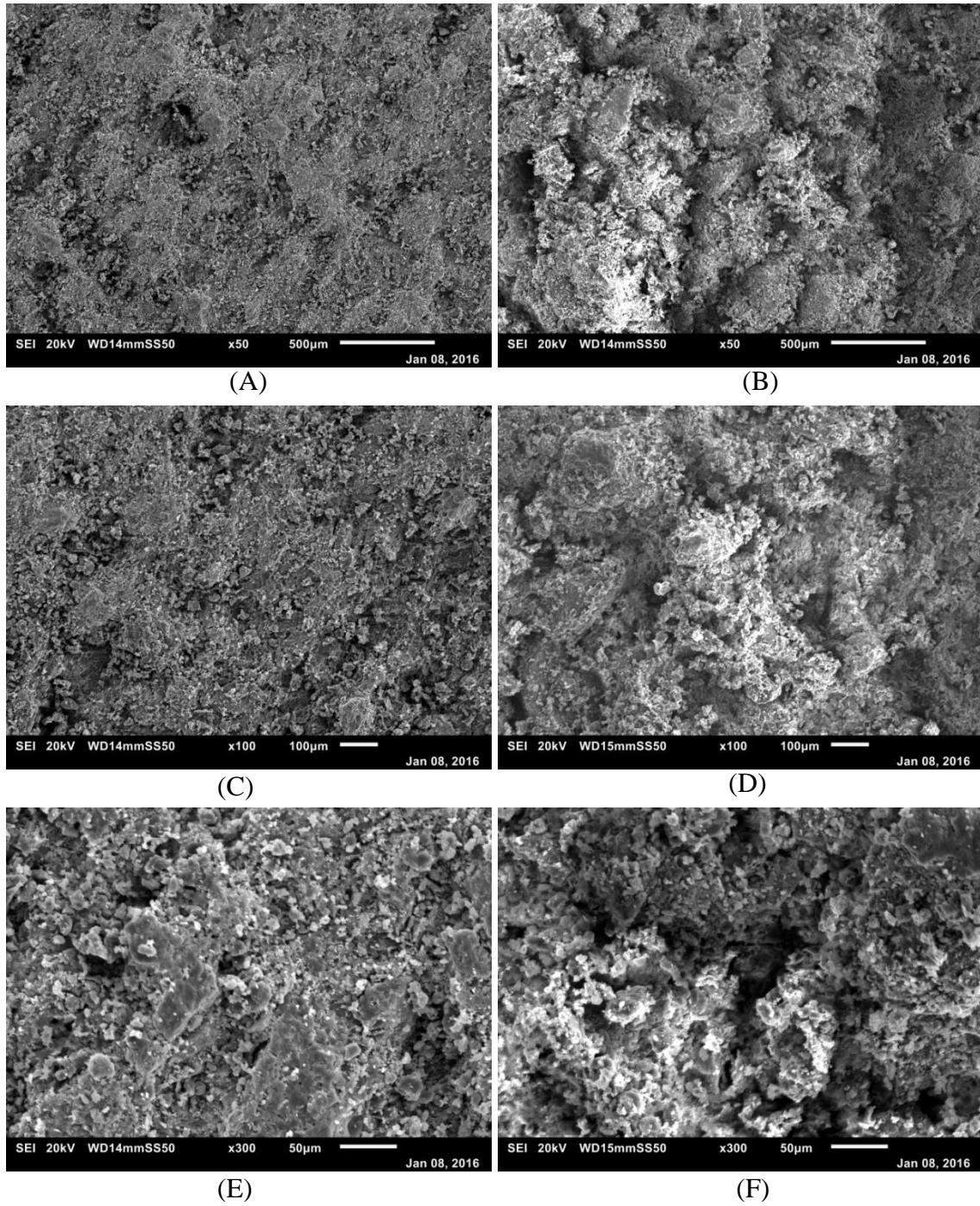


Figure B.17: SEM images for ribbons produced from lactose 21AN at 20 bar using the flat rollers; centre of ribbon (A, C, E) and edges of the ribbon (B, D, F), at 50× magnification (A, B), 100× (C, D), and 300× (E, F).

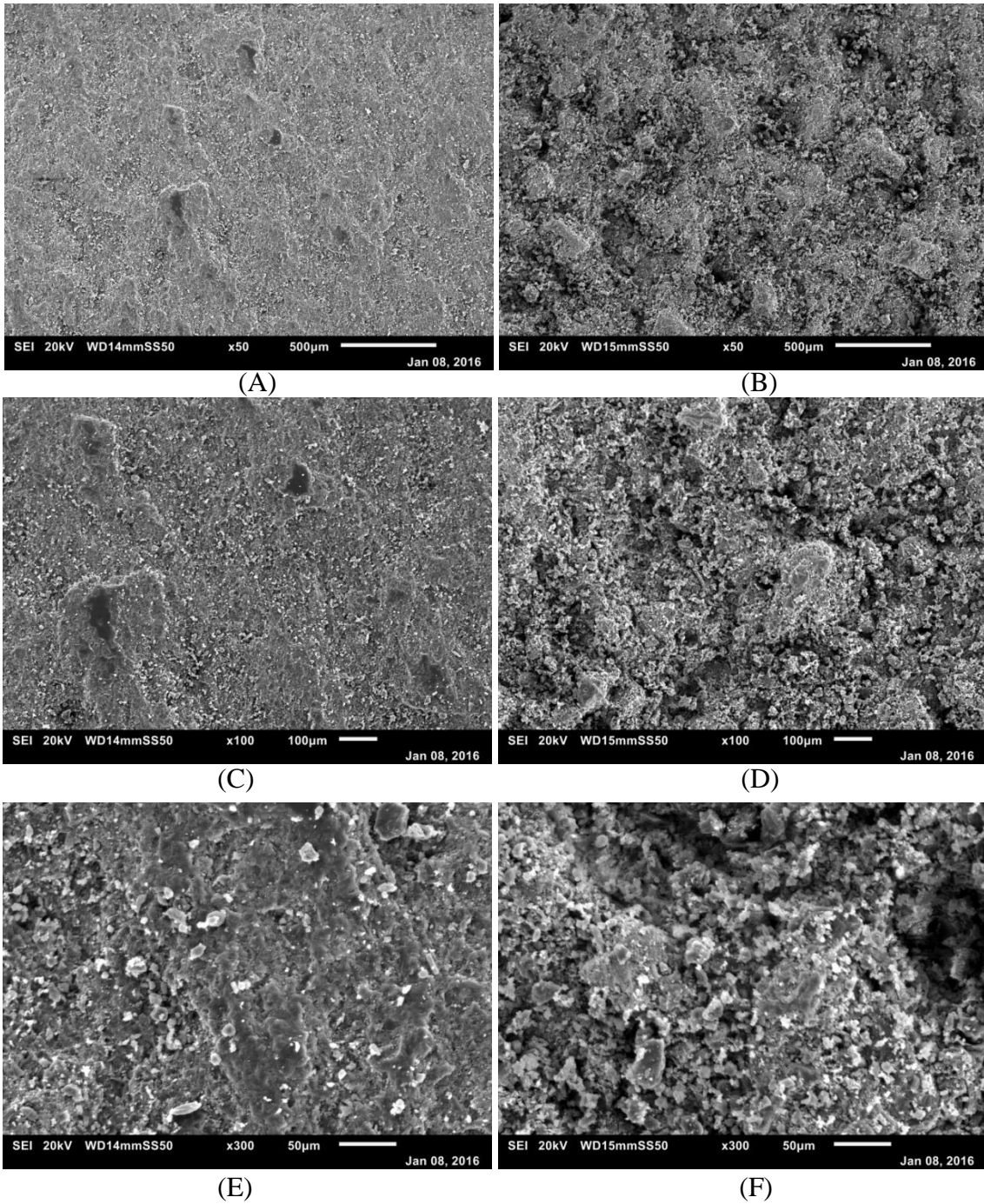


Figure B.18: SEM images for ribbons produced from lactose 21AN at 100 bar using the flat rollers; centre of ribbon (A, C, E) and edges of the ribbon (B, D, F), at 50 \times magnification (A, B), 100 \times (C, D), and 300 \times (E, F).

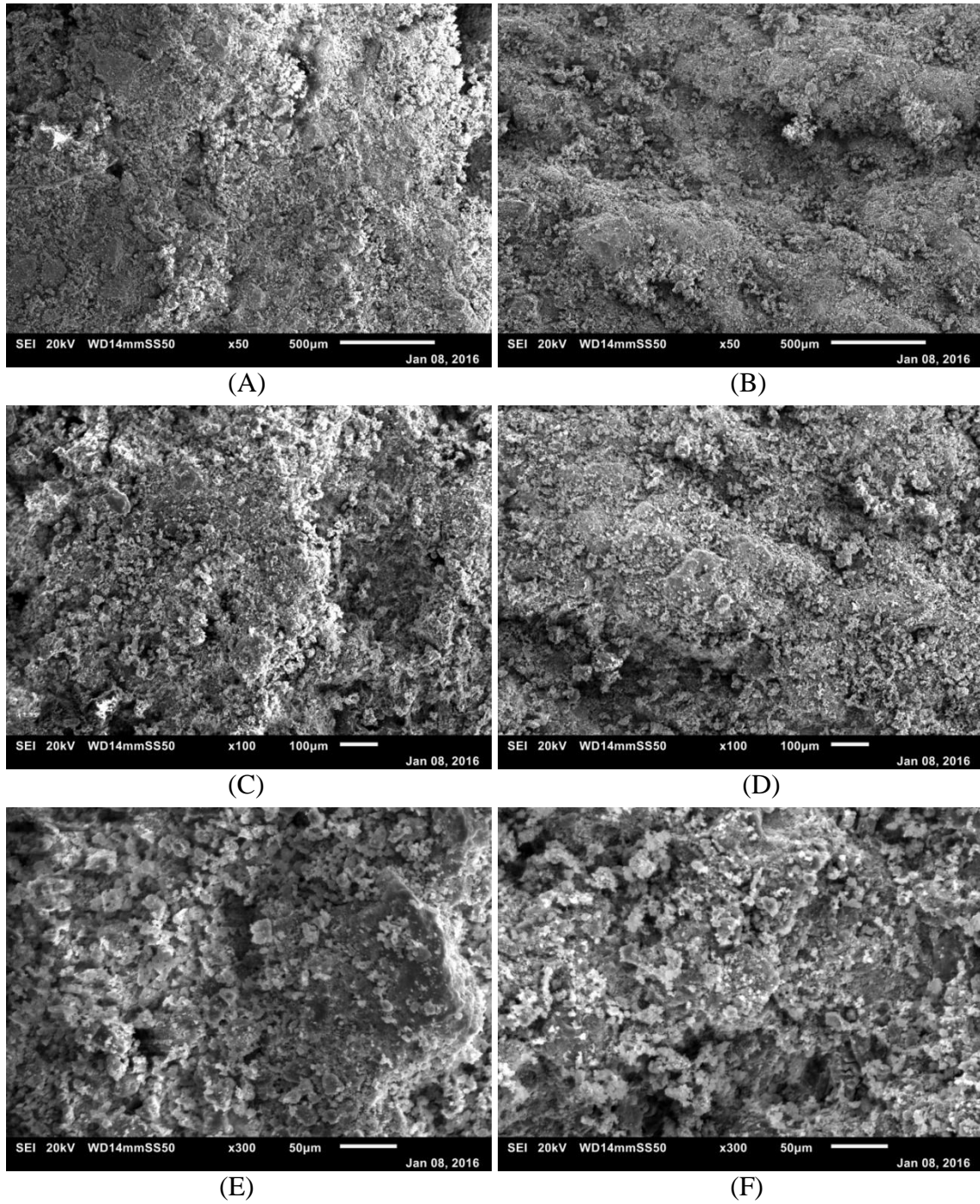


Figure B.19: SEM images for ribbons produced from lactose 21AN at 20 bar using the curved rollers; centre of ribbon (A, C, E) and edges of the ribbon (B, D, F), at 50× magnification (A, B), 100× (C, D), and 300× (E, F).

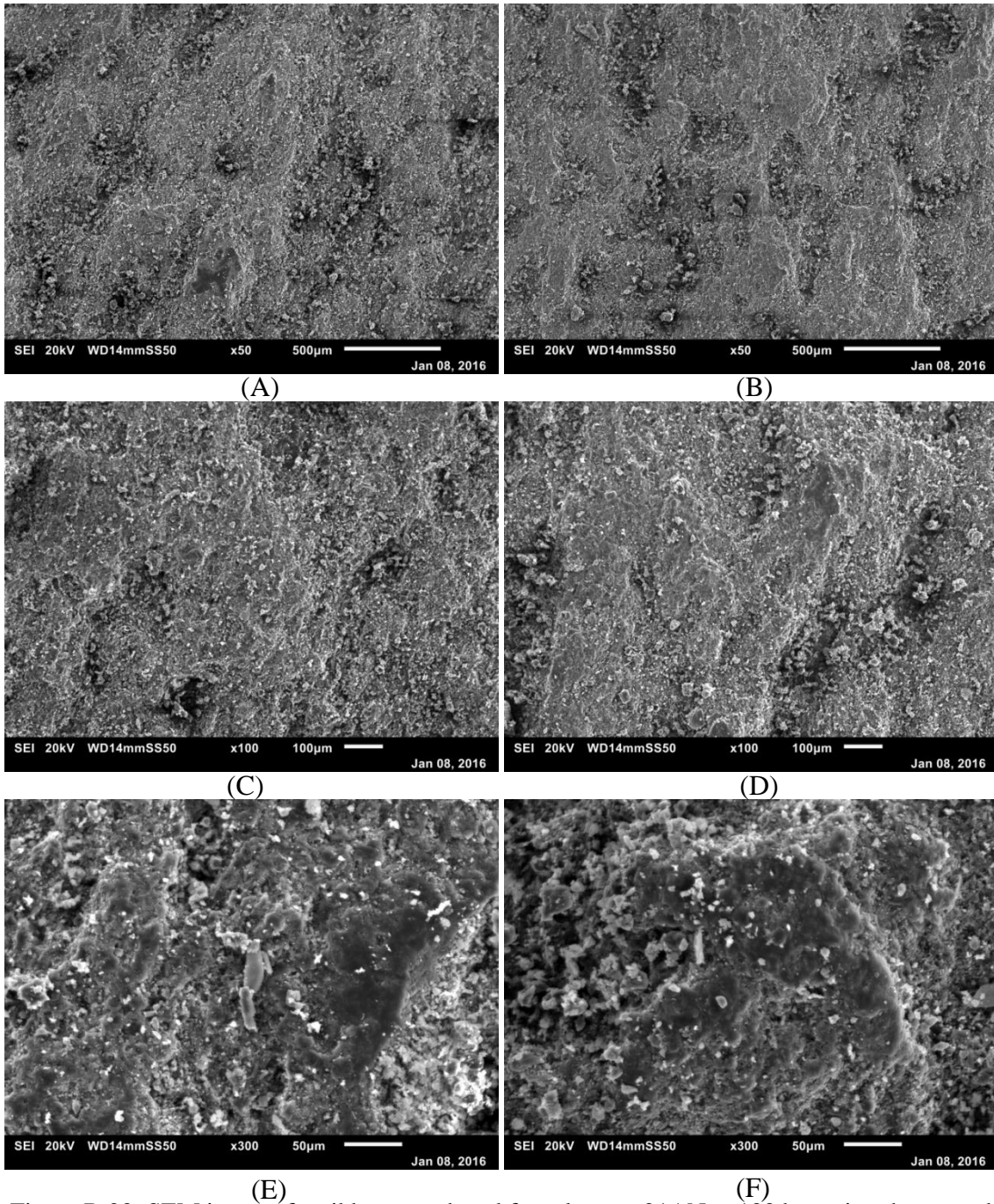


Figure B.20: SEM images for ribbons produced from lactose 21AN at 100 bar using the curved rollers; centre of ribbon (A, C, E) and edges of the ribbon (B, D, F), at 50 \times magnification (A, B), 100 \times (C, D), and 300 \times (E, F)

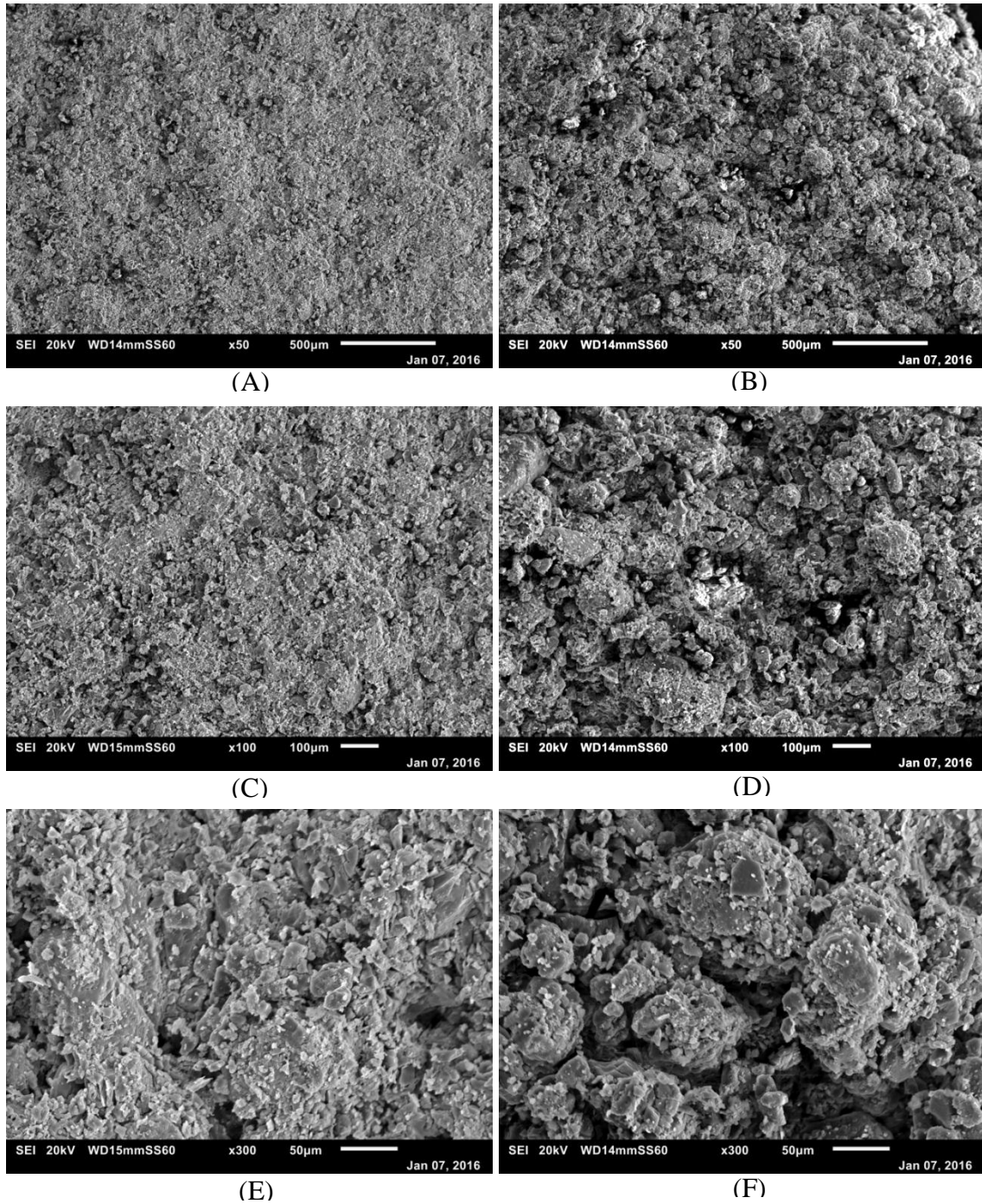


Figure B.21: SEM images for ribbons produced from lactose SD at 20 bar using the flat rollers; centre of ribbon (A, C, E) and edges of the ribbon (B, D, F), at 50× magnification (A, B), 100× (C, D), and 300× (E, F).

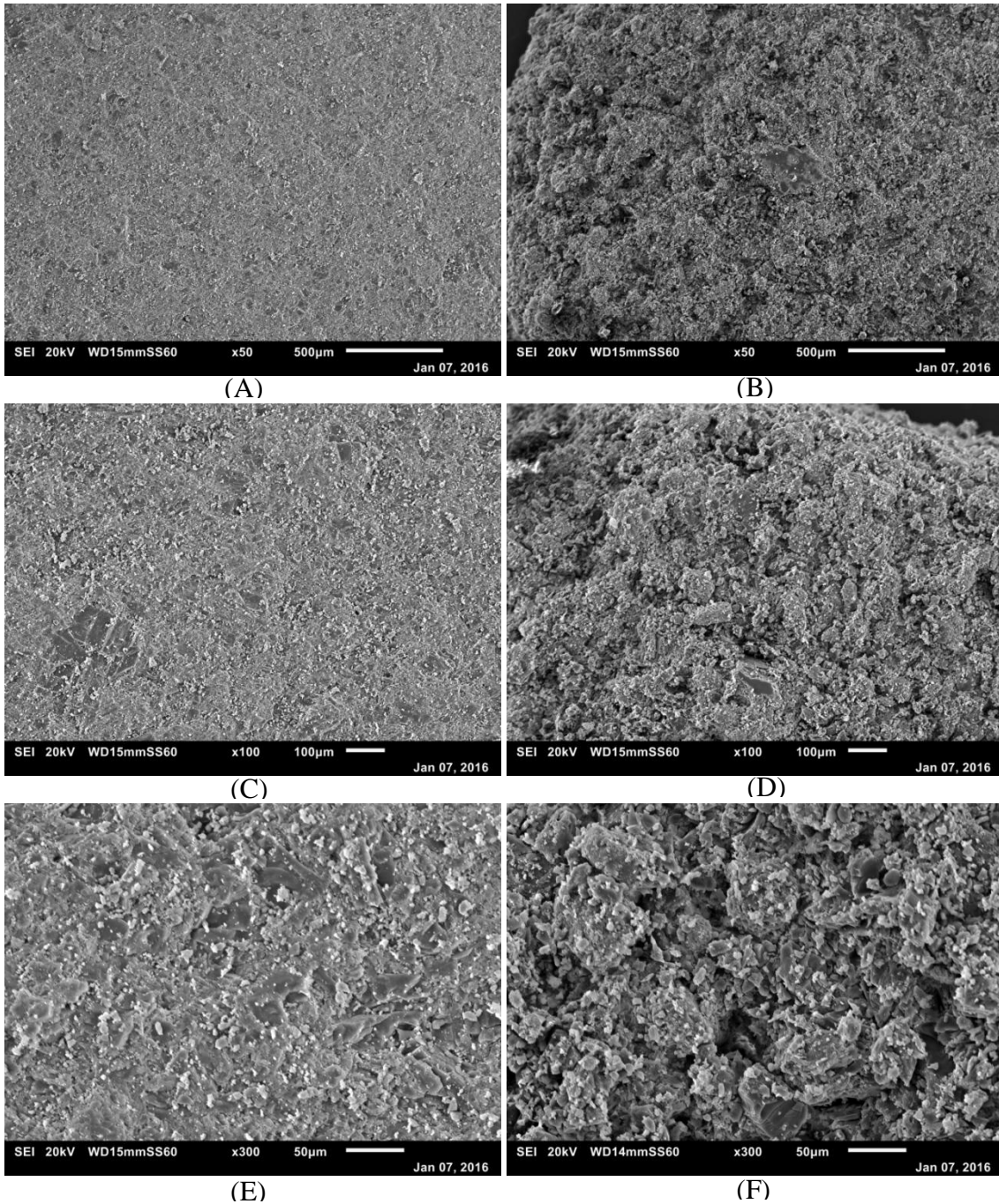


Figure B.22: SEM images for ribbons produced from lactose SD at 100 bar using the flat rollers; centre of ribbon (A, C, E) and edges of the ribbon (B, D, F), at 50× magnification (A, B), 100× (C, D), and 300× (E, F).

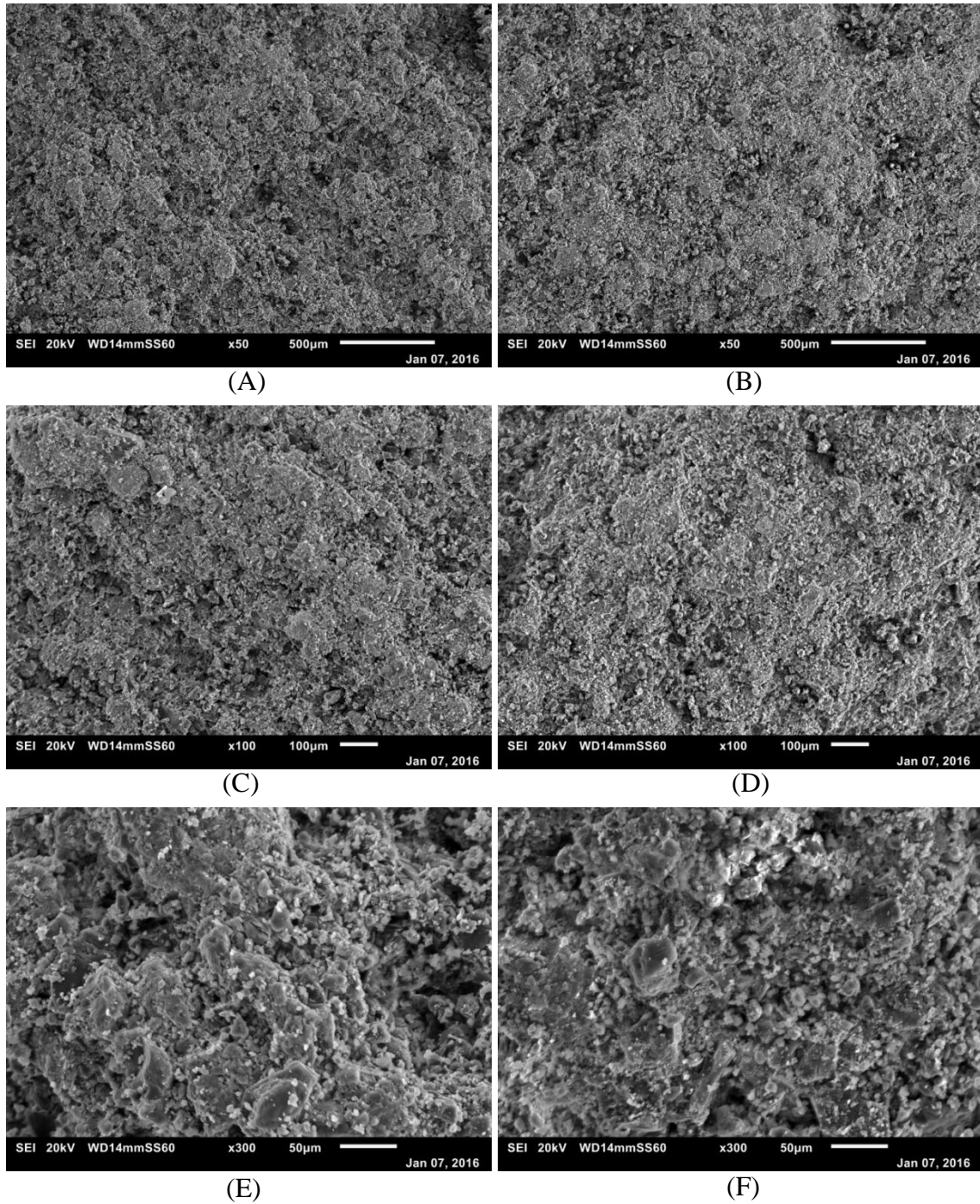


Figure B.23: SEM images for ribbons produced from lactose SD at 20 bar using the curved rollers; centre of ribbon (A, C, E) and edges of the ribbon (B, D, F), at 50× magnification (A, B), 100× (C, D), and 300× (E, F).

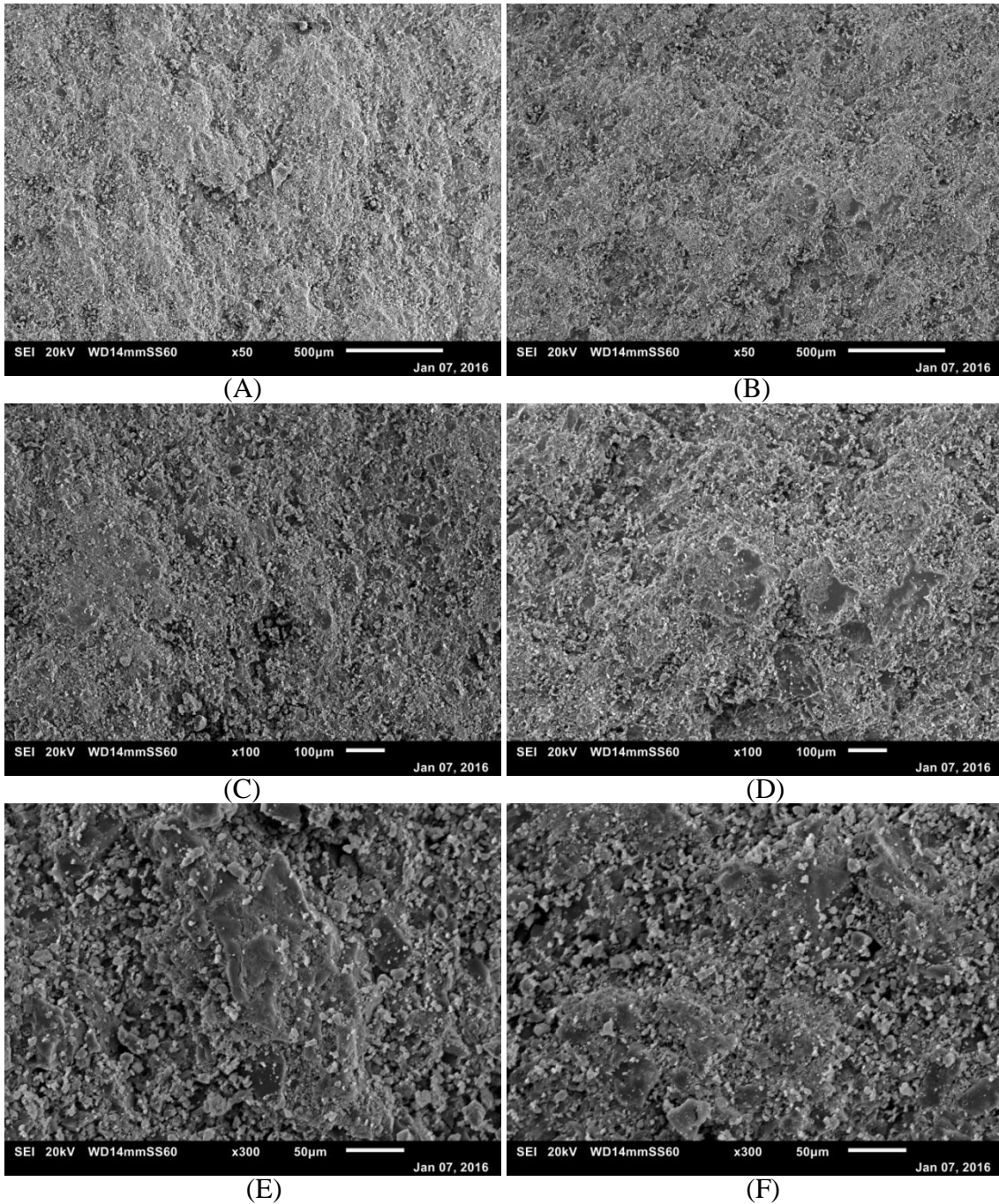


Figure B.24: SEM images for ribbons produced from lactose SD at 100 bar using the curved rollers; centre of ribbon (A, C, E) and edges of the ribbon (B, D, F), at 50× magnification (A, B), 100× (C, D), and 300× (E, F).

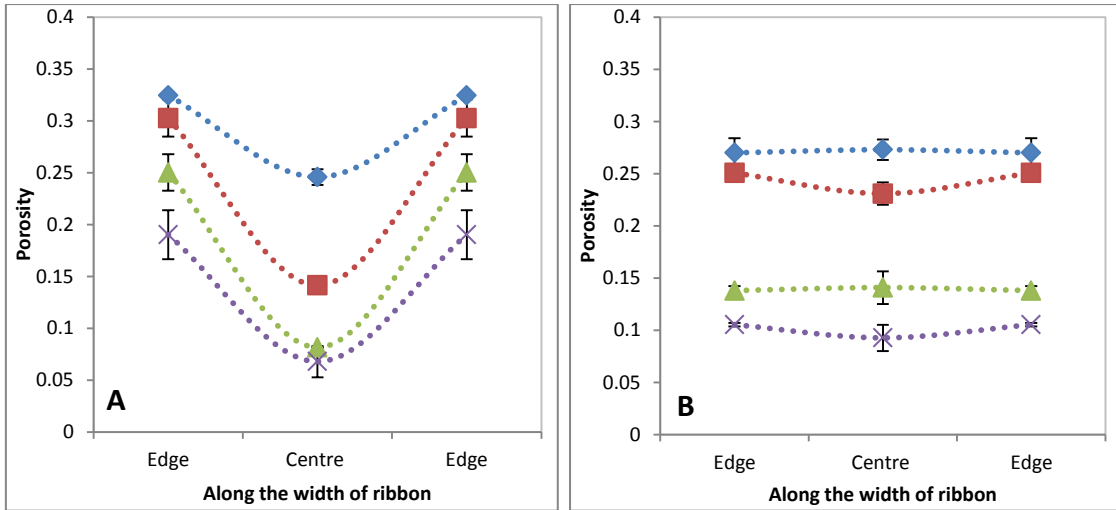


Figure B.25: Porosity across the width of ribbon of 21AN using the flat roller (A) and the curved roller (B) (◆ 20 bar, ■ 50 bar, ▲ 80 bar, × 100 bar).

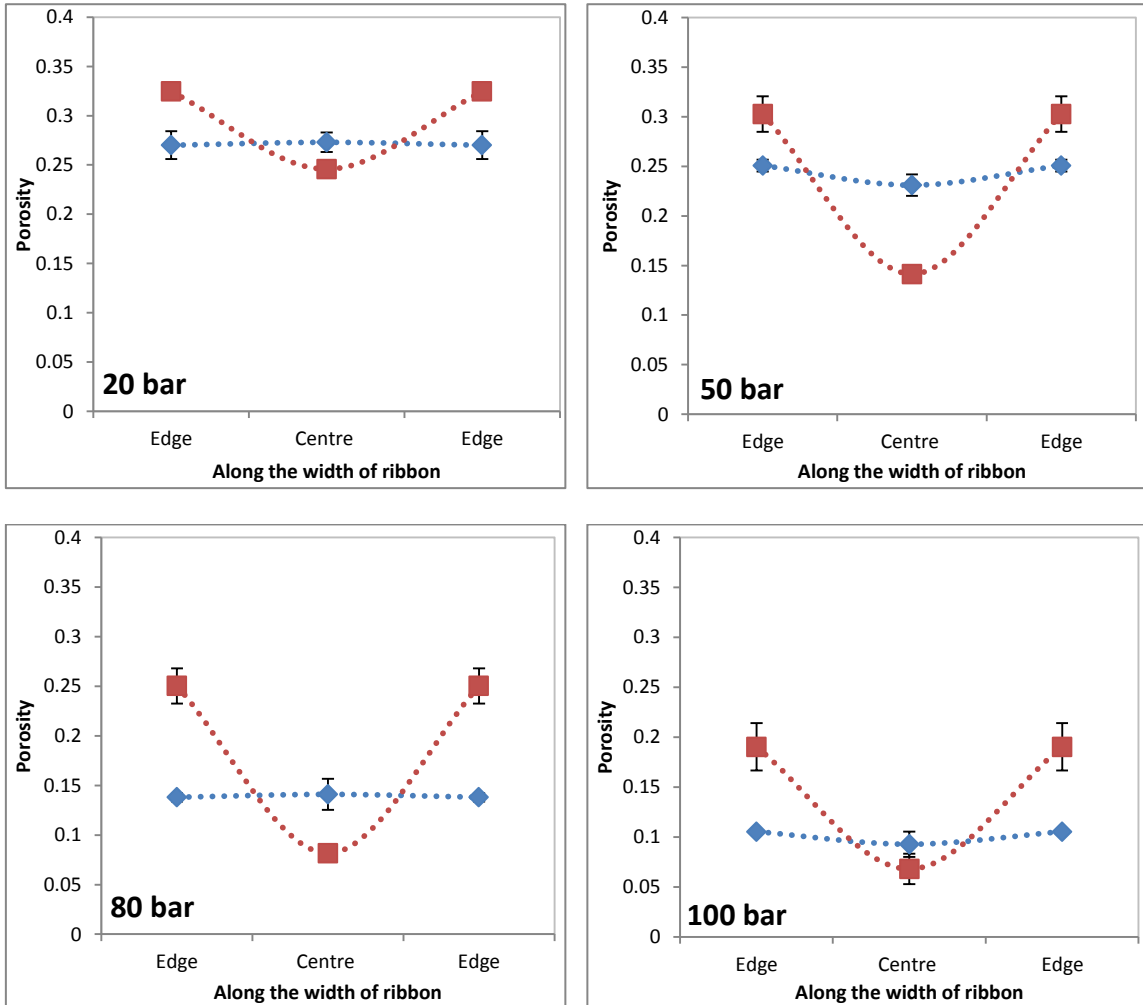


Figure B.26: Porosity across the width of ribbon produced from 21AN using the curved roller ◆, and the flat roller ■.

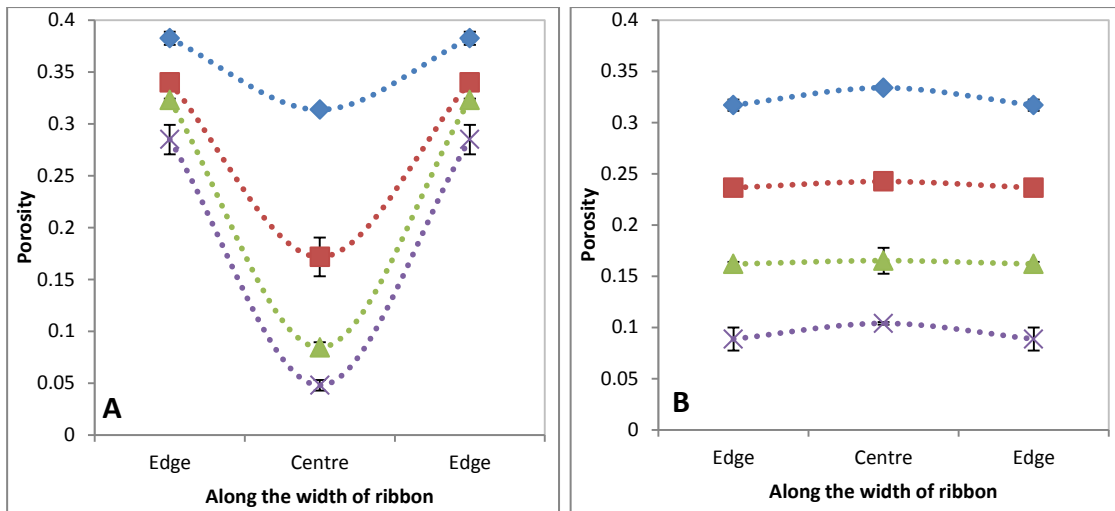


Figure B.27: Porosity across the width of ribbon of SD using the flat roller (A) and the curved roller (B) (◆ 20 bar, ■ 50 bar, ▲ 80 bar, × 100 bar).

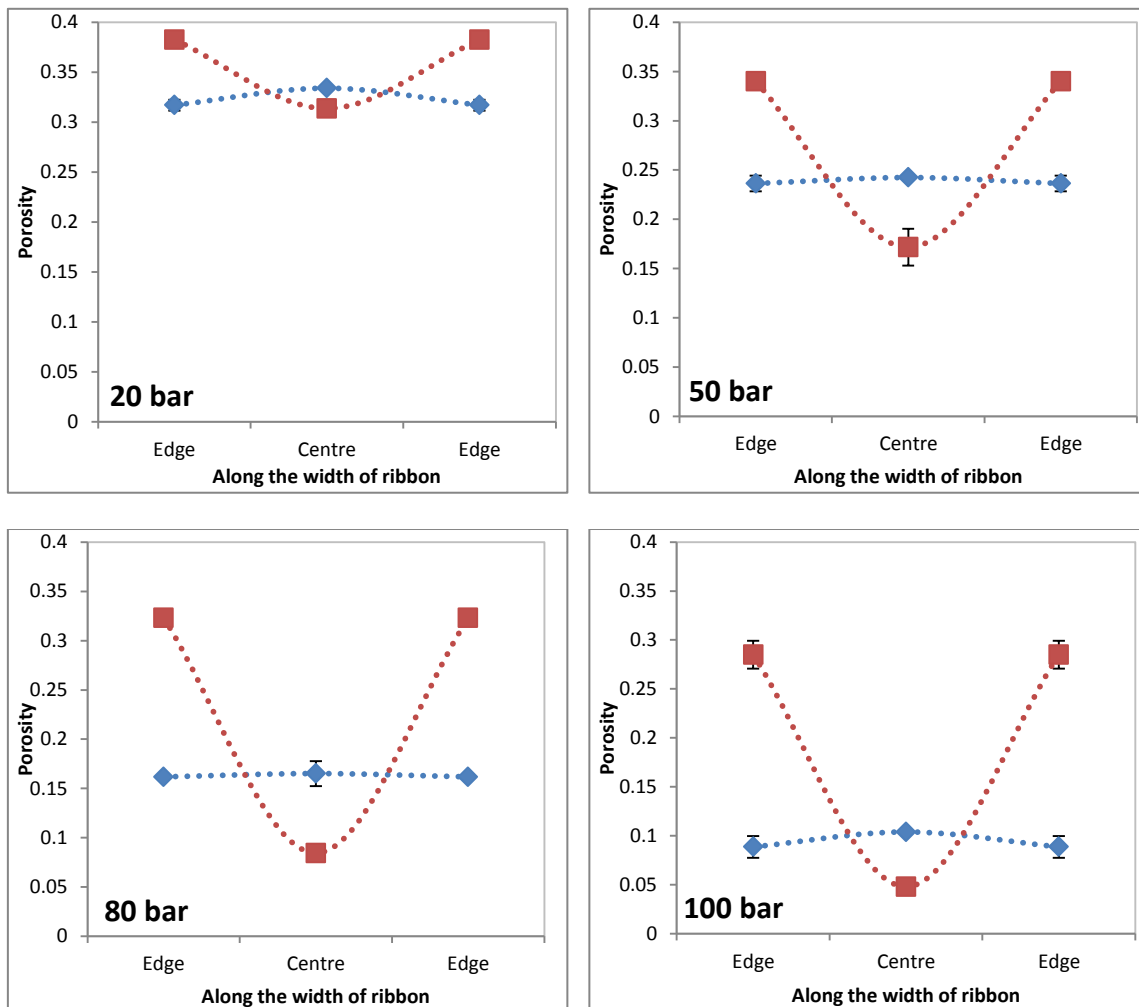


Figure B.28: Porosity across the width of ribbon produced from SD using the curved roller ◆, and the flat roller ■.

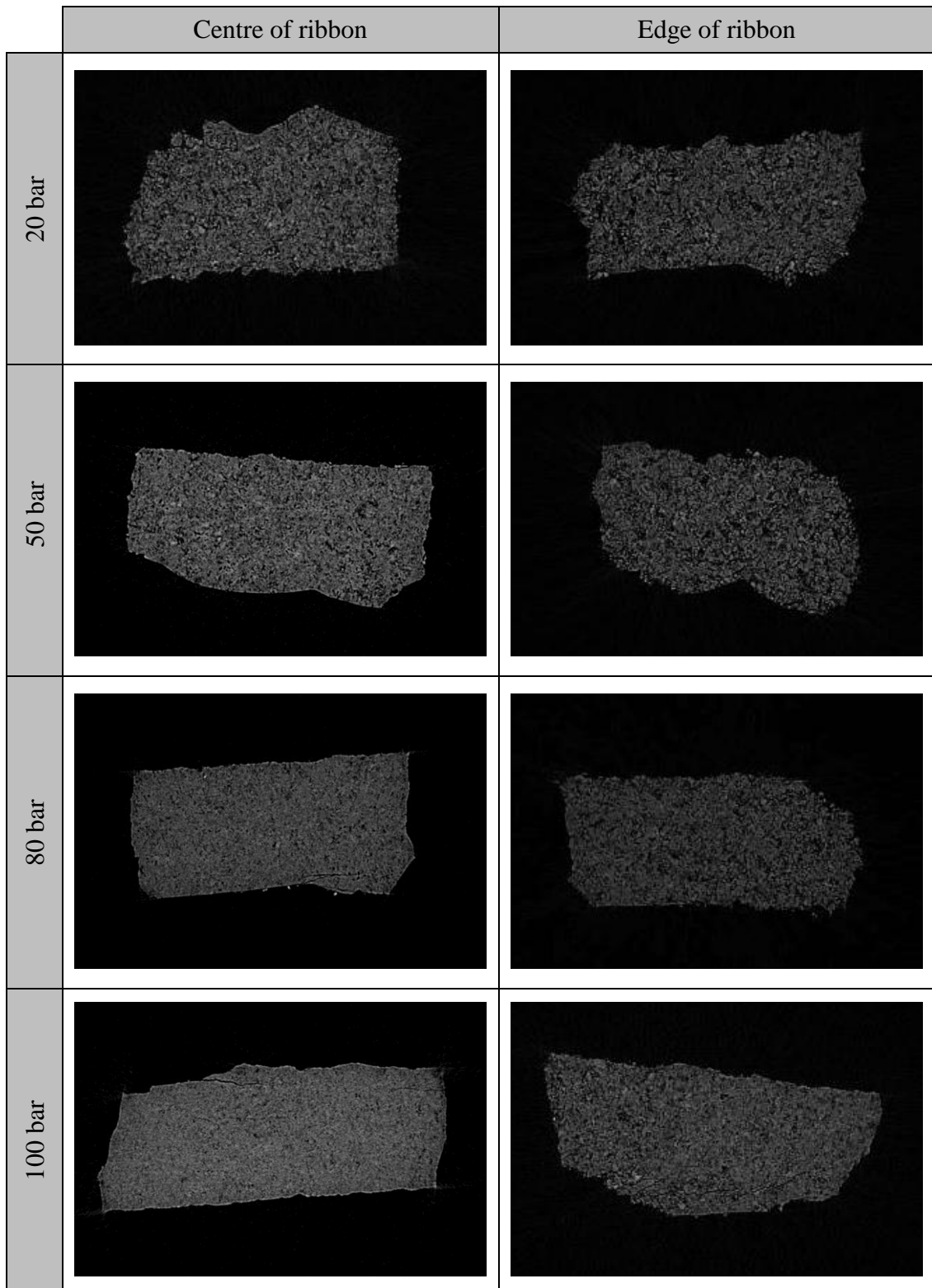


Figure B.29: X-ray images for ribbon produced from lactose 21AN using the flat rollers.

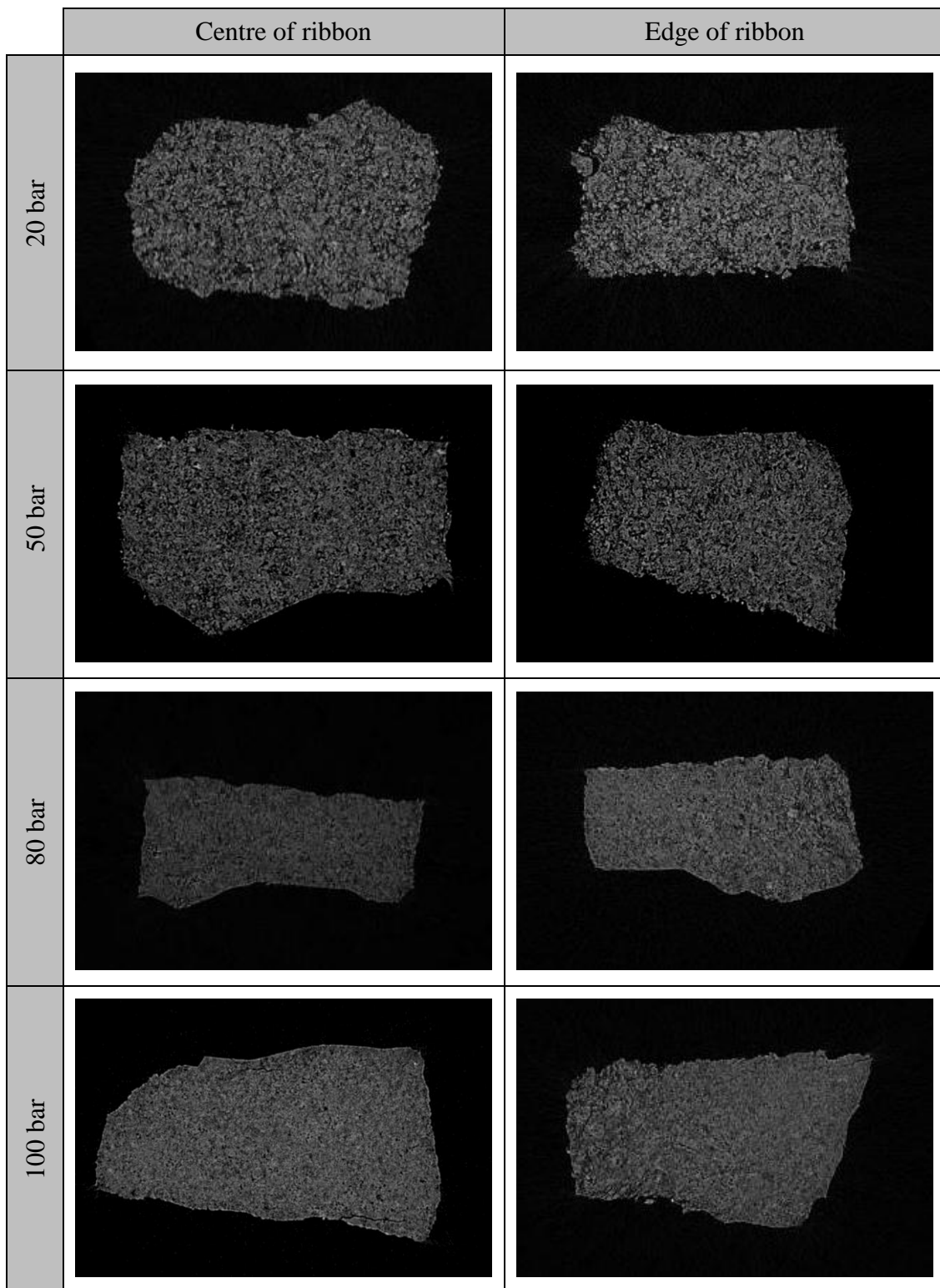


Figure B.30: X-ray images for ribbon produced from lactose 21AN using the curved rollers.

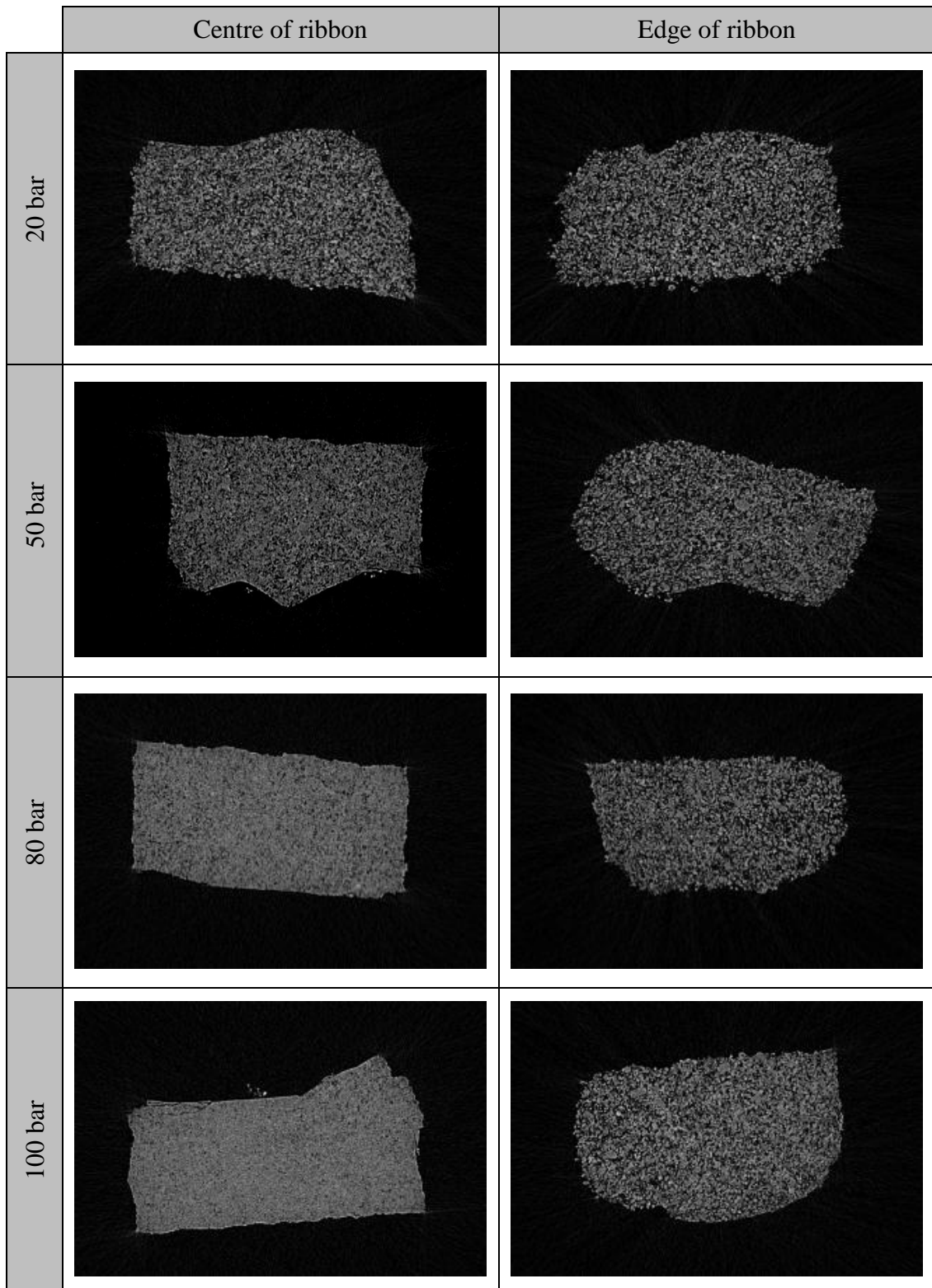


Figure B.31: X-ray images for ribbon produced from lactose SD using the flat rollers.

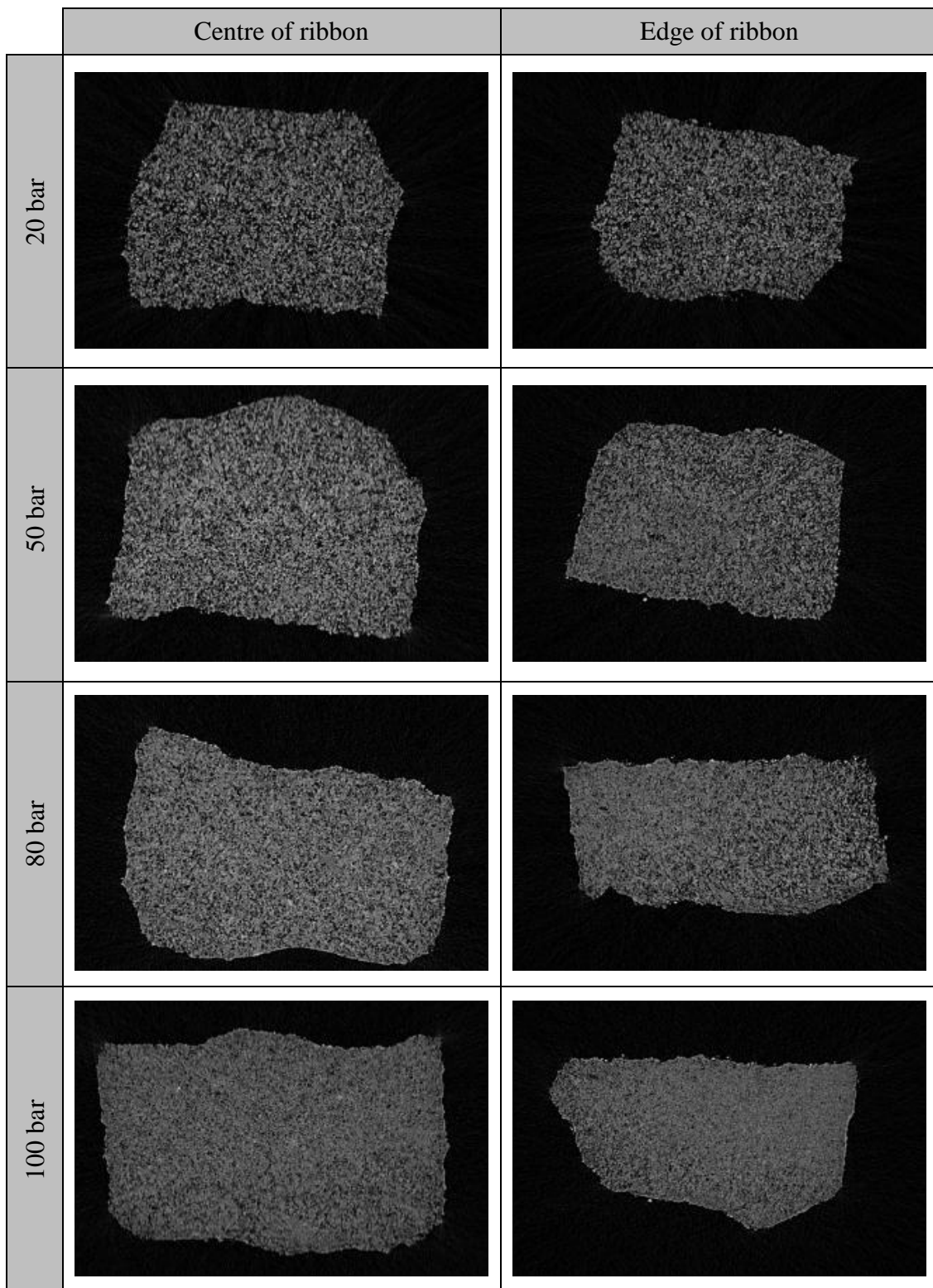


Figure B.32: X-ray images for ribbon produced from lactose SD using the curved rollers.